

School of Earth and Planetary Sciences

**Photic Zone Euxinia and Microbial Mat Development
in the Early Triassic of the Perth Basin, Western Australia:
Implications for Petroleum Systems**

Takashi Taniwaki

ORCID iD: 0000-0003-2425-8690

**This thesis is presented for the Degree of
Doctor of Philosophy
of
Curtin University**

December 2021

Declaration

To the best of my knowledge and belief this thesis contains no material previously published by any other person except where due acknowledgement has been made.

This thesis contains no material which has been accepted for the award of any other degree or diploma in any university.

Takashi Taniwaki

Perth, 1 December 2021

Abstract

The end-Permian mass extinction was the most profound extinction event in the Phanerozoic. Massive volcanic activity from the Siberian Traps produced a large amount of CO₂ and other gases, causing global warming and subsequent global anoxia and euxinia in the ancient seas. Photic zone euxinia (PZE) is established when the euxinic (elevated H₂S and anoxic) part of the water column overlaps with the sunlight zone. Under PZE, anoxygenic sulfur bacteria are active and live in a distinct vertical zonation of communities: purple sulfur bacteria at the top of the chemocline, green-green sulfur bacteria beneath, and green-brown sulfur bacteria beneath green-green sulfur bacteria. These bacteria make characteristic carotenoid pigments that give rise to specific biomarkers (okenane: purple sulfur bacteria, chlorobactane: green-green sulfur bacteria, and isorenieratane: green-brown sulfur bacteria) in sediments and petroleum samples. However, microbial mats (microbialites as lithofacies) are also known to contain anaerobic sulfur bacteria with abundant purple sulfur bacteria and green-green sulfur bacteria.

In the northern Perth Basin, the Kockatea Shale was deposited during the Late Permian to Early Triassic. Interpretation of seismic data suggests that basin geometry during the Early Triassic was largely inherited from Permian rifting and that intra-basinal structural highs controlled the distribution of the Lower Triassic sediments. Core and wireline logs provide details of the lithofacies present in the basal section of the Lower Triassic Kockatea Shale. The lateral distribution of the lithofacies, combined with organic geochemical signatures (biomarkers, stable carbon and sulfur isotopic data) shows the lateral extent of corresponding paleoenvironments.

The presence of carotenoid biomarkers derived from sulfur bacteria and other biomarkers related to anoxia and water column stratification show that dark coloured mudstones were deposited in the deeper part of the basin under PZE. Microbial mats developed in shallow water settings on intra-basinal structural highs away from basin margins. These mats also have carotenoid biomarkers derived from sulfur bacteria and developed under both oxic and PZE conditions. Cyanobacteria become more abundant

in the mats developed under oxic conditions compared with the mats developed under PZE. On the other hand, light coloured mudstones were deposited under oxygenated tidally influenced conditions in shallow water settings near the basin margins.

The source rock potential of both dark coloured mudstone and microbialite facies is demonstrated by total organic carbon (TOC) values between 0.3 and 3.4 % and hydrogen index (HI) values between 39 and 579 mg/gTOC. The light coloured mudstones, deposited under more aerobic tidal settings, have no to poor source rock potential and TOC values between 0.2 and 0.5% and HI values between 59 and 127 mg/gTOC.

Similar patterns of variations in biomarker abundances can be correlated between petroleum exploration wells, defining a chemo-isotope stratigraphy, which suggests cyclic fluctuation of PZE and oxic conditions. This can be explained by the fluctuation of the depth of the chemocline (the boundary between oxic and anoxic/euxinic conditions). When the chemocline is shallow, PZE develops basin-wide, but when the chemocline is deep, PZE is limited to deeper water or is absent altogether. This periodic fluctuation in PZE could correspond to the periodic anoxic episodes after the end-Permian mass extinction recognized in other basins globally.

Microbialites and PZE share similar biomarker features. However, several organic geochemical features differentiate microbialites and PZE. Microbialites have a higher relative abundance of okenane and C₃₃ *n*-alkylcyclohexane (*n*-C₃₃ ACH), and isotopically lighter values of $\delta^{13}\text{C}_{\text{OM}}$ and $\delta^{34}\text{S}$ of pyrite compared with PZE. Purple sulfur bacteria are more abundant in microbialites compared to PZE. Purple sulfur bacteria utilize the C₃ pathway of photosynthesis for their carbon fixation, which is relatively depleted in ¹³C, while green sulfur bacteria utilize the reversed TCA (tricarboxylic acid) cycle for their carbon fixation which is relatively enriched in ¹³C. The source of *n*-C₃₃ ACH is uncertain, but the high abundance of this compound in microbialites suggests that it is associated with microbialite facies. The fractionation of $\delta^{34}\text{S}$ values between PZE and microbialites appears to indicate that the difference of microbial community including the relative abundance of purple sulfur bacteria is a cause for the fractionation related to the difference of metabolism of each microbe as identified in other basins.

In this thesis, the petroleum samples from the Northern Carnarvon Basin are also analysed. The Northern Carnarvon Basin is located on the north-west margin of Australia and shares a similar evolution to the northern Perth Basin. Many of the analysed petroleum samples from both the Perth and Northern Carnarvon basins contain carotenoids (okenane, chlorobactane and isorenieratane) derived from sulfur bacteria, suggesting that their source rocks were deposited under conditions of PZE and/or derived from microbialites. In the northern Perth Basin, the major lithofacies contributing to the source rock are dark coloured mudstone associated with PZE and microbialite lithofacies. In the southern Perth Basin, there is a potential source in Permian strata based on the low concentrations or absence of carotenoids and *n*-C₃₃ ACH. There is also a strong possibility that the Lower Triassic Locker Shale (the equivalent of the Lower Triassic Kockatea Shale in the Perth Basin) is one of the source rocks for the petroleum in the Tubridgi field on the Peedamullah Shelf of the Northern Carnarvon Basin, based on the similarity of biomarkers to the Kockatea Shale, and Perth Basin petroleum. However, the possibility of charge from the Upper Jurassic Dingo Claystone cannot be excluded.

This thesis presents a practical integration of geology and organic geochemistry to investigate the basin-scale paleogeography and paleoenvironmental depositional conditions of the Early Triassic in the northern Perth Basin, and the application of them to source rock evaluation in the Perth and Northern Carnarvon basins. In addition, the integrated organic geochemical research reveals the organic geochemical difference between PZE and microbialites. This work shows the importance of understanding basin-scale paleoenvironmental conditions for comparing paleoenvironments between basins and predicting potential source rocks in a basin.

Acknowledgements

This PhD research was a great challenge, full of considerable experiences and conducted with great support from many brilliant people and institutes. I was lucky to come across them. Without their support, this research would not have been possible.

Firstly, I would like to thank my supervisor Professor Kliti Grice for accepting my application for PhD research and giving me a chance to engage in this project. She always gave me great support and discussion of my work with her profound academic knowledge and kindness. I stayed on right track with her academic advice. I am very thankful for the provision of the excellent laboratory of WA-OIGC and facilitating several analyses outside WA-OIGC.

Secondary I would also like to thank my co-supervisor Professor Chris Elders for providing an opportunity for the geological analysis of this project. He kept providing me considerable advice for my works with his great academic experience. I was able to keep on the right track of my research with his guidance. In addition, I would like to acknowledge technical support for online meetings for my milestone presentation and others during the restriction of COVID-19.

I would like to thank Adj. Professor Gregory Smith and Associate Professor Marco Coolen for many beneficial discussions or comments on my research and Alex Maftai for drawing the attention to the oil inclusions in the Pinhoe 1/ST1 well. Their scientific advice inspired me for the ways of works. I also would like to thank Mr Peter Hopper and Dr Alex Holman for much technical support and scientific advice. They kindly explained to me the methods for the experiments. In addition, I am very thankful for the technical support with GC-MS for biomarker analysis, elemental analysis for stable carbon isotope analysis and the arrangement of sending samples to Intertek, Massachusetts Institute of Technology (MIT) and The Leibniz Institute for Baltic Sea Research (IOW).

I am also thankful to my colleagues and staff at WA-OIGC and in the geology lab. They made my university life more joyful and fruitful with their friendly support in addition to the technical support for many aspects. I also acknowledge Professor Roger Summons for arranging and performing GC-MRM-MS analysis at MIT, Professor Michael Böttcher for the sulfur isotope and mercury concentration analysis at IOW and valuable comments for the manuscript, and Intertek for the TOC and Rock Eval analysis. I also would like to thank the Geoscience Australia for providing seismic and well log data and the department of Mines, Industry Regulation and Safety in Western Australia for permission to observe cores and sampling (G004177).

I would like to acknowledge INPEX Corporation for providing an opportunity and scholarship for this PhD research in addition to much support for the life and health issues during this period.

Finally, many thanks go to my beloved family and friends in both Perth and Japan for giving a great time for relaxing, support and understanding in every aspect during my PhD time. The life in Perth with them became fruitful and will be an unforgettable period in my life.

Primary publications

This thesis is combined by publications, which are published, submitted. The publications for each chapter are listed below.

Chapter 2

Taniwaki, T., Elders, C., Grice, K., 2021. Early Triassic paleogeography of the northern Perth Basin, and controls on the distribution of source rock facies. *Marine and Petroleum Geology*. 133, 105314, <https://doi.org/10.1016/j.marpetgeo.2021.105314>, impact factor 4.348.

Chapter 3

Taniwaki, T., Elders, C., Böttcher, M., E., Holman, A., I., Grice, K., Photic zone redox oscillations and microbial mat development recorded by Early Triassic sediments of the Perth Basin: A geochemical approach. *Geochimica et Cosmochimica Acta*, submitted Sept 2021, impact factor 5.010.

Chapter 4

Taniwaki, T., Elders, C., Holman, A., I., Grice, K., The potential extent of Kockatea Shale equivalent source rocks in the Northern Carnarvon and Perth Basins. *Petroleum Geoscience*, submitted Mar 2022, impact factor 2.323.

Secondary publications

Conference abstracts

Taniwaki, T., Grice, K., Elders, C., Lateral facies distribution in the Upper Permian to Lower Triassic Kockatea Shale in the Northern Perth Basin. Basin Workshop 2020, Perth and online, December 2020, oral presentation.

Taniwaki, T., Elders, C., Grice, K., Biomarkers indicative of photic zone euxinia and microbial mats in the northern Perth and northern Carnarvon basins. AAPG Geosciences Technology Workshop (GTW), Perth and online, March 2021, oral presentation.

Taniwaki, T., Elders, C., Holman, A., I., Böttcher, M., E., Grice, K., Basin scale evaluation: Organic geochemical characteristics of northern Perth Basin (Early Triassic). 30th International meeting of Organic Geochemistry (IMOG 2021), Montpellier, France and online, September 2021, poster.

Taniwaki, T., Elders, C., Holman, A., I., Grice, K., Basin scale paleoenvironmental conditions during deposition of the Early Triassic Kockatea Shale, northern Perth Basin. GSA Earth Science Student Symposia Western Australia (GESSS WA), Perth, November 2021, oral presentation.

Correlation of terminologies between chapters

Chapter	Microbial mat as biological term	Microbialite as lithological term	Dark coloured mudstone	Light coloured mudstone
1	Microbial mat	Microbialite	Dark coloured mudstone	Light coloured mudstone
2	Microbial mat	Microbial mat	Darker coloured mudstone	Lighter coloured mudstone
3	Microbial mat	Microbial mat	Dark coloured mudstone	Light coloured mudstone
4	Microbial mat	Microbial mat	Dark coloured mudstone	Light coloured mudstone
5	Microbial mat	Microbial mat	Dark coloured mudstone	Light coloured mudstone

Table of contents

Chapter 1: Introduction and overview

1	Objectives	2
2	Mass extinctions during the Phanerozoic and end-Permian mass extinction	2
2.1	Mass extinction events in the Phanerozoic	2
2.2	End-Permian mass extinction event	3
3	Geological setting	6
3.1	The northern Perth Basin, Western Australia.....	6
3.2	The Northern Carnarvon Basin, Western Australia	12
4	Significance of biomarkers and isotope analysis in organic geochemistry	15
4.1	Biomarker analysis.....	15
4.2	Stable isotope analysis	16
4.3	Reconstruction of paleoenvironments.....	19
4.3.1	Photic Zone Euxinia (PZE)	19
4.3.2	Microbial mats (Microbialites).....	22
5	Project Design.....	24
5.1	Geological analysis for the reconstruction of paleogeography	24
5.2	Organic geochemical analyses for the paleoenvironments	25
6	Scope of the thesis	27

Chapter 2: Early Triassic paleogeography of the northern Perth Basin, and controls on the distribution of source rock facies

Abstract	33
1 Introduction	33
2 Geological setting	35
3 Data & Methodology	36
3.1 Seismic data	36
3.2 Seismic interpretation.....	40
3.3 Well data for core description	41
3.4 TOC and Rock-Eval analyses	41
4 Results	42
4.1 Seismic interpretation.....	42
4.1.1 Seismic stratigraphy	42
4.1.2 Structure	43
4.1.3 Structural evolution	46
4.2 Core description	48
4.2.1 Mudstone facies (Lighter coloured mudstone facies, darker coloured mudstone facies and fossiliferous facies).....	48
4.2.2 Microbial mat facies.....	51
4.2.3 Tidal sandstone facies	51
4.2.4 Storm/gravity flow bed facies	52
4.2.5 Bioturbated Siltstone facies.....	52
4.3 Core- well log correlation	56
4.4 Microbial mat distribution.....	57

4.5	Source rock quality	57
5	Discussion	60
5.1	Lateral facies relationship	60
5.2	Basin morphology	61
5.3	Lower Triassic Paleogeography	62
5.4	Controls on microbial mat distribution	63
6	Conclusion	64
	Acknowledgements	70
	References	71
	Appendix	77

Chapter 3: Photic zone redox oscillations and microbial mat development recorded by Early Triassic sediments of the Perth Basin: A geochemical approach

	Abstract	80
1	Introduction	81
2	Geological setting	83
3	Data & Methodology	86
3.1	Samples and lithology	86
3.2	Extraction of sediments and fractionation.....	92
3.3	Analysis.....	92
3.3.1	Gas Chromatography-Mass Spectrometry & gas chromatography-metastable reaction monitoring-mass spectrometry.....	92
3.3.2	Bulk carbon isotopes of organic matter ($\delta^{13}\text{C}_{\text{OM}}$)	93

3.3.3	Mercury (Hg).....	94
3.3.4	Stable sulfur isotopes.....	94
4	Results	95
4.1	Thermal maturity.....	95
4.2	Characteristics of biomarkers, $\delta^{13}\text{C}_{\text{OM}}$, $\delta^{34}\text{S}$, Hg and Hg/TOC	98
4.3	Definition of zones	103
4.3.1	Zone 1	103
4.3.2	Zone 2.....	104
4.3.3	Zone 3.....	105
4.3.4	Zone 4.....	106
4.3.5	Zone 5.....	106
5	Discussion	115
5.1	Distinguishing the geochemical signatures of PZE and microbialites.....	115
5.2	Paleoenvironmental conditions and their organic geochemical characteristics	119
5.3	Lateral distribution of paleoenvironmental conditions and relationship with paleogeography	122
6	Conclusions	123
	Acknowledgements.....	127
	References	128
	Appendix	142

Chapter 4: The potential extent of Kockatea Shale equivalent source rocks in the Northern Carnarvon and Perth Basins

Abstract	144
1 Introduction	144
2 Geological setting	146
3 Data & Methodology	149
3.1 Samples	149
3.2 Fractionation of samples	149
3.3 Analysis.....	152
3.3.1 Gas Chromatography-Mass Spectrometry (GC-MS).....	152
3.3.2 GC-MS, metastable reaction monitoring- (GC-MRM-MS)....	152
3.3.3 Rock samples.....	153
4 Results and discussions.....	153
4.1 Thermal maturity influence.....	153
4.2 Characteristics of major biomarkers (Pr/Ph, C ₃₅ homohopane index, gammacerane index, and C ₂₇₋₂₉ regular sterane ratio).....	157
4.3 Carotenoid biomarkers (okenane, chlorobactane and isorenieratane) in petroleum samples.....	157
4.3.1 Okenane, isorenieratane and chlorobactane	157
4.3.2 Thermal maturity influence on okenane, chlorobactane and isorenieratane	160
4.3.3 Relative abundance of between okenane, chlorobactane and isorenieratane	161
4.4 Implications to source rocks.....	163
4.4.1 Perth Basin	163

4.4.2	Northern Carnarvon Basin.....	167
5	Conclusion	169
	Acknowledgements.....	170
	References	170

Chapter 5: Conclusions and significance

1	Summary of this PhD research.....	178
2	Significance of this research	182
2.1	Organic geochemical difference between PZE and microbialites	182
2.2	Application of chemo-isotope stratigraphy.....	183
2.3	Global variation in source rock quality around the end-Permian mass extinction	183
3	Future work	187
3.1	Application of the northern Perth Basin analogues: Source rock potential and distribution in the Bedout Sub-basin.....	187
	Bibliography	193
	Appendices	219
Appendix 1	220
Appendix 2	222
Appendix 3	225

List of Figures

Chapter 1: Introduction and overview

- Figure 1-1. The diversity of life during Phanerozoic and the five major mass extinction events (after Raup and Sepkoski, 1982). Cm = Cambrian, O = Ordovician, S = Silurian, D = Devonian, C = Carboniferous, P = Permian, Tr = Triassic, J = Jurassic, K = Cretaceous, T = Tertiary, Cz = Cenozoic. 3
- Figure 1-2. Locations of the northern Perth and Northern Carnarvon basins with gravity anomaly map as background showing the basin geometry. The public domain data used for the gravity map is published by the Scripps Institution of Oceanography (after Sandwell & Smith, 2009; Sandwell et al., 2013; Sandwell et al., 2014)..... 9
- Figure 1-3. Paleogeography and Eastern Gondwana Interior Rift (EGIR) (after Rollet et al., 2019)..... 10
- Figure 1-4. Stratigraphy of the northern Perth Basin (after Ferdinando et al., 2007; Mory et al., 2005). Light and dark grey: deeper water mudstone, yellow: shallow marine sandstone: brown: fluvial to deltaic sediments, bluish green (Nangetty Fm.): open marine glacial sediments, yellowish green (Eneabba and Woodada Fms.): fluvial to deltaic sediments. 11
- Figure 1-5. Stratigraphy of the Northern Carnarvon Basin (after I'Anson et al., 2019). Light and dark grey: deeper water mudstone, yellow: shallow marine sandstone: brown: fluvial to deltaic/marine sediments, blue- green: open marine glacial sediments. 14
- Figure 1-6. Schematic concept of biomarker formation. Each biolipid represents okenone, chlorobactene and isorenieratene from purple sulfur bacteria, green-green sulfur bacteria and green-brown sulfur bacteria, respectively. These biolipids turn into biomarkers (okenane, chlorobactane, and isorenieratane) through burial and thermal maturation in sediments. 17

Figure 1-7. Approximate $\delta^{13}\text{C}$ range of plants, phytoplankton, sulfur bacteria and hydrocarbons (after Schidlowski, 1988; Peters et al., 2004).....	18
Figure 1-8. Schematic illustration of photic zone euxinia, associated microbial community, and representative carotenoid pigments of each sulfur bacteria.	21
Figure 1-9. General internal structure of microbial mats and related carotenoid pigments of each sulfur bacteria. Photo courtesy of Kliti Grice.....	23
Figure 1-10. Workflow applied for this thesis, showing the integration of geology and organic geochemistry.	30
Figure 1-11. Workflow of organic geochemical analysis applied in this research. ...	31

Chapter 2: Early Triassic paleogeography of the northern Perth Basin, and controls on the distribution of source rock facies

Figure 2-1. Location of the study area within the northern Perth Basin, interpreted 3D seismic volumes, 2D seismic lines, calibrated wells, core interpreted wells, and the location of lines used in subsequent figures.....	37
Figure 2-2. Stratigraphy of the northern Perth Basin (after Ferdinando et al., 2007; Mory et al., 2005). Light and dark grey: deeper water mudstone, yellow: shallow marine sandstone: brown: fluvial to deltaic sediments, bluish green (Nangetty Fm.): open marine glacial sediments, yellowish green (Eneabba and Woodada Fms.): fluvial to deltaic sediments.	38
Figure 2-3. Typical seismic section from the offshore (A) and onshore (B) northern Perth Basin. Dark purple (Oldest horizon): Late Permian Unconformity, Blue: Base Kockatea Shale, Orange: Top Kockatea Shale, Cream yellow: Top Woodada Formation/Lesueur Sandstone, Green: Top Eneabba Formation, Pink: Intra Yarragadee Formation, Cream green: Valanginian Unconformity, Light blue: Top Winning Group, Light purple: Top Cretaceous. The location of the lines is shown in Figure 2-1.	44

Figure 2-4. Time structure maps of the (A) Top Kockatea Shale and (B) Base Kockatea Shale horizons and (C) time thickness map of the Kockatea Shale....	45
Figure 2-5. The seismic expression of Permian faults. The major fault at the west end of the section represents one of the remnant Permian faults, based on thickness variations within the Upper Permian Sandstones. Location of the line is shown in Figure 2-1. The colour of the seismic horizons is as in Figure 2-3.....	49
Figure 2-6. Thickness variation in (A) the Wagina Sandstone, (B) the Dongara Sandstone, (C) the Permian Kockatea Shale, and (D) Upper Permian (Wagina and Dongara Sandstones and Permian Kockatea Shale) based on well log data. The brown polygon in (A) shows the extent of the Wagina Sandstone. The orange polygon in (B) shows the limit of the Dongara Sandstone. The blue polygon in (C) shows the extent of Permian Kockatea Shale.....	50
Figure 2-7. Microbial mats in Cliff Head 4. Grey colour beds in (B) represent the microbial mats.....	53
Figure 2-8. Examples of typical lithologies observed in cores.....	54
Figure 2-9. Core observation logs and correlation of six wells. Points represent the location of samples for TOC and Rock-Eval analyses.	55
Figure 2-10. Well log correlation to microbial mat facies. The base Kockatea Shale is indicated by purple lines. The intervals between red lines correspond to either the presence of microbial mat facies in cores or the irregular log facies which indicates the development of microbial mats. Note that the GR log for Beharra Springs 2 is of poor quality. The microbial mat facies are absent from Jurien 1 and Woolmulla 1. Colours indicating the facies identified in core logs are the same as in Figure 2-9.	58
Figure 2-11. Irregular log facies distribution indicating the distribution of microbial mat facies on well logs.....	59
Figure 2-12. HI-OI and HI-TOC plots of each lithofacies.....	60

Figure 2-13. N-S oriented lateral facies relationship from Upper Permian Dongara and Wagina Sandstone to Lower Kockatea Shale. G. =Griesbachian and D. =Dienerian. Location of wells is shown in Figure 2-1..... 67

Figure 2-14. Map of (A) reconstructed basin morphology during Late Permian and Early Triassic and (B) paleogeography in Early Triassic. The blank area in (B) represents a hiatus during the Early Triassic or erosion during younger rifting..... 68

Figure 2-15. Paleogeographic model of the Early Triassic viewed from north. Not to scale..... 69

Chapter 3: Photic zone redox oscillations and microbial mat development recorded by Early Triassic sediments of the Perth Basin: A geochemical approach

Figure 3-1. (A) Inset map for B, showing the location of the study area within Australia. (B) Location map of the northern Perth Basin wells used for rock sample analysis, with gravity anomaly map as background showing the basin geometry. The public domain data used for the gravity map is published by the Scripps Institution of Oceanography (Sandwell et al., 2013, 2014; Sandwell and Smith, 2009). Black points represent the location of major towns within the map. 84

Figure 3-2. Stratigraphy of the northern Perth Basin (Ferdinando et al., 2007). Light and dark grey: deeper water mudstone, yellow: shallow marine sandstone: brown: fluvial to deltaic sediments, bluish green (Nangetty Fm.): open marine glacial sediments, yellowish green (Eneabba and Woodada Fms.): fluvial to deltaic sediments. Fm.=Formation, Fms=Formations, Sst.=Sandstone, and Mbr.=Member. 85

Figure 3-3. Well correlation panel of the basal section of the Kockatea Shale from Cliff Head 4, Dongara 4, Hovea 3, Beharra Springs 2, Woolmulla 1 and Jurien 1. Core lithology is based on core observation (Taniwaki et al., 2021), gamma ray

(GR) and sonic log (Sonic) are plotted. Wells are aligned by the approximate Permian/Triassic boundary.	88
Figure 3-4. Typical lithofacies of A) microbialite, B) dark coloured mudstone and C) light coloured mudstone.....	89
Figure 3-5 Carotenoid biomarkers from microbialites (Cliff Head 4, 1422.38m) identified using GC-MRM-MS by comparison with standard compounds. 'Paleo': paleorenieratane, 'ren': renieratane, 'rnp': renierapurpurane.	99
Figure 3-6. Composite panel of major biomarkers for Cliff Head 4, Dongara 4, and Hovea 3. C ₃₅ homohopane index (HI), pristine/phytane ratio (Pr/Ph), gammacerane index (GI), 2 α -methylhopane index (2MeHI), C ₃₀ sterane ratio, <i>n</i> -C ₃₃ ACH ratio are plotted. (Fox et al., 2020; Grice et al., 2005c; Peters et al., 2004; Summons et al., 1999; Tulipani et al., 2015). Cores are aligned on the approximate Permian/Triassic boundary.	100
Figure 3-7. Composite panel of carotenoids and related biomarkers for Cliff Head 4, Dongara 4, and Hovea 3. Okenane, chlorobactane, isorenieratane, ren+rnp/paleo+iso ratio, okenane ratio and aryl isoprenoids (C ₁₈₋₂₀) are plotted (Brocks and Schaeffer, 2008; Cui et al., 2020; Grice et al., 2005a; Schaefer et al., 2020; Summons and Powell, 1987). Cores are aligned on the approximate Permian/Triassic boundary.	101
Figure 3-8. Composite panel of isotope and Hg data for Cliff Head 4, Dongara 4, and Hovea 3. $\delta^{13}\text{C}_{\text{OM}}$, $\delta^{34}\text{S}$, Hg concentration and Hg/TOC are plotted (Brand and Coplen, 2012; Grasby et al., 2017; Hartmann and Nielsen, 2012). Cores are aligned on the approximate Permian/Triassic boundary.....	102
Figure 3-9. Okenane ratio of samples from each paleoenvironmental zone. Okenane ratio is defined as (okenane + chlorobactane + isorenieratane) / (chlorobactane + isorenieratane).....	110
Figure 3-10. <i>n</i> -C ₃₃ ACH ratio (C ₃₃ <i>n</i> -alkylcyclohexane/C ₃₄ <i>n</i> -alkane) in each paleoenvironmental zone (Grice et al., 2005c).	111
Figure 3-11. Plot of bulk $\delta^{13}\text{C}_{\text{OM}}$ in each paleoenvironmental zone.....	112

Figure 3-12. Plot of bulk $\delta^{34}\text{S}$ in each paleoenvironmental zone.	113
Figure 3-13. Cross plots of (A) TOC vs TRIS, (B) Hg vs TRIS and (C) Hg vs TOC. TOC/TRIS ratios (1 and 2.8) are shown in A. Major clusters mentioned by Shen et al. (2020) are shown in B and C.....	109
Figure 3-14. Cross plots of each parameter (Okenane ratio, $n\text{-C}_{33}$ ACH, $\delta^{13}\text{C}_{\text{OM}}$ and $\delta^{34}\text{S}$) used for principal component analysis. The dashed line in each plot represents an approximate trend line from PZE facies (red) to microbialite facies (green).	117
Figure 3-15. Plot of PC1 and PC2 based on the principal component analysis for okenane ratio, $n\text{-C}_{33}$ ACH, $\delta^{13}\text{C}_{\text{OM}}$ and $\delta^{34}\text{S}$	118
Figure 3-16. Paleoenvironmental setting sketch showing the fluctuation of PZE associated with the fluctuation of the depth of the chemocline.	125
Figure 3-17. The distribution of PZE and microbialites in the Early Triassic northern Perth Basin. A shows the basin during shallower chemocline and B shows the basin during deeper chemocline.....	126
Figure 3-S1. Composite panel of biomarkers, isotopes, and Hg for Jurien 1 (A) and Woolmulla 1 (B).	142

Chapter 4: The potential extent of Kockatea Shale equivalent source rocks in the Northern Carnarvon and Perth Basins

Figure 4-1. Location of both Perth and Northern Carnarvon basins and petroleum samples. A represents the location of both basins and samples with gravity anomaly map as background showing basin geometry. The public domain data used for the gravity map is published by the Scripps Institution of Oceanography (Sandwell et al., 2013, 2014; Sandwell and Smith, 2009). B shows the detailed sample location around the Tubridgi Field in the Northern Carnarvon Basin. C indicates the detailed sample location around the northern Perth Basin. Yellow

points represent the location of wells where rock sample analysis was conducted (Taniwaki et al., 2021).	147
Figure 4-2. Stratigraphy in both (A) northern Perth and (B) Northern Carnarvon basins (Ferdinando et al., 2007; I’Anson et al., 2019). Light and dark grey: deeper water mudstone, yellow: shallow marine sandstone: brown: fluvial to deltaic/marine sediments, blue- green: open marine glacial sediments.	148
Figure 4-3. GC-MRM-MS peaks of okenane, isorenieratane and chlorobactane from petroleum samples (A: Hovea 1, B: Tubridgi 5). Hovea 1 is located on the northern Perth Basin and Tubridgi 5 is located on the Peedamullah Shelf in the Northern Carnarvon Basin.	158
Figure 4-4. Distribution of carotenoid biomarkers (okenane, chlorobactane and isorenieratane). A shows the entire region covering samples from the Northern Carnarvon Basin to the southern Perth Basin. B represents the detailed distribution around the Tubridgi Field in the Northern Carnarvon Basin. C indicates the distribution around the northern Perth Basin.	162
Figure 4-5. The influence of thermal maturity on carotenoid biomarkers (A: okenane, B: chlorobactane, C: isorenieratane).	164
Figure 4-6. GC-MRM-MS peaks of okenane, isorenieratane and chlorobactane from petroleum samples of Tubridgi 2, 4, 5 and 7.	165
Figure 4-7. The thermal maturity influence on $n\text{-C}_{33}$ ACH ratio. $n\text{-C}_{33}$ ACH ratio = $n\text{-C}_{33}$ ACH / C_{34} $n\text{-alkane}$	166

Chapter 5: Conclusions and significance

Figure 5-1. Summary figures of this research, showing the basin scale extent of paleoenvironments and their fluctuation during deposition of the Early Triassic Kockatea Shale.	181
Figure 5-2. Plate reconstruction around 250Ma and locations of each basin (after Matthews et al., 2016; Scotese, 2003; Thomas et al., 2004; Zhu et al., 2019). The	

paleogeographic reconstruction in this figure shows the large continent around Meishan, but some other reconstructions show a micro-continental fragment (Matthews et al., 2016; Thomas et al., 2004)..... 185

Figure 5-3. Stratigraphy during the Early to Middle Triassic in the northern Perth (A) and Bedout (B) basins (after Ferdinando et al., 2007; Minken et al., 2019)..... 190

Figure 5-4. The distribution of the East Gondwana Interior Rift (EGIR) (after Minken et al., 2019). 191

Figure 5-5. Reconstructed paleogeography during the Early Triassic Olenekian to Middle Triassic Anisian (after Rollet et al., 2019). 192

List of Tables

Chapter 1: Introduction and overview

Table 1-1. Stable isotope abundance of carbon and sulfur (Faure and Mensing, 2005).	16
--	----

Chapter 2: Early Triassic paleogeography of the northern Perth Basin, and controls on the distribution of source rock facies

Table 2-1. Details of 3D seismic volumes used in this study	39
Table 2-S1. List of wells used for seismic interpretation and core observation. “*” symbol in the core column represents the wells used for core observation.	77

Chapter 3: Photic zone redox oscillations and microbial mat development recorded by Early Triassic sediments of the Perth Basin: A geochemical approach

Table 3-1. Depth, lithofacies (lithology and facies) and geological ages of each sample.	90
Table 3-2. $C_{32} 22S/(22S+22R)$ $\alpha\beta$ -homohopane ratio and $C_{29} 20S/(20S+20R)$ sterane ratio used for thermal maturity assessment.	96
Table 3-3. Summary of paleoenvironments and their organic geochemical characteristics.....	108
Table 3-4. Range of selected isotope and biomarker results in each zone.....	116

Chapter 4: The potential extent of Kockatea Shale equivalent source rocks in the Northern Carnarvon and Perth Basins

Table 4-1. Type of fluids, basin location, reservoir age and Formation and for each petroleum sample.	150
Table 4-2. C_{32} $22S/(22S+22R)$ $\alpha\beta$ -homohopane, Moretane/Hopane, C_{29} $20S/(20S+20R)$ ($\alpha\alpha\alpha+\alpha\beta\beta$) sterane ratio, $\alpha\beta\beta/(\alpha\beta\beta+\alpha\alpha\alpha)$ C_{29} Sterane, $Ts/(Ts+Tm)$ and $Dia/(Dia+Reg)$ of each sample for thermal maturity evaluation.	154
Table 4-3. Characteristics of major biomarkers (Pr/Ph , C_{35} homohopane index, gammacerane index, and C_{27-29} regular sterane ratio).....	159

Chapter 5: Conclusions and significance

No tables for Chapter 5

Chapter 1

Introduction and overview

1 Objectives

The end-Permian mass extinction is the most profound extinction event in the Phanerozoic and is characterized by anoxic, euxinic and photic zone euxinic (PZE) conditions caused by volcanic eruptions from the Siberian Traps. In this period, microbial mats (microbialite as lithofacies) were also extensively developed due to the establishment of harsh conditions for other organisms.

The aims of this research are to investigate the basin-scale extent of anoxic and euxinic conditions during the Early Triassic in the northern Perth Basin, Western Australia, by integrating organic geochemistry and geology, and to establish the contribution of microbialites to organic geochemical signatures, which share similar organic geochemical characteristics to PZE.

2 Mass extinctions during the Phanerozoic and end-Permian mass extinction

2.1 Mass extinction events in the Phanerozoic

The history of life on Earth shows a series of mass extinction events and recoveries from them (Figure 1-1) (Raup & Sepkoski, 1982; Twitchett, 2006; Whiteside & Grice, 2016). Many species were wiped out during mass extinctions, but the empty niches allowed surviving species to evolve and diversify during the subsequent period. Five large mass extinction events have been recognized in the Phanerozoic: the end Ordovician, Late Devonian, end-Permian, end-Triassic and end-Cretaceous. Several possible reasons for each extinction have been identified such as glaciation (end Ordovician), CO₂ reduction due to the rise of terrestrial plants (late Devonian), volcanic activity (end-Permian and end-Triassic), and asteroid impacts (end-Cretaceous). The severity of extinction differs in each event.

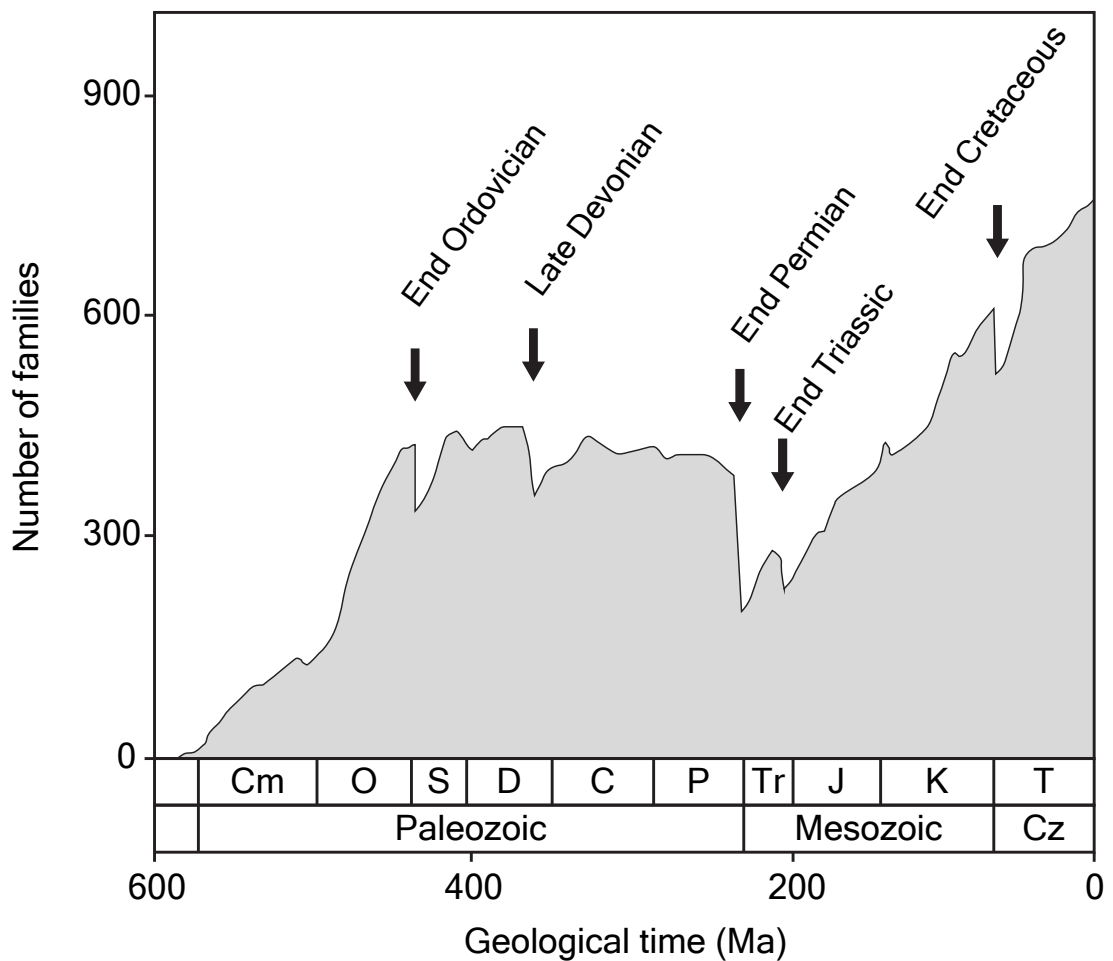


Figure 1-1. The diversity of life during Phanerozoic and the five major mass extinction events (after Raup and Sepkoski, 1982). Cm = Cambrian, O = Ordovician, S = Silurian, D = Devonian, C = Carboniferous, P = Permian, Tr = Triassic, J = Jurassic, K = Cretaceous, T = Tertiary, Cz = Cenozoic.

2.2 End-Permian mass extinction event

The end-Permian mass extinction event is the most profound extinction event of the Phanerozoic, and occurred between 251.94 and 251.88 Ma spanning 60 kyr (Figure 1-1) (Benton, 2016; Erwin, 1994; Hofman, 2016; Twitchett, 2006; Whiteside & Grice, 2016). Almost 95% of marine and 70% of terrestrial species were wiped out during

this event. The cause of this extinction event is believed to be the massive volcanic activity associated with the Siberian Traps, which released large amount of CO₂ and other gasses leading to global warming (Burgess & Bowring, 2015; Georgiev et al., 2020; Grasby et al., 2017; Herndon, 2017; Reichow et al., 2009; Sanei et al., 2012; Shen et al., 2019a, b; Sial et al., 2020; Thibodeau et al., 2016; Tian et al., 2014; Wang et al., 2019; Whiteside & Grice, 2016). Mercury (Hg) concentrations are high globally in this period (Grasby et al., 2017; Sanei et al., 2012; Scaife et al., 2017; Shen et al., 2019; Sial et al., 2020; Thibodeau et al., 2016; Wang et al., 2019). The main causes of high Hg concentration are considered to be volcanic activity, terrestrial input, and incorporation of atmospheric-derived Hg into sulfide precipitation in the water column (Cui et al., 2020; Grasby et al., 2017; Scaife et al., 2017; Shen et al., 2019a,b; Sial et al., 2020; Them et al., 2019; Wang et al., 2019). The globally high Hg concentration around the Permian-Triassic boundary is generally considered to be the result of atmospheric transport associated with volcanic activity from the Siberian Traps (Sanei et al., 2012). During this period, global warming resulted in sluggish water column conditions and the ocean became anoxic. This also resulted in increased activity of sulfate-reducing bacteria at the sediment-water interface, causing high concentrations of H₂S, resulting in euxinic conditions (Algeo et al., 2011; Fenton et al., 2007; Knoll et al., 1996; Kump et al., 2005; Pfenning, 1978; Song et al., 2014; Wignall & Twitchett, 1996; Zatoń et al., 2016). After the end-Permian mass extinction, anoxic conditions were established periodically until the beginning of the Middle Triassic. As a result, the recovery from the mass extinction took around 8-9 million years. This is a longer recovery period compared with other extinction events, and consequently biodiversity was profoundly damaged. However, local oxygenated shallow water settings are good refuges for biotic recovery (Beatty et al., 2008; Benton, 2016; Chen et al., 2012; Chen & Benton, 2012; Foster et al., 2015; Hallam, 1991; Hofmann et al., 2011; Kaiho et al., 2016; Knaust, 2010; Payne et al., 2004; Retallack et al., 1996; Sahney & Benton, 2008; Sedlacek et al., 2014; Shen et al., 2015; Shen et al., 2019a,b; Song et al., 2014; Twitchett et al., 2004; Wei et al., 2015; Woods et al., 1999; Zatoń et al., 2016; Zhang et al., 2014; Zhang et al., 2017).

Some authors have proposed a meteorite impact as a cause of the end-Permian mass extinction such as a possible impact on the Bedout High in the Roebuck Basin, offshore north western Australia (Becker et al., 2004). However, a meteorite impact cannot explain the periodic global anoxia and the protracted recovery after the mass extinction. Recovery after the end-Cretaceous mass extinction caused by a meteorite impact was rapid compared with recovery after the end-Permian mass extinction (Lowery et al., 2018). The interpretation of the Bedout High as an impact structure is also questioned (Müller et al., 2005).

PZE was developed globally in this period by overlapping of the photic zone and shallow euxinic conditions (Summons & Powell, 1987; Grice et al., 1996; Clifford et al., 1998; Pedentchouk et al., 2004; Grice et al., 2005a,c; Cao et al., 2009; Maslen et al., 2009; Nabbefeld et al., 2010; Sousa Júnior et al., 2013; Tulipani, 2013; French et al., 2015; Zhou et al., 2017; Connock et al., 2018; Fox et al., 2020; Schaefer et al., 2020). Within the PZE interval, anoxygenic photosynthetic bacteria such as sulfur bacteria occur near the chemocline (transition between oxic and euxinic conditions). Details of PZE are described in 4.3.

Paleozoic fauna was replaced by modern fauna across the end-Permian mass extinction (Benton, 2016). Major Paleozoic fauna such as brachiopods, rugose and tabulate corals, cephalopods, crinoids, trilobites, graptolites, and tetrapod synapsids became extinct, and many modern fauna such as neoselachians (modern sharks), neopterygians (modern fishes), teleosts (modern fishes), mammals, turtles, lepidosaurs (modern lizards), and archosaurs (dinosaurs and birds) emerged. On the other hand, major flora groups survived the end-Permian mass extinction and modern seed ferns, conifers and flowering plants emerged and expanded in the Cretaceous. Distinct characteristics of the end-Permian mass extinction are the “coral gap” and “coal gap”. After the extinction, coral reefs were missing for 10 million years until recovery in the Middle Triassic, and the coral types were replaced by modern scleractinian corals across the coral gap, indicating that harsh environments for coral building organisms continued for a longer time after the extinction. Coal beds are also missing for 10

million years after the extinction, indicating the absence of forests or a massive loss of plants at least near shorelines in this period.

The development of microbialites is another important feature following the extinction (Foster et al., 2020; Kershaw et al., 2012; Luo et al., 2018; Woods, 2014). Microbialites are generally common in the Proterozoic, but are also commonly recognized globally from the Lower Triassic. This indicates that severe conditions existed during and after the mass extinction which were not suitable for other organisms (Forel, 2013; Foster et al., 2020; Kershaw et al., 2012; Luo et al., 2018; Woods, 2014).

3 Geological setting

The study areas for this research are the northern Perth and Northern Carnarvon basins (Figure 1-2), with the main focus being the northern Perth Basin. These basins developed during several phases of rifting and uplift related to the break-up of the Pangea and Gondwana continents as part of the Eastern Gondwana Interior Rift (EGIR) (Domeier and Torsvik, 2014; Matthews et al., 2016; Olierook et al., 2019; Scholle et al., 1995).

3.1 The northern Perth Basin, Western Australia

The northern Perth Basin is the major focus of this thesis. It is located in Western Australia and has a north-south elongate basin geometry. In the basin, the Kockatea Shale was deposited during the Late Permian to Early Triassic, recording the end-Permian mass extinction and its recovery (Georgiev et al., 2020; Grice et al., 2005; Metcalfe et al., 2008; Thomas et al., 2004), and is one of the good quality source rocks in the basin (Boreham et al., 2000; Grosjean et al., 2017; Langhi et al., 2014; Scott, 1994; Thomas, 1979; Thomas et al., 2004). The basin developed as a narrow seaway between the Indian and Australian continents associated with the EGIR (Figure 1-3)

(Domeier and Torsvik, 2014; Matthews et al., 2016; Olierook et al., 2019; Scholle et al., 1995).

The regional structural trend in the basin is defined by NNW-SSE striking normal faults, parallel to the Darling Fault system which separates the Perth Basin from the Yilgarn Craton in the east (Jones et al., 2011; Song & Cawood, 2000). The basin is divided into sub-basins generally based on the present-day basin geometry (Hall & Kneale, 1992). For instance, the Beagle Ridge is a prominent intra-basinal high located near the present-day coastline. The Turtle Dove Ridge is an offshore structural high parallel to the Beagle Ridge. The Dandaragan Trough is the structural low between the Beagle Ridge and the eastern basin margin.

The tectonic evolution from the Devonian to Early Cretaceous has been described by many authors (Figure 1-4) (Cadman et al., 1994; Crostella, 1995; Crostella & Backhouse, 2000; Elders et al., 2018; Hall et al., 2017; Jablonski & Saitta, 2004; Jones & Hall, 2002; Mory, 1994; Norvick, 2004; Orlov et al., 2017; Owens et al., 2018; Playford et al., 1976; Quaife et al., 1994; Tupper et al., 2016). The Late Permian rifting and subsequent Late Permian Unconformity are significant geological features. The Lower Permian Nangetty Formation, Holmwood Shale, High Cliff Sandstone, Irwin River Coal Measures and Carynginia Formation were deposited in open marine, fluvial and deltaic settings, and are interpreted as pre-rift or syn-rift sequences (Mory & Iasky, 1996; Mory et al., 2005). In parts of the basin, the Upper Permian Wagina Sandstone, Beekeeper Formation and Dongara Sandstone were deposited in deltaic and shallow marine settings as the first post-rift sediments overlying the Late Permian Unconformity. Subsequently, in the Late Permian to Early Triassic, the thermal subsidence phase of the rift produced a local marine transgression with deposition of the Kockatea Shale facies in deeper water. At the same time, the Bookara Sandstone was developed in the shallow water parts of the basin. Deltaic sediments of the Middle Triassic Woodada Formation were deposited above the Kockatea Shale as a result of subsequent regression. The overlying Late Triassic to Late Jurassic Lesueur, Eneabba, Cattamarra Coal Measures, Cadda, and Yarragadee Formations were deposited during

subsequent rift events. Extensive uplift and erosion was caused by the breakup of Greater India in the Early Cretaceous (Jablonski and Saitta, 2004), and is especially prominent in the offshore northern Perth Basin, resulting in a significant unconformity that separates these sequences from the Lower Cretaceous Winning Group.

The Perth Basin is an oil and gas producing basin (Boreham et al., 2000; Crostella, 1995; Ellis & Bruce, 1998; Ghori, 2015, 2017; Jones et al., 2011; le Poidevin & Lowden, 1994; Tupper et al., 2016). One of the main sources of oil is the Lower Triassic Kockatea Shale (Boreham et al., 2000; Gorter et al., 2009; Grosjean et al., 2017; Langhi et al., 2014; Scott, 1994; Thomas, 1979; Thomas et al., 2004; Torghabeh et al., 2014). The source rock potential and organic geochemical characteristics of the Kockatea Shale are well documented based on biomarker and stable carbon and hydrogen isotopic studies (Dawson et al., 2005; Grice et al., 2007; Grice et al., 2005; Grice et al., 2005; Grice et al., 2005; McIlldowie & Alexander, 2005; Thomas & Barber, 2004). A unique biomarker named “C₃₃ *n*-alkylcyclohexane” (*n*-C₃₃ ACH) has been identified globally from the Lower Triassic, and is identified in the northern Perth Basin (Grice et al., 2007; Grice et al., 2005a,b,c; Grotheer et al., 2017; Hays et al., 2012; McIlldowie & Alexander, 2005; Nabbefeld et al., 2010; Thomas & Barber, 2004). This compound is utilized for the source-oil correlation and to identify the contribution of the Lower Triassic Kockatea Shale source rock to the petroleum system in the basin.

The basal section of the Lower Triassic Kockatea Shale is a good oil-prone source rock with high TOC and HI (Grosjean et al., 2017; Thomas et al., 2004). The good source rock interval corresponds to the development of PZE (Grice et al., 2005b; Thomas et al., 2004), but several ichnofossils and body fossils were also identified (Chen et al., 2012; Haig et al., 2015; Luo & Chen, 2014; Zhang et al., 2017), suggesting oxic conditions were also present during the Early Triassic. Microbialites are identified from the Kockatea Shale. These mats are well documented from outcrops in the Perth Basin (Chen et al., 2014; Luo et al., 2018; Luo and Chen, 2014), although they are less well-studied in the subsurface (Thomas et al., 2004).

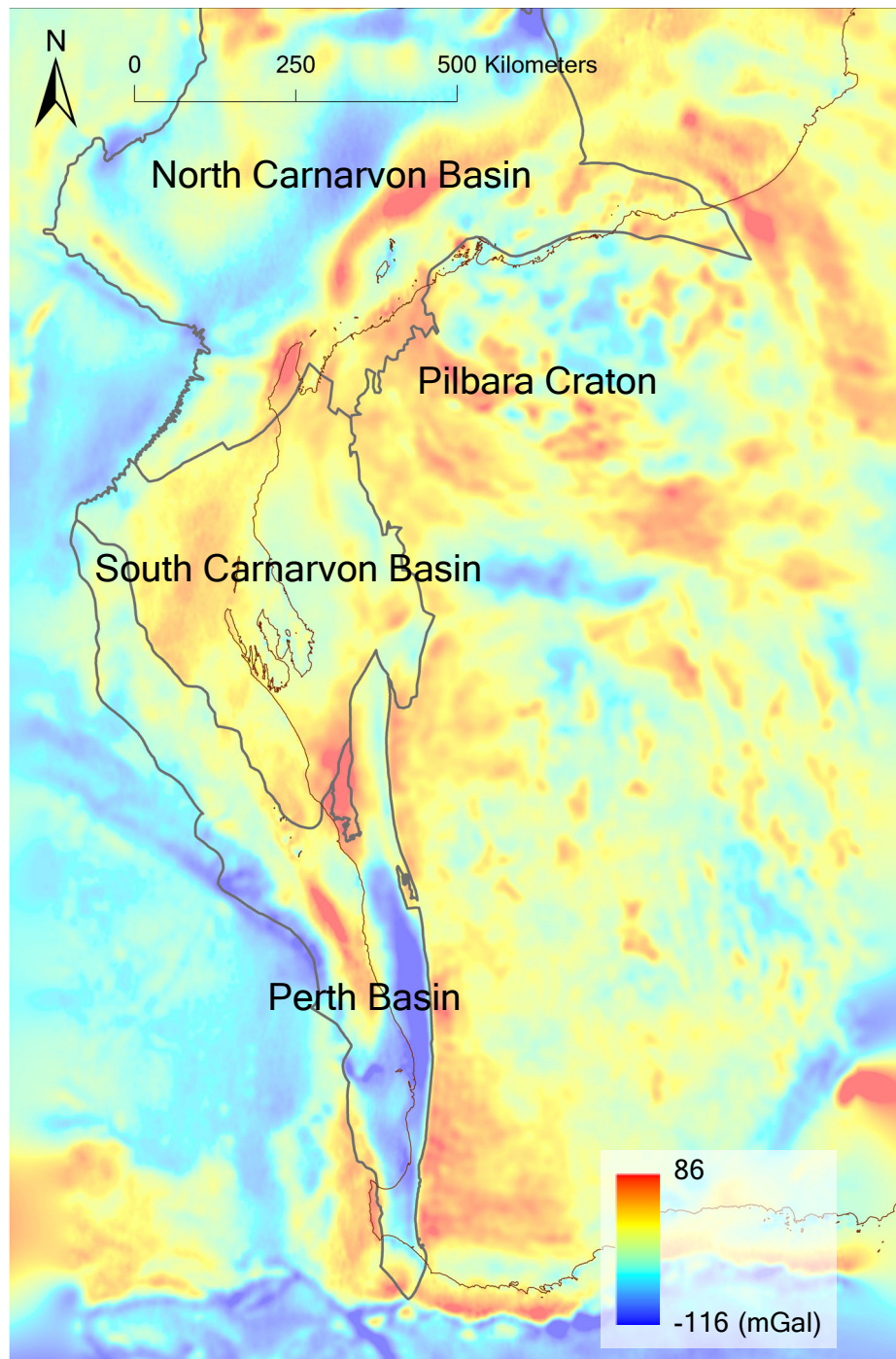


Figure 1-2. Locations of the northern Perth and Northern Carnarvon basins with gravity anomaly map as background showing the basin geometry. The public domain data used for the gravity map is published by the Scripps Institution of Oceanography (after Sandwell & Smith, 2009; Sandwell et al., 2013; Sandwell et al., 2014).

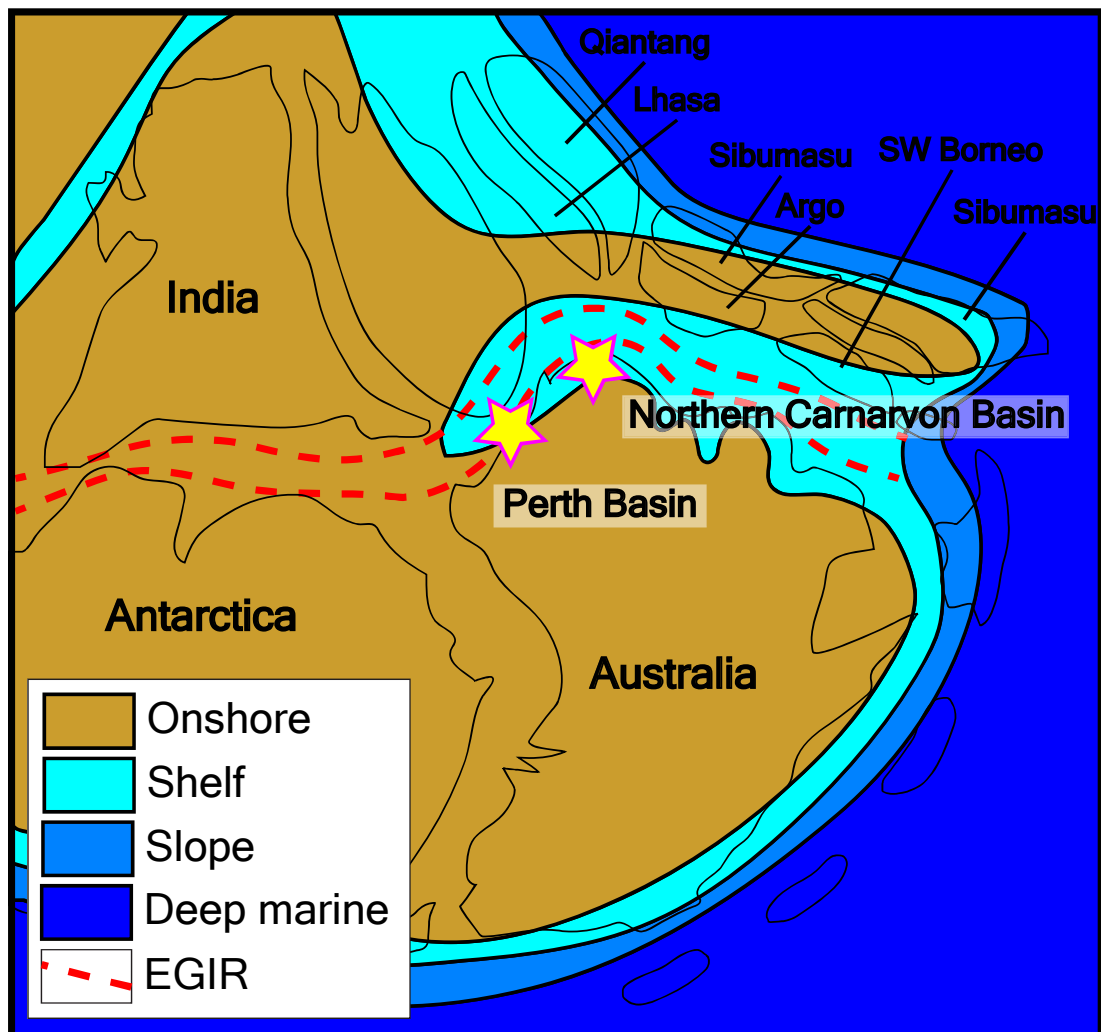


Figure 1-3. Paleogeography and Eastern Gondwana Interior Rift (EGIR) (after Rollet et al., 2019).

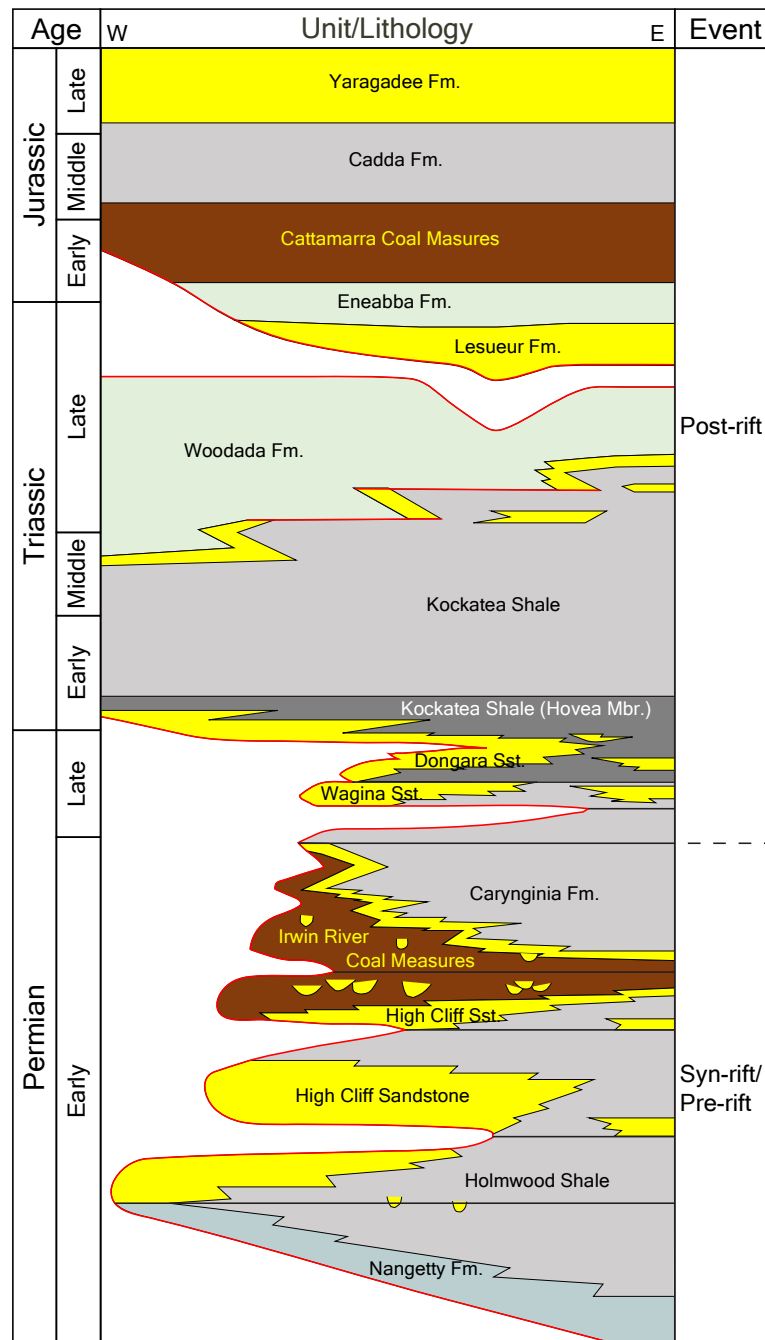


Figure 1-4. Stratigraphy of the northern Perth Basin (after Ferdinando et al., 2007; Mory et al., 2005). Light and dark grey: deeper water mudstone, yellow: shallow marine sandstone: brown: fluvial to deltaic sediments, bluish green (Nangetty Fm.): open marine glacial sediments, yellowish green (Eneabba and Woodada Fms.): fluvial to deltaic sediments.

3.2 The Northern Carnarvon Basin, Western Australia

The Northern Carnarvon Basin is located in the western part of the North West Shelf on the northern coast of Australia. In the basin, the Upper Jurassic Dingo Claystone and the Lower Triassic Locker Shale are considered potential source rocks (Grahame et al., 2017; Molyneux et al., 2016; van Aarssen et al., 1996; Volkman et al., 1983). The Locker Shale of the Northern Carnarvon Basin is an equivalent to the Lower Triassic Kockatea Shale in the northern Perth Basin and shares a similar depositional age and depositional setting to the Kockatea Shale. The Northern Carnarvon Basin is located on the eastern edge of the EGIR, bounded by the Sibmasu-Argo blocks and the Neo Tethys Ocean (Figure 1-3) (Domeier and Torsvik, 2014; Matthews et al., 2016; Minken et al., 2019; Scholle et al., 1995; Stephenson et al., 1998).

The Northern Carnarvon Basin shares a similar tectonic evolution and stratigraphy to the northern Perth Basin. The Locker Shale was deposited in a post-rift marine transgression setting. Deltaic facies are suggested for the Middle Triassic Mungaroo Formation in the Northern Carnarvon Basin (Figure 1-5) (Allgöwer and Lignum, 2019; Baillie et al., 1994; Ferdinando et al., 2007; Grahame et al., 2017; I'Anson et al., 2019; Iasky et al., 2002; Lech, 2013; Longley et al., 2002; Marshall and Lang, 2013; McGee et al., 2017; Müller et al., 2005; Smith et al., 1999; Tindale et al., 1998; Westphal and Aigner, 1997). The regional structural trend in the basin is NE-SW striking normal faults associated with small oblique faults responsible for lateral movement (Borel and Stampfli, 2002; Iasky et al., 2002; Paschke et al., 2018; Stephenson et al., 1998; Tindale et al., 1998; Yasin et al., 1998). The basin is divided into sub-basins generally based on depocentre locations. The Exmouth, Barrow, Dampier and Beagle Sub-basins are the main depocentres. On the other hand, the Enderby Terrace, Lambert and Peedamullah Shelves form the shelf margin on the southeast flank of the basin.

Late Permian rifting and the Late Permian Unconformity are prominent geological features in this basin (Minken et al., 2019). The Lower Triassic Locker

Shale was deposited as a post-rift transgressive deep water sequence (McGee et al., 2017; Tao et al., 2013). The Middle Triassic Mungaroo Formation and younger strata were deposited during subsequent periods of subsidence and rifting. The Upper Jurassic Dingo Claystone was also deposited in a deeper marine setting during a global anoxic event (Hocking, 1992). The basin experienced significant uplift and erosion in the Early Cretaceous, and the Valanginian Unconformity separates the passive margin sequences from older sediments as in the northern Perth Basin.

Although the largest fields in the Northern Carnarvon Basin are condensate and gas, the basin is also an oil producing basin (Bunt et al., 2001; Iasky et al., 2002; le Poidevin and Lowden, 1994; Lech, 2013; Thompson et al., 2018). In the Northern Carnarvon Basin, there are several potential source rocks. The Upper Jurassic Dingo Claystone is recognised as a source rock in the Barrow and Exmouth sub-basins (Tindale et al., 1998; van Aarssen et al., 1996; Volkman et al., 1983). The Lower Triassic Locker Shale also has source rock potential with high TOC and HI (Molyneux et al., 2016). Triassic or older strata have been cited as possible source rocks for the Tubridgi Field on the Peedamullah Shelf (Bunt et al., 2001; Edwards and Zumberge, 2005).

Age		W	Unit/Lithology	E	Event
Cretaceous	Late		Winning Group		Valanginian Unconformity
	Early		Barrow Group	Mardie Greensand Member Birdong Sandstone Nanutarra Formation Angel Formation	
Jurassic	Late		Dingo Claystone		
			Calypso Formation		
	Middle		Athol Formation		
	Early		Murat Siltstone		
			North Rankin Formation		
Triassic	Late		Brigadier Formation		
			Mungaroo Formation		
	Middle		Locker Shale		
	Early				
Permian	Late		Kennedy Group		Late Permian Unconformity
			Bryo Group		
	Early		Callytharra Formation		
			Wooramel Group		

Figure 1-5. Stratigraphy of the Northern Carnarvon Basin (after I'Anson et al., 2019).
 Light and dark grey: deeper water mudstone, yellow: shallow marine sandstone:
 brown: fluvial to deltaic/marine sediments, blue- green: open marine glacial sediments.

4 Significance of biomarkers and isotope analysis in organic geochemistry

Organic geochemistry is essential to investigate paleoenvironments and source rock characteristics (Peters et al., 2004; Peters, 1986). In this research, TOC and Rock-Eval, biomarker, stable carbon and sulfur isotope analyses are used. The principles of their application are discussed here.

4.1 Biomarker analysis

Biomarkers are “molecular fossils” and originate from biolipids of living organisms (Peters et al., 2004). These biolipids lose their reactive functional groups such as carbon-carbon double bonds through the thermal maturation process, and their basic carbon skeletons are preserved as biomarkers in sedimentary rocks and petroleum (Figure 1-6). The biomarker compositions represent ecological communities in geological time. The identification and quantification of biomarkers is utilized for the reconstruction of paleoenvironments, thermal maturity evaluation, and petroleum system analysis. Many biomarkers are produced by multiple organisms, but some specific biomarkers are sourced from particular species and utilized for paleoenvironment reconstruction. For instance, photosynthetic bacteria produce specific carotenoids depending on species: okenone from purple sulfur bacteria (*Chromatiaceae*), chlorobactene from green-brown sulfur bacteria (*Chlorobiaceae*), and isorenieratene from green-green sulfur bacteria (*Chlorobiaceae*) (Brocks & Schaeffer, 2008; Fox et al., 2020; Grice et al., 1997; Grice et al., 2005a; Schaefer et al., 2020; Summons & Powell, 1987). These bacteria generally develop under PZE and in microbialites. Biomarkers derived from these carotenoids (okenane, chlorobactane, isorenieratane) are a good proxy for the identification of these conditions.

4.2 Stable isotope analysis

Stable isotope data can also contribute to the reconstruction of paleoenvironments in combination with biomarkers (Grice et al., 2007, 1998, 1997; Hayes et al., 1990; Kuhn et al., 2010; Schouten et al., 1998).

Most elements have several stable isotopes. For carbon, ^{12}C is dominant with minor proportions of ^{13}C . For sulfur, ^{32}S is dominant with ^{33}S , ^{34}S and ^{36}S as minor portions (Table 1-1). The abundance of each stable isotope under natural conditions is relatively constant. However, the isotope fraction changes slightly through physical, chemical and biological processes such as photosynthesis (Peters et al., 2004; Schidlowski, 1988) (Figure 1-7).

Table 1-1. Stable isotope abundance of carbon and sulfur (Faure and Mensing, 2005).

	Carbon		Sulfur
^{12}C	98.90%	^{32}S	95.02%
^{13}C	1.10%	^{33}S	0.75%
		^{34}S	4.21%
		^{36}S	0.02%

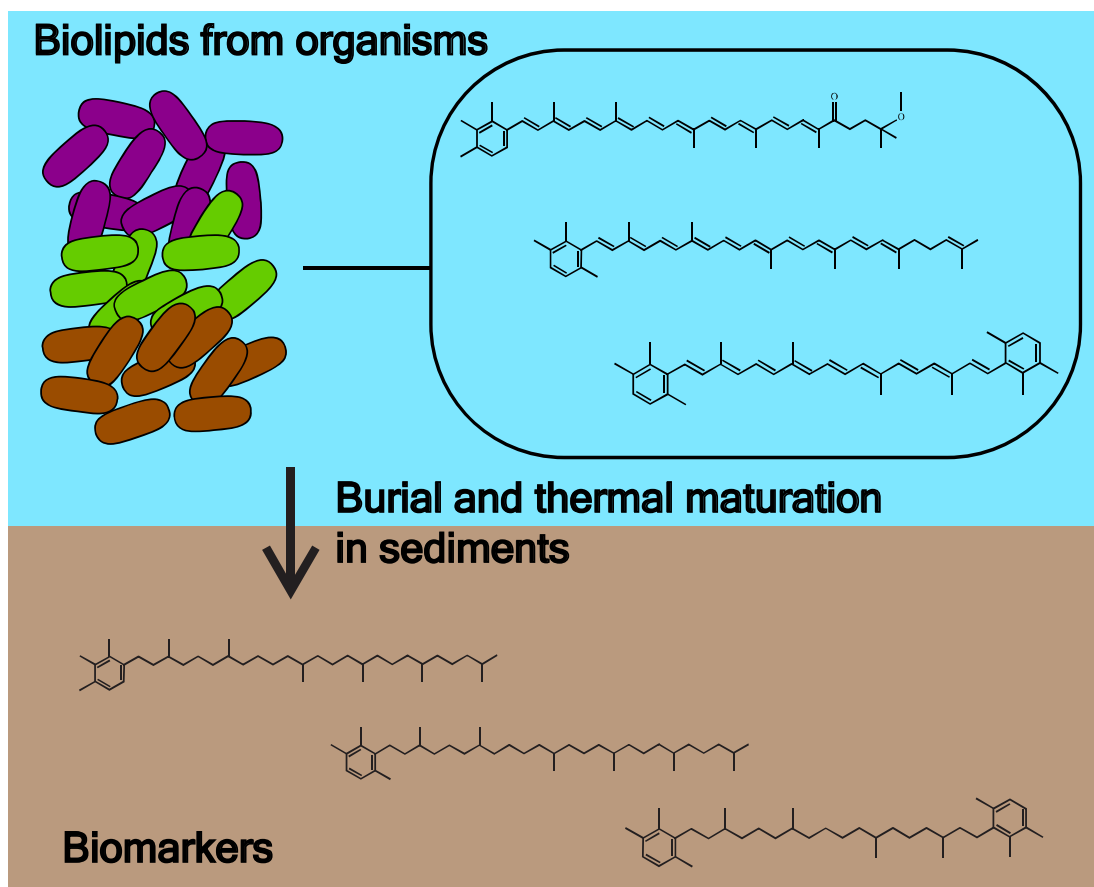


Figure 1-6. Schematic concept of biomarker formation. Each biolipid represents okenone, chlorobactene and isorenieratene from purple sulfur bacteria, green-green sulfur bacteria and green-brown sulfur bacteria, respectively. These biolipids turn into biomarkers (okenane, chlorobactane, and isorenieratane) through burial and thermal maturation in sediments.

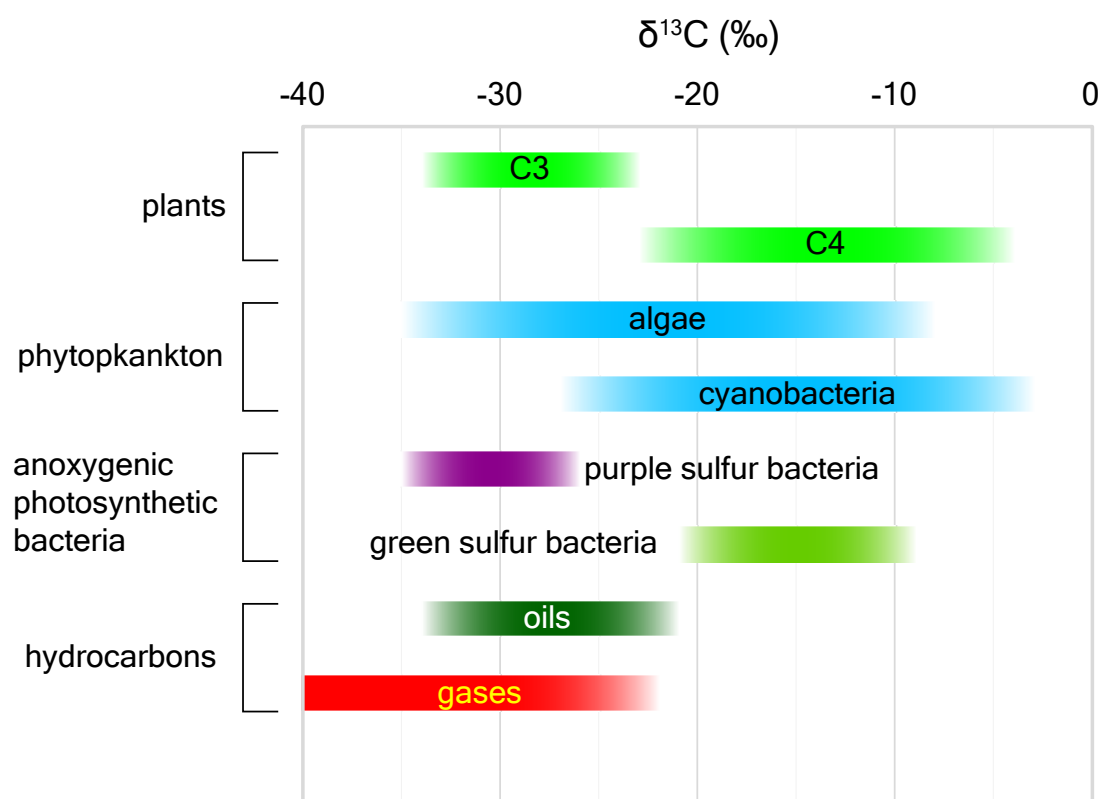


Figure 1-7. Approximate $\delta^{13}\text{C}$ range of plants, phytoplankton, sulfur bacteria and hydrocarbons (after Schidlowski, 1988; Peters et al., 2004).

For example, compounds derived from sulfur bacteria have different values of stable carbon isotope depending on the type of bacteria (Peters et al., 2004). Purple sulfur bacteria (*Chromatiaceae*) are active in settings with dissolved inorganic carbon depleted in ^{13}C , and utilize the C3 pathway for carbon fixation through their photosynthesis (Grice et al., 1997; Zyakun et al., 2009). Therefore, products from these bacteria become relatively depleted in ^{13}C . On the other hand, green sulfur bacteria (*Chlorobiaceae*) utilize the reversed TCA (tricarboxylic acid) cycle for carbon fixation through their photosynthesis, and their products are relatively enriched in ^{13}C .

Sulfur isotope fractionation is influenced by microbial metabolism under oxic and anoxic conditions and evaporite mineral formation (Bernasconi et al., 2017). For

example, $\delta^{34}\text{S}$ values of pyrite in PZE are isotopically lighter compared to oxic conditions (Böttcher et al., 2010; Canfield and Farquhar, 2009; Kaplan and Rittenberg, 1964; Schaefer et al., 2020). This difference follows the change in the sulfur isotope composition of seawater sulfate. This is related to pyrite formation and burial under anoxic conditions, and microbial sulfate reduction, due to the strong preference of ^{32}S over ^{34}S during this process. This trend is recognized globally around the Permian-Triassic boundary (Bernasconi et al., 2017).

4.3 Reconstruction of paleoenvironments

Source-specific biomarkers and stable isotopes can differentiate paleoenvironmental conditions. PZE and microbialites are the main focus of this research. The general conditions of each setting are described in this section.

4.3.1 Photic Zone Euxinia (PZE)

Under anoxic conditions with a stagnant water column, sulfate-reducing bacteria become active around the sediment-water interface and produce H_2S as a degradation product (Manske et al., 2005; Pfenning, 1978; Sass et al., 2001), and euxinic conditions are established with high H_2S concentration. PZE is established when the chemocline between oxic and euxinic water becomes shallow and occurs within the photic zone (Figure 1-8). It is identified in present day lakes and oceans such as the Black Sea (Jorgensen et al., 1991), Fayetteville Green Lake (Meyer et al., 2011) and North Sea fjords (Anderson et al., 1988). PZE is sometimes associated with mass extinctions, such as the Permian-Triassic boundary (Cao et al., 2009; Grice et al., 2005a; Hays et al., 2007) and the Middle to Late Devonian (Connock et al., 2018; George et al., 2014; Spaak et al., 2018).

Under PZE, anoxygenic photosynthetic bacteria such as sulfur bacteria become active and produce layers of bacterial communities depending on tolerance to oxygen (Brocks and Schaeffer, 2008; Cui et al., 2020; French et al., 2015, 2014; Hays et al.,

2007; Meyer et al., 2011; Nabbefeld et al., 2010). Green-brown sulfur bacteria (*Chlorobiaceae*) are located at the bottom, green-green sulfur bacteria (*Chlorobiaceae*) are in the middle, and purple sulfur bacteria (*Chromatiaceae*) are positioned at the top of the layer. Green sulfur bacteria (green-green and green-brown sulfur bacteria) are strict anaerobic phototrophs, and utilize H₂S as an electron donor for photosynthesis. They produce specific biolipids such as carotenoid pigments including chlorobactene from green-green sulfur bacteria, isorenieratene from green-brown sulfur bacteria, and bacteriochlorophylls such as Bchl *c*, *d* and/or *e*. These biolipids become biomarkers throughout thermal maturation: chlorobactane, isorenieratane, methyl *iso*-butyl maleimides, and aryl isoprenoids (Clifford et al., 1998; Grice et al., 1996; Grice et al., 2005a,b; Maslen et al., 2009; Naeher & Grice, 2015; Pedentchouk et al., 2004; Sousa Júnior et al., 2013; Summons & Powell, 1987; Tulipani et al., 2015). Green sulfur bacteria utilize the reversed TCA (tricarboxylic acid) cycle for carbon fixation for their photosynthesis. Therefore, their products tend to be relatively enriched in ¹³C (Grice et al., 1997). On the other hand, purple sulfur bacteria also utilize H₂S as an electron donor for photosynthesis but have more tolerance to oxygen. They also produce specific biolipids: okenone as the carotenoid pigment, and Bchl *a* and *b* as bacteriochlorophylls. Okenone becomes the carotenoid biomarker okenane. Purple sulfur bacteria utilize the C₃ pathway for carbon fixation for their photosynthesis. Therefore, the products from them tend to be relatively depleted in ¹³C.

The $\delta^{34}\text{S}$ values of pyrite tend to be isotopically lighter in euxinic conditions compared with oxic conditions (Böttcher et al., 2010; Canfield and Farquhar, 2009; Kaplan and Rittenberg, 1964; Schaefer et al., 2020). Under euxinic conditions, pyrite is formed under unlimited sulfate supply and preserves the large sulfur isotope fractionation between the sulfate pool and pyrite (Georgiev et al., 2020). On the other hand, under oxic conditions with limited sulfate supply, $\delta^{34}\text{S}$ values of pyrite tend to be isotopically heavier (Georgiev et al., 2020).

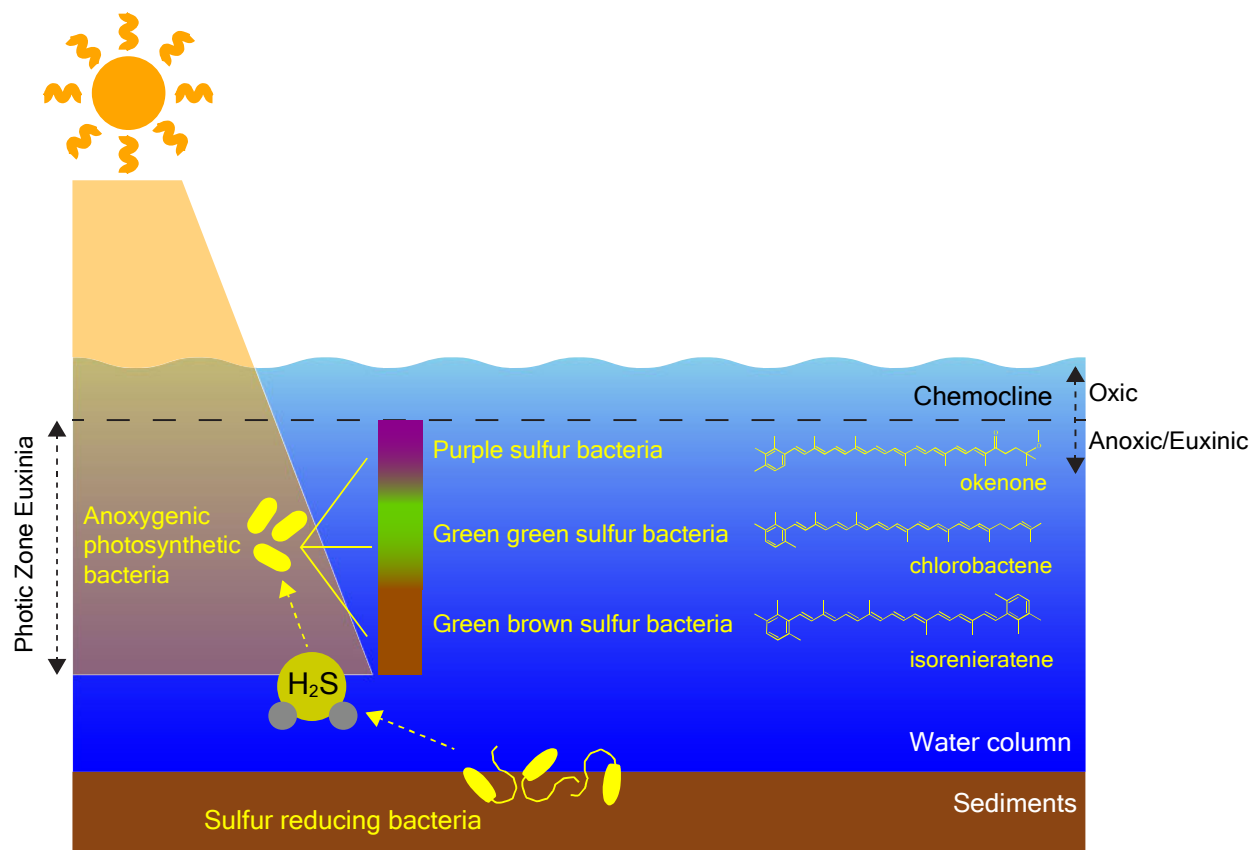


Figure 1-8. Schematic illustration of photic zone euxinia, associated microbial community, and representative carotenoid pigments of each sulfur bacteria.

4.3.2 Microbial mats (Microbialites)

Microbial mats are biogenic sediments composed of microorganisms such as bacteria, and have been identified from the Proterozoic to the present day, although these mats were more common in the Proterozoic (Noffke, 2010). The habitable zones for microbial mats are extensive, and include conditions that are harsh for other organisms such as high sulfate and hypersaline environments, geothermal springs and tidal flats. For instance, in the present day, they develop in Shark Bay under hypersaline conditions (Jahnert and Collins, 2013; Logan, 1974; Pagès et al., 2014) and Fayetteville Green Lake under high sulfate conditions (Meyer et al., 2011). During the Phanerozoic, microbialites have been identified around mass extinction events such as in the Early Triassic after the end-Permian mass extinction (Chen et al., 2014; Foster et al., 2020; Kershaw et al., 2012; Luo et al., 2018; Luo and Chen, 2014; Thomas et al., 2004; Woods, 2014), the End Triassic after the end- Triassic mass extinction (Fox et al., 2020) and in the Chicxulub crater after the end- Cretaceous mass extinction (Bralower et al., 2020; Schaefer et al., 2020).

The top layer of microbial mats contains oxygenic cyanobacteria and eukaryotic algae (Figure 1-9) (Armitage et al., 2012; Noffke, 2010; Stal et al., 1985). Anoxic conditions develop in the lower layers, and anaerobic sulfur bacteria become active using the light which penetrates from the top layer (Brocks and Schaeffer, 2008; Fox et al., 2020; Pagès et al., 2014; Schaefer et al., 2020). The sulfur bacterial layers of microbial mats share the same bacterial communities as PZE. Therefore biomarkers from microbial mats are similar to the biomarker composition of PZE. However, in general, purple sulfur bacteria and green-green sulfur bacteria are relatively more abundant than green sulfur bacteria in microbial mats compared with PZE (Brocks and Schaeffer, 2008; Meyer et al., 2011).

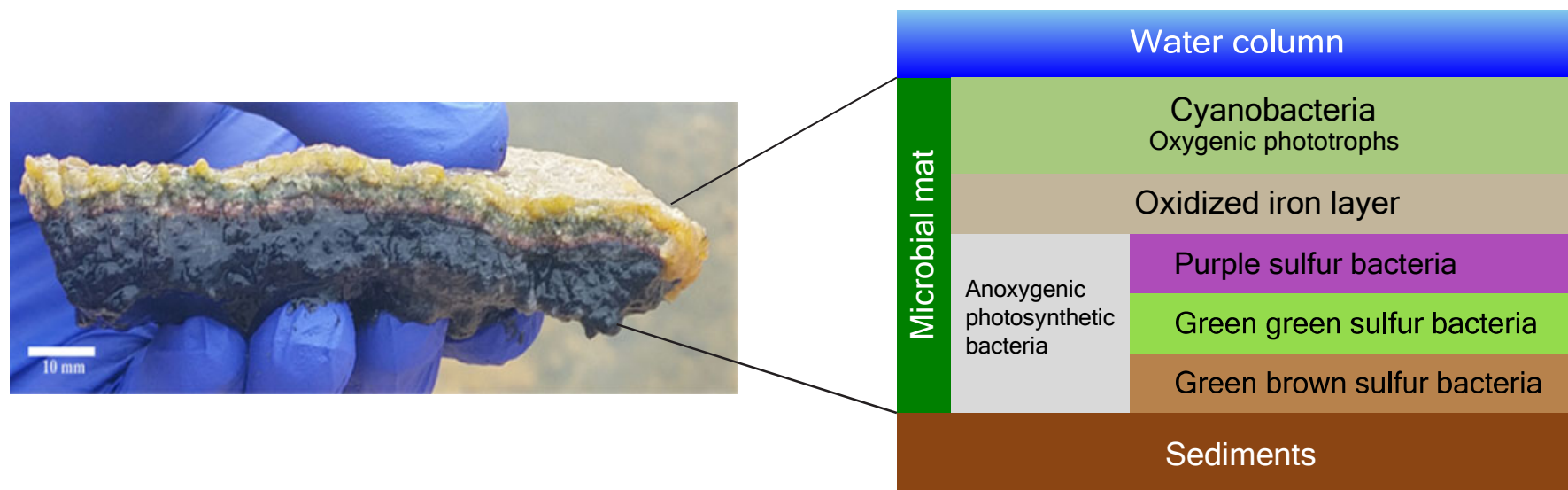


Figure 1-9. General internal structure of microbial mats and related carotenoid pigments of each sulfur bacteria. Photo courtesy of Kliti Grice.

5 Project Design

Geology and organic geochemistry were both utilised in this research (Figure 1-10). Seismic data, core and wireline logs were utilized for geological analyses, and Rock-Eval, biomarker, stable carbon isotope and sulfur isotope analyses were conducted for organic geochemistry analyses.

5.1 Geological analysis for the reconstruction of paleogeography

The reconstruction of basin geometry and paleogeography is based on geological analyses such as seismic interpretation, wireline log and core analyses. Seismic data with well calibrations define the tectono-stratigraphy, basin evolution and basin geometry for each period of geologic time. Detailed observation of each package in the seismic data indicates the timing of fault activity and their influence on the deposition of sediments. Well correlations are utilized with seismic data, but are also useful for understanding the tectono-stratigraphy of basins, especially when the quality of seismic data is poor and/or the sediment thickness is less than seismic resolution.

Cuttings show the lithology of nearly all of the drilled intervals, but cannot provide details of sedimentary structures or other features to evaluate sedimentary settings. On the other hand, core data provide detailed lithofacies information required for the investigation of depositional settings, although cores are generally limited to intervals such as reservoirs. The comparison of core lithofacies with wireline log characteristics can show the lateral distribution of lithofacies where core data is unavailable. In addition, the boundary of each lithofacies and the paleogeography can be defined in relation to the basin geometry established by seismic and well data.

Organic geochemistry is a useful tool for investigating paleoenvironmental conditions, but combining it with geologic analysis is necessary to reconstruct the basin-scale paleoenvironments and their geological controls.

5.2 Organic geochemical analyses for the paleoenvironments

The analytical approach for the organic geochemical analysis applied in this research is briefly described as follows (Figure 1-11). The detailed methodology of each analysis is presented in subsequent chapters.

Rock samples of 10 to 30 grams were initially ground into a fine powder and separated for different uses. TOC and Rock-Eval analyses were conducted by Intertek (Intertek Group plc) in Welshpool, Western Australia, for determining the source rock potential of each sample.

Soluble organic materials were extracted from powdered rock samples using Soxhlet extraction with a mixture of dichloromethane (DCM) and methanol. The extracted organic materials were eluted into saturated, aromatic, Ni-porphyrin, V=O-porphyrin and polar fractions. Petroleum samples were fractionated into saturated, aromatic and polar fractions. Short silica gel chromatography with appropriate solvents for eluting each fraction were used for the separation. These preparations were conducted at Curtin University.

For biomarker analysis, gas chromatography-mass spectrometry (GC-MS) & gas chromatography-metastable reaction monitoring-mass spectrometry (GC-MRM-MS) were used, and measured biomarkers were identified and quantified. D4-C₂₇ $\alpha\alpha\alpha$ cholestane was added as an internal standard for quantification of the GC-MRM-MS analyses. GC-MS analysis was conducted at Curtin University and GC-MRM-MS analysis was conducted at Massachusetts Institute of Technology in the United States.

The residual sediments were used for the stable carbon isotope and sulfur isotope analyses. For the stable carbon isotope analysis, the bulk stable carbon isotope composition ($^{13}\text{C}/^{12}\text{C}$) of organic matter was measured. Carbonate minerals were removed with hydrochloric acid (HCl). A Thermo Flash 2000 HT elemental analyser (EA) connected to a Delta V Advantage isotope ratio mass spectrometer (irMS) *via* a ConFlo IV was used to measure the ratio of ^{13}C and ^{12}C of kerogen. Each sample was analysed in triplicate. This analysis was conducted at Curtin University. Measured

values were normalised to the Vienna Pee Dee Belemnite (VPDB) scale. The $\delta^{13}\text{C}$ values are the ratio of ^{13}C to ^{12}C relative to the reference standard in ‰ (Equation 1). This analysis was conducted at Curtin University.

$$\delta^{13}\text{C}_{\text{sample}}(\text{‰}) = \left(\frac{R_{\text{sample}}}{R_{\text{standard}}} - 1 \right) * 1000 \quad (\text{Equation 1})$$

$$R = \frac{^{13}\text{C}}{^{12}\text{C}}$$

The stable sulfur isotope composition ($^{34}\text{S}/^{32}\text{S}$) of the total reduced inorganic sulfur (TRIS; considered to essentially represent pyrite (FeS_2)) was also measured. A Thermo Scientific Flash EA Isolink Elemental Analyzer, connected to a Thermo Finnigan MAT 253 gas mass spectrometer *via* a Thermo Conflo IV split interface was used for the extracted sulfur to measure the ratio of ^{34}S and ^{32}S of each sample. This analysis was conducted at Leibniz-Institute for Baltic Sea Research (IOW) in Germany. Measured values were normalised to the Vienna-Canyon Diablo Troilite (VCDT) scale. The $\delta^{34}\text{S}$ values are the ratio of ^{34}S to ^{32}S relative to the reference standard in ‰ (Equation 2). This analysis was conducted at the Leibniz Institute for Baltic Sea Research (IOW) in Germany.

$$\delta^{34}\text{S}_{\text{sample}}(\text{‰}) = \left(\frac{R_{\text{sample}}}{R_{\text{standard}}} - 1 \right) * 1000 \quad (\text{Equation 2})$$

$$R = \frac{^{34}\text{S}}{^{32}\text{S}}$$

The Hg concentrations were measured using a Direct Mercury Analyser (DMA)-90. Calibration was conducted with both the BCR 142 R CRM and SRM 2709 reference materials. Although it has been observed that Hg may bond to different sedimentary phases such as organic matter, sulfides, or clay minerals (e.g., Shen et al., 2020), normalized data only with reference to TOC were used in this research. This analysis was conducted at IOW in Germany.

6 Scope of the thesis

PZE has been identified by previous authors during the Early Triassic in the northern Perth Basin (Grice et al., 2007; Grice et al., 2005a,b; Thomas & Barber, 2004), and recognized as the conditions under which source rocks were deposited (Boreham et al., 2000; Grosjean et al., 2017; Langhi et al., 2014; Scott, 1994; Thomas, 1979; Thomas et al., 2004). However, the identification has been based on limited wells, and the basin scale paleoenvironmental conditions have not yet been fully evaluated (Dargahi and Rezaee, 2014). In addition, microbialites have been identified in the Lower Triassic Kockatea Shale from both outcrop and in the subsurface (Chen et al., 2014; Luo et al., 2018; Luo and Chen, 2014; Thomas et al., 2004), but their organic geochemical characteristics and source rock potential have not been fully evaluated.

The main objectives of this research are to reconstruct the basin scale paleoenvironmental conditions and investigate their controlling factors during the Early Triassic in the northern Perth Basin by integrating organic geochemistry and geology, and to distinguish between organic geochemical characteristics of PZE and/or microbialites. A further aim is to investigate the petroleum system in the northern Perth and Northern Carnarvon basins by applying the concept of paleoenvironmental distribution and organic geochemical characteristics of PZE and/or microbialites to petroleum samples.

Chapter 2 reconstructs the basin morphology and paleogeography during the Early Triassic in the northern Perth Basin and investigates the controls on the distribution of source rock facies. The facies distribution in the Lower Triassic Kockatea Shale is an important factor for investigating the distribution of paleoenvironments and source rock potential in this period. This research utilizes cores, wireline logs and seismic data. The chapter focuses on the reconstruction of basin geometry and paleogeography and the basin-scale distribution of source rock facies during the Early Triassic. This chapter was prepared for submission to *Marine and Petroleum Geology* (accepted on

29 August 2021 and published in volume 133 in November 2021). Some information mentioned in other chapters is repeated here.

Chapter 3 investigates the basin-scale distribution of paleoenvironmental conditions during the Early Triassic in the northern Perth Basin and the organic geochemical difference between PZE and microbialites. Biomarker, stable carbon isotopes of organic matter, sulfur isotopes of pyrite and Hg concentration analyses are applied. This chapter focuses on the chemo-isotope stratigraphic description of organic geochemical characteristics to investigate basin-scale paleoenvironments and to identify the organic geochemical difference between PZE and microbialites. This chapter was submitted to *Geochimica et Cosmochimica Acta* on 1 September 2021. Some information mentioned in other chapters is repeated here.

Chapter 4 evaluates the potential source rocks in both the Perth and Northern Carnarvon basins. Biomarker analysis (by GC-MRM-MS) is applied to petroleum samples from both the Perth and Northern Carnarvon basins, especially for targeting carotenoid biomarkers derived from sulfur bacteria related to the development of PZE and/or microbialites. This chapter focuses on the investigation of the source rock facies contributing to the petroleum system in the northern Perth Basin and the potential source rocks for the petroleum samples in the Northern Carnarvon Basin, especially the Tubridgi Field in the Peedamullah Shelf, applying source-oil and oil-oil correlation. This chapter was submitted to *Petroleum Geoscience* on 26 March 2022. Some information mentioned in other chapters is repeated here.

Chapter 5 concludes this thesis and discuss its significant findings. It compares the major findings of this research to global characteristics of the end-Permian mass extinction event such as the multiple episodes of harsh environmental conditions that developed after the event and which have been identified globally. The comparison with other basins suggests possible controls on Early Triassic source rock potential but also indicates the importance of basin scale paleoenvironmental reconstruction even for the comparison between basins. The potential source rock distribution in the

Bedout Sub-basin in the North West Shelf, which has recent significant oil discoveries, is presented by comparing the basin scale source rock quality between the Bedout and the northern Perth basins.

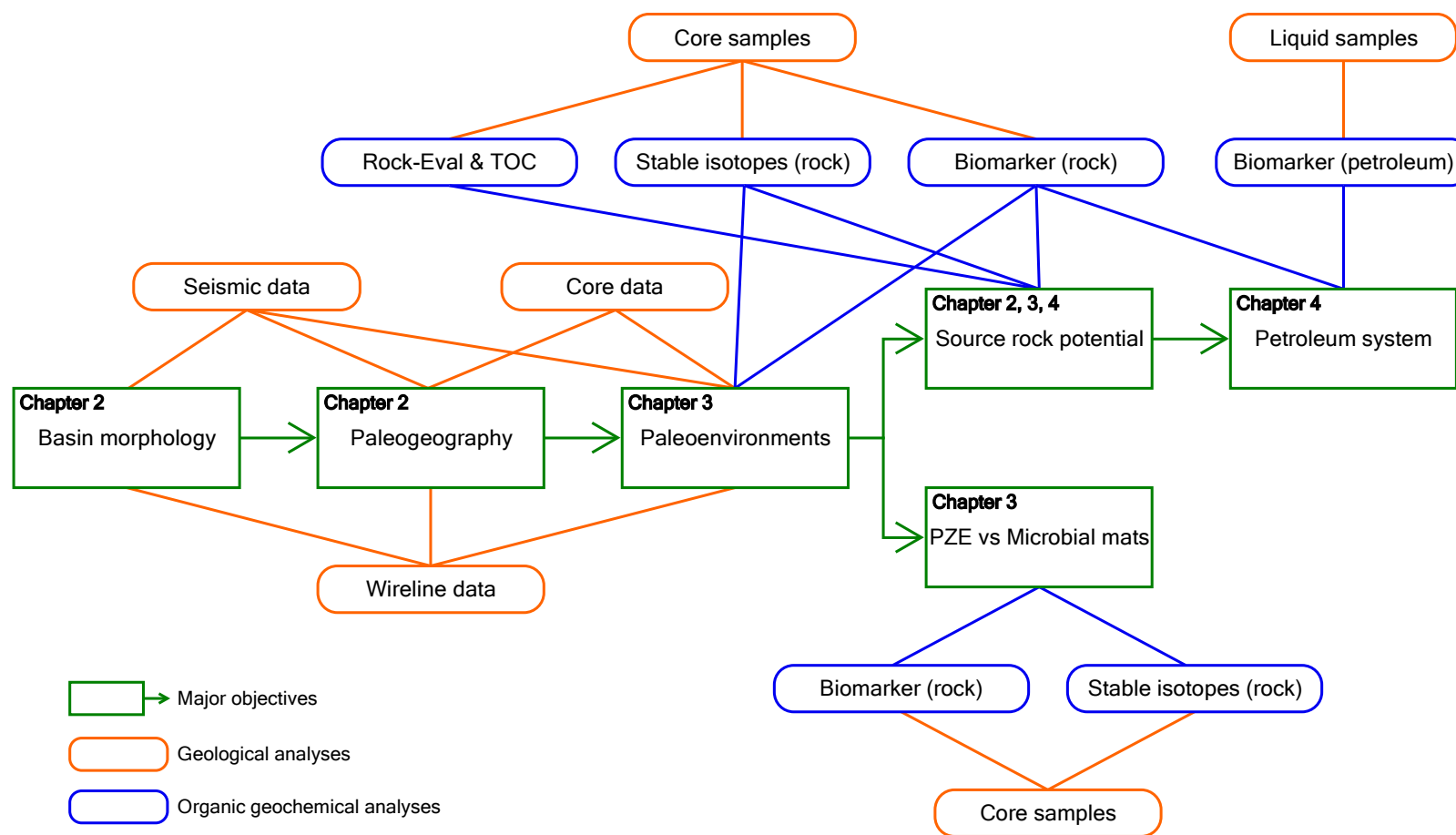


Figure 1-10. Workflow applied for this thesis, showing the integration of geology and organic geochemistry.

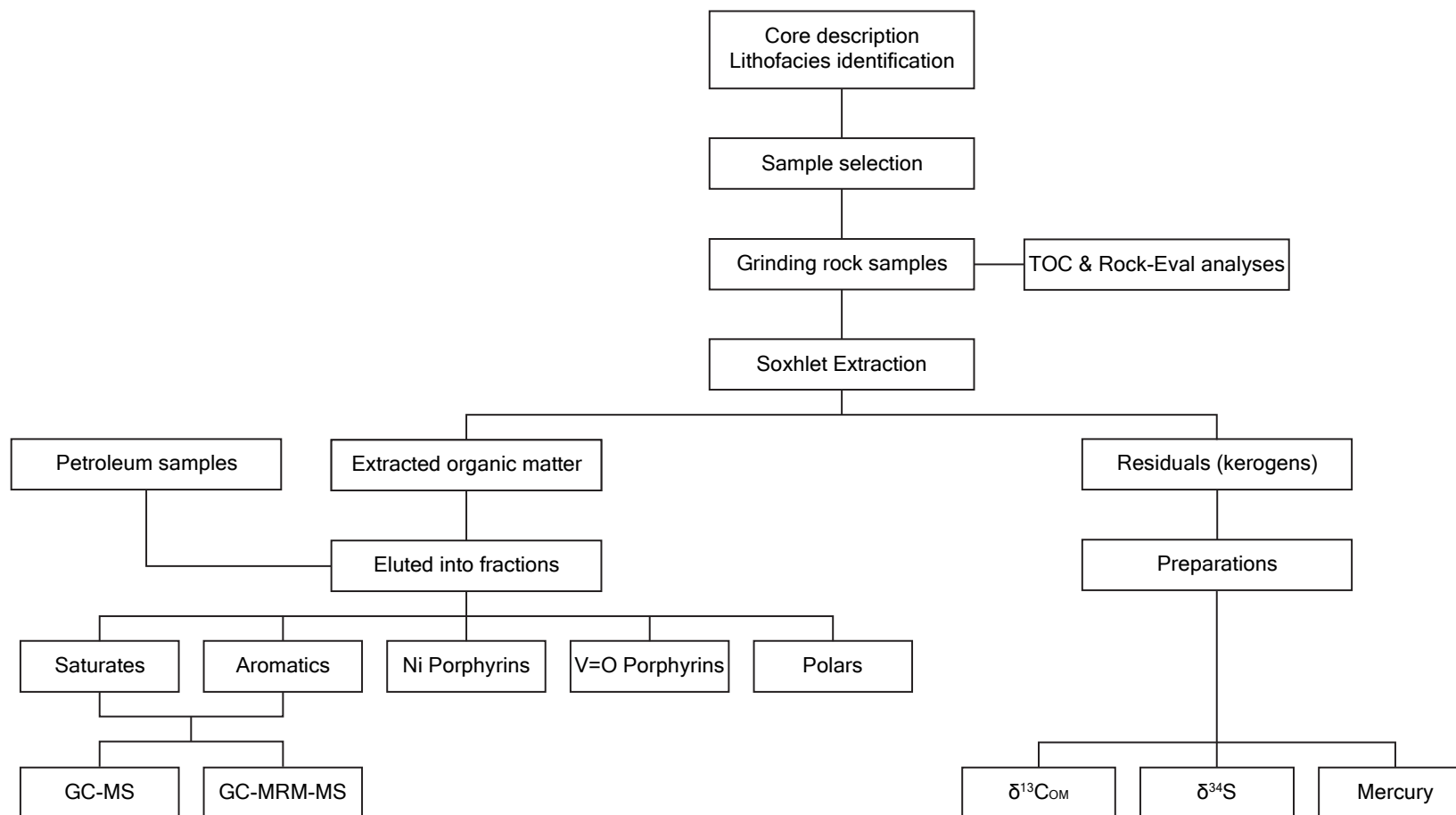


Figure 1-11. Workflow of organic geochemical analysis applied in this research.

Chapter 2

Early Triassic paleogeography of the northern Perth Basin, and controls on the distribution of source rock facies

Takashi Taniwaki, Chris Elders and Kliti Grice

Marine and Petroleum Geology 133 (2021) 105314

Submitted: 12 April 2021

Accepted: 29 August 2021

Published: November 2021

Abstract

The facies distribution of the Lower Triassic Kockatea Shale in the northern Perth Basin is an important factor for assessing the Lower Triassic source rock potential in the basin. Seismic interpretation and well analyses demonstrate that Permian-aged faults are responsible for the morphology of the basin in the Early Triassic and created remnant topography that controls the deposition of Lower Triassic sediments. Cores from petroleum wells and their correlated wireline logs show the lithological variation and lateral distribution of facies across the base of the Kockatea Shale. Darker coloured mudstones were deposited under anoxic conditions in the deeper part of the basin, while lighter coloured mudstones and tidally influenced sediments with bioturbation were deposited under oxic conditions in a shallow marine setting. Microbial mats developed in shallower water depths on structural highs (Beagle Ridge and Turtle Dove Ridge) in the anoxic parts of the basin.

The distribution of microbial mats is controlled by two factors during the period of ecological recovery from the end-Permian mass extinction: 1) the presence of topographic highs and, 2) distance from the edge of the basin. The source rock potential of both darker coloured mudstone and microbial mat facies is demonstrated by TOC values between 0.3 and 3.4 % and HI values between 39 and 579 mg/gTOC. On the other hand, the lighter coloured mudstones, deposited under more oxic tidal settings, have poor source rock quality and TOC values between 0.2 and 0.5% and HI values between 59 and 127 mg/gTOC.

1 Introduction

The Perth Basin is an oil- and gas-producing basin located on the western coast of Australia (Crostellla, 1995; Ghori, 2015; Jones et al., 2011). One of the main sources of oil is the Lower Triassic Kockatea Shale (Boreham et al., 2000; Grosjean

et al., 2017; Langhi et al., 2014; Scott, 1994; Thomas, 1979; Thomas et al., 2004), the source rock potential and organic geochemical characteristics of which are well documented based on biomarker and carbon and hydrogen stable isotopic studies (Dawson et al., 2005; Grice et al., 2007; Grice et al., 2005a,b,c; McIlldowie & Alexander, 2005; Thomas & Barber, 2004). The basal section of the Kockatea Shale is distinctive and displays increased total organic carbon (TOC) and hydrogen index (HI) values both of which are good indicators of oil source rock quality. Key biomarker correlation confirms that this part of the Kockatea Shale is the primary source of hydrocarbons in many fields of the Perth Basin (e.g. Hovea, North Yandanogo, Dongara, Mt Horner, Jingemia and Woodada) (Thomas and Barber, 2004).

The Kockatea Shale was deposited from the Late Permian to the Early Triassic, and therefore spans a part of the end-Permian mass extinction. The development of anoxic condition and photic zone euxinia (PZE) around this mass extinction is recognized globally, and is thought to be related to volcanic activity of the Siberian Trap eruptions (Erwin, 1994; Grice et al., 2005a; Knoll et al., 1996; Nabbefeld et al., 2010; Song et al., 2014; Twitchett et al., 2004; Whiteside & Grice, 2016; Wignall & Twitchett, 1996). The presence of these conditions in the Perth Basin has been established on the basis of biomarker analysis (Grice et al., 2005c), and they played an important role in the development of organic-rich source rocks in the Kockatea Shale (Grosjean et al., 2017; Thomas and Barber, 2004). In addition, the development of microbial mats following the mass extinction is recognized globally and is an indication of the severe conditions that existed during and after the mass extinction which were not suitable for other organisms (Foster et al., 2020; Kershaw et al., 2012; Luo et al., 2018; Woods, 2014). Microbial mats are well documented from outcrops of the Kockatea Shale in the Perth Basin (Chen et al., 2014; Luo et al., 2018; Luo and Chen, 2014), although they are less well-studied in the subsurface (Thomas et al., 2004).

Although it is expected that the Kockatea Shale is widely distributed in the northern Perth Basin, the lateral extent of organic matter-rich source rock facies within the Kockatea Shale is poorly constrained (Crostella, 1995; Crostella & Backhouse, 2000; Haig et al., 2015; Mory, 1994). Recognising the factors that influence facies distribution, and microbial mat development in particular, will contribute to understanding the controls on source rock distribution and quality, as well as the impact of the end-Permian mass extinction on the Perth Basin. In this study, we identify several lithofacies, including microbial mats, from the base of the Kockatea Shale from a selection of petroleum exploration wells, and document lithological variation in the Kockatea Shale from cores. Seismic data is utilized to demonstrate the extent to which Permian rifting influenced basin geomorphology in the Early Triassic. Core data is correlated to well logs to investigate the lateral distribution of lithofacies and source rock quality. These results are integrated to evaluate the paleogeography, and identify controls on microbial mat development and distribution. Source rock analysis is also conducted to investigate the source rock potential of these beds.

2 Geological setting

The northern Perth Basin (Figure 2-1) has experienced several rift, subsidence, and uplift events from the Devonian to the Early Cretaceous (Jablonski and Saitta, 2004; Norvick, 2004). Late Permian rifting is one of the most prominent events in the evolution of the basin (Jablonski and Saitta, 2004). The Lower Permian Nangetty Formation, Holmwood Shale, High Cliff Sandstone, Irwin River Coal Measures and Carynginia Formation were deposited in open marine, fluvial and deltaic settings, and are interpreted as pre-rift or syn-rift sequences (Mory & Iasky, 1996; Mory et al., 2005) (Figure 2-2). The Late Permian Unconformity was developed regionally at the end of this rift event (Jablonski and Saitta, 2004; Jones et al., 2011). In parts of the basin, the Upper Permian Wagina Sandstone, Beekeeper Formation and Dongara

Sandstone were deposited in deltaic and shallow marine settings as the first post-rift sediments. Subsequently, in the Late Permian to Early Triassic, the thermal subsidence phase of the rift produced a local marine transgression with deposition of the Kockatea Shale facies in deeper water. At the same time, the Bookara Sandstone was developed in the shallow water parts of the basin. Deltaic sediments of the Middle Triassic Woodada Formation were deposited after deposition of the Kockatea Shale as a result of subsequent regression. The overlying Late Triassic to Late Jurassic Lesueur, Eneabba, Cattamarra Coal Measures, Cadda, and Yarragadee Formations were deposited during subsequent rift events. Extensive uplift and erosion caused by the breakup of Greater India in the Early Cretaceous is prominent (Jablonski and Saitta, 2004), especially in the offshore northern Perth Basin, resulting in a significant unconformity that separates these sequences from the Lower Cretaceous Winning Group.

3 Data & Methodology

3.1 Seismic data

A large amount of public domain 2D and 3D seismic data is available from the northern Perth Basin. The 3D seismic surveys used in this study are listed in Table 2-1. In addition, the location of 2D and 3D seismic data is shown in Figure 2-1.

The quality of both 2D and 3D seismic data is generally good offshore and poor to moderate onshore. Onshore 2D seismic lines were mainly acquired pre-2000. Seismic resolution of both 2D and 3D seismic data is generally good enough for interpretation as far down as the Late Permian Unconformity. However, the 2D seismic data in the southern portion of the onshore basin is relatively poor. Therefore it is difficult to identify horizons with a high degree of confidence in the regions covered solely by 2D seismic data.

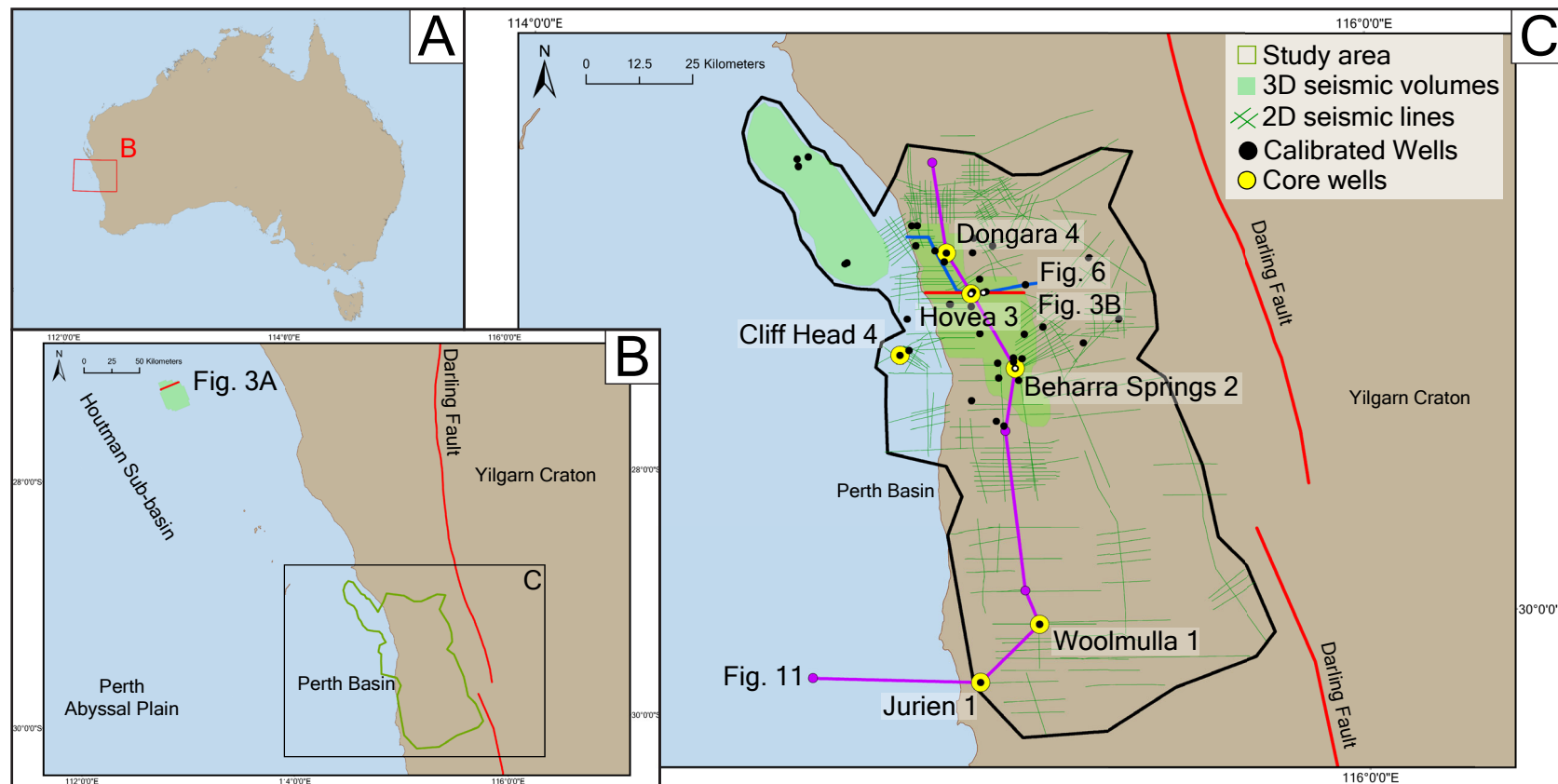


Figure 2-1. Location of the study area within the northern Perth Basin, interpreted 3D seismic volumes, 2D seismic lines, calibrated wells, core interpreted wells, and the location of lines used in subsequent figures.

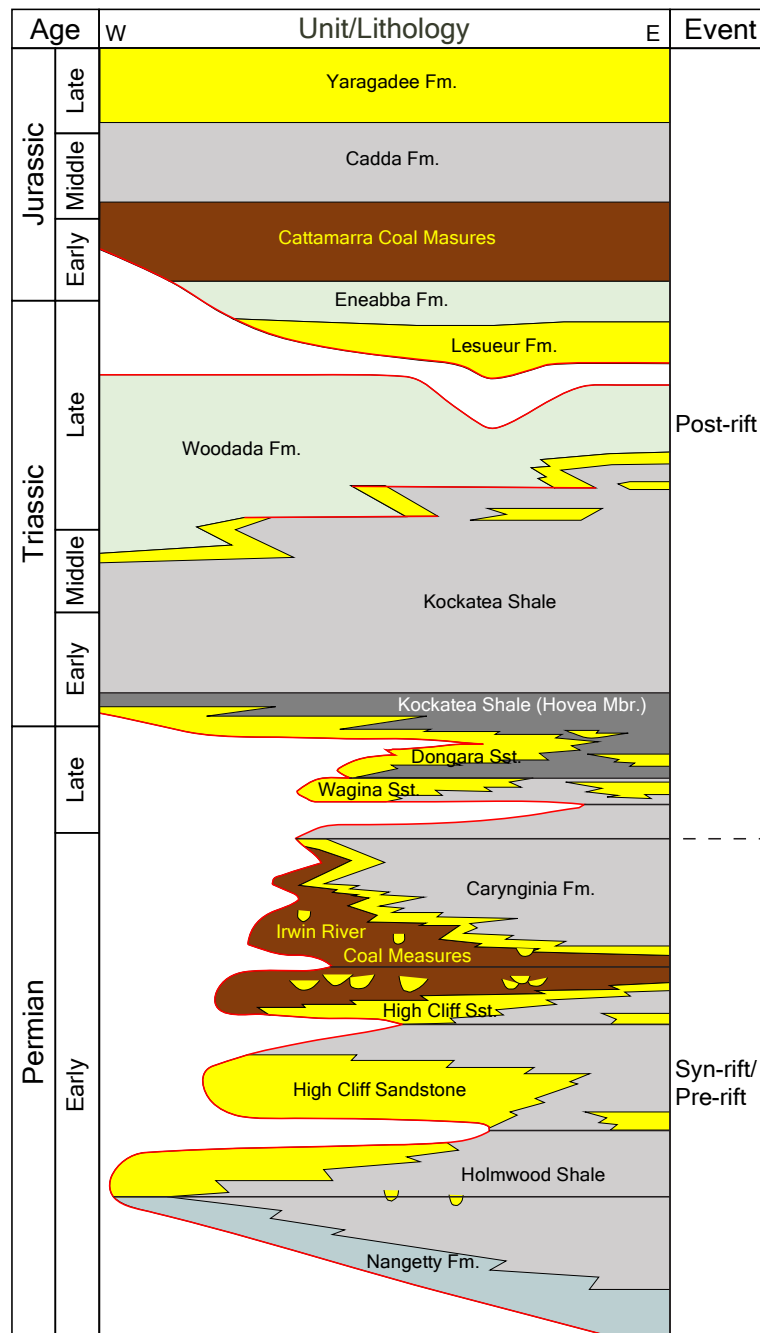


Figure 2-2. Stratigraphy of the northern Perth Basin (after Ferdinando et al., 2007; Mory et al., 2005). Light and dark grey: deeper water mudstone, yellow: shallow marine sandstone: brown: fluvial to deltaic sediments, bluish green (Nangetty Fm.): open marine glacial sediments, yellowish green (Eneabba and Woodada Fms.): fluvial to deltaic sediments.

Table 2-1. Details of 3D seismic volumes used in this study

Survey name	Setting	Year acquired	Area (km²)	Record depth (s)	Inline spacing (m)	Crossline spacing (m)
Beharra Springs 3D	Onshore	2002	210	3.8	20	20
Denison 3D	Onshore	2004	580	4.2	20	20
Dongara North 3D	Onshore	1994	70	4	12.5	12.5
Diana 3D	Marine	2008	620	4	25	12.5
Macallan 3D	Marine	2003	550	5.6	25	25

3.2 Seismic interpretation

Interpretation was conducted on time domain data in Petrel 2017 Software (Schlumberger). Interpreted seismic horizons were picked based on well tops from 46 wells (Figure 2-1 and Table 2-1), and synthetic seismograms were created for 3 wells (Beharra Springs 2, Hovea 3 and Apium 1) to confirm the tie between well tops and seismic data. Horizons were created for each 2D and 3D survey. All interpreted horizons were merged into a single horizon after eliminating overlap. The merged horizon data was used to create surfaces.

The Base and Top Kockatea Shale are the main seismic horizons interpreted for this study, and are used to identify basin geometry and paleogeography from the Late Permian to the Early Triassic. The Late Permian Unconformity was also interpreted where it is distinct from the Base Kockatea Shale, and where the Dongara and/or Wagina Sandstone are also present. The Late Permian Unconformity is a prominent unconformity in the northern Perth Basin. It forms an angular unconformity in the offshore, but it is represented by a disconformity or a subtle angular unconformity onshore. The Base Kockatea Shale is generally defined as a continuous reflection above the Late Permian Unconformity where the Dongara and/or Wagina Sandstone are present. The Top Kockatea Shale is defined as a continuous reflection at the top of the low amplitude seismic facies that represents the Kockatea Shale. However, the Woodada Formation, which generally lies above the Kockatea Shale, sometimes shares a similar lithology. Therefore, the seismic reflection corresponding to the Top Kockatea Shale is unclear in these places. In this case, the nearest reflection was picked. Based on correlation with wells, the vertical difference between the Top Kockatea Shale and the nearest picked reflection is small (~20ms), and this approximation does not affect the interpretation of regional structural trends and thickness variations.

3.3 Well data for core description

Forty-one wells cored some part of the Kockatea Shale in the northern Perth Basin. Six wells were selected for core description and interpretation (Beharra Springs 2, Cliff Head 4, Dongara 2, Hovea 3, Jurien 1 and Woolmulla 1; Figure 2-1 and Table 2-S1) because they contain cores near the base of the Kockatea Shale, covering both the Upper Permian and Lower Triassic sections, and have well-defined formation tops, well reports and mostly complete well logs. Furthermore, these wells are sufficiently well-spaced to evaluate the basin-scale lateral distribution of lithofacies and depositional setting. All core materials are stored in the Perth Core Library managed by the Department of Mines, Industry Regulation and Safety, Government of Western Australia.

3.4 TOC and Rock-Eval analyses

A set of 69 samples of the basal section of the Kockatea Shale from cores of 6 wells were selected and analysed for TOC and Rock-Eval analyses (Figure 2-9).

Samples were subjected to sonication for three intervals of 15 minutes each in a 9:1 DCM:MeOH (Dichloromethane:Methanol) mixture to remove any surface contamination. Sonicated samples were then ground into fine powder using a Rocklabs BTRM 1A rock grinder. TOC and Rock-Eval analyses was applied to ~1g rock samples.

A LECO Carbon Sulphur analyser was used for the TOC measurement after treatment with 3M HCl to remove carbonate. For the pyrolysis analysis, Vinci Technologies Rock-Eval 6 equipment was used with powdered rock samples. Thermal maturity was evaluated by measuring S1 (Free hydrocarbon in mg/g rock measured at lower temperatures), S2 (Hydrocarbon in mg/g rock measured through thermal cracking of kerogens at higher temperatures), T_{max} (temperature of maximum hydrocarbon production in °C) and S3 (amount of CO₂ in mg/g rock) using

IFP1600000 as standard. For the analysis, the initial temperature was set at 300 °C with 3 minutes holding time and programmed to heat to 650 °C at a rate of 25 °C/min. The derivative parameters such as HI ($S2*100/TOC$) and OI ($S3*100/TOC$) were also calculated.

The rock samples were ground at Curtin University and TOC and Rock-Eval analyses were conducted by Intertek (Intertek Group plc) in Welshpool, Western Australia.

4 Results

4.1 Seismic interpretation

4.1.1 Seismic stratigraphy

The seismic cross sections in Figure 2-3 shows typical structural and stratigraphic features from the northern Perth Basin. Below the Late Permian Unconformity, reflections generally dip to the west-southwest and are segmented by normal faults. Parallel reflector packages are correlated to the pre-rift High Cliff Sandstone and older sediments. The overlying wedge-shaped packages are correlated to the syn-rift Irwin River Coal Measures and Carynginia Formation. The Dongara and Wagina sandstones are thin, and are represented by only a few reflections on seismic data, making them difficult to distinguish. Where present, they are expressed as high-amplitude, flat-lying parallel reflectors overlying the angular Late Permian Unconformity.

The Kockatea Shale conformably overlies the Dongara Sandstone, and is expressed as a package of low-amplitude, parallel to semi-parallel reflections. Both time-thickness maps and seismic sections suggest limited variations in the thickness of this formation, although several local depocentres are evident on the time-thickness map (Figure 2-4C). A number of large normal faults cut the Kockatea

Shale; however, there are no obvious thickness variations across these faults, which are interpreted as being post-depositional.

The Woodada Formation conformably overlies the Kockatea Shale and generally shows higher amplitude reflections than in the Kockatea Shale. The Lesueur Sandstone conformably overlies the Woodada Formation and the top of the Lesueur Sandstone is eroded by the Valanginian Unconformity in the offshore. Where they are not eroded, the Eneabba and Cadda Formations conformably overlie the Lesueur Sandstone and show significant thickness variations across large normal faults. The Yarragadee Formation conformably overlies the Cadda Formation with poor definition of the top of the Yarragadee Formation due to poor seismic quality at shallower depth. The Cretaceous Winning Group overlies the Valanginian Unconformity. The reflections are sub-parallel to the seabed and are low amplitude. Paleogene and Neogene packages with low amplitude reflections downlap onto the top Cretaceous horizon.

4.1.2 Structure

Both Top and Base Kockatea Shale structure maps and seismic sections show large normal faults (Figures 2-3 and 2-4). The identified normal faults are consistent with faults that were previously identified by other authors (Cadman et al., 1994; Crostella & Backhouse, 2000; Hall & Kneale, 1992; Jablonski & Saitta, 2004; Jones et al., 2011; Mory et al., 2005; Quaife et al., 1994; Song & Cawood, 2000). The orientation of most onshore normal faults is NNW-SSE. The orientation rotates to NW-SE for the offshore normal faults. Faults dip to the east onshore and to the west offshore. In the northern onshore, NE-SW trending normal faults are also identified, such as the Allanooka Fault (Hall and Kneale, 1992). This fault dips to the south.

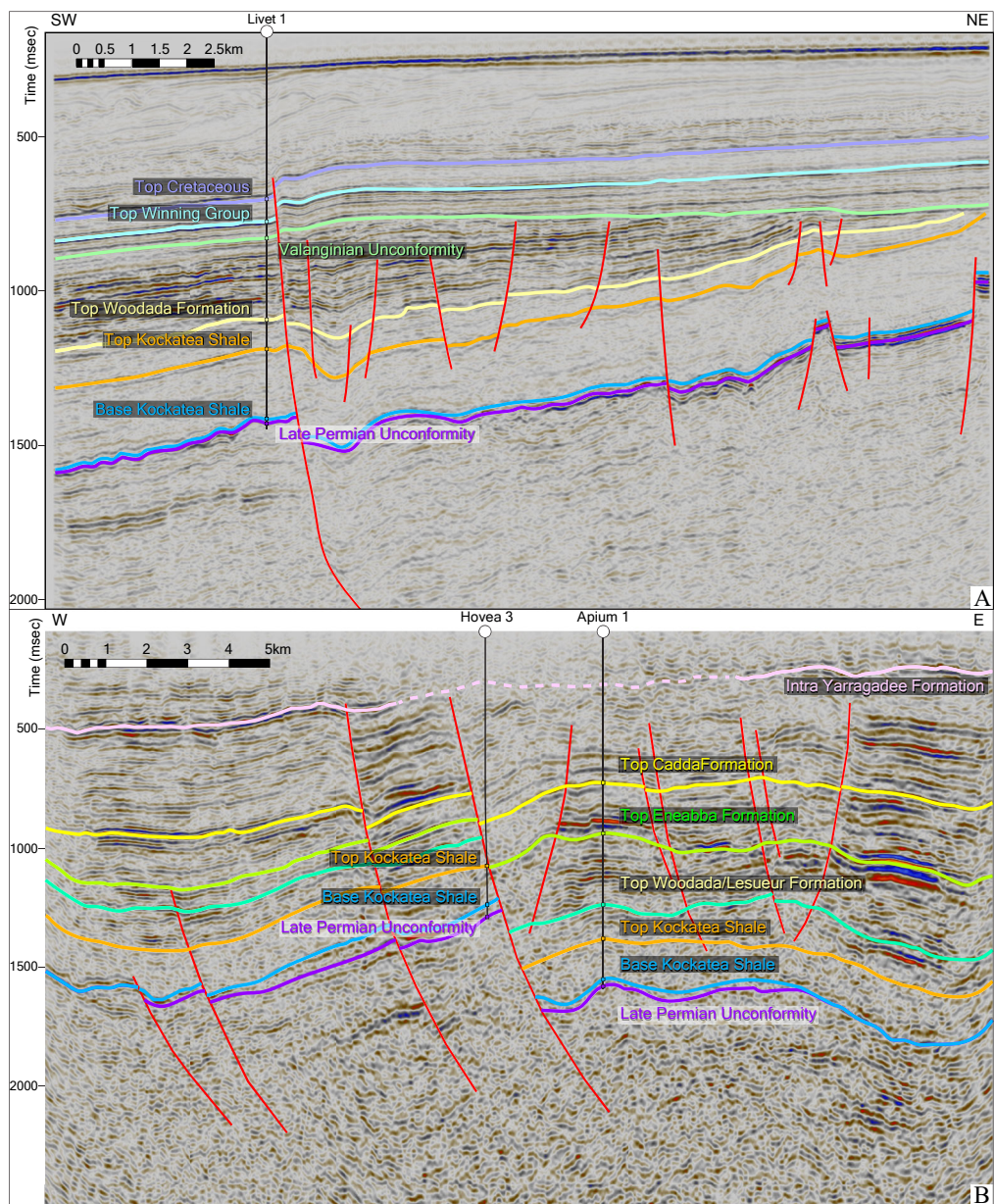


Figure 2-3. Typical seismic section from the offshore (A) and onshore (B) northern Perth Basin. Dark purple (Oldest horizon): Late Permian Unconformity, Blue: Base Kockatea Shale, Orange: Top Kockatea Shale, Cream yellow: Top Woodada Formation/Lesueur Sandstone, Green: Top Eneabba Formation, Pink: Intra Yarragadee Formation, Cream green: Valanginian Unconformity, Light blue: Top Winning Group, Light purple: Top Cretaceous. The location of the lines is shown in Figure 2-1.

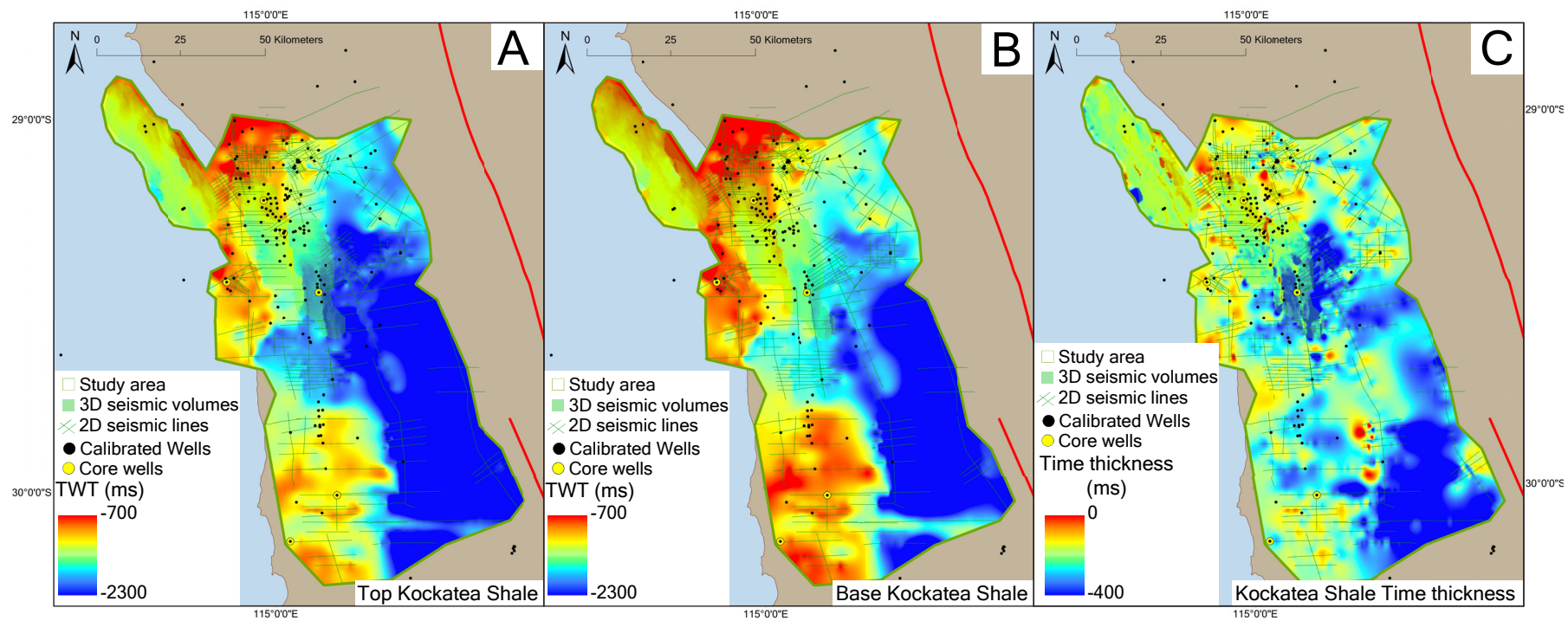


Figure 2-4. Time structure maps of the (A) Top Kockatea Shale and (B) Base Kockatea Shale horizons and (C) time thickness map of the Kockatea Shale.

4.1.3 Structural evolution

4.1.3.1 Permian rifting

The large normal faults in the offshore are associated with inclined Permian packages that are truncated by the Late Permian Unconformity, indicating pre- and syn-rift sediments, suggesting that these faults were active during the Permian rifting phase. However, the seismic reflections beneath the Late Permian Unconformity in the onshore seismic data are not as clearly inclined, and indicate that the focus of Permian rifting occurs offshore.

4.1.3.2 Early post-rift

The Wagina Sandstone directly overlies the Late Permian Unconformity, but is limited to the middle part of the Dandaragan Trough (Figure 2-6A). It is overlain by the Dongara Sandstone, which is more widespread and sits directly above the Late Permian Unconformity where the Wagina Sandstone is absent. Both units are absent from the south of the study area (Figure 2-6B). The Permian Kockatea Shale developed in the middle part of study area around Hovea 3 and Beharra Springs 2 (Figure 2-6C and D) and the Triassic Kockatea Shale sits directly above the Late Permian Unconformity in the south. The combined thickness of these Upper Permian units is variable (Figure 2-6D). They are thinner (~0-35 m) in the western part of the study area, which corresponds to the Beagle Ridge, and become thicker (> 50 m) away from the ridge, toward the Dandaragan Trough. This is also evident from seismic data. For example, in the Denison 3D seismic survey both the Dongara and Wagina Sandstones are recognised in wells and can be identified as a single unit on seismic data. An arbitrary seismic section (Figure 2-5) shows a major normal fault at the west end of the section, but the Dongara Sandstone can only be interpreted to the east of the fault, and is too thin (below seismic resolution) or absent to the west. The thickness variation, facies distribution and seismic stratigraphic relationships suggest a progressive infilling of remnant topography that remained after the Late Permian rift event. Alternatively, the thickness variation of the Upper Permian could be a

result of erosion of more widespread Upper Permian units above structural highs. Either way, this indicates the persistence of remnant topography following Permian rifting.

The thickness of both Kockatea Shale and Woodada Formation is similar across most large faults (Figure 2-3) which, combined with their position above the Late Permian Unconformity, allows these sequences to be interpreted as post-rift. However, there are some faults that propagate up from beneath the base of the Kockatea Shale, but do not cut the entire sequence (Figure 2-3), indicating that minor movement continued from the Permian rift event in some places. The Kockatea Shale also shows significant thickness variations across-faults in a few instances (i.e. ~280-470m in the foot wall and ~660-850m in the hanging wall, Figure 2-4C), indicating continued fault activity, or alternatively, additional infilling of remnant topography created by the Late Permian rift event.

4.1.3.3 Late Triassic to Early Cretaceous reactivation

The Permian structure is partly disguised by fault reactivation in the Upper Triassic to Early Cretaceous. This is indicated by distinct thickness variations in the Upper Triassic to Middle Jurassic Eneabba and Cadda Formations across large normal faults (Figure 2-3). On the other hand, the Upper Jurassic Yarragadee Formation is uniform in thickness, indicating a cessation of fault activity. In the offshore, the Upper Triassic Lesueur Sandstone package and younger units are rotated by fault movement after the deposition of this package because seismic reflections are parallel and uniform. The faults and the rotated sediments are truncated by the Valanginian Unconformity, and the thickness of the overlying post-Valanginian sediments, such as the Winning Group, are almost uniform. Therefore, the activity on these faults can be constrained to after the Middle Jurassic and before the development of the Valanginian Unconformity. Reactivation of older Permian faults is indicated by the greater rotation of Permian packages beneath the Late

Permian Unconformity. In addition, a number of new faults formed at this time, some of which detach in the Kockatea Shale.

4.2 Core description

Several different lithofacies are recognized in the Kockatea Shale, although “Shale” is used as a lithostratigraphic term in well reports. The Kockatea Shale contains dark and light coloured mudstones, microbial mat beds, storm/gravity sandstones, bioturbated siltstone and tidal sandstones (Figures 2-8 and 2-9).

4.2.1 Mudstone facies (Lighter coloured mudstone facies, darker coloured mudstone facies and fossiliferous facies)

Mudstone dominated intervals are identified in five of the six wells, but the mudstone type is variable and they are distinguished as: lighter coloured mudstone facies (medium grey mudstone), darker coloured mudstone facies (dark grey mudstone and black mudstone) and fossiliferous facies (Figure 2-8). The latest Permian section is dominated by lighter coloured mudstones and fossiliferous grey mudstones which contain shells, small fossil fragments and erosional features. Bioturbation is less common in the latest Permian mudstone interval of Hovea 3. In the lowest Triassic section, black and dark-grey mudstone (darker coloured mudstone) are dominant in the northern wells (Hovea 3, Dongara 4). Black mudstone is common in Hovea 3 and dark grey mudstone is mainly observed in Dongara 4. Parallel laminations are commonly observed in all the mudstone facies, suggesting that the original sedimentary structures are preserved. Mudstone from the southern wells (Jurien 1, Woolmulla 1) are a medium grey colour (lighter coloured mudstone). This facies is lighter in colour than both the darker coloured mudstone and microbial mat facies in the northern wells.

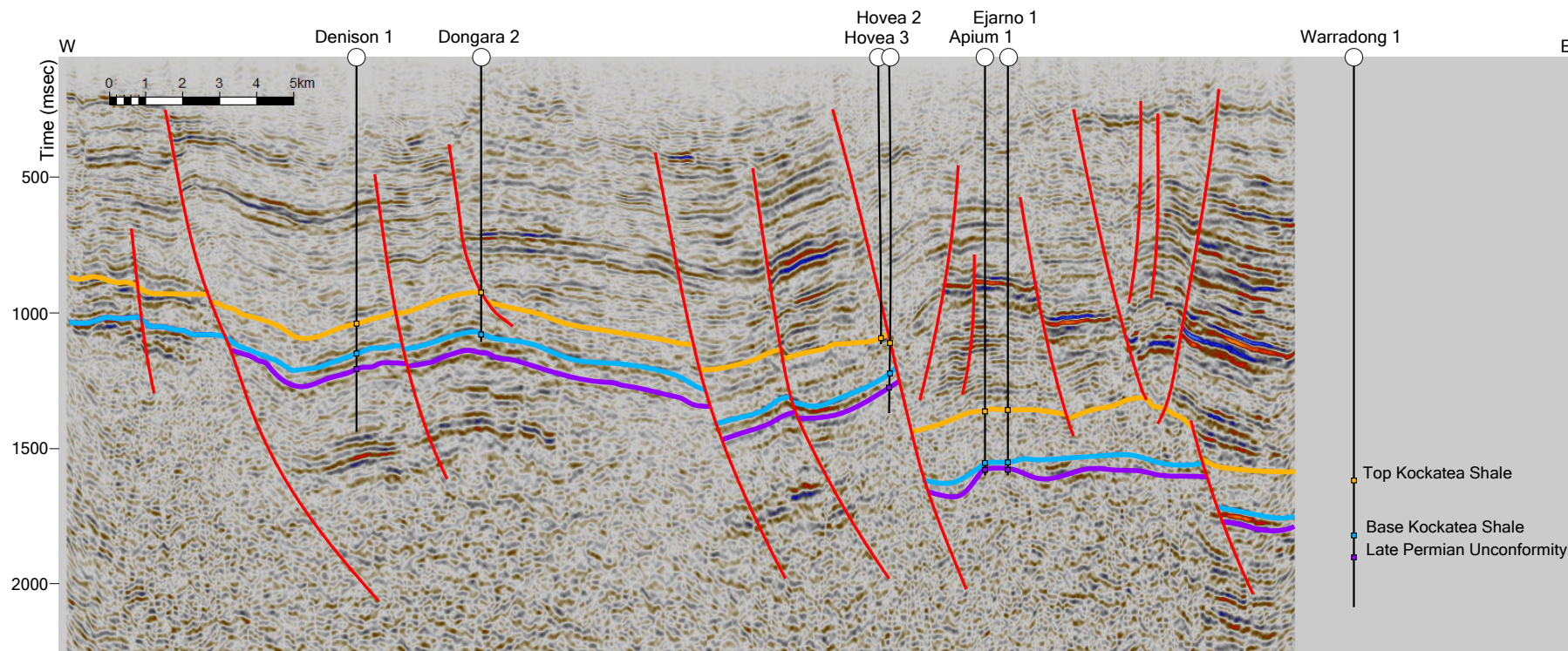


Figure 2-5. The seismic expression of Permian faults. The major fault at the west end of the section represents one of the remnant Permian faults, based on thickness variations within the Upper Permian Sandstones. Location of the line is shown in Figure 2-1. The colour of the seismic horizons is as in Figure 2-3.

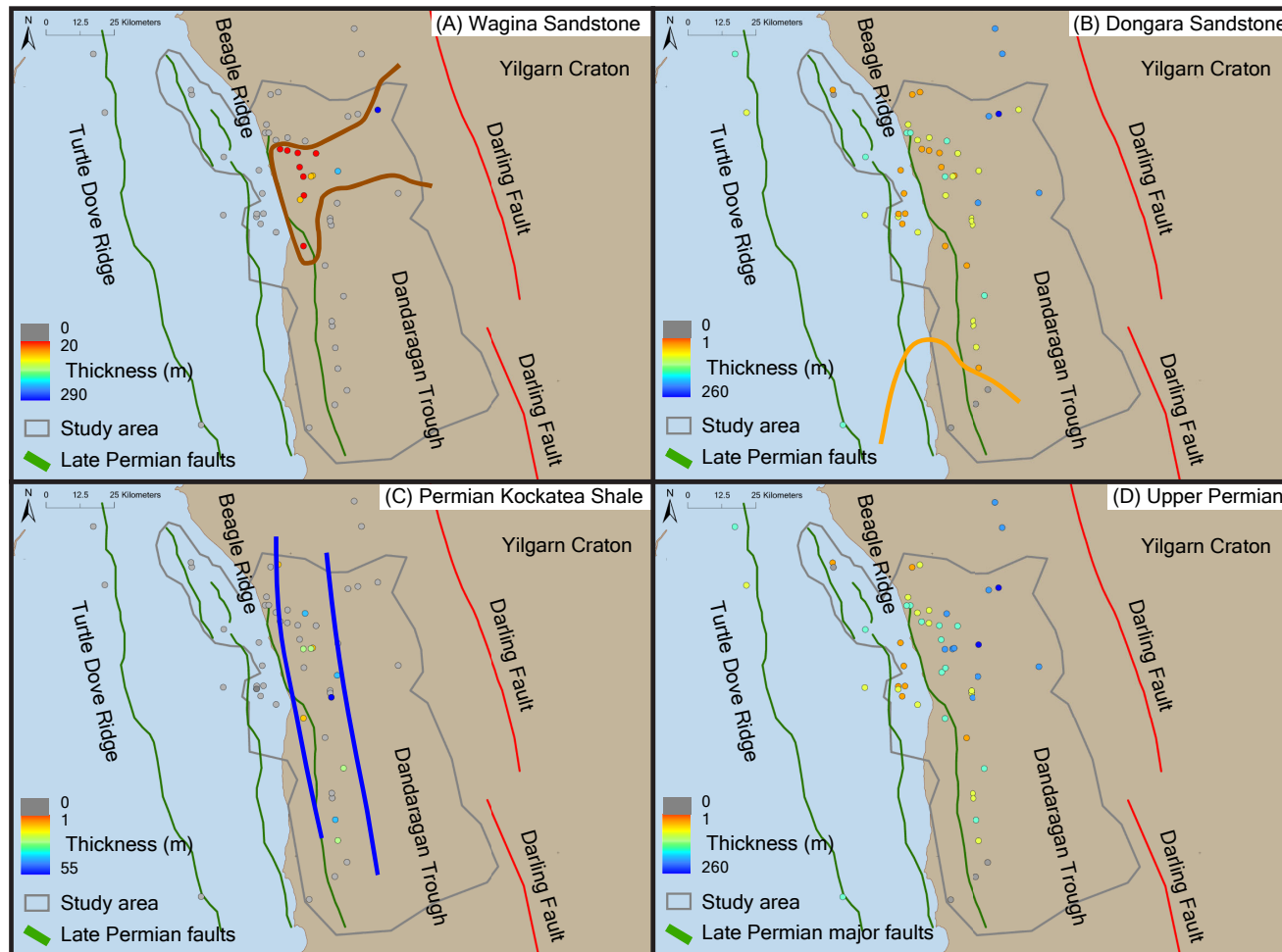


Figure 2-6. Thickness variation in (A) the Wagina Sandstone, (B) the Dongara Sandstone, (C) the Permian Kockatea Shale, and (D) Upper Permian (Wagina and Dongara Sandstones and Permian Kockatea Shale) based on well log data. The brown polygon in (A) shows the extent of the Wagina Sandstone. The orange polygon in (B) shows the limit of the Dongara Sandstone. The blue polygon in (C) shows the extent of Permian Kockatea Shale.

4.2.2 Microbial mat facies

Cliff Head 4, Hovea 3 and Dongara 4 contain layered carbonates exhibiting a mounded or swelling geometry, with the colour of the carbonate layers varying from grey to cream (Figures 2-7 and 2-8). Because of the mounded shape, the lateral thickness variation across individual beds is large, and is between 1 and 47 cm. The features of this lithofacies are similar to the cross-sections of stromatolites observed in outcrop (Chen et al., 2014; Luo and Chen, 2014), and this lithofacies was described as microbial beds in Hovea 3 by Thomas et al. (2004). Based on these features we interpret this lithofacies as containing microbial mats. In the Cliff Head 4 and Dongara 4 wells, the microbial mats are interbedded with dark grey mudstone. Both dark grey mudstone and black mudstone are interbedded with microbial mats in Hovea 3. The mudstone in this facies has no obvious bioturbation and parallel laminations are preserved, which are likely the original sedimentary structure. The contact between mudstone and microbial mat is sharp with no indication of a gradual lithologic change.

4.2.3 Tidal sandstone facies

Jurien 1 and Woolmulla 1 show alternations of sandstone and lighter coloured mudstone. Sandstone with wavy to flaser-like sedimentary structures and mud drapes are common in both wells (Figure 2-8). This indicates that the sandstone was probably deposited in a shallow water setting with a tidal influence. The thickness of each bed ranges from 1 to 45 cm. The contacts between sandstone and mudstone are generally sharp and the base of some sandstone units shows erosion into the underlying mudstone. Bioturbation is not apparent in Jurien 1, indicating that the original sedimentary structures are preserved in this well. Conversely, tidal sandstones in Woolmulla 1 experienced significant bioturbation with vertical burrows such as *Planolites* and *Cylindrichnus*. However, the bioturbation cannot be easily identified in mudstone within this facies. In addition, the intensity of the bioturbation is not enough to completely destroy the original sedimentary structures,

indicating a relatively sparse fauna. The preserved sedimentary structures of the sandstone units in Woolmulla 1 are similar to sandstones in Jurien 1 and indicate a probable tidal environment. The interbedded mudstone is medium-grey with parallel laminations.

4.2.4 Storm/gravity flow bed facies

Cliff Head 4 and Dongara 4 have an interval of interbedded mudstone and sandstone above and beneath the microbial mat facies. The thickness of the sandstone beds is generally 1-3 cm, and they are cream-yellow in colour. The sandstones are very fine to fine grained, and are massive, or contain weak parallel laminations (Figure 2-8). There is a gradation from massive to finer grained parallel laminated units, which suggests deposition by a waning current. In places they also show boudin-like thickness variations, and are interbedded with laminated mudstone, suggesting deposition by a storm or gravity flow.

4.2.5 Bioturbated Siltstone facies

Beharra Springs 2 contains chaotic, very poorly sorted siltstones in the Upper Permian. The facies is generally massive to weakly bedded. Bivalves and gastropods are frequently observed, although fossils are rare in other facies (Figure 2-8). The original sedimentary structures are not obvious, and individual trace fossils are also rare in this facies, implying intense bioturbation, although in some cases vertical *Ophiomorpha*-like trace fossils are identified. The facies is medium-dark grey in colour and lighter than both the mudstone in the microbial mat facies and the darker coloured mudstone facies.

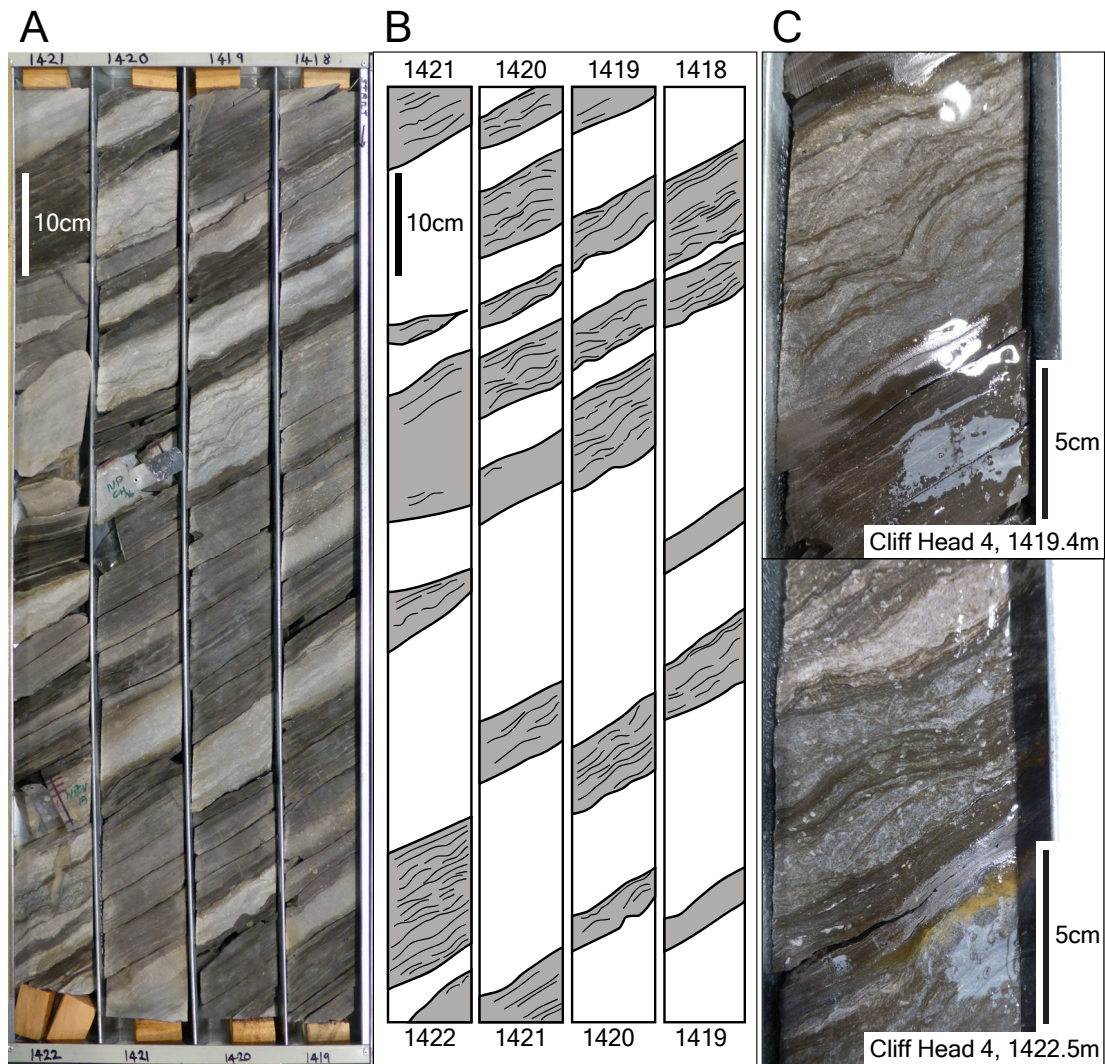


Figure 2-7. Microbial mats in Cliff Head 4. Grey colour beds in (B) represent the microbial mats.

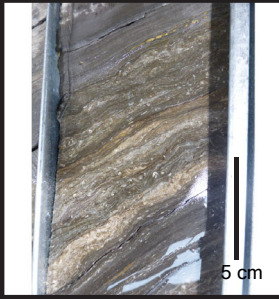
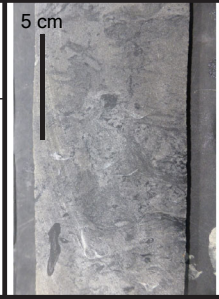
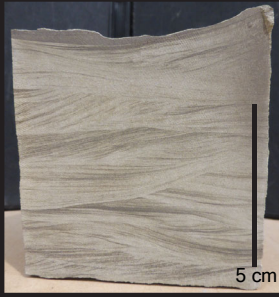
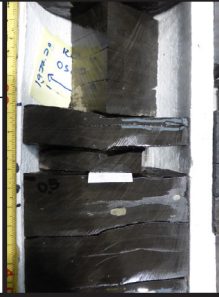
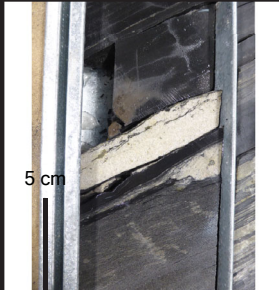

	<p>Microbial mat beds</p> <p>Cliff Head 4, Dongara 4, Hovea 3</p> <p>Calcareous mounded or swelling geometry. Various colour and thickness.</p>		<p>Bioturbated siltstone beds</p> <p>Beharra Springs 2</p> <p>Chaotic and very poorly sorted siltstones. Shells and trace fossils.</p>
	<p>Tidal sandstone</p> <p>Jurien 1, Woolmulla 1</p> <p>Wavy to flaser like sedimentary structures with mud drapes. Bioturbation in Woolmulla 1.</p>		<p>Darker coloured mudstone</p> <p>Dongara 4, Hovea 3</p> <p>Black mudstone, Dark grey mudstone. Less bioturbation in Lower Triassic preserving original sedimentary structures.</p>
	<p>Storm/gravity flow beds</p> <p>Cliff Head 4, Dongara 4</p> <p>Grading from massive to parallel lamination. Boundin-like thickness variation.</p>		<p>Lighter coloured mudstone</p> <p>Jurien 1, Woolmulla 1</p> <p>Medium grey mudstone. Less bioturbation preserving original sedimentary structures.</p>

Figure 2-8. Examples of typical lithologies observed in cores.

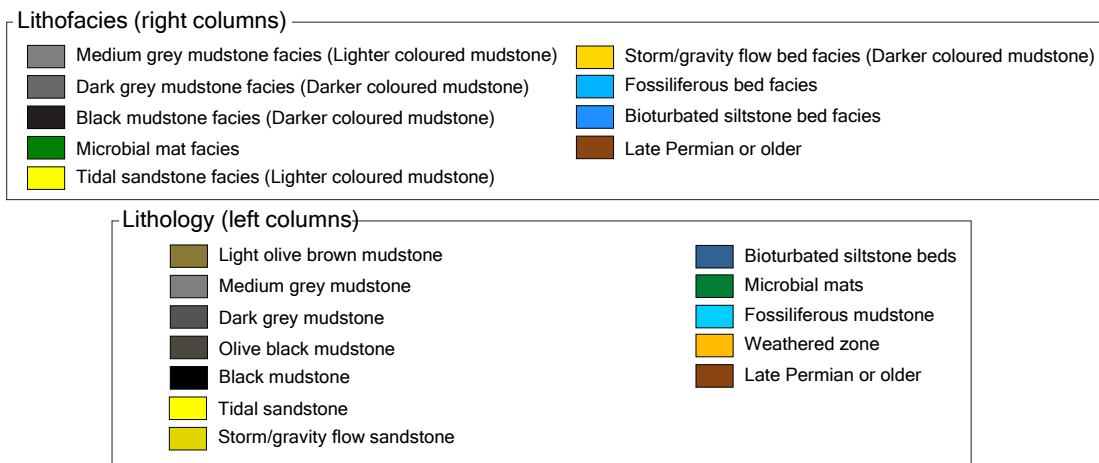
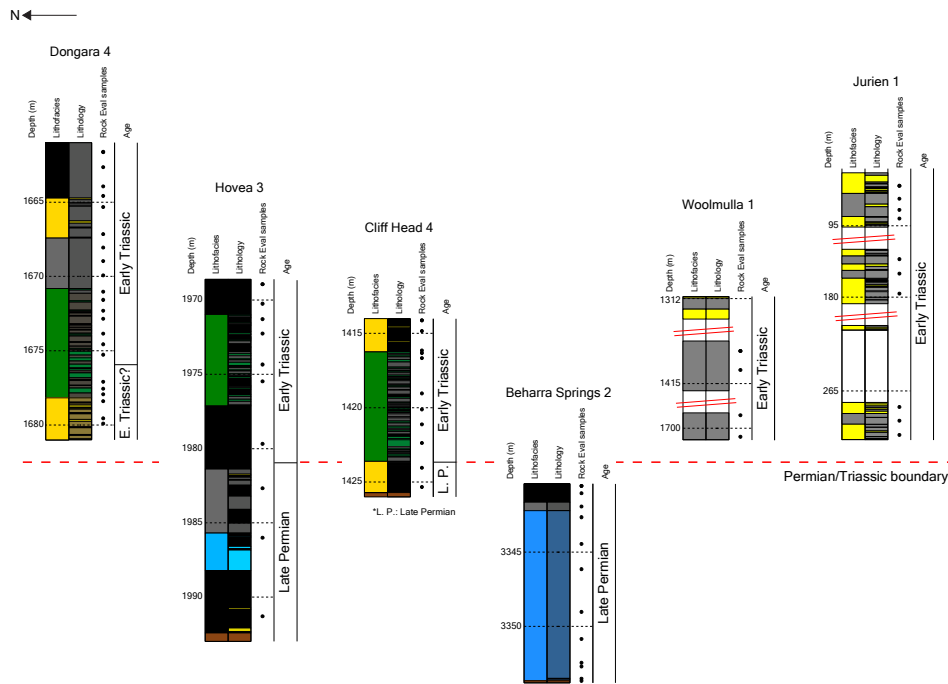


Figure 2-9. Core observation logs and correlation of six wells. Points represent the location of samples for TOC and Rock-Eval analyses.

4.3 Core- well log correlation

There is a good correlation between core observations and well log response. Figure 2-10 shows well logs (gamma ray (GR), sonic log, density log, neutron porosity log and resistivity log) where available and core logs of the six wells from which cores were described.

The typical response of the upper parts of the Kockatea Shale shows constant values of GR, sonic log, and neutron, with the high values of GR indicating the presence of mudstone. By contrast, some wells show an irregular log response in the lower part of the Kockatea Shale. In the irregular log facies, the GR shows a serrated pattern and has lower values. The sonic log also shows a similar serrated pattern to GR, with slightly higher values that tend to decrease at the top of the irregular log facies. The neutron porosity log also shows a serrated pattern similar to the GR and sonic logs, and a decrease in values at the top of the irregular log facies. In the interval below the irregular log facies, the GR shows large variation in values. The sonic log decreases to typical Kockatea Shale values. The neutron porosity log tends to be higher in value compared the irregular log facies and typical Kockatea Shale.

The microbial mat facies is identified in three cores (Cliff Head 4, Dongara 4, Hovea 3), and in all cases the lithofacies corresponds to the irregular log facies (Figure 2-10). In addition, cuttings description from these wells indicate the presence of limestone or calcareous lithofacies in the interval corresponding to the irregular log facies and microbial mats. Taken together, these observations indicate that the irregular log facies is a good proxy for identifying the development of microbial mats from wireline logs.

Beharra Springs 2, which does not contain the microbial mat facies in core, does not have this irregular log facies in the cored interval. However, an irregular log facies is identified on both the sonic and neutron porosity logs above the cored interval (Figure 2-10), although GR cannot be used because of poor data quality. In addition, the cuttings description of Beharra Springs 2 also show the presence of

limestone in the irregular log facies interval. Therefore, Beharra Springs 2 may have a microbial mat facies outside the cored interval. On the other hand, Jurien 1 and Woolmulla 1, which do not have microbial mat facies in the cored section, do not show the irregular log response in the cored interval or elsewhere in the well (Figure 2-10).

4.4 Microbial mat distribution

Well logs from 63 wells were analysed to identify the irregular log facies (Figure 2-11), starting from the cored wells (Dongara 4, Cliff Head 4, and Hovea 3), and extending to other wells. Wells with irregular log facies are well developed around Dongara 4, Hovea 3 and Cliff Head 4 which are located around the northern Beagle Ridge. On the other hand, wells without irregular log facies tend to be located on the southern Beagle Ridge and in the Dandaragan Trough. Wells with irregular log facies are also identified on the Turtle Dove Ridge (Batavia 1 and Geelvink 1).

4.5 Source rock quality

The darker coloured mudstone have high TOC and HI and low OI (TOC: up to 2.7 %, HI: up to 502 mg/gTOC, OI: 7-65mg/gTOC), suggesting good source rock potential with type II-III kerogen (Figure 2-12). The microbial mat facies also have high TOC and HI, as well as slightly high OI compared with the darker coloured mudstone (TOC: up to 3.4 %, HI: up to 579 mg/gTOC, OI: 16-410 mg/gTOC), suggesting similar or slightly enhanced source rock potential compared to the darker coloured mudstones (Figure 2-12). On the other hand, the lighter coloured mudstone has low TOC and HI and high OI indicating type III kerogen (TOC: 0.2-0.5 %, HI: 59-127 mg/gTOC, OI: 68-340 mg/gTOC), suggesting poor source rock potential (Figure 2-12).

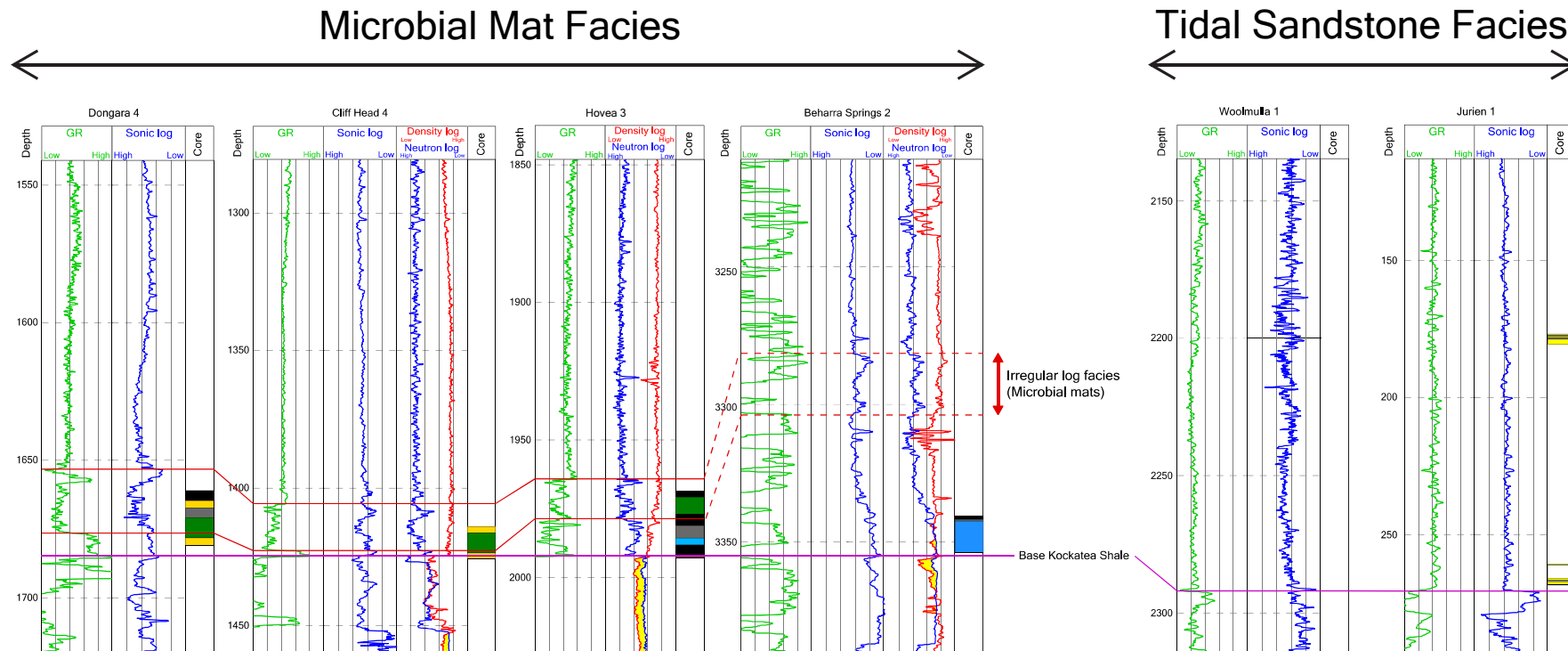


Figure 2-10. Well log correlation to microbial mat facies. The base Kockatea Shale is indicated by purple lines. The intervals between red lines correspond to either the presence of microbial mat facies in cores or the irregular log facies which indicates the development of microbial mats. Note that the GR log for Beharra Springs 2 is of poor quality. The microbial mat facies are absent from Jurien 1 and Woolmulla 1. Colours indicating the facies identified in core logs are the same as in Figure 2-9.

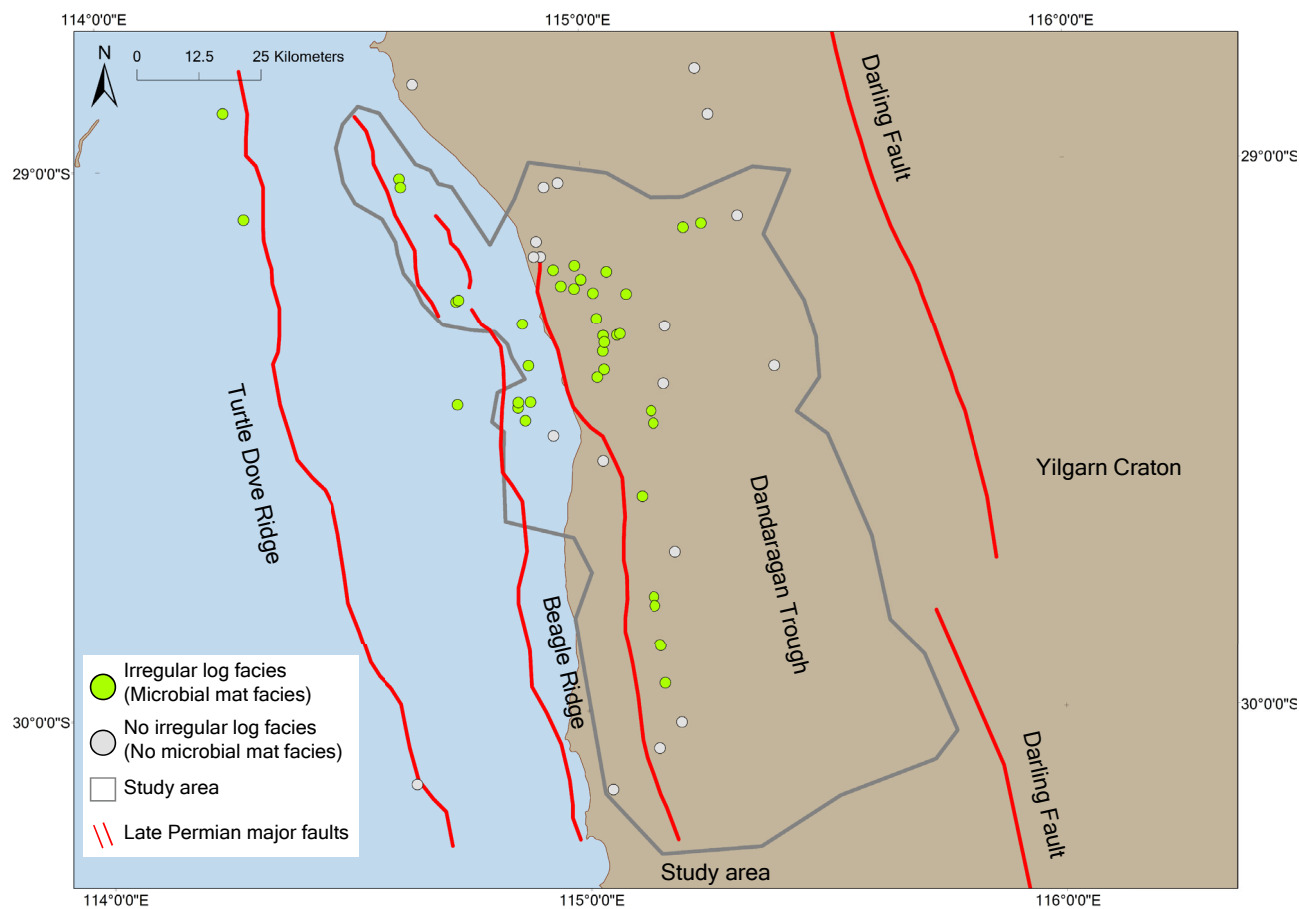


Figure 2-11. Irregular log facies distribution indicating the distribution of microbial mat facies on well logs.

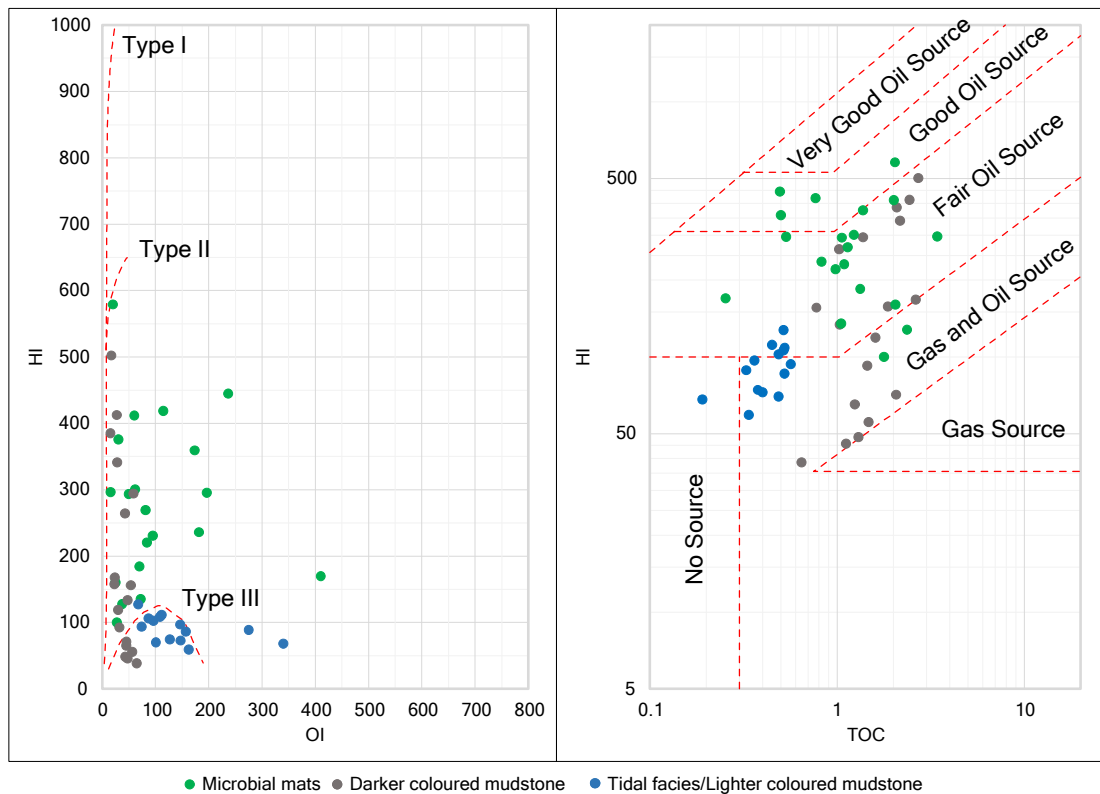


Figure 2-12. HI-OI and HI-TOC plots of each lithofacies.

5 Discussion

5.1 Lateral facies relationship

The distribution of different facies in the lower part of Kockatea Shale, based on core observations and well log analysis, is illustrated in Figure 2-13.

The age of the formations in each well is based on post-drill palynological studies (Georgiev et al., 2020; Gorter et al., 2009; Metcalfe et al., 2008; Thomas et al., 2004). The Wagina Sandstone is Lower Wuchiapingian in age. The Permian Kockatea Shale is the same age as the Changhsinian and Upper Wuchiapingian Dongara Sandstone, and thus they are considered lateral equivalents.

The cored Early Triassic sections of the Kockatea Shale are assigned to both the Griesbachian and Dienerian, which are parts of the Induan stage in the earliest Triassic. All of the microbial mats for which biostratigraphic samples are available indicate an Early Triassic age. Therefore it is highly likely that they are local representatives of typical Lower Triassic lithofacies, following a global pattern of microbial mat development (Foster et al., 2020; Kershaw et al., 2012; Luo et al., 2018; Woods, 2014). The Permo-Triassic boundary is located at the boundary of the sandstone (Dongara Sandstone) and mudstone (Kockatea Shale) in most wells, although this boundary is positioned within the Kockatea Shale in some wells where the Permian Kockatea Shale is present. The South Turtle Dove 1B well, located approximately 40 km west of Jurien 1, has a high proportion of sandstone in the lower part of the Lower Triassic which is assigned to the Bookara Sandstone, and is of equivalent age to the Kockatea Shale. The Permo-Triassic boundary in this well is positioned within sandstone facies, between the Dongara Sandstone and Bookara Sandstone.

5.2 Basin morphology

The morphology of the basin was created by Late Permian rifting. This persisted into the latest Permian and early Triassic post-rift phase either as remnant topography or as a consequence of minor continued fault movement, and influenced the distribution of both the Dongara and Wagina Sandstones and the Kockatea Shale (Figure 2-14A). The Beagle Ridge formed a structural high at this time. A second ridge, comprising the Turtle Dove Ridge and Geelvink High (Jones et al., 2011) is located offshore and is parallel to the Beagle Ridge. The evolution of this ridge is less easy to define because of poor seismic resolution above it. However, several 2D seismic sections indicate thickening of Permian strata beneath the Late Permian Unconformity in the footwall of major faults that bound the ridge, indicating that the faults were active during Permian rifting and that the ridge also formed a structural

high during the Upper Permian and Early Triassic. Structural lows such as the Dandaragan Trough are located both east and west of these highs. These structural lows form the main depocentres and Upper Permian to Lower Triassic sedimentary sequences become thin, or are affected by hiatuses or erosion on the structural highs.

5.3 Lower Triassic Paleogeography

Thomas and Barber (2004) identified the Permo-Triassic boundary in the Kockatea Shale although Georgiev et al. (2020) and Grice et al. (2005c) suggest that it may correspond to a short-lived hiatus. A major transgression commenced around the Permo-Triassic boundary. Consequently, mudstone deposition became dominant in the Early Triassic (Figure 2-14B and Figure 2-15). The main depocentres of the Kockatea Shale correspond to structural lows (Figure 2-4C). In addition, the onlap of reflections at the base of the Lower Triassic Kockatea Shale against a Permian fault (Figure 2-3) shows that the morphology created by Permian faults continued to influence the deposition of the lower part of the Kockatea Shale.

The Bookara Sandstone is interpreted to have been deposited in a shallow marine setting with higher clastic input (Mory & Iasky, 1996) in the southern part of the Turtle Dove Ridge. Interbedding of the sandstone with mudstone containing coal fragments in South Turtle Dove 1B suggests that there is terrigenous input. The tidal sandstone facies recognised in Jurien 1 and Woolmulla 1 developed in the southern part of the Beagle Ridge. The high proportion of sandstone interbedded with mudstone in the tidal sandstone facies also suggests proximity to clastic input or the basin margin.

The association of the tidal sandstone facies with the lighter coloured mudstone in both Jurien 1 and Woolmulla 1 suggests oxic conditions, resulting in the deposition of a poor quality source rock. The sediments of Cliff Head 4, Dongara 4 and Hovea 3 are dominated by darker coloured mudstone without significant

bioturbation, suggesting that the mudstone was deposited under anoxic to euxinic conditions, resulting in higher source rock quality. Anoxic to euxinic conditions have been reported by other authors (Grice et al., 2005a; Thomas & Barber, 2004) and related to global anoxia or euxinia after the end-Permian mass extinction (Erwin, 1994; Grice et al., 2005a; Knoll et al., 1996; Nabbefeld et al., 2010; Song et al., 2014; Twitchett et al., 2004; Whiteside & Grice, 2016; Wignall & Twitchett, 1996). In the north, some wells located on the Beagle Ridge (Bookara 1, Conder 1, Dibblers 1, Eleven Mile 1, and Wye 1) contain thin sandstone beds which are also assigned to the Bookara Sandstone, suggesting that clastic input and a shallower marine setting also developed in this area. The extent to which the Beagle Ridge persisted is unclear as other wells, such as Wakeford 1, are missing the Kockatea Shale as well as the Dongara and Wagina Sandstone and overlying units. This could either indicate a persistent high with a sedimentary hiatus during the latest Permian and Early Triassic or could be a result of erosion during Late Triassic to Early Cretaceous rifting.

Microbial mats are associated with the darker coloured mudstone found in the northern wells (Figures 2-9 and 2-11). In addition, the distribution of wells containing the irregular log facies shows that microbial mats were mainly developed on the Beagle Ridge, on its eastern flank and on the Turtle Dove Ridge (i.e. in shallower water depths) in the anoxic part of the basin. They are absent from the Dandaragan Trough (i.e. greater water depths) and from the southern part of the basin where there was greater clastic input (Bookara Sandstone) and more oxygenated waters (tidal sandstone facies and lighter coloured mudstones).

5.4 Controls on microbial mat distribution

Figure 2-15 shows a three dimensional representation of Early Triassic paleogeography showing the relationship between microbial mat development, clastic input, the presence of structural highs and relative paleo water depth.

Global anoxia or euxinia after the end-Permian mass extinction has been reported by several authors (Erwin, 1994; Grice et al., 2005a; Knoll et al., 1996; Nabbefeld et al., 2010; Song et al., 2014; Twitchett et al., 2004; Whiteside & Grice, 2016; Wignall & Twitchett, 1996) and created the conditions globally for the development of microbial mats during the post-extinction recovery phase (Foster et al., 2020; Kershaw et al., 2012; Luo et al., 2018; Woods, 2014). However, these global conditions were not developed uniformly throughout the northern Perth Basin.

It is clear from the occurrence of bioturbated sediments that oxic conditions existed in shallow water conditions on the southern margin of the basin. These are associated with tidal sediments and clastic input (Bookara Sandstone) which may have provided nutrients that supported the establishment of grazing organisms that would in turn have inhibited the development of microbial mats.

Anoxic and euxinic conditions were established in the northern part of the basin, due to a combination of its restricted nature and greater water depth. While the absence of other fauna in this setting promoted the development of microbial mats, they are restricted to the intra-basinal structural highs (Beagle Ridge and Turtle Dove Ridge) where substrates were shallow enough for sufficient light to penetrate for the mats to develop. Anoxic mudstones were deposited in the adjacent deeper water troughs which are less favourable settings for mat development.

6 Conclusion

Core observation reveals a large variation in lithofacies at the base of the Kockatea Shale: darker coloured mudstone, lighter coloured mudstone, microbial mats, tidal sandstone, storm/gravity sandstones and bioturbated mudstones. The microbial mats in cores correspond to an irregular log facies on wireline logs and this facies is recognized in several wells. In addition, seismic interpretation demonstrates that the paleogeography during the Late Permian and Early Triassic was influenced

by remnant topography from Permian faults. The integrated analysis of core, well logs and seismic data shows the lateral facies distribution within the Kockatea Shale and the factors that control the development and distribution of microbial mats in the northern Perth Basin.

The lighter coloured mudstones and interbedded tidal sandstone were deposited in an oxygenated tidal setting along with the shallow marine Bookara Sandstone. Anoxic to euxinic conditions were established elsewhere in the basin due to a combination of its restricted nature and its greater water depths, resulting in the deposition of darker coloured mudstone with higher TOC values. Microbial mats developed in association with the darker coloured mudstone, but were confined to intra-basinal structural highs (Beagle Ridge and Turtle Dove Ridge) which were shallow enough for sufficient light to penetrate to allow the development of mats, but in harsh conditions for other fauna.

During the period of ecological recovery that followed the end-Permian mass extinction, the development of microbial mats was controlled by two local factors.

1) Paleogeographic control: anoxic conditions away from the basin margin inhibited grazing organisms, allowing microbial mats to flourish while oxic, shallow marine, tidal settings with major clastic input closer to the basin margins promoted grazing organisms, which are unfavourable for microbial mat forming organisms.

2) Topographic control: topographic highs in the anoxic part of the basin provided good habitats with sufficient light for microbial mat forming organisms.

Therefore, the combination of global and local controls are important for the development of microbial mats.

The microbial mats and darker coloured mudstone have good source rock potential with higher TOC and HI. The distribution of these lithofacies matches the distribution of discovered hydrocarbon fields highlighting the more prospective parts

of the basin. On the other hand, the lighter coloured shale deposited under oxic condition has poor source rock quality with lower TOC and HI.

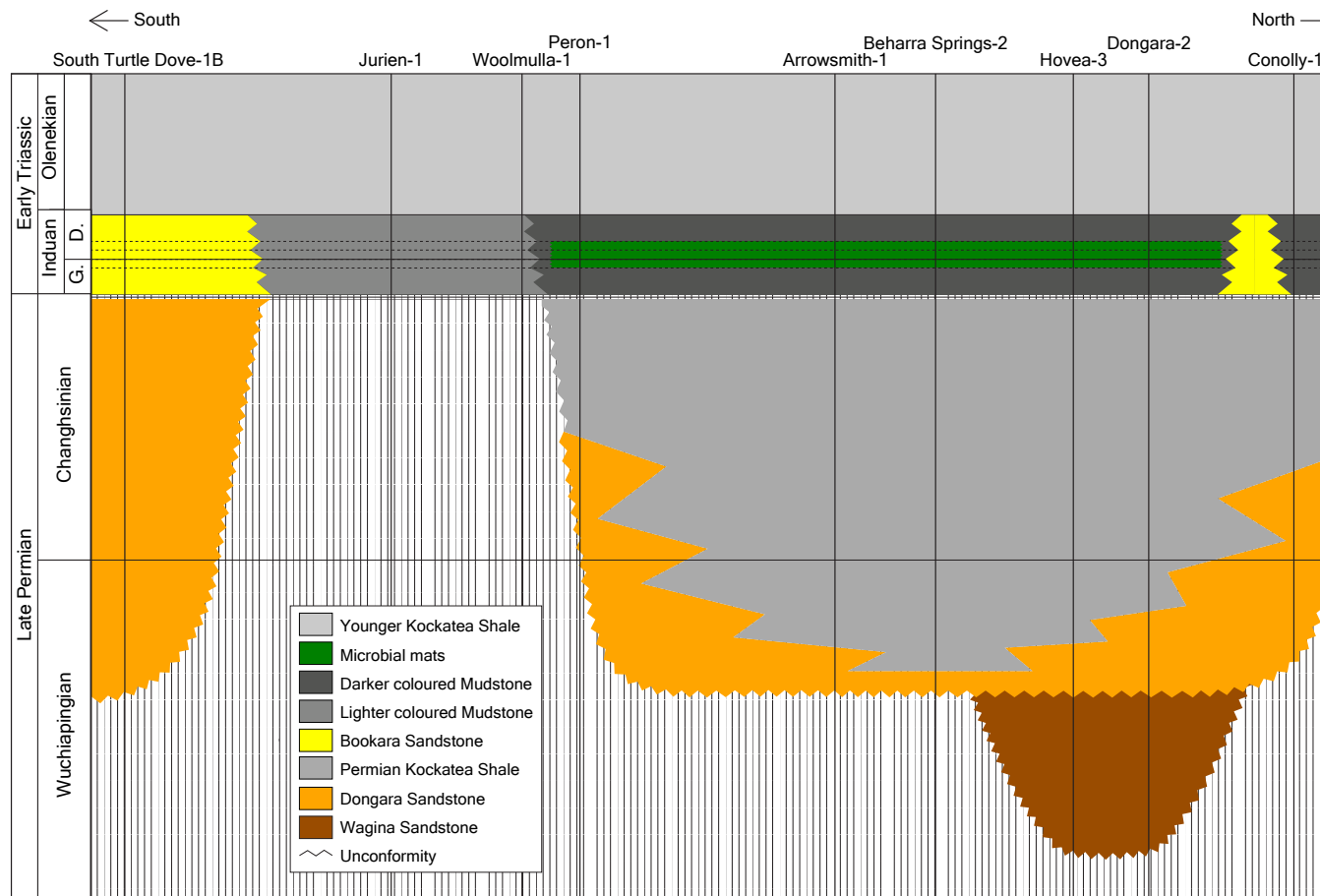


Figure 2-13. N-S oriented lateral facies relationship from Upper Permian Dongara and Wagina Sandstone to Lower Kockatea Shale. G. =Griesbachian and D. =Dienerian. Location of wells is shown in Figure 2-1.

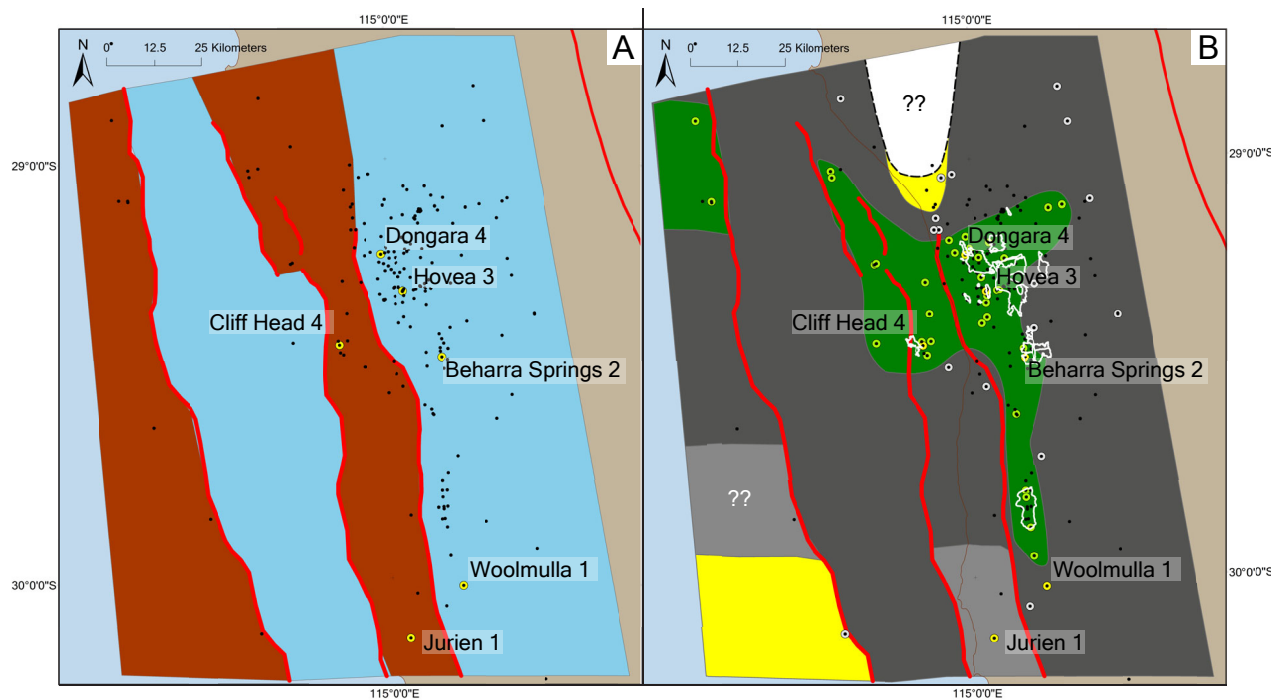


Figure 2-14. Map of (A) reconstructed basin morphology during Late Permian and Early Triassic and (B) paleogeography in Early Triassic. The blank area in (B) represents a hiatus during the Early Triassic or erosion during younger rifting.

Basin morphology (A)

Early Triassic paleographic map (B)

- Structural highs
- Structural lows

- Bookara Sandstone
- Lighter Mudstone (Oxic & Tidal)
- Darker Mudstone (Anoxic/Euxinic)

- Microbial Mats
- Field polygons

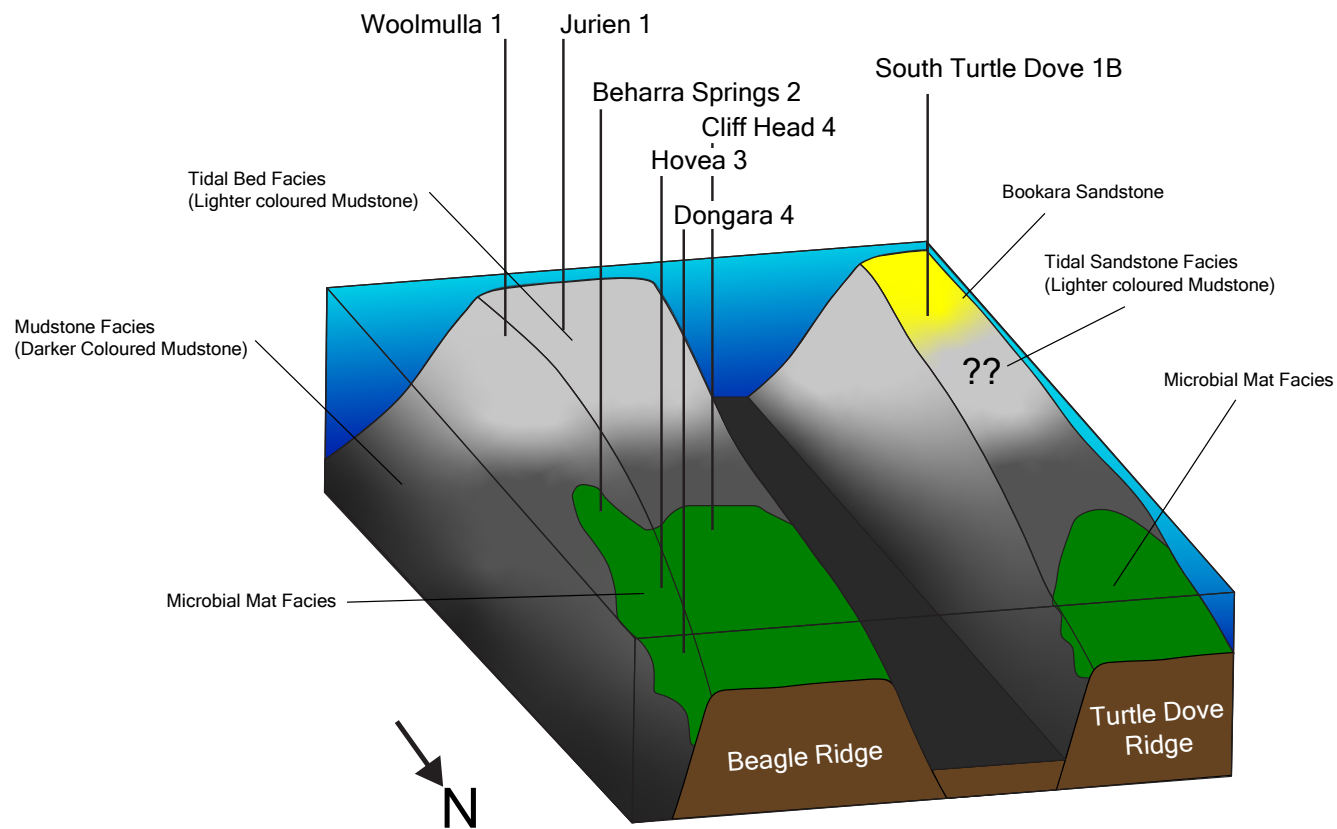


Figure 2-15. Paleogeographic model of the Early Triassic viewed from north. Not to scale.

Acknowledgements

This study is a part of PhD research by the first author funded by INPEX Corporation. The authors thank Geoscience Australia and the Geological Survey of Western Australia for providing seismic and well log data. The Geological Survey of Western Australia is also thanked for permission to observe cores and collect rock samples (G004177), Intertek for TOC and Rock-Eval analyses, Schlumberger for providing Petrel interpretation software and ESRI for providing ArcGIS software. We also thank Darren Ferdinando and an anonymous referee for reviews of an earlier version of the manuscript which have improved it significantly.

References

- Boreham, C.J., Hope, J.M., Hartung-Kagi, B., van Aarssen, B.J.K., 2000. More sources for gas and oil in Perth Basin. *AGSO Res. Newsl.* 5–9.
- Cadman, S.J., Pain, L., Vuckovic, V., 1994. Perth Basin, Western Australia. *Aust. Pet. Accumulations Rep.* 10, 1–103.
- Chen, Z.Q., Wang, Y., Kershaw, S., Luo, M., Yang, H., Zhao, L., Feng, Y., Chen, J., Yang, L., Zhang, L., 2014. Early Triassic stromatolites in a siliciclastic nearshore setting in northern Perth Basin, Western Australia: Geobiologic features and implications for post-extinction microbial proliferation. *Glob. Planet. Change* 121, 89–100. <https://doi.org/10.1016/j.gloplacha.2014.07.004>
- Crostella, A., 1995. An evaluation of the hydrocarbon potential of the onshore northern perth basin, western australia. *Geol. Surv. West. Aust. Report* 43, 67p.
- Crostella, A., Backhouse, J., 2000. *Geology and Petroleum Exploration of the Central and Southern Perth Basin.* West. Aust. Geol. Surv. Report 57, 85p.
- Dawson, D., Grice, K., Alexander, R., 2005. Effect of maturation on the indigenous δD signatures of individual hydrocarbons in sediments and crude oils from the Perth Basin (Western Australia). *Org. Geochem.* 36, 95–104. <https://doi.org/10.1016/j.orggeochem.2004.06.020>
- Erwin, D.H., 1994. The Permo-Triassic extinction. *Nature* 367, 231–236.
- Ferdinando, D., Baker, J.C., Gongora, A., Pidgeon, B.A., 2007. Illite/Smectite clays preserving porosity at depth in Lower Permian reservoirs, northern Perth Basin. *APPEA J.* 47, 69–88. <https://doi.org/10.1071/aj06004>
- Foster, W.J., Heindel, K., Richoz, S., Gliwa, J., Lehrmann, D.J., Baud, A., Kolar-Jurkovšek, T., Aljinović, D., Jurkovšek, B., Korn, D., Martindale, R.C., Peckmann, J., 2020. Suppressed competitive exclusion enabled the proliferation of Permian/Triassic boundary microbialites. *Depos. Rec.* 6, 62–74.

<https://doi.org/10.1002/dep2.97>

- Georgiev, S. V., Stain, H.J., Yang, G., Hannah, J.L., Böttcher, M.E., Grice, K., Holman, A.I., Turgeon, S., Simonsen, S., Cloquet, C., 2020. Late Permian–Early Triassic environmental changes recorded by multi-isotope (Re-Os-N-Hg) data and trace metal distribution from the Hovea-3 section, Western Australia. *Gondwana Res.* 88, 353–372. <https://doi.org/10.1016/j.bbamem.2019.183135>
- Ghori, K.A.R., 2015. Petroleum systems of the Perth Basin, Western Australia. *Search Discov.* 10805, 20p.
- Gorter, J., Nicoll, R.S., Metcalfe, I., Willink, R., Ferdinando, D., 2009. The Permian–Triassic boundary in Western Australia: evidence from the Bonaparte and Northern Perth basins—exploration implications. *APPEA J.* 49, 311–336. <https://doi.org/10.1071/AJ08020>
- Grice, K., Cao, C., Love, G.D., Böttcher, M.E., Twitchett, R.J., Grosjean, E., Summons, R.E., Turgeon, S.C., Dunning, W., Jin, Y., 2005a. Photic zone euxinia during the Permian-Triassic superanoxic event. *Science.* 307, 706–709. <https://doi.org/10.1126/science.11104323>
- Grice, K., Nabbefeld, B., Maslen, E., 2007. Source and significance of selected polycyclic aromatic hydrocarbons in sediments (Hovea-3 well, Perth Basin, Western Australia) spanning the Permian-Triassic boundary. *Org. Geochem.* 38, 1795–1803. <https://doi.org/10.1016/j.orggeochem.2007.07.001>
- Grice, K., Summons, R.E., Grosjean, E., Twitchett, R.J., Dunning, W., Wang, S.X., Böttcher, M.E., 2005b. Depositional conditions of the Northern Onshore Perth Basin (Basal Triassic). *APPEA J.* 45, 263–274.
- Grice, K., Twitchett, R.J., Alexander, R., Foster, C.B., Looy, C., 2005c. A potential biomarker for the Permian-Triassic ecological crisis. *Earth Planet. Sci. Lett.* 236, 315–321. <https://doi.org/10.1016/j.epsl.2005.05.008>

-
- Grosjean, E., Hall, L., Boreham, C., Buckler, T., 2017. Source rock geochemistry of the offshore northern Perth Basin: regional hydrocarbon prospectivity of the offshore northern Perth Basin. *Rec. 2017/18. Geosci. Aust. Canberra*.
<https://doi.org/10.11636/Record.2017.018>
- Haig, D.W., Martin, S.K., Mory, A.J., McLoughlin, S., Backhouse, J., Berrell, R.W., Kear, B.P., Hall, R., Foster, C.B., Shi, G.R., Bevan, J.C., 2015. Early Triassic (early Olenekian) life in the interior of East Gondwana: Mixed marine-terrestrial biota from the Kockatea Shale, Western Australia. *Palaeogeogr. Palaeoclimatol. Palaeoecol.* 417, 511–533.
<https://doi.org/10.1016/j.palaeo.2014.10.015>
- Hall, P.B., Kneale, R.L., 1992. Perth Basin rejuvenated. *APPEA J.* 32, 33–43.
- Jablonski, D., Saitta, A.J., 2004. Permian To Lower Cretaceous Plate Tectono-Stratigraphic Development of the Western Australian Margin. *APPEA J.* 44, 287–328. <https://doi.org/10.1071/AJ03011>
- Jones, A., Kennard, J.M., Nicholson, C.J., Bernardel, G., Mantle, D., Grosjean, E., Boreham, C.J., Jorgensen, D.C., Robertson, D., 2011. New exploration opportunities in the offshore northern Perth Basin. *APPEA J.* 51, 45–78.
<https://doi.org/10.1071/aj10003>
- Kershaw, S., Crasquin, S., Li, Y., Collin, P.Y., Forel, M.B., Mu, X., Baud, A., Wang, Y., Xie, S., Maurer, F., Guo, L., 2012. Microbialites and global environmental change across the Permian-Triassic boundary: A synthesis. *Geobiology* 10, 25–47. <https://doi.org/10.1111/j.1472-4669.2011.00302.x>
- Knoll, A.H., Bambach, R.K., Canfield, D.E., Grotzinger, J.P., 1996. Comparative earth history and late Permian mass extinction. *Science.* 273, 452–457.
<https://doi.org/10.1126/science.273.5274.452>
- Langhi, L., Ross, A., Crooke, E., Jones, A., Nicholson, C., Stalvies, C., 2014. Integrated hydroacoustic flares and geomechanical characterization reveal

-
- potential hydrocarbon leakage pathways in the Perth Basin, Australia. *Mar. Pet. Geol.* 51, 63–69. <https://doi.org/10.1016/j.marpetgeo.2013.11.016>
- Luo, M., Chen, Z.Q., 2014. New arthropod traces from the Lower Triassic Kockatea Shale Formation, northern Perth Basin, Western Australia: Ichnology, taphonomy and palaeoecology. *Geol. J.* 49, 163–176. <https://doi.org/10.1002/gj.2506>
- Luo, M., Chen, Z.Q., Shi, G.R., Feng, X., Yang, H., Fang, Y., Li, Y., 2018. Microbially induced sedimentary structures (MISSs) from the Lower Triassic Kockatea Formation, northern Perth Basin, Western Australia: Palaeoenvironmental implications. *Palaeogeogr. Palaeoclimatol. Palaeoecol.* 519, 236–247. <https://doi.org/10.1016/j.palaeo.2018.06.040>
- McIlldowie, M., Alexander, R., 2005. Identification of a novel C33 n-alkylcyclohexane biomarker in Permian-Triassic sediments. *Org. Geochem.* 36, 1454–1458. <https://doi.org/10.1016/j.orggeochem.2005.06.009>
- Metcalf, I., Nicoll, R.S., Willink, R.J., 2008. Conodonts from the Permian-Triassic transition in Australia and position of the Permian-Triassic boundary. *Aust. J. Earth Sci.* 55, 365–377. <https://doi.org/10.1080/08120090701769480>
- Mory, A.J., 1994. Structural evolution of the onshore northern Perth basin, Western Australia. *Sediment. Basins West. Aust. Proc. Pet. Explor. Soc. Aust. Symp. Perth 1994* 781–790.
- Mory, A.J., Haig, D.W., McLoughlin, S., Hocking, R.M., 2005. Geology of the northern Perth Basin, Western Australia- A field guide. *Geol. Surv. West. Aust.* 2005/9, 71p.
- Mory, A.J., Iasky, R.P., 1996. Stratigraphy and structure of the onshore northern Perth Basin, Western Australia. *Geol. Surv. West. Aust. Report 46*, 101pp.
- Nabbefeld, B., Grice, K., Summons, R.E., Hays, L.E., Cao, C., 2010. Significance of

polycyclic aromatic hydrocarbons (PAHs) in Permian/Triassic boundary sections. *Appl. Geochemistry* 25, 1374–1382.

<https://doi.org/10.1016/j.apgeochem.2010.06.008>

Norvick, M.S., 2004. Tectonic and Stratigraphic History of the Perth Basin. *Geosci. Aust.* 2004/16, 18p.

Quaife, P., Rosser, J., Pagnozzi, S., 1994. The structural architecture and stratigraphy of the offshore northern Perth Basin, Western Australia, in: *The Sedimentary Basins of Western Australia: Proceedings of the Petroleum Exploration Society of Australia Symposium*. pp. 811–822.

Scott, J., 1994. Source rocks of Western Australia - distribution, character and models, in: *The Sedimentary Basins of Western Australia: Proceedings of the Petroleum Exploration Society of Australia Symposium*. pp. 141–155.

Song, H.H.H., Wignall, P.B., Chu, D., Tong, J., Sun, Y., Song, H., He, W., Tian, L., 2014. Anoxia/high temperature double whammy during the Permian-Triassic marine crisis and its aftermath. *Sci. Rep.* 4, 4132.
<https://doi.org/10.1038/srep04132>

Song, T., Cawood, P.A., 2000. Structural styles in the Perth Basin associated with the Mesozoic break-up of Greater India and Australia. *Tectonophysics* 317, 55–72.
[https://doi.org/10.1016/S0040-1951\(99\)00273-5](https://doi.org/10.1016/S0040-1951(99)00273-5)

Thomas, B.M., 1979. Geochemical analysis of hydrocarbon occurrences in northern Perth Basin, Australia. *Am. Assoc. Pet. Geol. Bull.* 63, 1092–1107.
<https://doi.org/10.1306/2F9184BE-16CE-11D7-8645000102C1865D>

Thomas, B.M., Barber, C.J., 2004. A re-evaluation of the hydrocarbon habitat of the northern Perth Basin. *APPEA J.* 44, 59–92.

Thomas, B.M., Willink, R.J., Grice, K., Twitchett, R.J., Purcell, R.R., George, A.D., Tye, S., Alexander, R., Foster, C.B., Barber, C.J., George, A.D., Tye, S.,

Alexander, R., Foster, C.B., Unique, C.J.B., Barber, C.J., 2004. Unique marine Permian-Triassic boundary section from Western Australia. *Aust. J. Earth Sci.* 51, 423–430.

Twitchett, R.J., Krystyn, L., Baud, A., Wheeley, J.R., Richoz, S., 2004. Rapid marine recovery after the end-Permian mass-extinction event in the absence of marine anoxia. *Geology* 32, 805–808. <https://doi.org/10.1130/G20585.1>

Whiteside, J.H., Grice, K., 2016. Biomarker Records Associated with Mass Extinction Events. *Annu. Rev. Earth Planet. Sci.* 44, 581–612. <https://doi.org/10.1146/annurev-earth-060115-012501>

Wignall, P.B., Twitchett, R.J., 1996. Oceanic anoxia and the end permian mass extinction. *Science* (80-.). 272, 1155–1158. <https://doi.org/10.1126/science.272.5265.1155>

Woods, A.D., 2014. Assessing Early Triassic paleoceanographic conditions via unusual sedimentary fabrics and features. *Earth-Science Rev.* 137, 6–18. <https://doi.org/10.1016/j.earscirev.2013.08.015>

Appendix

Supplementary data

Table 2-S1. List of wells used for seismic interpretation and core observation. “*” symbol in the core column represents the wells used for core observation.

Well name	Longitude	Latitude
Apium 1	115.0710306	-29.3159611
Apium North 1	115.0626222	-29.2868222
Arramall 1	115.0972073	-29.5897553
Beharra Springs 1	115.1411643	-29.464129
Beharra Springs 2*	115.1449391	-29.4780041
Beharra Springs 3	115.1408531	-29.4554399
Beharra Springs South 1	115.1528667	-29.5035833
Bonniefield 1	114.9144776	-29.1702867
Central Yardarino 1	115.0513492	-29.199241
Cliff Head 4*	114.8673558	-29.4460592
Denison 1	114.9561116	-29.2244036
Dongara 2	114.9781396	-29.2484314
Dongara 4*	114.9835006	-29.2294589
Drakea 2	115.0609389	-29.4030139
Dunsborough 1	114.6254361	-29.0241028
Dunsborough 2	114.628175	-29.0392889
Ejarno 1	115.0773318	-29.3138419
Erregulla 1	115.398944	-29.3759831
Frankland 1	114.7386889	-29.249525

Frankland 2	114.743679	-29.246809
Hakia 1	115.0960339	-29.2159313
Hovea 1	115.0422111	-29.3168333
Hovea 2	115.0447361	-29.3135778
Hovea 3*	115.041275	-29.3179778
Illyarrie 1	115.0466834	-29.2296897
Jingemia 1	114.9909917	-29.3394861
Jingemia 2	114.9897139	-29.3392722
Jurien 1*	115.0483333	-30.1444444
Lilac 1	114.6523192	-29.0198047
Mentelle 1	114.8891708	-29.43592
Mooratara 1	114.9102669	-29.2128481
Mountain Bridge 1	115.1153792	-29.6001207
Mt Adams 1	115.1681145	-29.4057102
Mungenooka 1	115.2135018	-29.3909879
North Erregulla 1	115.3275556	-29.2443172
North Yardanogo 1	115.1027273	-29.4663213
Rakrani 1	114.9011942	-29.170209
Redback 1	115.1620861	-29.4577917
Redback 2	115.1616028	-29.4575944
Robb 1	115.0383406	-29.5453188
South Yardanogo 1	115.1045209	-29.497936
Twin Lions 1	114.88645	-29.3695361
Warradong 1	115.1727495	-29.3002664
West Erregulla 1	115.3103839	-29.4258069
West White Point 1	115.0411759	-29.3448758
Woolmulla 1*	115.1942326	-30.0232145

Chapter 3

Photic zone redox oscillations and microbial mat development recorded by Early Triassic sediments of the Perth Basin: A geochemical approach

Takashi Taniwaki, Chris Elders, Michael E. Böttcher, Alex I. Holman and Kliti Grice

Geochimica et Cosmochimica Acta, submitted

Submitted: 1 September 2021

Abstract

Photic zone euxinia (PZE) has previously been identified in the Early Triassic Kockatea Shale of the northern Perth Basin, based on the presence of biomarkers such as isorenieratane derived from isorenieratene of green sulfur bacteria. However, green and purple sulfur bacteria can also occur in microbial mats. In this study we present a basin-scale assessment of biomarkers associated with open water column PZE and/or microbialites. The lithofacies from the Early Triassic of the northern part of the northern Perth Basin consist of dark coloured mudstones (black to dark grey) with microbialites, which were deposited away from basin margins. These samples were found to contain okenane, chlorobactane and isorenieratane derived from carotenoid pigments of purple, green-green and green-brown sulfur bacteria, respectively. These biomarkers were not observed in the light coloured mudstones (medium grey) formed under oxic conditions in a tidal environment with higher clastic input close to the basin margins in the southern part of the basin where shallow marine sandstones were also deposited. Okenane and chlorobactane were abundant in facies containing microbialites which developed in a shallow water setting on intra-basinal structural highs. The development of oxic conditions near the basin margins in the Perth Basin provided refuges for organisms during the mass extinction event. Okenane was more abundant in the microbialite facies compared with the dark coloured mudstone deposited under PZE. C_{33} *n*-alkylcyclohexane (C_{33} ACH) has previously been described as a biomarker associated with ecosystem collapse during the lower Triassic, and its ratio relative to the C_{34} *n*-alkane was elevated in facies that contain abundant microbialites. Mercury (Hg)-total reduced inorganic sulfur (TRIS) and Hg-total organic carbon (TOC) plots show a positive correlation, supporting the development of euxinia as sulfide sequesters Hg. The high Hg/TRIS values in microbialite facies supports mat development with high Hg concentrations. The values of $\delta^{13}C_{OM}$ and $\delta^{34}S$ were isotopically lighter in microbialite facies when compared with mudstones formed under PZE, although samples deposited under oxic conditions showed the isotopically lightest $\delta^{13}C_{OM}$ and

isotopically heaviest $\delta^{34}\text{S}$. The variation in $\delta^{13}\text{C}_{\text{COM}}$ probably reflects the different carbon fixation pathways of various sulfur bacteria while it appears that the fractionation of $\delta^{34}\text{S}$ values between PZE and microbialites is a result of the differences in the microbial community structure and the higher relative abundance of purple sulfur bacteria. In addition, fluctuations between PZE and oxic conditions were identified throughout the sampled intervals attributed to fluctuations in the depth of the chemocline. Under the shallower chemocline, PZE developed widely in the basin, even in shallower waters. Under the deeper chemocline PZE was absent or limited to deeper water, and oxic conditions developed in shallower water. The fluctuations of PZE and oxic conditions in the northern Perth Basin suggests the development of multiple episodes of harsh environmental conditions after the end-Permian mass extinction, similar to those identified in other regions (e.g., Meishan in China and Peace River in Canada).

1 Introduction

The Late Permian mass extinction is the largest extinction event of the Phanerozoic (Whiteside and Grice, 2016). During this time, about 95 % of marine and 70 % of terrestrial species were wiped out. It is assumed that volcanic activity associated with a Large Igneous Province (LIP) related to the break-up of Pangea led to the mass extinction (Reichow et al., 2009; Whiteside and Grice, 2016). After the end-Permian mass extinction, anoxic conditions were established periodically until the beginning of the Middle Triassic. As a result, the recovery from the mass extinction took around 8-9 million years. This is a longer recovery period compared to other extinction events, and consequently biodiversity was profoundly damaged. However, local oxygenated shallow water settings are good refuges for biotic recovery (Beatty et al., 2008; Benton, 2016; Chen et al., 2012; Chen & Benton, 2012; Foster et al., 2015; Hallam, 1991; Hofmann et al., 2011; Kaiho et al., 2016; Knaust, 2010; Payne et al., 2004; Retallack et al., 1996; Sahney & Benton, 2008; Sedlacek et al., 2014; Shen et al., 2015; Shen et al., 2019a,b; Song et al., 2014; Twitchett et al.,

2004; Wei et al., 2015; Woods et al., 1999; Zatoń et al., 2016; Zhang et al., 2014; Zhang et al., 2017). The LIP released large quantities of CO₂ and other gases leading to a rise in global temperature by up to 6°C. It has been shown previously that the Panthalassa and Paleo Tethys Seas were devoid of oxygen (Grice et al., 2005a; Hays et al., 2007; Nabbefeld et al., 2010; Wignall and Twitchett, 1996). In many global locations, photic zone euxinia (PZE) in ancient seas has been identified based on the abundance of the biomarker isorenieratane at or across the extinction horizon (Grice et al., 2005a). PZE is characterized by the development of sulfidic anoxic bottom waters separated from the oxic surface waters by a chemocline within the photic zone. H₂S is derived from sulfate-reducing bacteria which anaerobically degrade organic matter in sediments and/or at the water column interface (Manske et al., 2005; Pfenning, 1978; Sass et al., 2001). Under PZE, different types of anoxygenic photosynthetic sulfur bacteria reside at the chemocline. These include purple, green-green and green-brown sulfur bacteria that utilise H₂S as an electron donor in photosynthesis to fix carbon dioxide in the presence of sunlight. These organisms make specific carotenoid pigments (purple sulfur bacteria: okenone; green-green sulfur bacteria: chlorobactene; green-brown sulfur bacteria: isorenieratene) and bacteriochlorophylls (Bchls) (purple sulfur bacteria: Bchl *a* and *b*; green-green and green-brown sulfur bacteria: Bchls *c*, *d* and *e*) to be able to capture longer wavelengths of the electromagnetic spectrum for photosynthesis. Such pigments can give rise to a range of biomarkers in sediments (*e.g.*, okenane, chlorobactane, isorenieratane and methyl *iso*-butyl maleimides derived from the macrocycle of Bchls *c*, *d* and *e*). These biomarkers have been reported in oils and sediments and are thus indicators of open water column PZE (Clifford et al., 1998; Grice et al., 2005a, 2005c, 1996; Maslen et al., 2009; Pedentchouk et al., 2004; Sousa Júnior et al., 2013; Tulipani et al., 2015). However, similar anaerobic photosynthetic sulfur bacteria can occur in microbialites, which are especially dominated by purple sulfur bacteria (Brocks and Schaeffer, 2008; Fox et al., 2020; Pagès et al., 2014; Schaefer et al., 2020).

In the northern Perth Basin located on the western coast of Western Australia (WA), the development of PZE has been identified in Early Triassic source rocks and crude oils based on biomarker distributions (Thomas and Barber, 2004; Grice et al., 2005a,b). Microbialite facies have been documented in both outcrops and cores (Chen et al., 2014; Luo et al., 2018; Luo and Chen, 2014; Thomas et al., 2004). However, the organic geochemical characteristics of microbialites across the Perth Basin have not been fully evaluated. In this study, we conducted biomarker and stable isotope analyses of Kockatea Shale rock samples including microbialites to evaluate the geochemical characteristics of such facies and to explore the basin-scale extent of PZE. Sedimentary mercury (Hg) contents have been used to estimate the impact of disturbances like volcanic activity on the paleoenvironment (Georgiev et al., 2020; Grasby et al., 2017; Scaife et al., 2017; Shen et al., 2019a, 2019b; Sial et al., 2020; Wang et al., 2019), including a West-Australian section (Georgiev et al., 2020). These investigations were extended in the present study.

2 Geological setting

The northern Perth Basin experienced several rift, subsidence and uplift events from the Devonian through to the Early Cretaceous (Figures 3-1 and 3-2) (Jablonski and Saitta, 2004; Norvick, 2004). One of the most prominent events is Late Permian rifting, the end of which is marked by the angular Late Permian Unconformity (Taniwaki et al., 2021). NNW-SSE to NW-SE trending normal faults were developed during this phase of rifting. The Late Permian to Early Triassic post-rift geometry of the basin was shaped by topographic remnants of this rift event (Beagle Ridge, Turtle Dove Ridge and associated structural lows such as the Dandaragan Trough). This in turn controlled the distribution of the Late Permian sediments and the distribution of facies at the base of the Early Triassic Kockatea Shale (Figures 3-1 and 3-2) (Taniwaki et al., 2021).

The Late Permian Wagina Sandstone was deposited as post-rift sediment above the Late Permian Unconformity. This was followed by deposition of the Late Permian to Early Triassic Kockatea Shale in a post-rift transgressive deeper water setting. The Permian part of the Kockatea Shale follows deposition of the Wagina Sandstone and is in part laterally equivalent to the Dongara Sandstone. The Early Triassic part of the Kockatea Shale conformably overlies all of the Permian sediments and during this phase of deposition the Kockatea Shale is laterally equivalent to the shallow marine Bookara Sandstone which was developed near the basin margins (Mory and Iasky, 1996). The overlying sediments of Middle Triassic to Late Jurassic age include the Woodada Formation, Lesueur, Eneabba and Cattamarra Coal Measures, and Cadda and Yarragadee formations, and Lower Cretaceous Winning Group.

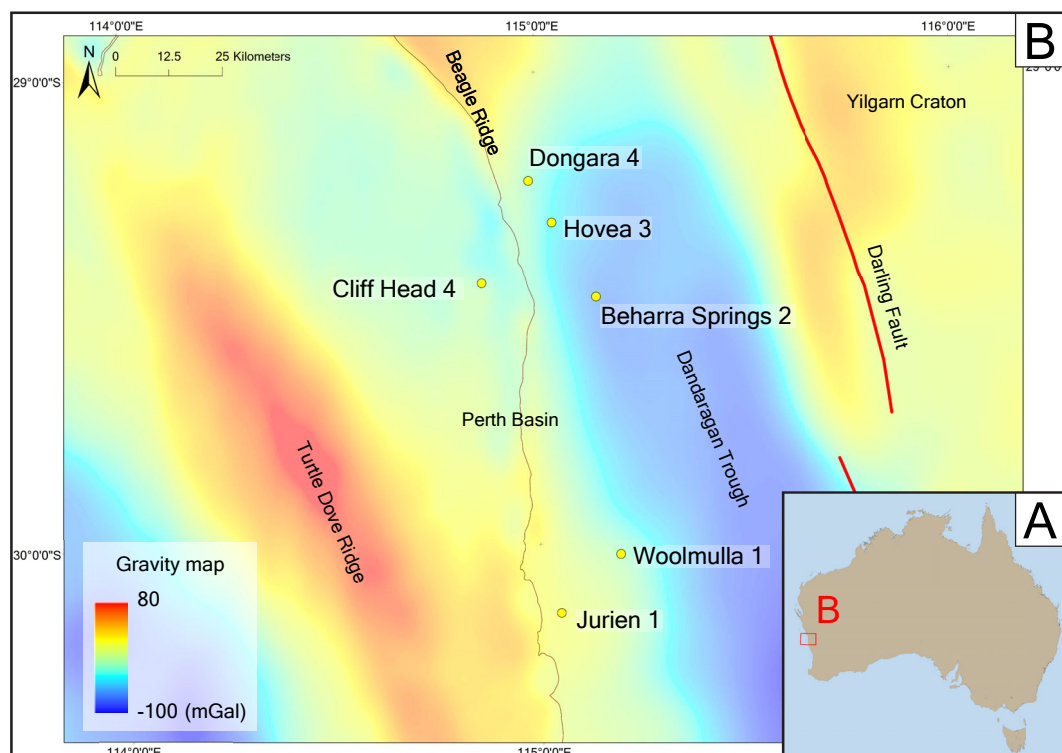


Figure 3-1. (A) Inset map for B, showing the location of the study area within Australia. (B) Location map of the northern Perth Basin wells used for rock sample

analysis, with gravity anomaly map as background showing the basin geometry. The public domain data used for the gravity map is published by the Scripps Institution of Oceanography (Sandwell et al., 2013, 2014; Sandwell and Smith, 2009). Black points represent the location of major towns within the map.

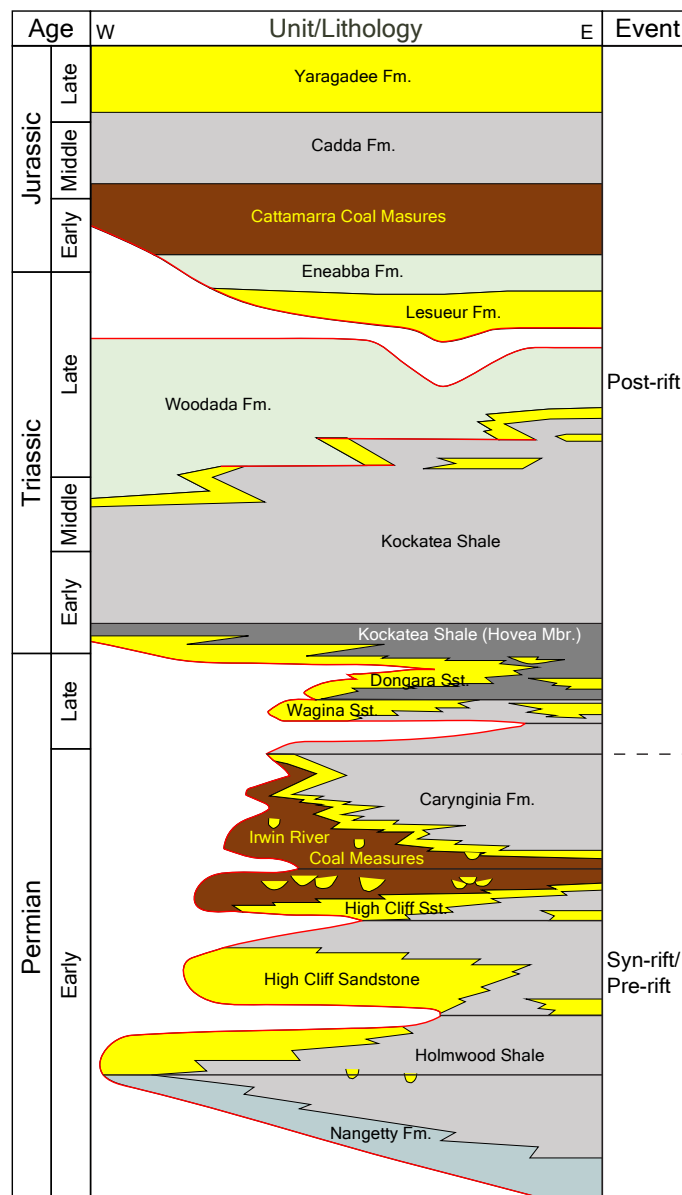


Figure 3-2. Stratigraphy of the northern Perth Basin (Ferdinando et al., 2007). Light and dark grey: deeper water mudstone, yellow: shallow marine sandstone: brown:

fluvial to deltaic sediments, bluish green (Nangetty Fm.): open marine glacial sediments, yellowish green (Eneabba and Woodada Fms.): fluvial to deltaic sediments. Fm.=Formation, Fms=Formations, Sst.=Sandstone, and Mbr.=Member.

3 Data & Methodology

3.1 Samples and lithology

Core material was obtained from the Perth Core Library managed by the Department of Mines, Industry Regulation and Safety, Government of Western Australia. A set of 38 rock samples obtained from the base of the Kockatea Shale from six wells (Beharra Springs 2, Cliff Head 4, Dongara 4, Hovea 3, Jurien 1 and Woolmulla 1) covering the Late Permian to Early Triassic were used in this study (Figures 3-1-3-3 and Table 3-1). All rock samples were assigned to specific lithofacies (dark coloured mudstone, light coloured mudstone and microbialites) based on core observations (Figure 3-4) (Taniwaki et al., 2021) and their geological age was determined from post-drill well reports and publications (Thomas et al., 2004; Metcalfe et al., 2008; Gorter et al., 2009; Georgiev et al., 2020). Other facies that were identified, but not sampled, include sandstone deposited by storm/gravity flows and tidal facies

The dark coloured mudstone in each facies other than the tidal facies consists of black and dark grey mudstones, and is dominant in the northern wells (Hovea 3, Dongara 4, and Cliff Head 4). Black mudstone is commonly observed in Hovea 3 and Cliff Head 4 and dark grey mudstone is common in Dongara 4 and Cliff Head 4. Parallel laminations are commonly identified in the dark coloured mudstone, suggesting that the original sedimentary structures are preserved.

Microbialites were only identified from the northern wells (Cliff Head 4, Hovea 3, and Dongara 4), and consist of layered calcareous beds with mounded or swelling geometry. Dark coloured mudstones (dark grey to black) are always interbedded with

microbialites. In Cliff Head 4 and Dongara 4, dark grey mudstones are interbedded with microbialites. In Hovea 3, both black and dark grey mudstones are associated with microbialites.

The light coloured mudstone facies are distinguished from the dark coloured mudstone facies by their medium grey colour and are dominant in the southern wells (Jurien 1 and Woolmulla 1). These mudstones are characterised by parallel laminations, and are interbedded with tidal sandstones. The interbedded tidal sandstones and light coloured mudstones show some degree of bioturbation.

3.2 Extraction of sediments and fractionation

Rock samples were gently sonicated for 15 minutes (three times) in 9:1 dichloromethane: methanol (DCM: MeOH) to remove any surface contamination. Samples were then powdered using a Rocklabs BTRM 1A rock grinder. Powdered samples (10-30 g) were Soxhlet extracted (72 hours with 9:1 DCM: MeOH). A small amount of activated copper turnings was placed in the round-bottom flask with extracted bitumen to remove elemental sulfur.

The extracts were weighed and fractionated into saturated hydrocarbon, aromatic hydrocarbon, Ni-porphyrin, V=O-porphyrin and polar fractions with small-scale silica gel column chromatography. Samples (~10 mg) were placed on a 5.5 cm column containing activated silica gel (160 °C, overnight). The saturated hydrocarbon fraction was eluted with *n*-hexane (4 mL). The aromatic hydrocarbon fraction was eluted using a mixture of 9:1 *n*-hexane (3.6 mL): DCM (0.4 mL). The Ni-porphyrin fraction was eluted using a 3:1 mixture of *n*-hexane (3 mL) and DCM (1 mL). The V=O-porphyrin fraction was eluted with DCM (4 mL). The polar fraction was recovered with a 1:1 mixture of MeOH (2 mL) and DCM (2 mL). The solvent of each fraction was removed with a nitrogen purge and then the fraction was weighed.

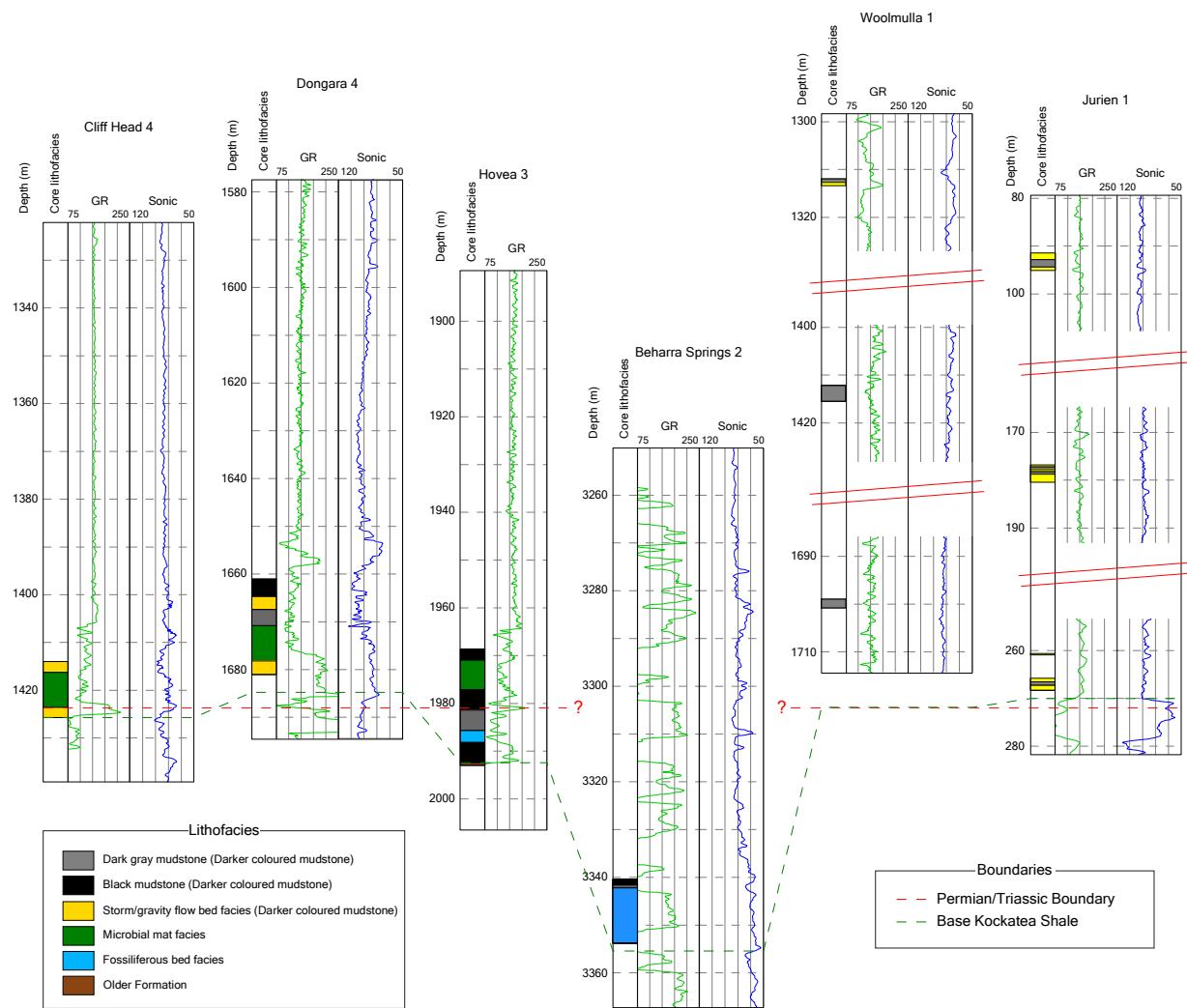
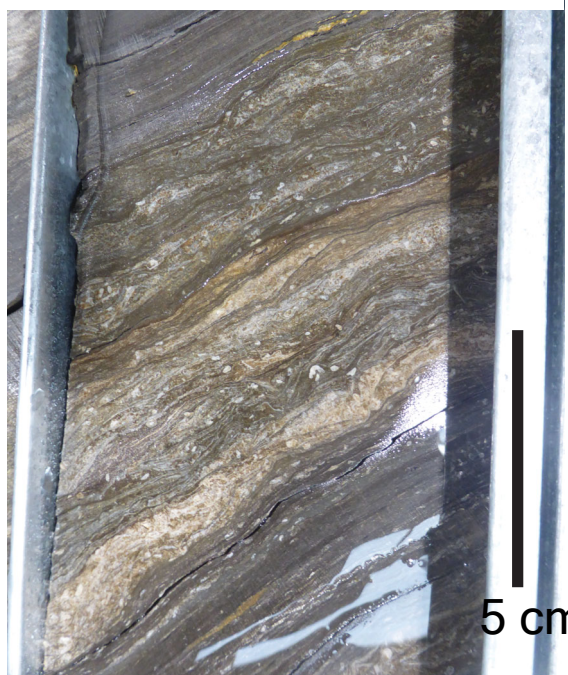
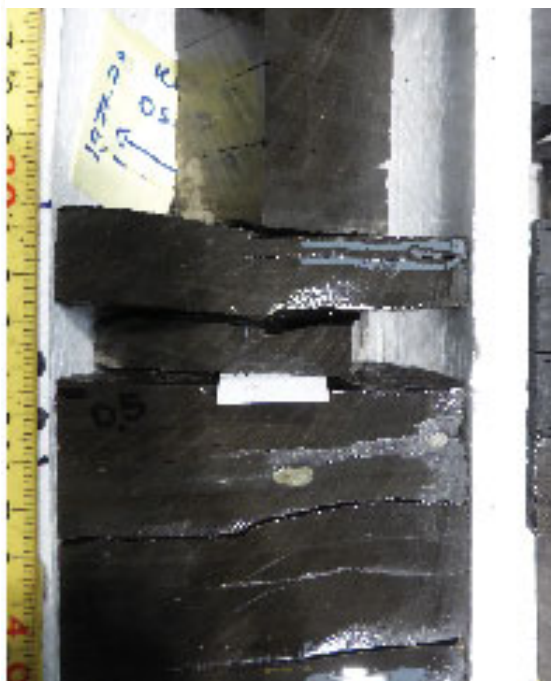


Figure 3-3. Well correlation panel of the basal section of the Kockatea Shale from Cliff Head 4, Dongara 4, Hovea 3, Beharra Springs 2, Woolmulla 1 and Jurien 1. Core lithology is based on core observation (Taniwaki et al., 2021), gamma ray (GR) and sonic log (Sonic) are plotted. Wells are aligned by the approximate Permian/Triassic boundary.

(A) Microbialite



(B) Dark coloured mudstone



(C) Light coloured mudstone



Figure 3-4. Typical lithofacies of A) microbialite, B) dark coloured mudstone and C) light coloured mudstone.

Table 3-1. Depth, lithofacies (lithology and facies) and geological ages of each sample.

Well	Depth (m)	Lithology Description	Facies type	Age
Beharra Springs 2	3340.54	Black Shale	Black Shale	Permian
Beharra Springs 2	3342.65	Bioturbated Deposit	Bioturbated bed	Permian
Beharra Springs 2	3352.70	Bioturbated Deposit	Bioturbated bed	Permian
Beharra Springs 2	3353.67	Black Shale	Bioturbated bed	Permian
Cliff Head 4	1414.84	Black Shale	Storm bed (Black Shale)	Triassic/Permian
Cliff Head 4	1416.15	Black Shale	Storm bed (Black Shale)	Triassic/Permian
Cliff Head 4	1416.66	Dark Grey Shale	Microbialite	Triassic/Permian
Cliff Head 4	1419.04	Dark Grey Shale	Microbialite	Triassic/Permian
Cliff Head 4	1420.12	Microbialite	Microbialite	Triassic/Permian
Cliff Head 4	1421.12	Black Shale	Microbialite	Triassic/Permian
Cliff Head 4	1422.38	Microbialite	Microbialite	Triassic/Permian
Cliff Head 4	1424.05	Black Shale	Storm bed (Black Shale)	Permian
Cliff Head 4	1425.34	Black Shale	Storm bed (Black Shale)	Permian
Dongara 4	1661.62	Dark Grey Shale	Dark Grey Shale	Triassic
Dongara 4	1665.32	Dark Grey Shale	Storm bed (Dark Grey Shale)	Triassic
Dongara 4	1667.15	Dark Grey Shale	Storm bed (Dark Grey Shale)	Triassic
Dongara 4	1668.06	Dark Grey Shale	Dark Grey Shale	Triassic
Dongara 4	1668.96	Dark Grey Shale	Dark Grey Shale	Triassic
Dongara 4	1669.93	Dark Grey Shale	Dark Grey Shale	Triassic
Dongara 4	1672.31	Microbialite	Microbialite	Triassic

Dongara 4	1672.85	Olive Black Shale	Microbialite	Triassic
Dongara 4	1673.85	Microbialite	Microbialite	Triassic
Dongara 4	1674.57	Olive Black Shale	Microbialite	Triassic
Dongara 4	1675.27	Microbialite	Microbialite	Triassic
Dongara 4	1677.09	Olive Black Shale	Microbialite	Triassic
Dongara 4	1677.56	Microbialite	Microbialite	Triassic
Dongara 4	1678.40	Light Olive Brown Shale	Storm bed (Light Olive Brown Shale)	Triassic
Hovea 3	1970.24	Black Shale	Black Shale	Triassic
Hovea 3	1971.28	Black Shale	Microbialite	Triassic
Hovea 3	1972.25	Microbialite	Microbialite	Triassic
Hovea 3	1974.34	Microbialite	Microbialite	Triassic
Hovea 3	1975.47	Black Shale	Microbialite	Triassic
Hovea 3	1979.68	Black Shale	Black Shale	Triassic
Hovea 3	1982.67	Black Shale	Dark Grey Shale	Permian
Hovea 3	1986.00	Black Shale	Fossiliferous Shale	Permian
Jurien 1	267.01	Medium Grey Shale	Medium Grey Shale	Triassic
Jurien 1	267.97	Medium Grey Shale	Tidal Bed	Triassic
Woolmulla 1	1699.12	Medium Grey Shale	Medium Grey Shale	Triassic

3.3 Analysis

3.3.1 Gas Chromatography-Mass Spectrometry & gas chromatography-metastable reaction monitoring-mass spectrometry

Both saturated and aromatic hydrocarbon fractions were analysed by gas chromatography-mass spectrometry (GC-MS), and gas chromatography-metastable reaction monitoring-mass spectrometry (GC-MRM-MS). GC-MS was conducted at Curtin University and GC-MRM-MS was carried out at the Massachusetts Institute of Technology.

For the saturated hydrocarbon fractions, GC-MS analysis was conducted using an Agilent 5977B MSD interfaced to an Agilent 7890B gas chromatograph. A J&W Scientific DB-1MS column with 60 m length, 250 μm inner diameter and 0.25 μm film thickness was used. The GC oven was programmed from 40 $^{\circ}\text{C}$ to 325 $^{\circ}\text{C}$ with a heating rate of 3 $^{\circ}\text{C}/\text{min}$. Initial and final holding times were 1 and 30 minutes, respectively. The MS was operated with an ionisation energy of 70 eV and scanned a mass range from 50 to 550 Daltons.

For the aromatic hydrocarbon fractions, GC-MS analysis was performed on an Agilent 5975B MSD interfaced to an Agilent 6890N gas chromatograph. A J&W DB-5MS column with 60 m length, 250 μm inner diameter and 0.25 μm film thickness was used. The settings of temperature, heating rate, holding times, and scanning mass range were the same as used for the saturated hydrocarbon analysis.

Equal amounts of saturated and aromatic hydrocarbon fractions were combined for GC-MRM-MS analysis. GC-MRM-MS was performed with an Agilent 7890B GC interfaced to an Agilent 7010B Triple Quadrupole MS operated in metastable reaction monitoring (MRM) mode. A DB-5MS UI capillary column with 60 m length, 250 μm inner diameter and 0.25 μm film thickness was used. The GC oven was programmed from 40 $^{\circ}\text{C}$ to 325 $^{\circ}\text{C}$ with a heating rate of 4 $^{\circ}\text{C}/\text{min}$. Holding time for the final temperature was 20.75 minutes. The MS was operated with an ionisation

energy of 50 eV. The QQQ temperature was set at 150°C. D4-C₂₇ $\alpha\alpha\alpha$ cholestane (10 μ L of 10 μ g/mL concentration) was added as an internal standard. The identification of compounds was conducted based on comparison with reference standards, matching retention times and elution order (Cui et al., 2020; French et al., 2014; Kaiho et al., 2016; Schaefer et al., 2020; Spaak, 2017).

3.3.2 Bulk carbon isotopes of organic matter ($\delta^{13}\text{C}_{\text{OM}}$)

For the bulk stable carbon isotope composition ($^{13}\text{C}/^{12}\text{C}$) measurement of the organic matter, carbonate minerals were removed with 1M HCl. The bulk $\delta^{13}\text{C}_{\text{OM}}$ analysis was conducted at Curtin University with a Thermo Flash 2000 HT elemental analyser (EA) connected to a Delta V Advantage isotope ratio mass spectrometer (irMS) *via* a Conflo IV. Samples (~2 mg) were placed in tin cups and combusted to CO₂ in the nitrogen-carbon reactor (1020 °C). CO₂ passed through the Conflo IV interface into the irMS measuring m/z 44, 45 and 46. Measured $\delta^{13}\text{C}$ values were calculated by Thermo Isodat software, and then normalised to the Vienna Pee Dee Belemnite (VPDB) scale with multiple reference materials of NBS 19 (+1.95 ‰) and L-SVEC (-46.6 ‰) (Coplen et al., 2006). In addition, IAEA-600 (-27.77 ‰) was also measured to evaluate the accuracy of normalisation. Each sample was analysed in triplicate.

3.3.3 Mercury (Hg)

The total Hg concentrations were measured using a DMA-90 analyser with a detection limit of approximately 0.15 μ g/kg of rock powder. Signal calibration was conducted with both the BCR 142 R CRM and SRM 2709 reference materials. The relative standard deviations of reference materials were measured to be less than $\pm 5\%$ of relative deviations from the mean value (Leipe et al., 2013). Although it has been observed that Hg may bond to different sedimentary phases such as organic matter, sulfides, or clay minerals (e.g., Shen et al., 2020), we present normalized data

with TOC and TRIS. The analyses were conducted at the Leibniz Institute for Baltic Sea Research (IOW).

3.3.4 Stable sulfur isotopes

The stable sulfur isotope composition ($^{34}\text{S}/^{32}\text{S}$) of total reduced inorganic sulfur (TRIS; considered to essentially represent pyrite (FeS_2)) was measured on powdered rock samples. Hydrogen sulfide was generated by applying hot acid chromium (II) chloride distillation (Fossing and Jørgensen, 1989). The generated H_2S was transported in a stream of N_2 through a Zn acetate solution trap and where it was precipitated quantitatively as ZnS. The sulfide concentration was measured spectrophotometrically (Specord 40 spectrophotometer) using the methylene blue method (Cline, 1969). The concentration was then converted to solid phase contents.

The ZnS was transformed to Ag_2S using a 1M AgNO_3 solution for further preparation. Ag_2S was washed and dried, and combusted in Sn cups in a Thermo Scientific Flash EA Isolink Elemental Analyzer, connected to a Thermo Finnigan MAT 253 gas mass spectrometer via a Thermo Conflo IV split interface as described by Pollmann et al. (2021). The isotope results are given in the δ notation, where the measurements given in ‰ are equivalent to mU (milli Urey; Brand and Coplen, 2012). International isotope IAEA and NBS intercomparison materials were used to convert the isotope ratios to the VCDT scale (Mann et al., 2009), with a precision of better than $\pm 0.2\text{‰}$. These analyses were conducted at IOW.

4 Results

4.1 Thermal maturity

The thermal maturity of each sample was determined by $\text{C}_{32} \text{22S}/(\text{22S}+\text{22R})$ $\alpha\beta$ -homohopane and $\text{C}_{29} \text{20S}/(\text{20S}+\text{20R})$ sterane ratios (Peters et al., 2004) Table 3-2). Most samples have not reached their thermal equilibrium values, indicating relatively low thermal maturity. However, the thermal maturity varies slightly between wells

depending on the burial depth. Beharra Springs 2 has higher thermal maturity than Cliff Head 4 and Hovea 3, most likely due to deeper burial. The thermal maturity of both Jurien 1 and Woolmulla 1 is higher than for other wells. These wells are located near an area of uplift which exposes the Kockatea Shale in outcrop (Mory et al., 2005) suggesting the maximum burial depth was much greater than the current burial depth. The numerical comparison of biomarker distributions between wells requires caution because of the small thermal maturity differences between the wells. On the other hand, the effect of thermal maturity is minimal when comparing biomarker distributions within a single well.

Table 3-2. C₃₂ 22*S*/(22*S*+22*R*) αβ-homohopane ratio and C₂₉ 20*S*/(20*S*+20*R*) sterane ratio used for thermal maturity assessment.

Well	Depth (m)	C ₃₂ 22 <i>S</i> /(22 <i>S</i> +22 <i>R</i>) αβ-homohopane ratio	C ₂₉ 20 <i>S</i> /(20 <i>S</i> +20 <i>R</i>)
Beharra Springs 2	3340.54	0.60	0.48
Beharra Springs 2	3342.65	0.54	0.45
Beharra Springs 2	3352.70	0.62	0.53
Beharra Springs 2	3353.67	0.63	0.38
Cliff Head 4	1414.84	0.49	0.17
Cliff Head 4	1416.15	0.50	0.16
Cliff Head 4	1416.66	0.51	0.16
Cliff Head 4	1419.04	0.47	0.17
Cliff Head 4	1420.12	0.50	0.18
Cliff Head 4	1421.12	0.44	0.16
Cliff Head 4	1422.38	0.48	0.20
Cliff Head 4	1424.05	0.59	0.43
Cliff Head 4	1425.34	0.59	0.43
Dongara 4	1661.62	0.54	0.20
Dongara 4	1665.32	0.56	0.23
Dongara 4	1667.15	0.54	0.24
Dongara 4	1668.06	0.54	0.22
Dongara 4	1668.96	0.53	0.22
Dongara 4	1669.93	0.54	0.22
Dongara 4	1672.31	0.55	0.21

Dongara 4	1672.85	0.55	0.19
Dongara 4	1673.85	0.52	0.23
Dongara 4	1674.57	0.53	0.24
Dongara 4	1675.27	0.52	0.23
Dongara 4	1677.09	0.52	0.24
Dongara 4	1677.56	0.51	0.23
Dongara 4	1678.40	0.53	0.26
Hovea 3	1970.24	0.59	0.44
Hovea 3	1971.28	0.59	0.39
Hovea 3	1972.25	0.59	0.42
Hovea 3	1974.34	0.59	0.42
Hovea 3	1975.47	0.59	0.43
Hovea 3	1979.68	0.57	0.43
Hovea 3	1982.67	0.58	0.36
Hovea 3	1986.00	0.57	0.39
Jurien 1	267.01	0.56	0.48
Jurien 1	267.97	0.60	0.45
Woolmulla 1	1699.12	0.62	0.36

4.2 Characteristics of biomarkers, $\delta^{13}\text{C}_{\text{OM}}$, $\delta^{34}\text{S}$, Hg and Hg/TOC

One of the distinct characteristics of the Lower Triassic is the presence of carotenoid biomarkers (okenane, chlorobactane and isorenieratane) (Figure 3-5). The northern wells (Cliff Head 4, Dongara 4 and Hovea 3) contain high abundances of carotenoid biomarkers, and display fluctuations in concentration (Figures 3-6-3-8). In addition, other biomarkers, $\delta^{13}\text{C}_{\text{OM}}$, $\delta^{34}\text{S}$, Hg and Hg/TOC show repeated fluctuations of their concentrations and ratios (Figures 3-6-3-8) similar to the fluctuation of carotenoid biomarkers. Hopane and gammacerane indices [hopane index: C_{35} (22S+22R) $\alpha\beta$ -homohopane/ C_{34} (22S+22R) $\alpha\beta$ -homohopane, gammacerane index: (gammacerane)/(gammacerane+ $\text{C}_{30}\alpha\beta$ -homohopane)] show a positive correlation with the concentration of carotenoid biomarkers, while Pr/Ph is negatively correlated. Values of the 2 α -methylhopane index (2MeHI: 2 α -methyl $\alpha\beta$ -hopane/(2 α -methyl $\alpha\beta$ -hopane+ $\text{C}_{30}\alpha\beta$ -homohopane)) and (renieratane and renierapurpurane)/(paleorenieratane+isorenieratane) ratio ((ren+rnp)/(paleo+iso)) are variable but tend to be high in the interval with low hopane and gammacerane indices and high Pr/Ph within the microbialite lithofacies. The relative abundance of okenane to chlorobactane and isorenieratane (okenane ratio) and the concentration of aryl isoprenoids (C_{18} , C_{19} , and C_{20} with a 2,3,6 methyl substitution pattern) show opposite trends. High okenane ratios and low concentrations of aryl isoprenoids are typically identified in the interval with lower hopane and gammacerane indices and higher Pr/Ph within the microbialite lithofacies. The C_{33} *n*-alkylcyclohexane ratio (*n*- C_{33} ACH ratio, $n\text{-C}_{33}\text{ACH}/n\text{-C}_{34}$) is high in the microbialite lithofacies. The relative abundance of C_{30} steranes is high in the basal part of the Lower Triassic near the Permian-Triassic boundary. TRIS values are similar across the sampled interval. Hg concentration and normalized Hg/TOC, Hg/TRIS and TOC/TRIS values are also high in the basal part of the Lower Triassic, corresponding to the interval with a higher abundance of C_{30} steranes (C_{30} steranes/ $\Sigma(\text{C}_{27-30}$ steranes). Values of $\delta^{13}\text{C}_{\text{OM}}$ and $\delta^{34}\text{S}$ are isotopically light in the microbialite facies although the isotopically

lightest $\delta^{34}\text{S}$ values in the Lower Triassic are mainly identified near the Permian-Triassic boundary.

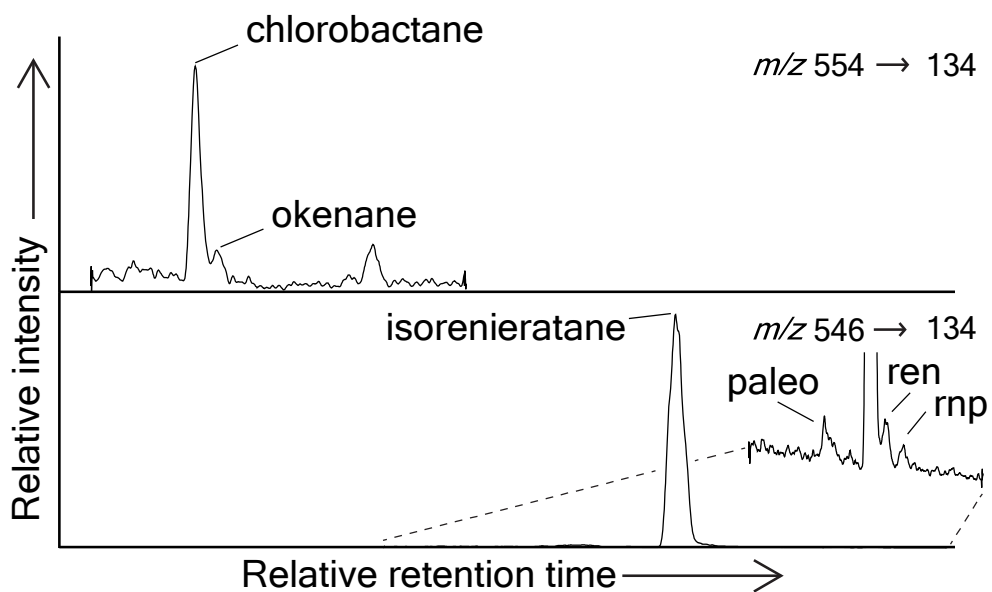


Figure 3-5 Carotenoid biomarkers from microbialites (Cliff Head 4, 1422.38m) identified using GC-MRM-MS by comparison with standard compounds. 'Paleo': paleorenieratane, 'ren': renieratane, 'rnp': renierapurpurane.

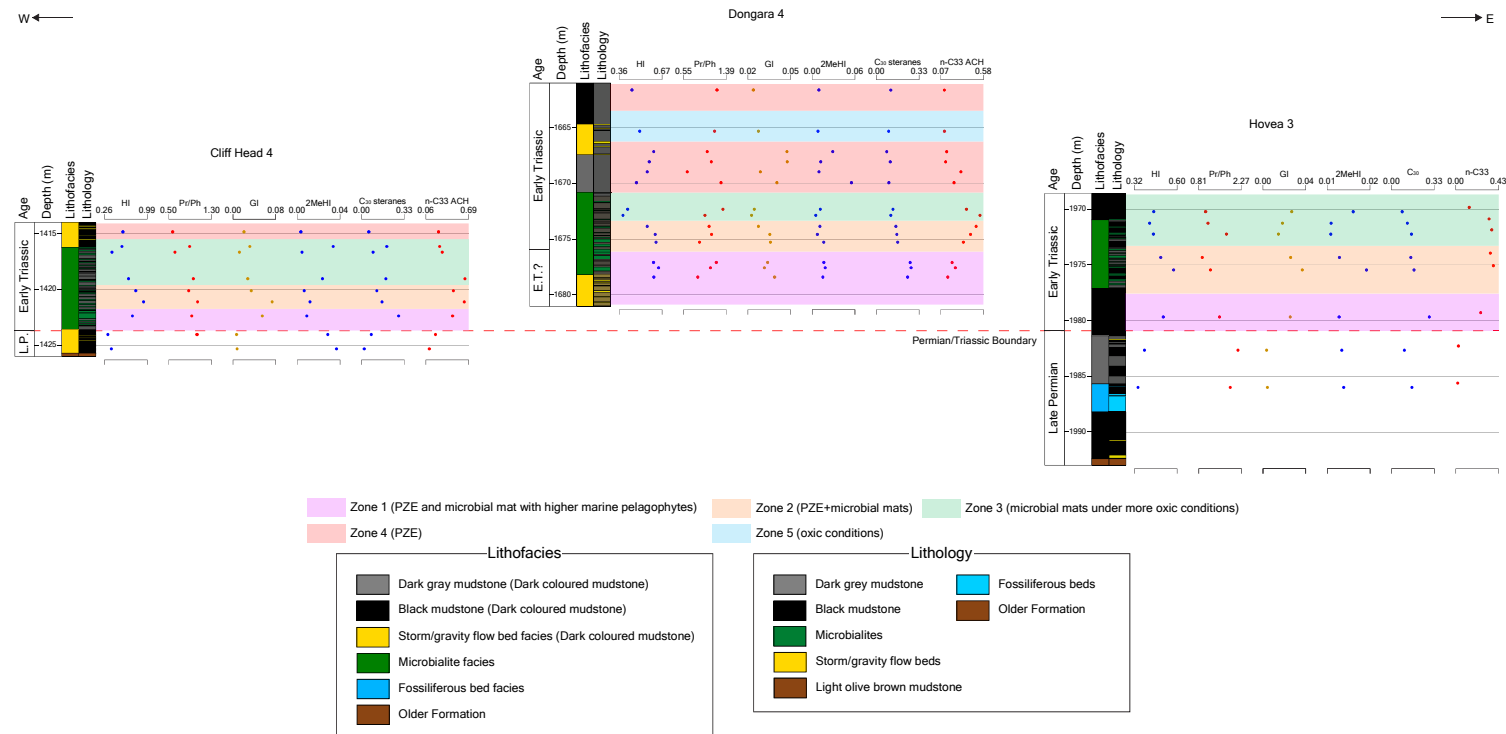


Figure 3-6. Composite panel of major biomarkers for Cliff Head 4, Dongara 4, and Hovea 3. C₃₅ homohopane index (HI), pristane/phytane ratio (Pr/Ph), gammacerane index (GI), 2 α -methylhopane index (2MeHI), C₃₀ sterane ratio, n-C₃₃ ACH ratio are plotted. (Fox et al., 2020; Grice et al., 2005c; Peters et al., 2004; Summons et al., 1999; Tulipani et al., 2015). Cores are aligned on the approximate Permian/Triassic boundary.

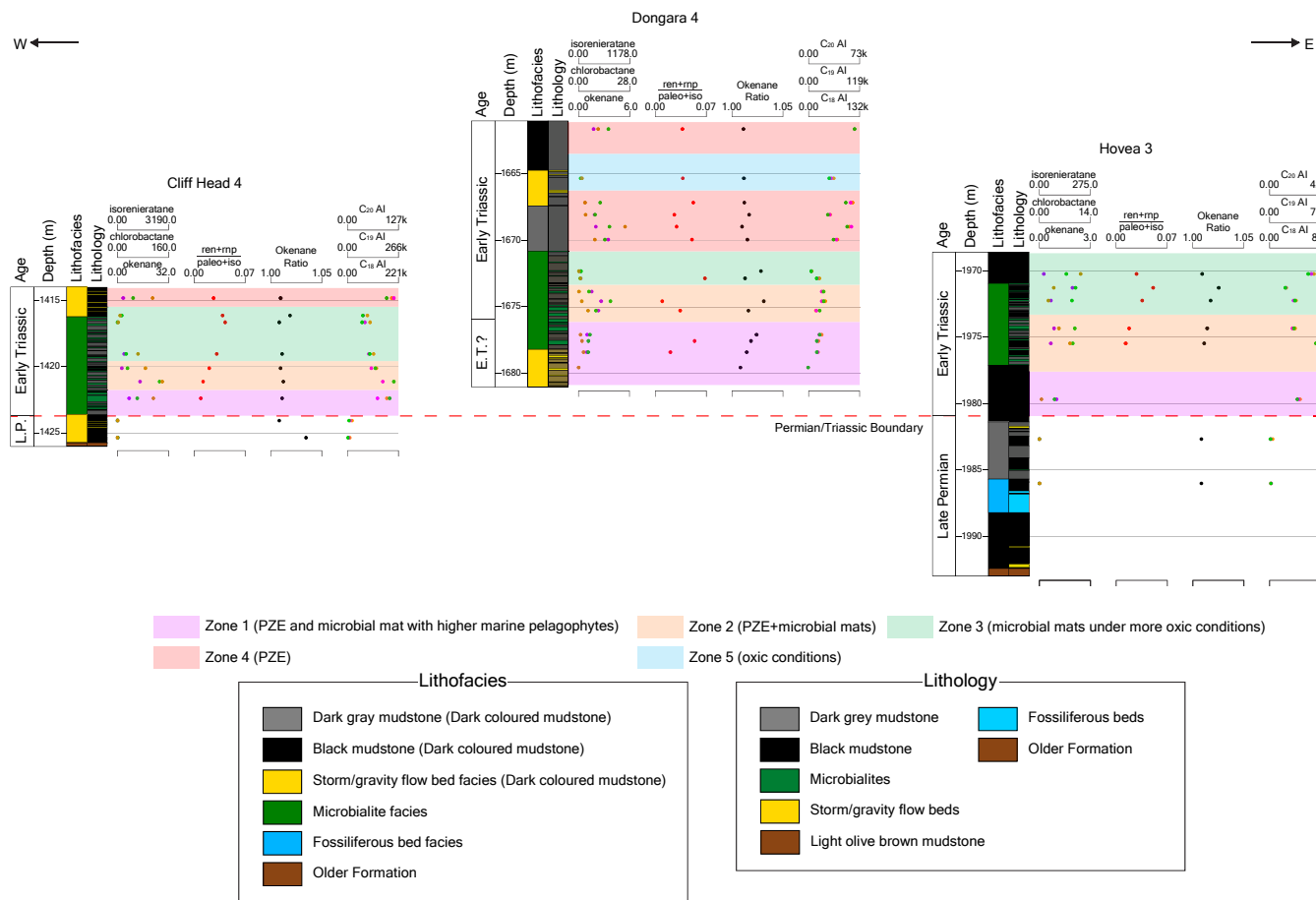


Figure 3-7. Composite panel of carotenoids and related biomarkers for Cliff Head 4, Dongara 4, and Hovea 3. Okenane, chlorobactane, isorenieratane, ren+rnp/paleo+iso ratio, okenane ratio and aryl isoprenoids (C₁₈₋₂₀) are plotted (Brocks and Schaeffer, 2008; Cui et al., 2020; Grice et al., 2005a; Schaefer et al., 2020; Summons and Powell, 1987). Cores are aligned on the approximate Permian/Triassic boundary.

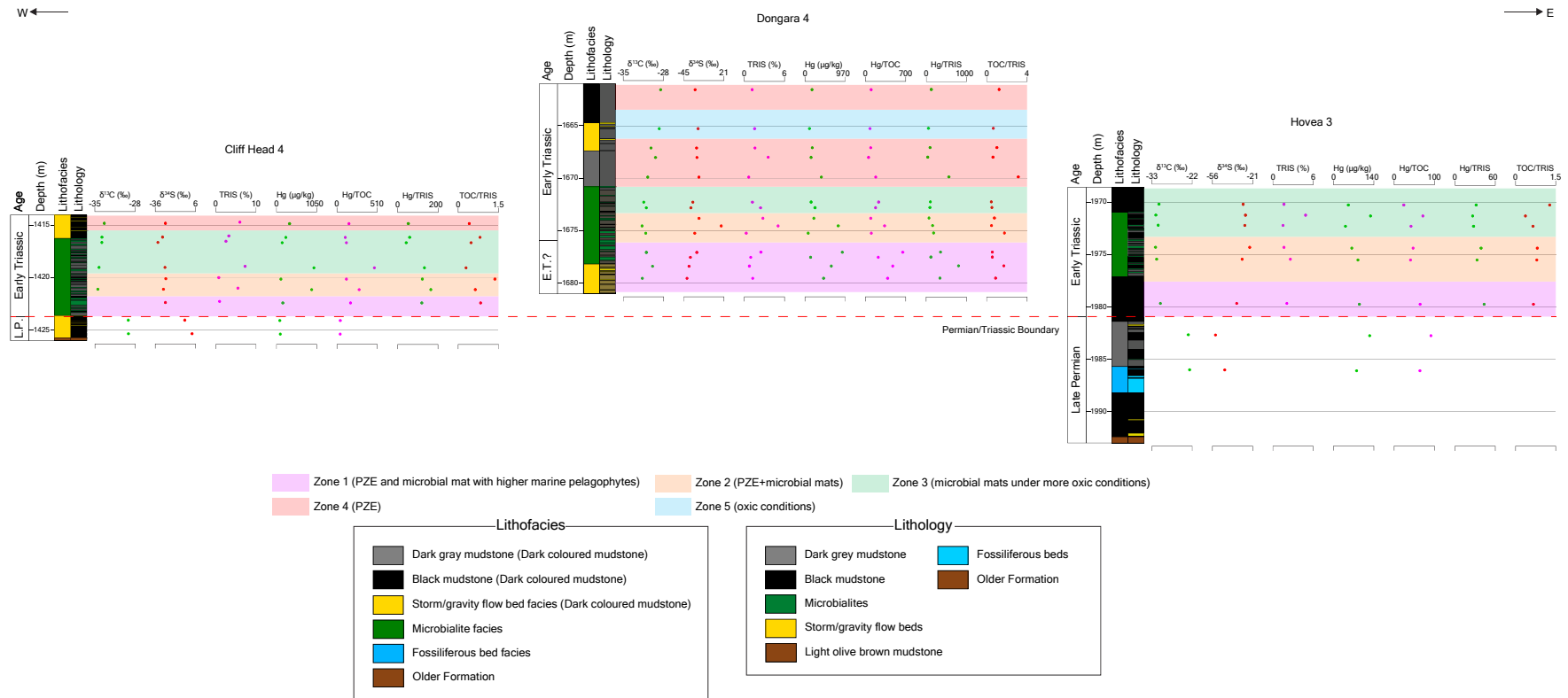


Figure 3-8. Composite panel of isotope and Hg data for Cliff Head 4, Dongara 4, and Hovea 3. $\delta^{13}\text{C}_{\text{OM}}$, $\delta^{34}\text{S}$, Hg concentration and Hg/TOC are plotted (Brand and Coplen, 2012; Grasby et al., 2017; Hartmann and Nielsen, 2012). Cores are aligned on the approximate Permian/Triassic boundary.

4.3 Definition of zones

Late Permian Kockatea Shale samples represent relatively more oxic depositional conditions with less water column stratification compared with Early Triassic Kockatea Shale samples based on hopane and gammacerane indices and Pr/Ph. In addition, carotenoid biomarkers related to sulfur bacteria were not identified in the Late Permian Kockatea Shale samples.

Paleoenvironmental depositional conditions in the Early Triassic were established using several biomarkers, bulk carbon isotopes of organic matter, sulfur isotope ratios and Hg contents (Figures 3-6-3-12 and 3-S1, Table 3-3). The analysed Early Triassic intervals are divided into five zones based on the relative abundances of biomarkers, rather than absolute values because of the variation caused by thermal maturation characteristics (section 4.1). The zones are Zone 1 (PZE and microbialites with higher marine pelagophytes), Zone 2 (PZE with microbialite), Zone 3 (Microbialites living under relatively more oxic conditions), Zone 4 (PZE), and Zone 5 (oxic condition).

4.3.1 Zone 1

This interval is identified in Cliff Head 4, Dongara 4, and Hovea 3. The dark coloured mudstones and microbialites represent the major lithofacies.

Persistent water column PZE was established based on high hopane and gammacerane indices, low Pr/Ph (Figure 3-6) and high concentrations of okenane, chlorobactane and isorenieratane indicating the abundance of phototrophic sulfur bacteria (Figure 3-7). Gammacerane index values reported herein are generally low compared with values reported in other publications (e.g. Tulipani et al., 2015), but there is a subtle variation of values within this range, consistent with other parameters. The concentration of okenane, chlorobactane and isorenieratane is generally high in this zone and the other zones associated with PZE (Zone 1, 2 and 4). The okenane ratio is variable, with slightly lower values indicating a slightly

lower abundance of purple sulfur bacteria. Aryl isoprenoid concentrations are generally high, suggesting a greater abundance of green sulfur bacteria (Summons and Powell, 1987). In addition, a low relative abundance of cyanobacteria in Zone 1 is inferred based on the low 2MeHI and (ren+rnp)/(paleo+iso) (Bralower et al., 2020; Cui et al., 2020; Fox et al., 2020; Schaefer et al., 2020; Summons et al., 1999). The *n*-C₃₃ ACH ratio is elevated in the zones with microbialites (Zone 1 to 3) relative to other zones (Figure 3-10) (Grice et al., 2005c). The high abundance of C₃₀ steranes observed in Zone 1, suggests abundant marine pelagophytes during the onset of major marine transgression or an intense bloom of pelagophytes after the mass extinction (Fox et al., 2020). Hg concentrations and normalized Hg/TOC values are generally high (Figure 3-8).

TRIS ranges from 0.76% to 2.5%. Hg/TRIS and TOC/TRIS are elevated and show the largest values of any of the zones (Figures 3-8 and 3-13). The bulk $\delta^{13}\text{C}_{\text{OM}}$ in Zones 1 and 2, which share similar paleoenvironmental conditions, ranges from \sim -30 ‰ to \sim -32.5 ‰ (Figure 3-11). $\delta^{34}\text{S}$ values range from \sim -20 ‰ to \sim -40 ‰ and are isotopically lighter than samples formed under oxic conditions (Figure 3-12).

The paleoenvironment in Zone 1 is interpreted as PZE with microbialite facies and a higher abundance of marine pelagophytes (elevated C₃₀ sterane ratio).

4.3.2 Zone 2

This interval is identified in Cliff Head 4, Dongara 4, and Hovea 3. Zone 2 shares similar lithofacies and most organic geochemical characteristics to Zone 1, except the relative abundance of C₃₀ sterane, which is low in Zone 2 and subsequent zones. TRIS ranges from 0.56% to 5.45%. Hg/TRIS and TOC/TRIS which is similar to the range of values in Zone 1 in Cliff Head 4 and Hovea 3, but lower than in Zone 1 in Dongara 4 (Figures 3-8 and 3-13). Figure 3-12 shows one sample has isotopically heavier $\delta^{34}\text{S}$ reaching to +15‰ in this zone. It appears to be an outlier and is excluded from the range of $\delta^{34}\text{S}$ values used to characterise this paleoenvironment.

The paleoenvironment in Zone 2 is interpreted as a combination of PZE and microbialites.

4.3.3 Zone 3

This interval is identified in Cliff Head 4, Dongara 4, and Hovea 3. The dominant lithofacies are similar to Zone 1 (dark coloured mudstone and microbialites), but more oxic conditions with less water column stratification are indicated by low hopane and gammacerane indices, and high Pr/Ph (Figure 3-6). The concentration of carotenoid biomarkers is generally variable. The okenane ratio is higher than in Zones 1, 2 and 4 where PZE developed with or without microbialites (Figure 3-7), indicating a higher contribution of purple sulfur bacteria (Figure 3-9). The significant separation of values between PZE (Zone 4) and microbialites (Zone 3) in Figure 3-9 shows there is very strong difference of okenane ratio between these facies. Aryl isoprenoid concentrations are low, indicating lower contributions of green sulfur bacteria (Figure 3-7). A high abundance of cyanobacteria is also evident based on the generally elevated 2MeHI in some wells (Cliff Head 4 and Hovea 3) and high (ren+rnp)/(paleo+iso) (Figure 3-7). The *n*-C₃₃ ACH ratio is elevated and is probably related to microbialites as described in Zone 1 (Figure 3-10). Most of the samples in Zone 3 and subsequent zones have a low Hg concentration and Hg/TOC compared with the underlying zones.

TRIS ranges from 1.2% to 7.2%. It shows slightly higher values than Zones 1 and 2 in Cliff Head 4 and Hovea 3, but values overlap significantly with other zones. The values of Hg/TRIS decrease from Zone 2. TOC/TRIS ranges are almost constant in Dongara 4 and Hovea 3 and slightly decrease in Cliff Head 4 (Figures 3-8 and 3-13). The bulk $\delta^{13}\text{C}_{\text{OM}}$ ranges from -31 to -32‰ and is isotopically lighter compared to Zone 4 (-28.5 to -31‰) (Figure 3-11). $\delta^{34}\text{S}$ values range from ~-25 to -35 ‰ which is isotopically lighter than the PZE interval without microbialites (Zone 4) (-20 to -25‰) (Figure 3-12).

The paleoenvironment in Zone 3 is interpreted as microbialites formed under relatively more oxic conditions.

4.3.4 Zone 4

This interval is identified in Cliff Head 4 and Dongara 4, but is mainly based on the characteristics of Dongara 4 because Cliff Head 4 has only one sample. The dark coloured mudstone represents the dominant lithofacies.

PZE is inferred based on high hopane and gammacerane indices, low Pr/Ph (Figure 3-6), and high concentrations of carotenoid biomarkers (Figure 3-7). The low okenane ratio and relatively high aryl isoprenoid concentration supports a low abundance of purple sulfur bacteria and greater abundance of green sulfur bacteria. The low ratios of both 2MeHI and (ren+rnp)/(paleo+iso) suggest a low abundance of cyanobacteria. The *n*-C₃₃ ACH ratio is also low in this interval (Figure 3-10).

TRIS ranges from 0.7% to 6.0%, showing a similar range to other zones. The values of TOC/TRIS increase compared with Zone 3 in Dongara 4 and are similar to Zone 3 in Cliff Head 4. Hg/TRIS is slightly low compared with Zone 3 (Figures 3-8 and 3-13). The bulk $\delta^{13}\text{C}_{\text{OM}}$ ranges from -28.5 ‰ to -31 ‰ and is isotopically heavier than the microbialite interval (Zone 3) (-31 to -32‰) (Figure 3-11). $\delta^{34}\text{S}$ ranges from -20 to -25‰ which is within a range of isotopically lighter values indicating the development of PZE, although it is isotopically heavier than the microbialite interval (-25 to -35‰) (Figure 3-12).

Zone 4 shows PZE depositional conditions. The uppermost part of the cored interval in Dongara 4 may also be assigned to PZE although there are inconsistencies between biomarkers, bulk $\delta^{13}\text{C}_{\text{OM}}$ and $\delta^{34}\text{S}$.

4.3.5 Zone 5

This interval is identified in Jurien 1, Woolmulla 1 (southern wells, Figure 3-S1) and Dongara 4 (northern well). One sample from Woolmulla 1 and two samples from Jurien 1 with the medium grey shale (light coloured mudstone) are assigned to this

zone. One sample from the dark grey mudstone (dark coloured mudstone) is assigned to this zone in Dongara 4.

Oxic conditions with less water column stratification are identified based on low hopane and gammacerane indices and high Pr/Ph (Figure 3-6). The carotenoid biomarkers are absent, indicating no PZE development and no microbialite source. The *n*-C₃₃ ACH ratio is quite low (Figures 3-10 and 3-S1).

TRIS ranges from 0.17% to 0.77% in Jurien 1 and Woolmulla 1 and is 1.6% in Dongara 4. TOC/TRIS and Hg/TRIS show higher values compared with other zones in Jurien 1 and Woolmulla 1. In Dongara 4 these values are in the same range as Zones 1 to 4 (Figures 3-8 and 3-13). The bulk $\delta^{13}\text{C}_{\text{OM}}$ ranges from about -32 to -34 ‰ and is isotopically lighter than the other zones (Figures 3-11 and 3-S1). Figure 3-11 shows one sample which has isotopically heavier $\delta^{13}\text{C}_{\text{OM}}$ reaching -29‰. It appears to be an outlier, hence this sample is excluded from the range of $\delta^{13}\text{C}_{\text{OM}}$ used to characterise this paleoenvironment. $\delta^{34}\text{S}$ values from Jurien 1 and Woolmulla 1 range from 0 to 25‰ and are isotopically heavier than the PZE and microbialite intervals (Figures 3-6 and 3-12).

In Dongara 4 (northern well), one sample from the dark grey mudstones is assigned to this zone based on biomarker characteristics. On the other hand, this zone in Dongara 4 has an isotopically lighter $\delta^{34}\text{S}$ value (-21.7 ‰) similar to the adjacent zones related to PZE. It appears to be an outlier compared with other samples. The lithofacies for the sample from Dongara 4 is a dark coloured mudstone interbedded with PZE intervals. In addition, aryl isoprenoids are present in small concentrations although carotenoids (isorenieratane, chlorobactane and okenane) are absent. There are some inconsistencies for this sample although many parameters favour oxic conditions.

Table 3-3. Summary of paleoenvironments and their organic geochemical characteristics

	Zone 1	Zone 2	Zone 3	Zone 4	Zone 5
Identified wells	Cliff Head 4 Dongara 4 Hovea 3	Cliff Head 4 Dongara 4 Hovea 3	Cliff Head 4 Dongara 4 Hovea 3	Cliff Head 4 Dongara 4	Jurien 1 Woolmulla 1 Dongara 4?
Lithofacies	dark coloured mudstone microbialites	dark coloured mudstone microbialites	dark coloured mudstone microbialites	dark coloured mudstone	light coloured mudstone dark grey mudstone
Paleoenvironment	PZE+Microbialites with higher abundance of marine pelagophytes	PZE+Microbialites	Microbialite under oxic conditions	PZE	Oxic conditions
C ₃₅ homohopane index (Hopane index)	High	High	Low	High	Low
Pr/Ph	Low	Low	High	Low	High
Gammacerane index	High	High	Low	High	Low
Okenane, chlorobactane, isorenieratane	High concentration	High concentration	Variable	High concentration	Absent
Okenane ratio	Low (variable)	Low (variable)	High	Low	Not available
Aryl isoprenoids	High concentration	High concentration	Low concentration	High concentration	Low concentration
2MeHI	Low	Low	High	Low	Low
(ren+rnp)/(paleo+iso)	Low	Low	High	Low	Not available
<i>n</i> -C ₃₃ ACH ratio	High	High	High	Low	Low

C ₃₀ sterane ratio	High	Low	Low	Low	Low
Hg & Hg/TOC	High	High	Low	Low	Low
¹³ C _{OM}	-30.0 to 32.5 ‰	-30.0 to 32.5 ‰	-31.0 to -32.0 ‰	-28.5 to -31.0 ‰	-32.0 to -34.0 ‰
³⁴ S	-20 to -40 ‰	-20 to -40 ‰	-25 to -35 ‰	-20 to -25 ‰	0 to +25 ‰

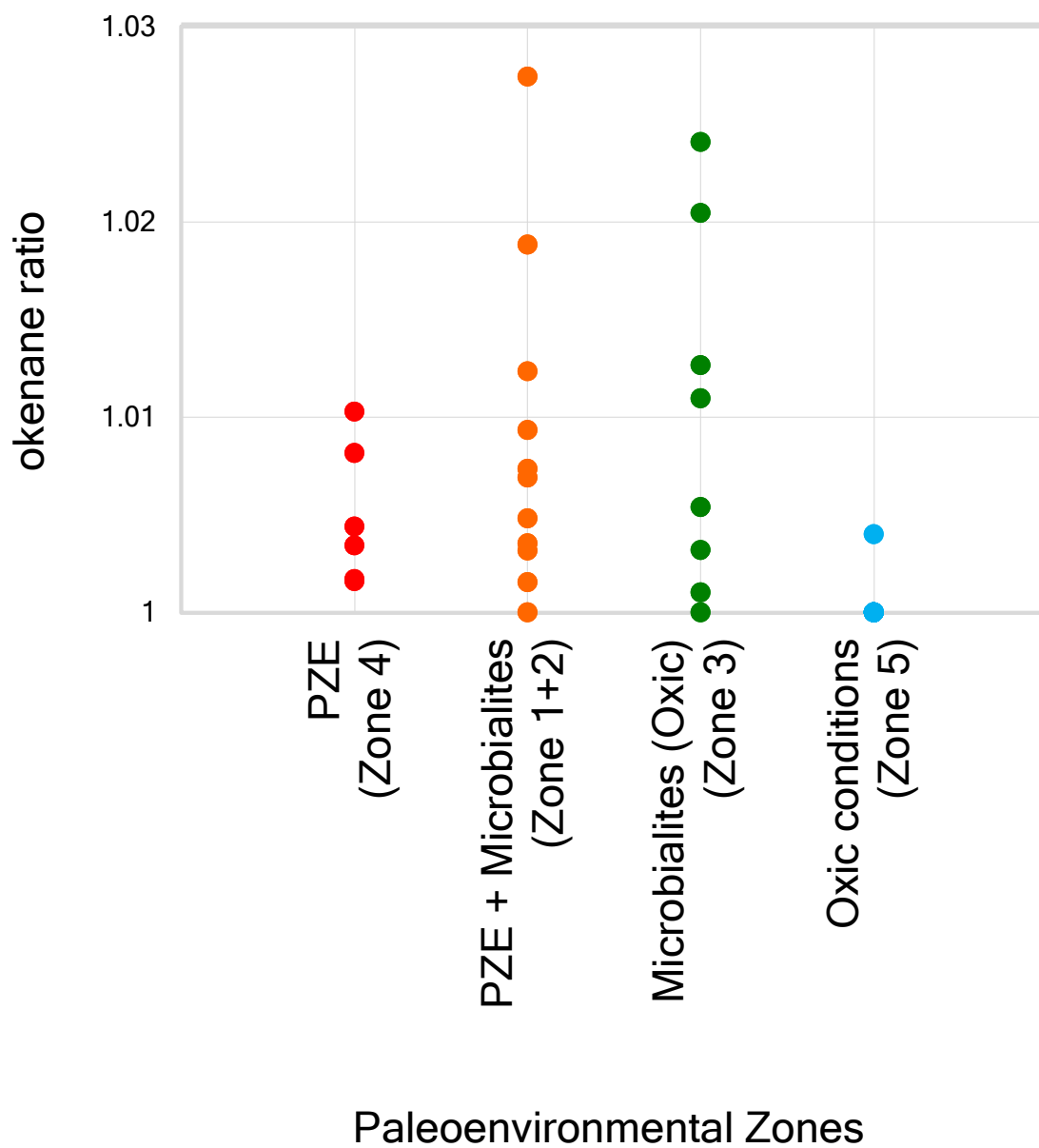


Figure 3-9. Okenane ratio of samples from each paleoenvironmental zone. Okenane ratio is defined as $(\text{okenane} + \text{chlorobactane} + \text{isorenieratane}) / (\text{chlorobactane} + \text{isorenieratane})$.

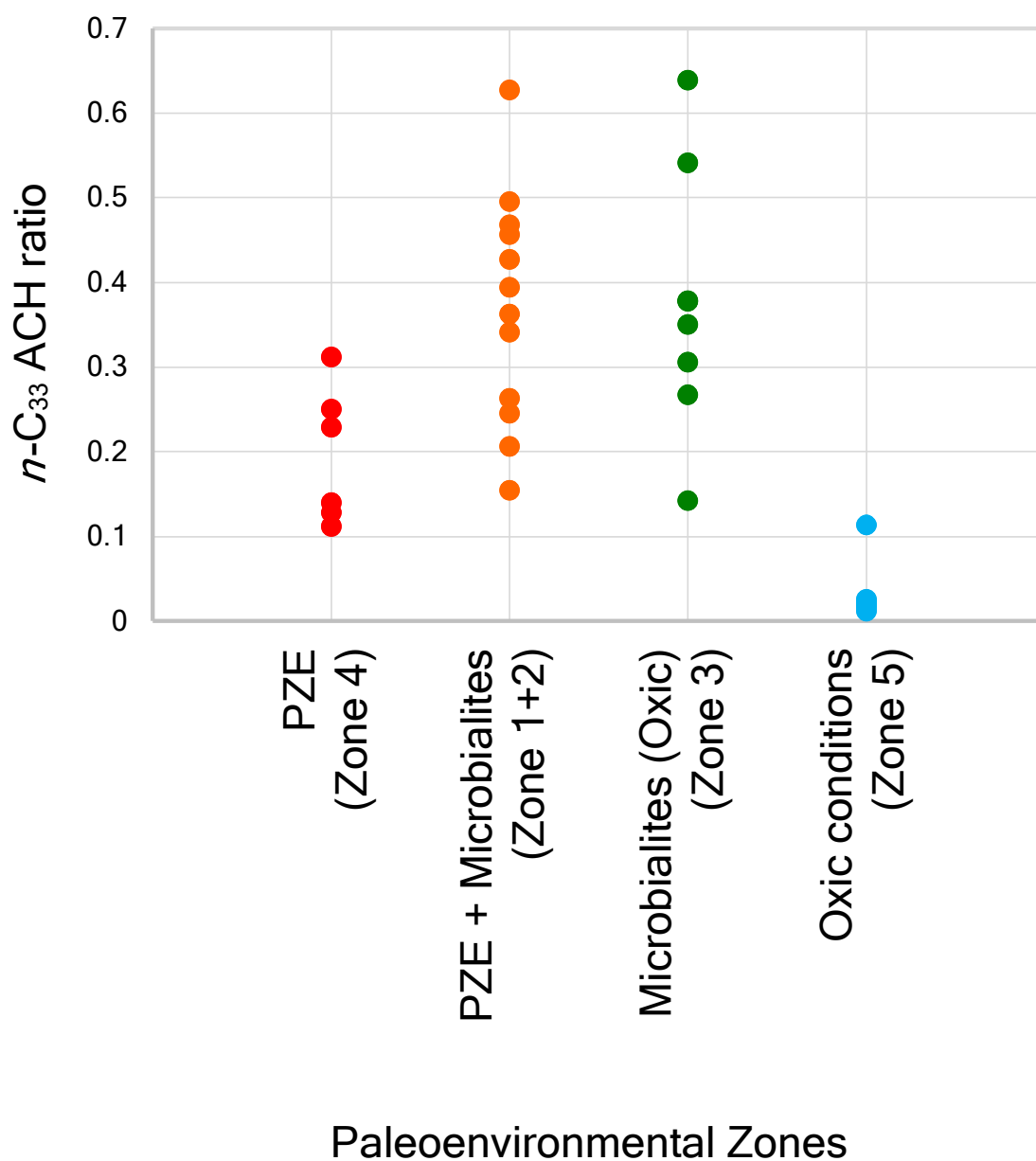


Figure 3-10. $n\text{-C}_{33}$ ACH ratio (C_{33} n -alkylcyclohexane/ C_{34} n -alkane) in each paleoenvironmental zone (Grice et al., 2005c).

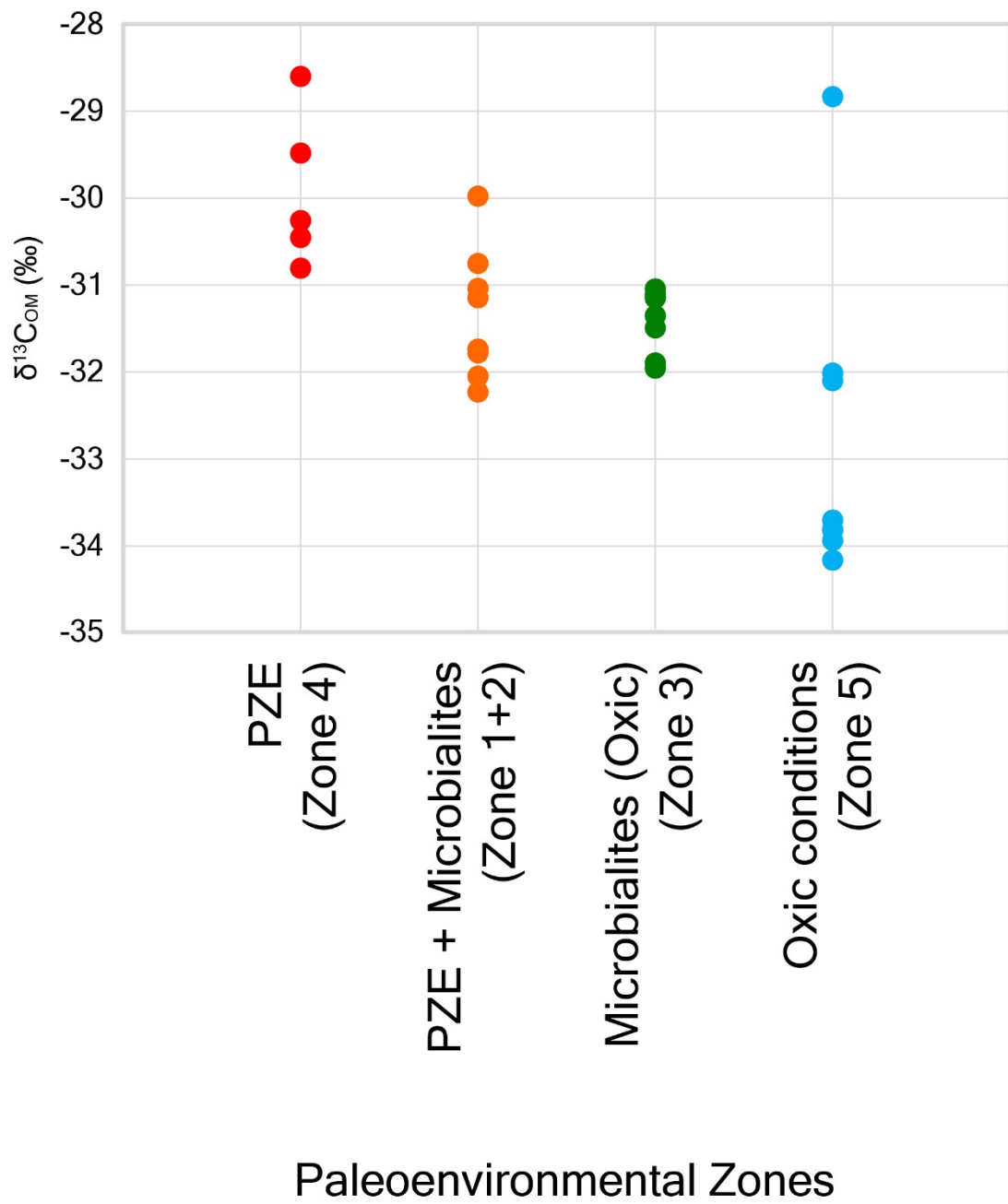


Figure 3-11. Plot of bulk $\delta^{13}\text{C}_{\text{COM}}$ in each paleoenvironmental zone.

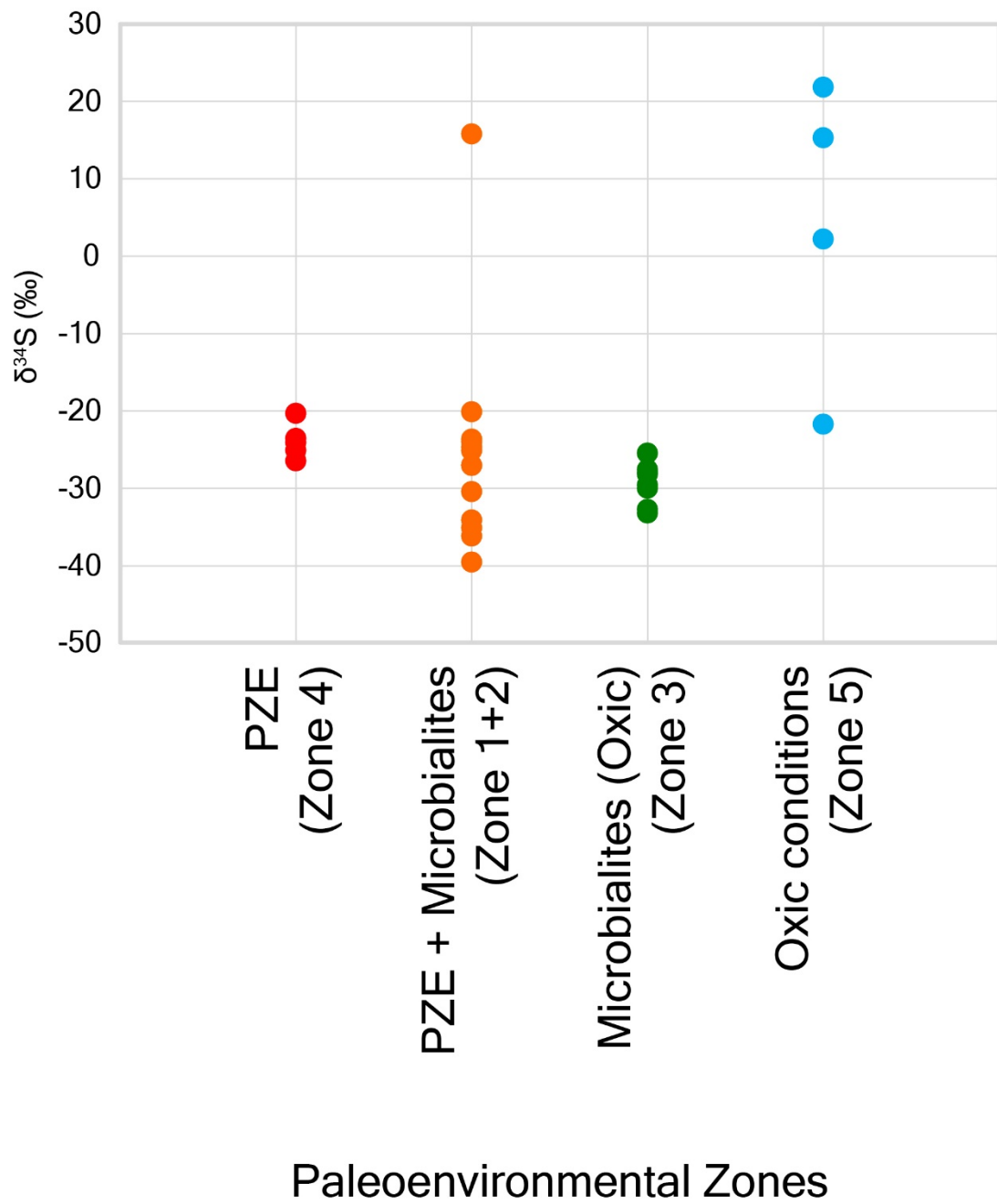


Figure 3-12. Plot of bulk $\delta^{34}\text{S}$ in each paleoenvironmental zone.

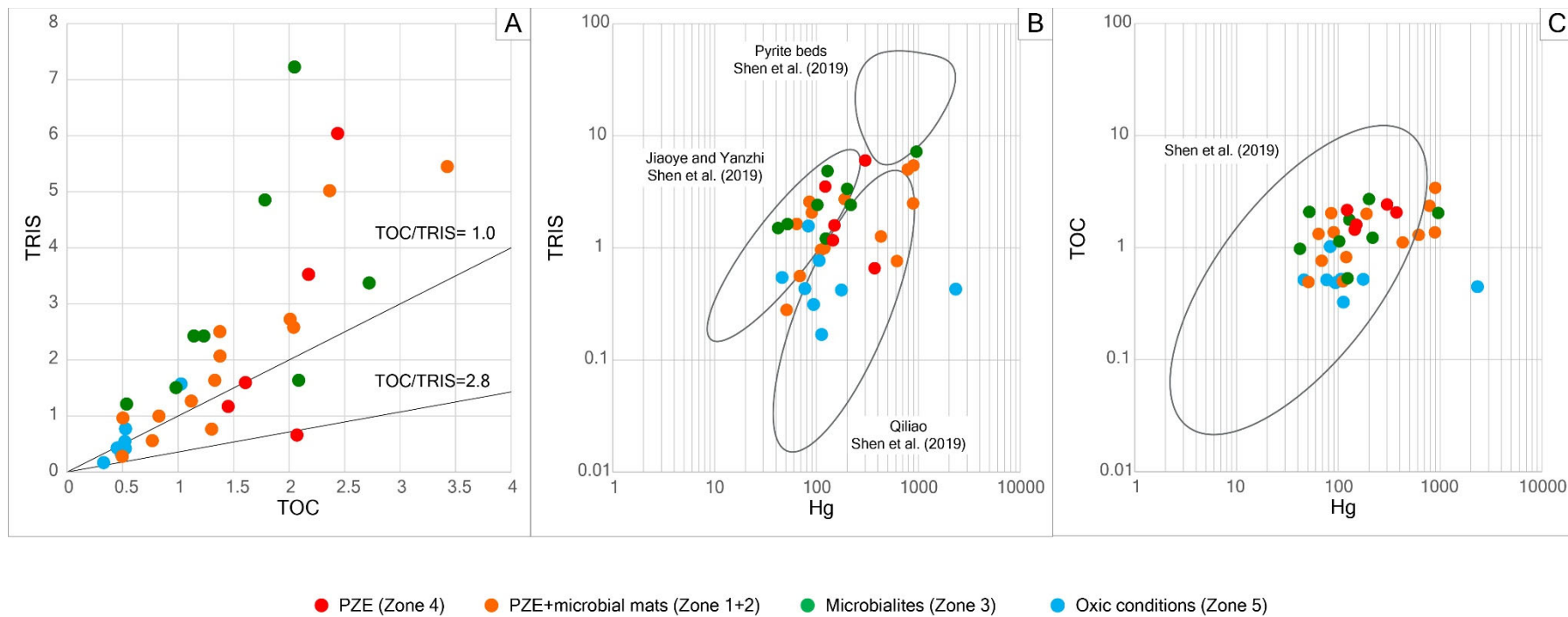


Figure 3-13. Cross plots of (A) TOC vs TRIS, (B) Hg vs TRIS and (C) Hg vs TOC. TOC/TRIS ratios (1 and 2.8) are shown in A. Major clusters mentioned by Shen et al. (2020) are shown in B and C.

5 Discussion

5.1 Distinguishing the geochemical signatures of PZE and microbialites

Okenane ratios, n -C₃₃ ACH, $\delta^{13}\text{C}_{\text{OM}}$ and $\delta^{34}\text{S}$ values show a difference between PZE and microbialite facies (Figures 3-9 and 3-12). Principal component analysis (PCA) has been carried out to determine the correlation between these parameters (Figures 3-14 and 3-15, Table 3-4). The correlation between n -C₃₃ ACH and $\delta^{13}\text{C}_{\text{OM}}$ is strongest (R^2 : -0.82) while the correlations between other parameters are very weak (R^2 (okenane ratio vs $\delta^{13}\text{C}_{\text{OM}}$)= -0.19, R^2 (n -C₃₃ ACH vs $\delta^{13}\text{C}_{\text{OM}}$)= -0.16, and R^2 ($\delta^{34}\text{S}$ vs $\delta^{13}\text{C}_{\text{OM}}$)= 0.06), probably because of the scattered distribution of samples from “PZE+microbialite facies (Zones 1 and 2)”.

In the plot of PC1, PC2 and PC3 (Figure 3-15), there is clear separation between PZE (Zone 4) and microbialite (Zone 3) facies. The samples from PZE+microbialite facies (Zones 1 and 2) mainly plot near the microbialite facies (Zone 3), probably because the PZE+microbialite facies (Zones 1 and 2) share similar biomarker characteristics based on okenane ratio and n -C₃₃ ACH (Figures 3-9 and 3-12). However, there are distinct differences of biomarker features in hopane index, 2MeHI and (ren+rno)/(paleo+iso) between microbialite (Zone 3) and PZE+microbialite (Zones 1 and 2) facies (Figures 3-9 and 3-12), resulting in the separation of these two facies on the PCA plot. When compared to the microbialite facies, the PZE samples have isotopically heavy $\delta^{13}\text{C}_{\text{OM}}$ and $\delta^{34}\text{S}$, and low okenane ratio and n -C₃₃ACH. PZE+microbialite samples have intermediate values between PZE and microbialite samples.

The $\delta^{13}\text{C}_{\text{OM}}$ associated with the high purple sulfur bacteria communities is depleted in ¹³C compared with high green sulfur bacterial communities due to their different carbon fixation pathways (Grice et al., 1997). The results of the PCA correspond to these characteristics. The isotopically lightest $\delta^{13}\text{C}_{\text{OM}}$ from microbialites has the largest PC1 value, while the isotopically heaviest $\delta^{13}\text{C}_{\text{OM}}$ from PZE facies shows the smallest value. The variation of PC1 values represents the

$\delta^{13}\text{C}_{\text{OM}}$ variation and correlates to the variation of $n\text{-C}_{33}\text{ACH}$ and other parameters. Based on the relationship between $\delta^{13}\text{C}_{\text{OM}}$ and sulfur bacterial community, in combination with okenane ratio, $n\text{-C}_{33}\text{ACH}$, and $\delta^{34}\text{S}$, the contribution of purple (microbialite) versus green (PZE) sulfur bacteria can be evaluated. The relative abundance of $n\text{-C}_{33}\text{ACH}$ in microbialites also suggests that this compound is related to facies containing microbialites.

Table 3-4. Range of selected isotope and biomarker results in each zone.

	$\delta^{34}\text{S}$		$\delta^{13}\text{C}_{\text{OM}}$		$n\text{-C}_{33}\text{ACH}$		Okenane Ratio	
	Max	Min	Max	Min	Max	Min	Max	Min
PZE	-20.3	-26.5	-28.6	-30.8	0.25	0.11	1.01	1.00
Mat	-25.5	-33.2	-31.1	-32.0	0.64	0.14	1.02	1.00
PZE+Microbialites	-23.7	-36.2	-30.0	-32.2	0.63	0.15	1.02	1.00

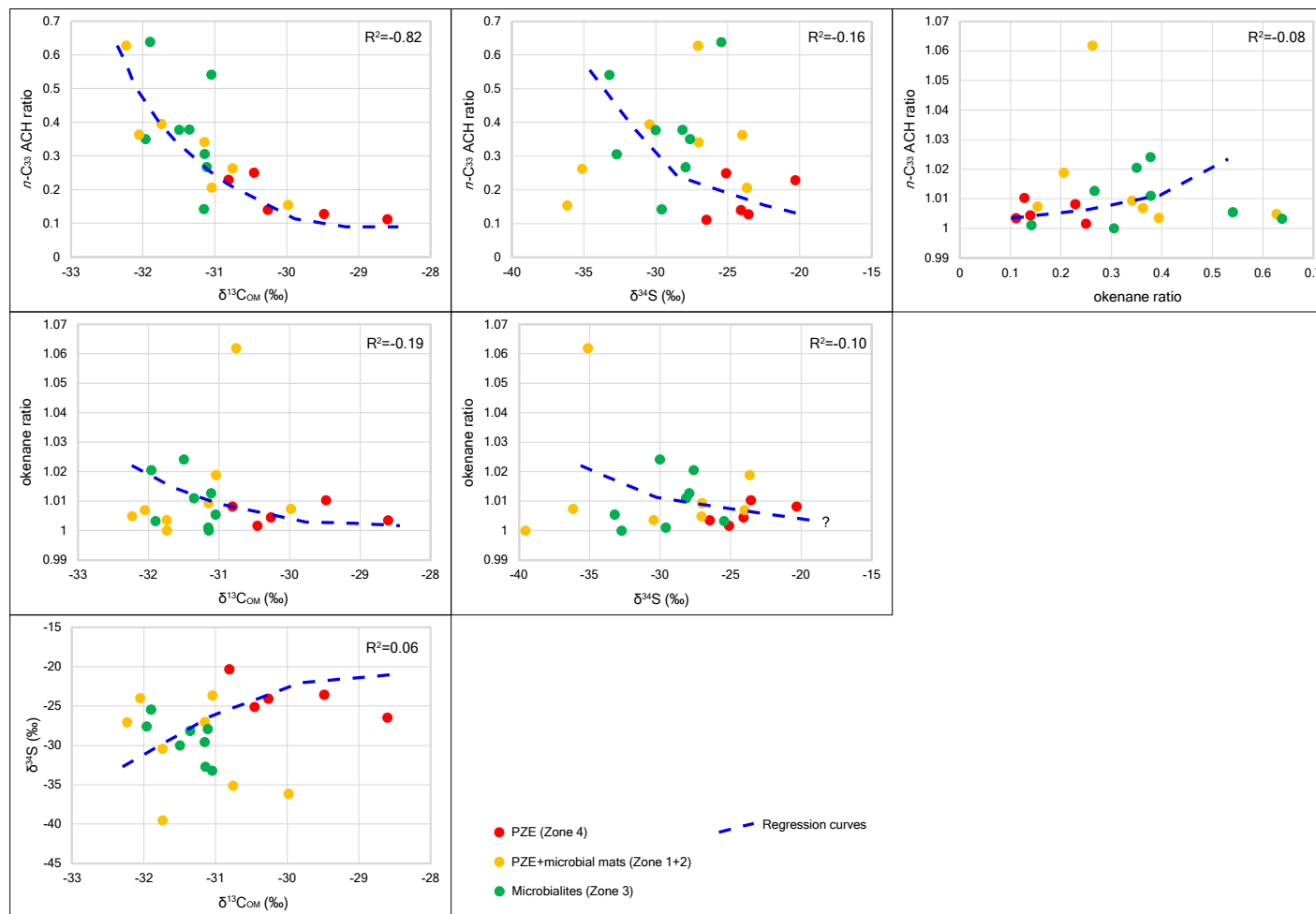


Figure 3-14. Cross plots of each parameter (Okenane ratio, $n\text{-C}_{33}$ ACH, $\delta^{13}\text{C}_{\text{OM}}$ and $\delta^{34}\text{S}$) used for principal component analysis. The dashed line in each plot represents an approximate trend line from PZE facies (red) to microbialite facies (green).

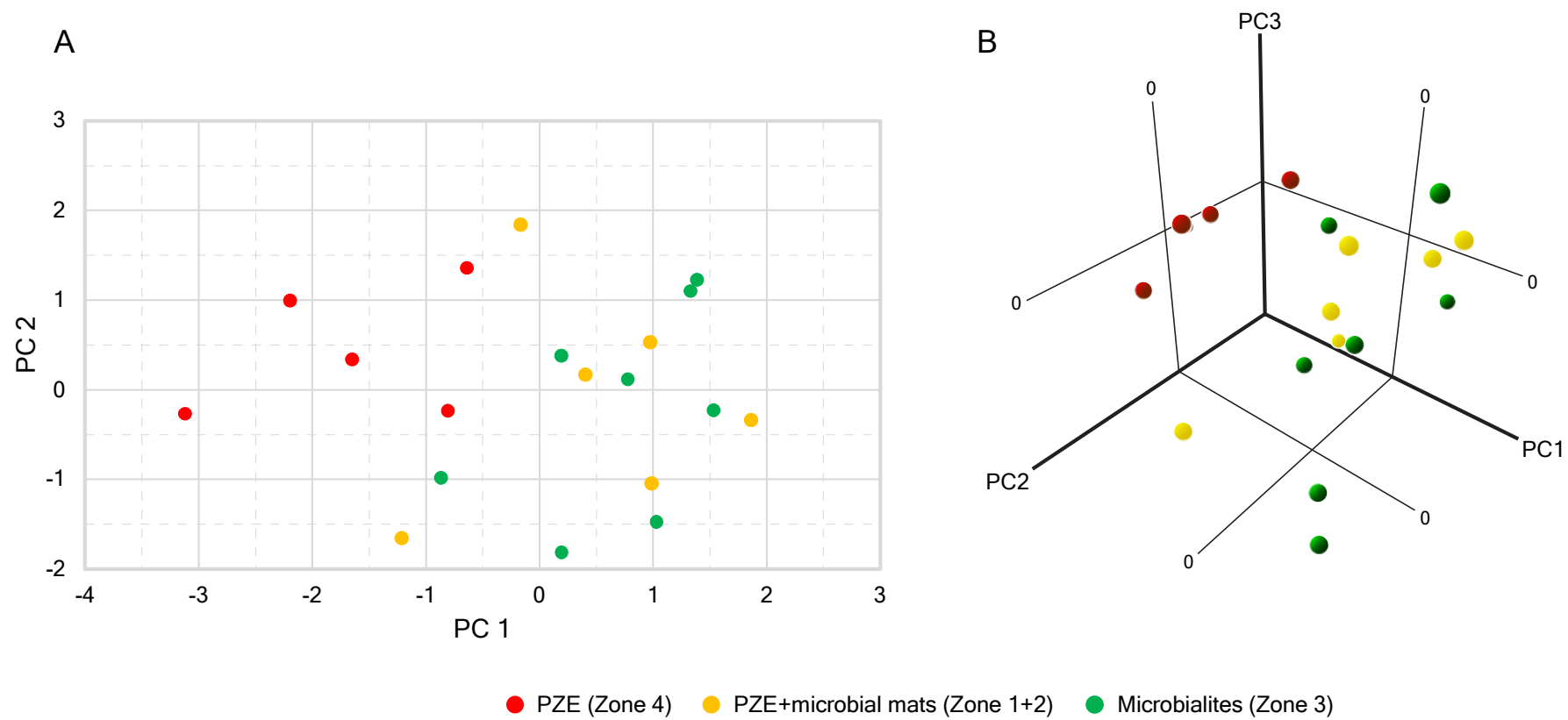


Figure 3-15. Plot of PC1 and PC2 based on the principal component analysis for okenane ratio, n -C₃₃ ACH, $\delta^{13}\text{C}_{\text{OM}}$ and $\delta^{34}\text{S}$.

5.2 Paleoenvironmental conditions and their organic geochemical characteristics

The northern wells (Cliff Head 4, Dongara 4, and Hovea 3) show fluctuating paleoenvironmental transitions between PZE and oxic conditions based on the biomarker and stable isotope characteristics. The lower part of the cored intervals (Zones 1 to 3) is associated with microbialites.

The fluctuation between PZE and oxic conditions suggests changes in the depth of the chemocline (transition between oxic and anoxic water) (Figure 3-16). As there is no evidence of changes in lithofacies, it is unlikely that this could be explained by changes in water depth. Under the shallower chemocline, PZE appears to have occurred across the region. On the other hand, when the chemocline was deeper, oxic conditions developed in shallower waters and PZE was either absent in the basin or persistent only in deeper water.

Microbialites developed under both PZE and oxic conditions. These mats are characterized by the high abundance of purple sulfur bacteria compared to green sulfur bacteria, regardless of PZE vs. oxic conditions. The mats can be distinguished by the relative abundance of cyanobacteria with a high relative abundance of cyanobacteria identified in the microbialites developed under oxic conditions.

Purple sulfur bacteria are active in settings with dissolved inorganic carbon depleted in ^{13}C , and utilize the C3 pathway for carbon fixation (Grice et al., 1997 and references therein). Therefore, the biosynthetic products of these bacteria tend to be relatively depleted in ^{13}C . On the other hand, green sulfur bacteria (green green sulfur bacteria and green brown sulfur bacteria) utilize the reversed TCA cycle for their carbon fixation, giving products which are relatively enriched in ^{13}C (Grice et al., 1997 and references therein)

The results obtained in this study are consistent with this, whereby the microbialite facies in Zone 3 show isotopically lighter $\delta^{13}\text{C}_{\text{OM}}$ values compared with PZE intervals (Zone 4) (Figure 3-11), indicating a higher proportion of purple sulfur

bacteria in microbialites (Zone 3) relative to PZE (Zone 4). This indicates that conditions of dissolved inorganic carbon depleted in ^{13}C were established at the time of microbialite development (Zone 3) in the northern Perth Basin.

$\delta^{34}\text{S}$ under oxic conditions (Zone 5) is isotopically heavier than under other conditions, and values of $\delta^{34}\text{S}$ are more negative in microbialites (Zone 3) than in the PZE intervals (Zone 4) (Figure 3-12). Sulfur isotope fractionation is influenced by microbial metabolism under oxic and anoxic conditions and evaporite mineral formation (Bernasconi et al., 2017). For example, $\delta^{34}\text{S}$ values of pyrite in PZE are often found to be isotopically lighter compared to oxic bottom water conditions (Jørgensen et al., 2004; Schaefer et al., 2020; Wijsman et al., 2001). This difference is controlled by both the actual sulfur isotope composition of seawater sulfate and the overall isotope fractionation derived from the superimposition of biological and abiotic processes shaping the sulfur isotope composition of sulfide. The isotopic composition of pyrite is close to that of the dissolved sulfide (Butler et al., 2004; Price and Shieh, 1979). The strongest isotope effect is related to pyrite formation and burial under anoxic conditions driven by microbial sulfate reduction under open system conditions (wrt. sulfate) which is associated with a strong preference of ^{32}S over ^{34}S during this process (Canfield and Farquhar, 2009; Hartmann and Nielsen, 2012; Kaplan and Rittenberg, 1964). This trend is recognized globally around the Permian-Triassic boundary (Bernasconi et al., 2017). $\delta^{34}\text{S}$ characteristics in this research reflect regional paleoenvironmental impacts on the incorporation of sulfur isotopes into sedimentary pyrite (Hartmann and Nielsen, 2012; Ohmoto et al., 1993). The fractionation of $\delta^{34}\text{S}$ values between PZE and microbialites appears to indicate that the difference in the microbial community, including the relative abundance of purple sulfur bacteria, is a cause for the fractionation and is related to the difference of metabolism of each microbe, as identified in other settings (Hartmann and Nielsen, 2012; Ohmoto et al., 1993).

Zones 1 and 2 have elevated Hg concentration and Hg/TOC compared with overlying zones. Hg-TRIS and Hg-TOC correlate well and are consistent with the

data shown by Georgiev et al. (2020) and Shen et al. (2019a) (Figure 3-13). There are several possible causes of high Hg concentrations, including a transported atmospheric fraction associated with volcanic activity such that of the Siberian Traps (Grasby et al., 2017; Scaife et al., 2017; Shen et al., 2019b; Sial et al., 2020; Wang et al., 2019), terrestrial input (suggesting increasing continental runoff; Them et al., 2019), or incorporation of atmospheric-derived Hg into sulfides precipitating under anoxic conditions in the water column or bottom waters (indicating intensifying anoxia; Shen et al., 2019a, 2020). Given the age of the sediments in the northern Perth Basin, the origin of Hg is likely to be a result of volcanic input (Georgiev et al., 2020; Jones and Hall, 2002; MacNeill et al., 2018; Paschke et al., 2018). Georgiev et al. (2020) identified two intervals with high Hg concentrations near to the Permian-Triassic boundary in Hovea 3, but the Hg data in this study are obtained from different samples to those reported by Georgiev et al. (2020). In addition, the reasons for high Hg concentrations in microbialites have never been fully explored, but Camacho et al. (2015) suggested that growth rate might be an important factor accounting for elevated Hg concentration in microbialites. In this study, the higher concentration of Hg in Zones 1 and 2 can be explained as the result of a combination of volcanic input and the high exposure of Hg to microbialites.

The fluctuations of PZE and oxic conditions in the northern Perth Basin suggest the development of multiple episodes of harsh environmental conditions after the end-Permian mass extinction. The similarity of the superposition in each well shows similar environmental transitions through time and across the basin and is consistent with the recurrent environmental perturbations observed during the Early Triassic in other regions (south China and northern India) (Wei et al., 2015). However, due to the limited resolution of stratigraphic control, it cannot be proven that the chronological scale of changes identified in this research corresponds to the fluctuations in other basins.

5.3 Lateral distribution of paleoenvironmental conditions and relationship with paleogeography

The intra-basinal structural highs (Beagle Ridge and Turtle Dove Ridge) present during the Early Triassic are the topographic remnants of the Late Permian rifting, reconstructed based on seismic data, wireline and core data (Taniwaki et al., 2021). The basin morphology controlled the distribution and deposition of the Early Triassic sediments. During this time, a shallow marine sandstone (the Bookara Sandstone) mainly developed in the southern part of the basin near to its margins. The light coloured mudstone interbedded with tidal sandstone was located near these shallow marine sandstones around Jurien 1 and Woolmulla 1. More distant from the shallow marine sandstone and basin margins, microbialites developed in the intra-basinal structural highs in relatively shallow water, and the dark coloured mudstones (without microbialites) were deposited in greater water in the adjacent troughs.

Paleoenvironmental settings reconstructed on the basis of organic geochemical characteristics show a high level of consistency with the paleogeography reconstructed from geological analysis (Taniwaki et al., 2021) (Figure 3-17). The light coloured mudstones from Jurien 1 and Woolmulla 1 developed under tidally influenced oxic conditions. The dark coloured mudstones from the northern wells (Cliff Head 4, Dongara 4, and Hovea 3) show fluctuations between PZE and oxic conditions. Under the shallower chemocline, PZE developed even in the shallower water on the structural highs (Figure 3-17A), but these locations experienced oxic conditions during periods of deeper chemocline (deeper PZE) (Figure 3-17B).

Highly diverse ichnofossil assemblages during the Early Triassic in northwest Pangea in oxygenated shallow-marine settings have been identified as refuges from the end-Permian mass extinction (Beatty et al., 2008). Haig et al. (2015) recorded a range of fossils including bivalves, gastropods, ammonoids and fish from the outcrop of the Early Triassic Kockatea Shale. Our research shows the development of oxic

conditions near the basin margins which were also refuges for organisms which survived the mass extinction.

6 Conclusions

The combination of organic and isotope geochemical investigations (biomarkers, bulk $\delta^{13}\text{C}_{\text{OM}}$ and $\delta^{34}\text{S}$) and a geologic analysis (core observational data, well analysis and seismic interpretation) has revealed the basin scale paleoenvironmental conditions of the northern Perth Basin during the Early Triassic.

Tidally influenced oxic conditions developed near basin margins in the southern part of the basin and the lighter coloured mudstone was deposited. Far from the basin margins, microbial mats developed in shallower water depth on the intra-basinal structural highs (Beagle Ridge and Turtle Dove Ridge) and PZE developed in greater water depth. In the microbial mat facies, purple sulfur bacteria appears to be more abundant compared with green sulfur bacteria. High abundances of cyanobacterial biomarkers were identified from microbial mats developed under oxic conditions. The *n*-C₃₃ ACH is observed to be abundant in the microbial mats, supporting its strong association with this facies.

The $\delta^{13}\text{C}_{\text{OM}}$ of bulk organic materials and $\delta^{34}\text{S}$ of pyrite are isotopically lighter in the microbial mat than in the PZE facies. The isotopically light $\delta^{13}\text{C}_{\text{OM}}$ in microbial mat facies could support an abundance of purple sulfur bacteria utilizing the C₃ pathway for their carbon fixation which is relatively depleted in ¹³C. The fractionation of $\delta^{34}\text{S}$ values between PZE and microbial mats appears to indicate that the difference of microbial community including the relative abundance of purple sulfur bacteria is a cause for the fractionation. The concentration of Hg and Hg/TOC are high around the interval with high C₃₀ sterane ratio indicating that this interval most likely developed after the mass extinction event, with the Hg being associated with volcanic activity. The okenane ratio, *n*-C₃₃ACH, $\delta^{13}\text{C}_{\text{OM}}$ and $\delta^{34}\text{S}$ are good proxies for distinguishing

PZE and microbial mat facies, related to the relative abundance of purple and green sulfur bacteria. Therefore, these values are useful for identifying the contribution of PZE and microbial mats in geological samples.

The biomarker and isotope data for organic matter in this study seems to be strongly influenced by microbial mats and PZE conditions. This basin-scale study and the $\delta^{13}\text{C}_{\text{OM}}$ data interpretations have the potential to be applied to all mass extinction events, including a reappraisal of chemo-isotope stratigraphical correlations.

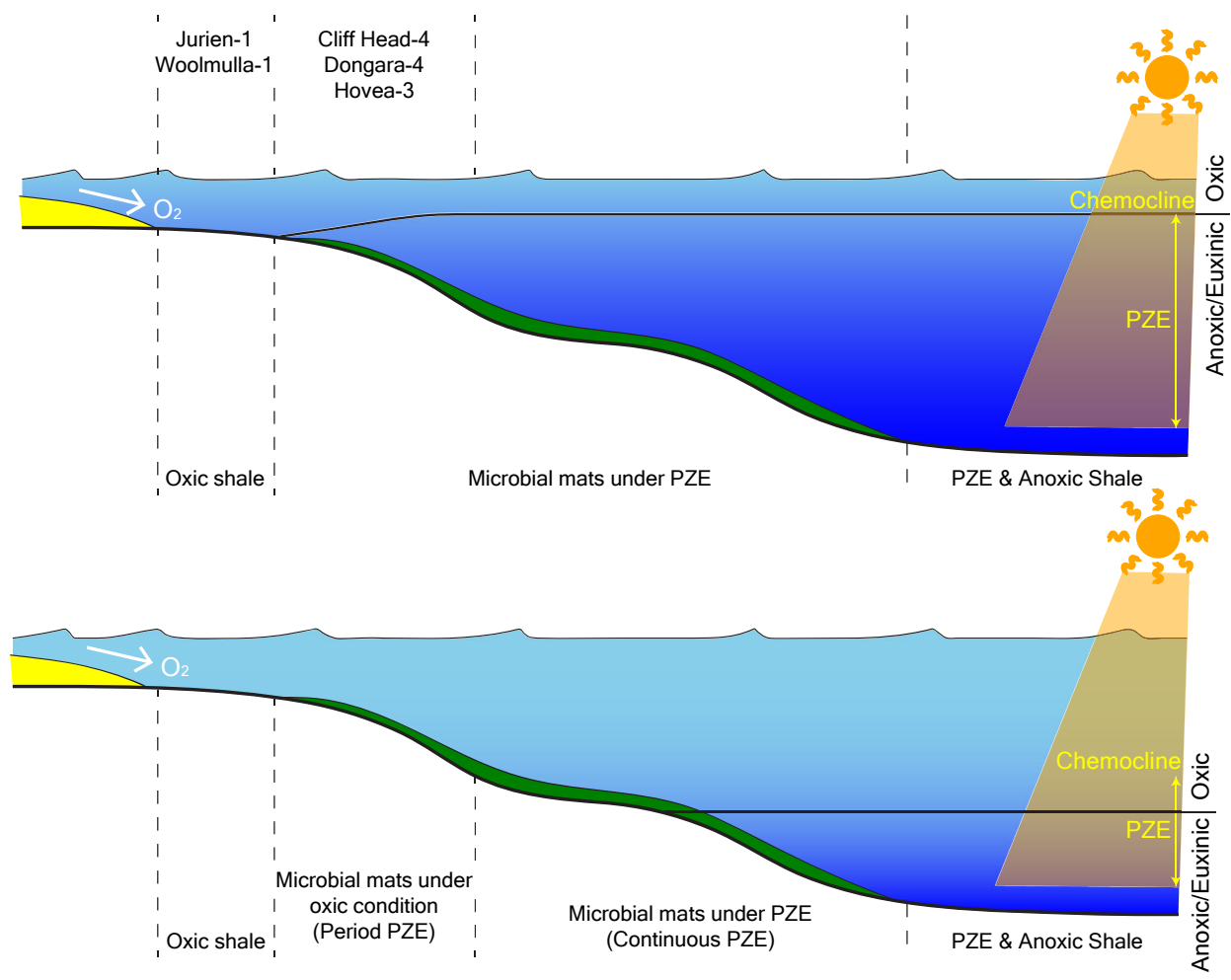


Figure 3-16. Paleoenvironmental setting sketch showing the fluctuation of PZE associated with the fluctuation of the depth of the chemocline.

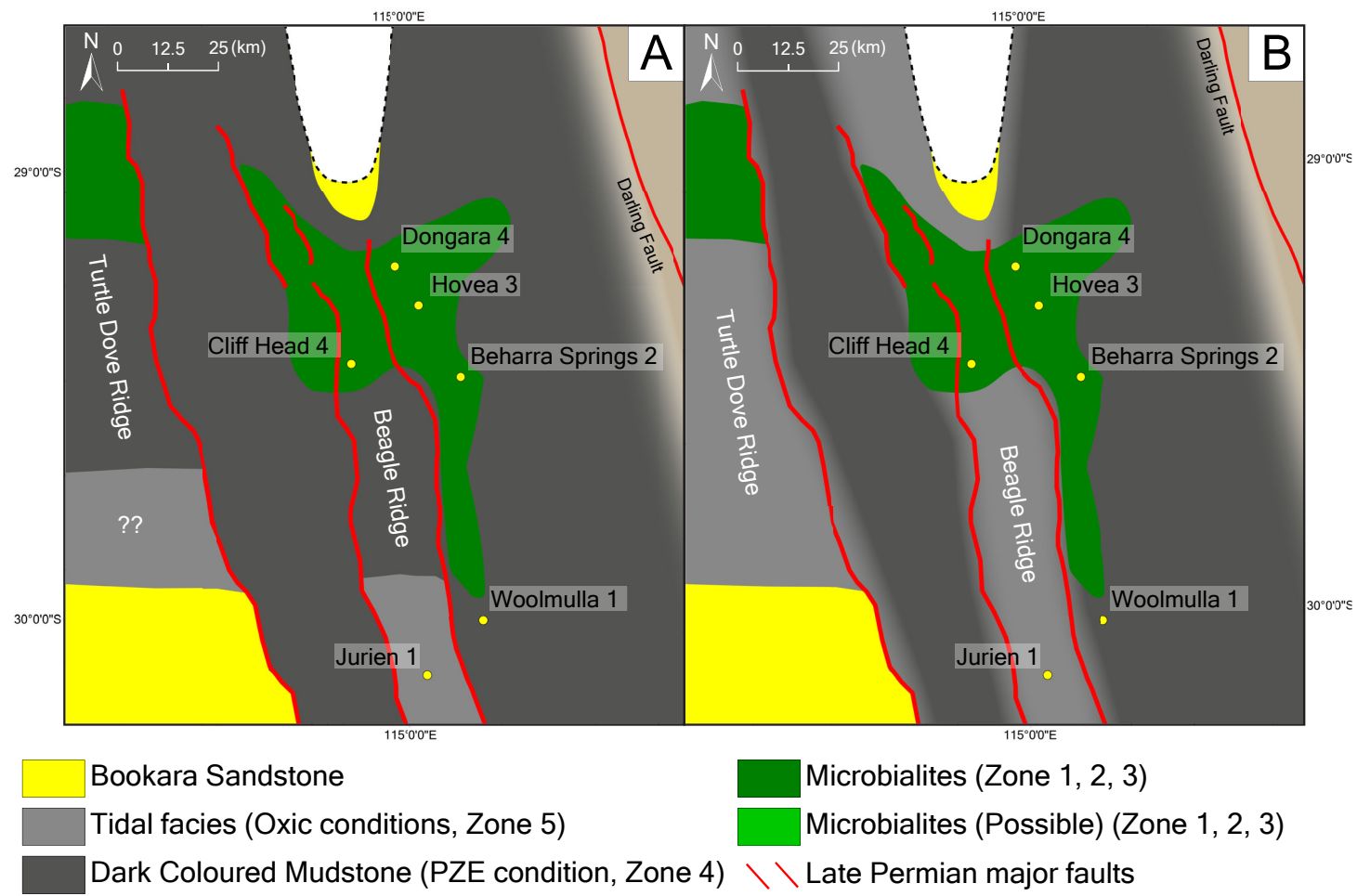


Figure 3-17. The distribution of PZE and microbialites in the Early Triassic northern Perth Basin. A shows the basin during shallower chemocline and B shows the basin during deeper chemocline.

Acknowledgements

This study was part of the PhD research of the first author, funded by INPEX Corporation. The authors thank the Geological Survey of Western Australia for permission to collect rock samples (G004177), Peter Hopper for the technical support, and Roger Summons for the arrangement of GC-MRM-MS analysis.

References

- Beatty, T.W., Zonneveld, J.P., Henderson, C.M., 2008. Anomalously diverse Early Triassic ichnofossil assemblages in northwest Pangea: A case for a shallow-marine habitable zone. *Geology* 36, 771–774.
<https://doi.org/10.1130/G24952A.1>
- Benton, M.J., 2016. The Triassic. *Curr. Biol.* 26, R1214--R1218.
<https://doi.org/10.1016/j.cub.2016.10.060>
- Bernasconi, S.M., Meier, I., Wohlwend, S., Brack, P., Hochuli, P.A., Bläsi, H., Wortmann, U.G., Ramseyer, K., 2017. An evaporite-based high-resolution sulfur isotope record of Late Permian and Triassic seawater sulfate. *Geochim. Cosmochim. Acta* 204, 331–349. <https://doi.org/10.1016/j.gca.2017.01.047>
- Bralower, T.J., Cosmidis, J., Heaney, P.J., Kump, L.R., Morgan, V., Harper, D.T., Lyons, S.L., Freeman, K.H., Grice, K., Wendler, E., Zachos, J.C., Artemieva, N., Athena, S., Gulick, S.P.S., House, C.H., Jones, H.L., Lowery, C.M., Nims, C., Schaefer, B., Thomas, E., Vajda, V., 2020. Origin of a global carbonate layer deposited in the aftermath of the Cretaceous-Paleogene boundary impact. *Earth Planet. Sci. Lett.* 548, 116476. <https://doi.org/10.1016/j.epsl.2020.116476>
- Brand, W.A., Coplen, T.B., 2012. Stable isotope deltas: Tiny, yet robust signatures in nature. *Isotopes Environ. Health Stud.* 48, 393–409.
<https://doi.org/10.1080/10256016.2012.666977>
- Brocks, J.J., Schaeffer, P., 2008. Okenane, a biomarker for purple sulfur bacteria (Chromatiaceae), and other new carotenoid derivatives from the 1640 Ma Barney Creek Formation. *Geochim. Cosmochim. Acta* 72, 1396–1414.
<https://doi.org/10.1016/j.gca.2007.12.006>
- Butler, I.B., Böttcher, M.E., Rickard, D., Oldroyd, A., 2004. Sulfur isotope partitioning during experimental formation of pyrite via the polysulfide and hydrogen sulfide pathways: Implications for the interpretation of sedimentary

- and hydrothermal pyrite isotope records. *Earth Planet. Sci. Lett.* 228, 495–509.
<https://doi.org/10.1016/j.epsl.2004.10.005>
- Camacho, A., Rochera, C., Hennebelle, R., Ferrari, C., Quesada, A., 2015. Total mercury and methyl-mercury contents and accumulation in polar microbial mats. *Sci. Total Environ.* 509–510, 145–153.
<https://doi.org/10.1016/j.scitotenv.2014.09.012>
- Canfield, D.E., Farquhar, J., 2009. Animal evolution, bioturbation, and the sulfate concentration of the oceans. *Proc. Natl. Acad. Sci. U. S. A.* 106, 8123–8127.
<https://doi.org/10.1073/pnas.0902037106>
- Chen, Z.-Q., Benton, M.J., 2012. The timing and pattern of biotic recovery following the end-Permian mass extinction. *Nat. Geosci.* 5, 375–383.
<https://doi.org/10.1038/ngeo1475>
- Chen, Z.-Q., Fraiser, M.L., Bolton, C., 2012. Early Triassic trace fossils from Gondwana Interior Sea: Implication for ecosystem recovery following the end-Permian mass extinction in south high-latitude region. *Gondwana Res.* 22, 238–255. <https://doi.org/10.1016/j.gr.2011.08.015>
- Chen, Z.Q., Wang, Y., Kershaw, S., Luo, M., Yang, H., Zhao, L., Feng, Y., Chen, J., Yang, L., Zhang, L., 2014. Early Triassic stromatolites in a siliciclastic nearshore setting in northern Perth Basin, Western Australia: Geobiologic features and implications for post-extinction microbial proliferation. *Glob. Planet. Change* 121, 89–100. <https://doi.org/10.1016/j.gloplacha.2014.07.004>
- Clifford, D.J., Clayton, J.L., Sinninghe Damsté, J.S., 1998. 2,3,6-/3,4,5-Trimethyl substituted diaryl carotenoid derivatives (Chlorobiaceae) in petroleums of the Belarussian Pripyat River Basin. *Org. Geochem.* 29, 1253–1267.
[https://doi.org/10.1016/S0146-6380\(98\)00086-2](https://doi.org/10.1016/S0146-6380(98)00086-2)
- Coplen, T.B., Brand, W.A., Gehre, M., Grhning, M., Meljer, H.A.J., Toman, B., Verkouteren, R.M., 2006. New Guidelines for $\delta^{13}\text{C}$ Measurements. *Anal.*

Chem. 78, 2439–2441.

- Cui, X., Liu, X.L., Shen, G., Ma, J., Husain, F., Rocher, D., Zumberge, J.E., Bryant, D.A., Summons, R.E., 2020. Niche expansion for phototrophic sulfur bacteria at the Proterozoic–Phanerozoic transition. *Proc. Natl. Acad. Sci. U. S. A.* 117, 17599–17606. <https://doi.org/10.1073/pnas.2006379117>
- Ferdinando, D., Baker, J.C., Gongora, A., Pidgeon, B.A., 2007. Illite/smectite clays preserving porosity at depth in Lower Permian reservoirs, northern Perth Basin. *APPEA J.* 47, 69–88. <https://doi.org/10.1071/aj06004>
- Fossing, H., Jørgensen, B.B., 1989. Measurement reduction of a single-step chromium method Evaluation of a single-step chromium reduction method. *Biogeochemistry* 8, 205–222.
- Foster, W.J., Danise, S., Sedlacek, A., Price, G.D., Hips, K., Twitchett, R.J., 2015. Environmental controls on the post-Permian recovery of benthic, tropical marine ecosystems in western Palaeotethys (Aggtelek Karst, Hungary). *Palaeogeogr. Palaeoclimatol. Palaeoecol.* 440, 374–394. <https://doi.org/10.1016/j.palaeo.2015.09.004>
- Fox, C.P., Cui, X., Whiteside, J.H., Olsen, P.E., Summons, R.E., Grice, K., 2020. Molecular and isotopic evidence reveals the end-Triassic carbon isotope excursion is not from massive exogenous light carbon. *Proc. Natl. Acad. Sci.* 117, 30171–30178. <https://doi.org/10.1073/pnas.1917661117>
- French, K.L., Sepúlveda, J., Trabucho-Alexandre, J., Gröcke, D.R., Summons, R.E., 2014. Organic geochemistry of the early Toarcian oceanic anoxic event in Hawsker Bottoms, Yorkshire, England. *Earth Planet. Sci. Lett.* 390, 116–127. <https://doi.org/10.1016/j.epsl.2013.12.033>
- Georgiev, S. V., Stain, H.J., Yang, G., Hannah, J.L., Böttcher, M.E., Grice, K., Holman, A.I., Turgeon, S., Simonsen, S., Cloquet, C., 2020. Late Permian–Early Triassic environmental changes recorded by multi-isotope (Re-Os-N-Hg)

- data and trace metal distribution from the Hovea-3 section, Western Australia. *Gondwana Res.* 88, 353–372. <https://doi.org/10.1016/j.bbamem.2019.183135>
- Gorter, J., Nicoll, R.S., Metcalfe, I., Willink, R., Ferdinando, D., 2009. The Permian–Triassic boundary in Western Australia: evidence from the Bonaparte and Northern Perth basins—exploration implications. *APPEA J.* 49, 311–336. <https://doi.org/10.1071/AJ08020>
- Grasby, S.E., Shen, W., Yin, R., Gleason, J.D., Blum, J.D., Lepak, R.F., Hurley, J.P., Beauchamp, B., 2017. Isotopic signatures of mercury contamination in latest Permian oceans. *Geology* 45, 55–58. <https://doi.org/10.1130/G38487.1>
- Grice, K., Cao, C., Love, G.D., Böttcher, M.E., Twitchett, R.J., Grosjean, E., Summons, R.E., Turgeon, S.C., Dunning, W., Jin, Y., 2005a. Photic zone euxinia during the Permian-Triassic superanoxic event. *Science*. 307, 706–709. <https://doi.org/10.1126/science.1104323>
- Grice, K., Gibbison, R., Atkinson, J.E., Schwark, L., Eckardt, C.B., Maxwell, J.R., 1996. Maleimides (1H-pyrrole-2,5-diones) as molecular indicators of anoxygenic photosynthesis in ancient water columns. *Geochim. Cosmochim. Acta* 60, 3913–3924. [https://doi.org/10.1016/0016-7037\(96\)00199-8](https://doi.org/10.1016/0016-7037(96)00199-8)
- Grice, K., Schaeffer, P., Schwark, L., Maxwell, J.R., 1997. Changes in palaeoenvironmental conditions during deposition of the Permian Kupferschiefer (Lower Rhine Basin, northwest Germany) inferred from molecular and isotopic compositions of biomarker components. *Org. Geochem.* 26, 677–690.
- Grice, K., Summons, R.E., Grosjean, E., Twitchett, R.J., Dunning, W., Wang, S.X., Böttcher, M.E., 2005b. Depositional conditions of the Northern Onshore Perth Basin (Basal Triassic). *APPEA J.* 45, 263–274.
- Grice, K., Twitchett, R.J., Alexander, R., Foster, C.B., Looy, C., 2005c. A potential biomarker for the Permian-Triassic ecological crisis. *Earth Planet. Sci. Lett.*

236, 315–321. <https://doi.org/10.1016/j.epsl.2005.05.008>

Haig, D.W., Martin, S.K., Mory, A.J., McLoughlin, S., Backhouse, J., Berrell, R.W., Kear, B.P., Hall, R., Foster, C.B., Shi, G.R., Bevan, J.C., 2015. Early Triassic (early Olenekian) life in the interior of East Gondwana: Mixed marine-terrestrial biota from the Kockatea Shale, Western Australia. *Palaeogeogr. Palaeoclimatol. Palaeoecol.* 417, 511–533. <https://doi.org/10.1016/j.palaeo.2014.10.015>

Hallam, A., 1991. Why was there a delayed radiation after the end-palaeozoic extinctions? *Hist. Biol.* 5, 257–262. <https://doi.org/10.1080/10292389109380405>

Hartmann, M., Nielsen, H., 2012. $\delta^{34}\text{S}$ values in recent sea sediments and their significance using several sediment profiles from the western Baltic Sea. *Isotopes Environ. Health Stud.* 48, 7–32. <https://doi.org/10.1080/10256016.2012.660528>

Hays, L.E., Beatty, T., Henderson, C.M., Love, G.D., Summons, R.E., 2007. Evidence for photic zone euxinia through the end-Permian mass extinction in the Panthalassic Ocean (Peace River Basin, Western Canada). *Palaeoworld* 16, 39–50. <https://doi.org/10.1016/j.palwor.2007.05.008>

Hofmann, R., Goudemand, N., Wasmer, M., Bucher, H., Hautmann, M., 2011. New trace fossil evidence for an early recovery signal in the aftermath of the end-Permian mass extinction. *Palaeogeogr. Palaeoclimatol. Palaeoecol.* 310, 216–226. <https://doi.org/10.1016/j.palaeo.2011.07.014>

Jablonski, D., Saitta, A.J., 2004. Permian To Lower Cretaceous Plate Tectono-Stratigraphic Development of the Western Australian Margin. *APPEA J.* 44, 287–328. <https://doi.org/10.1071/AJ03011>

Jones, N.T., Hall, a D., 2002. The Cliff Head Oil Discovery – Offshore Perth Basin, in: *The Sedimentary Basins of Western Australia 3: Proceedings of the*

Petroleum Exploration Society of Australia Symposium. pp. 901–909.

Jørgensen, B.B., Böttcher, M.E., Lüschen, H., Neretin, L.N., Volkov, I.I., 2004.

Anaerobic methane oxidation and a deep H₂S sink generate isotopically heavy sulfides in Black Sea sediments. *Geochim. Cosmochim. Acta* 68, 2095–2118.
<https://doi.org/10.1016/j.gca.2003.07.017>

Kaiho, K., Saito, R., Ito, K., Miyaji, T., Biswas, R., Tian, L., Sano, H., Shi, Z.,

Takahashi, S., Tong, J., Liang, L., Oba, M., Nara, F.W., Tsuchiya, N., Chen,

Z.Q., 2016. Effects of soil erosion and anoxic–euxinic ocean in the Permian–

Triassic marine crisis. *Heliyon* 2. <https://doi.org/10.1016/j.heliyon.2016.e00137>

Kaplan, I.R., Rittenberg, S.C., 1964. Microbiological fractionation of sulphur

isotopes. *J. Gen. Microbiol.* 34, 195–212. <https://doi.org/10.1099/00221287-34-2-195>

Knaust, D., 2010. The end-Permian mass extinction and its aftermath on an

equatorial carbonate platform: Insights from ichnology. *Terra Nov.* 22, 195–202. <https://doi.org/10.1111/j.1365-3121.2010.00934.x>

Leipe, T., Moros, M., Kotilainen, A., Vallius, H., Kabel, K., Endler, M., Kowalski,

N., 2013. Mercury in Baltic Sea sediments-Natural background and

anthropogenic impact. *Chemie der Erde* 73, 249–259.

<https://doi.org/10.1016/j.chemer.2013.06.005>

Luo, M., Chen, Z.Q., 2014. New arthropod traces from the Lower Triassic Kockatea

Shale Formation, northern Perth Basin, Western Australia: Ichnology,

taphonomy and palaeoecology. *Geol. J.* 49, 163–176.

<https://doi.org/10.1002/gj.2506>

Luo, M., Chen, Z.Q., Shi, G.R., Feng, X., Yang, H., Fang, Y., Li, Y., 2018.

Microbially induced sedimentary structures (MISSs) from the Lower Triassic

Kockatea Formation, northern Perth Basin, Western Australia:

Palaeoenvironmental implications. *Palaeogeogr. Palaeoclimatol. Palaeoecol.*

519, 236–247. <https://doi.org/10.1016/j.palaeo.2018.06.040>

- MacNeill, M., Marshall, N., McNamara, C., 2018. New Insights into a major Early-Middle Triassic Rift Episode in the NW Shelf of Australia, in: ASEG 2018 Extended Abstracts. pp. 1–5. https://doi.org/10.1071/ASEG2018abM3_3B
- Mann, J.L., Vocke, R.D., Kelly, W.R., 2009. Revised $\delta^{34}\text{S}$ reference values for IAEA sulfur isotope reference materials S-2 and S-3. *Rapid Commun. Mass Spectrom.* 23, 1116–1124. <https://doi.org/10.1002/rcm.3977>
- Manske, A.K., Glaeser, J., Kuypers, M.M.M., Overmann, J., 2005. Physiology and phylogeny of green sulfur bacteria forming a monospecific phototrophic assemblage at a depth of 100 meters in the Black Sea. *Appl. Environ. Microbiol.* 71, 8049–8060. <https://doi.org/10.1128/AEM.71.12.8049-8060.2005>
- Maslen, E., Grice, K., Gale, J.D., Hallmann, C., Horsfield, B., 2009. Crocetane: A potential marker of photic zone euxinia in thermally mature sediments and crude oils of Devonian age. *Org. Geochem.* 40, 1–11. <https://doi.org/10.1016/j.orggeochem.2008.10.005>
- Metcalf, I., Nicoll, R.S., Willink, R.J., 2008. Conodonts from the Permian-Triassic transition in Australia and position of the Permian-Triassic boundary. *Aust. J. Earth Sci.* 55, 365–377. <https://doi.org/10.1080/08120090701769480>
- Mory, A.J., Haig, D.W., McLoughlin, S., Hocking, R.M., 2005. Geology of the northern Perth Basin, Western Australia- A field guide. *Geol. Surv. West. Aust.* 2005/9, 71p.
- Mory, A.J., Iasky, R.P., 1996. Stratigraphy and structure of the onshore northern Perth Basin, Western Australia. *Geol. Surv. West. Aust. Report* 46, 101pp.
- Nabbefeld, B., Grice, K., Twitchett, R.J., Summons, R.E., Hays, L., Böttcher, M.E., Asif, M., 2010. An integrated biomarker, isotopic and palaeoenvironmental study through the Late Permian event at Lusitaniadalen, Spitsbergen. *Earth*

-
- Planet. Sci. Lett. 291, 84–96. <https://doi.org/10.1016/j.epsl.2009.12.053>
- Norvick, M.S., 2004. Tectonic and Stratigraphic History of the Perth Basin. *Geosci. Aust.* 2004/16, 18p.
- Ohmoto, H., Kakegawa, T., Lowe, D.R., 1993. 3.4-billion-year-old biogenic pyrites from Barberton, South Africa: Sulfur isotope evidence. *Science*. 262, 555–557. <https://doi.org/10.1126/science.11539502>
- Pagès, A., Grice, K., Vacher, M., Welsh, D.T., Teasdale, P.R., Bennett, W.W., Greenwood, P., 2014. Characterizing microbial communities and processes in a modern stromatolite (Shark Bay) using lipid biomarkers and two-dimensional distributions of porewater solutes. *Environ. Microbiol.* 16, 2458–2474. <https://doi.org/10.1111/1462-2920.12378>
- Paschke, C., O’Halloran, G., Dempsey, C., O’Halloran, G., 2018. Interpretation of a Permian conjugate basin margin preserved on the outer Northwest Shelf of Australia, in: *AEGC 2018 Extended Abstracts*. pp. 1–8. https://doi.org/10.1071/ASEG2018abM3_2B
- Payne, J.L., Lehrmann, D.J., Wei, J., Orchard, M.J., Schrag, D.P., Knoll, A.H., 2004. Large perturbations of the carbon cycle during recovery from the end-Permian extinction. *Science*. 305, 506–509. <https://doi.org/10.1126/science.1097023>
- Pedentchouk, N., Freeman, K.H., Harris, N.B., Clifford, D.J., Grice, K., 2004. Sources of alkylbenzenes in Lower Cretaceous lacustrine source rocks, West African rift basins. *Org. Geochem.* 35, 33–45. <https://doi.org/10.1016/j.orggeochem.2003.04.001>
- Peters, K., Walters, C., Moldowan, J., 2004. *The Biomarker Guide*, 2nd ed. Cambridge University Press.
- Pfenning, N., 1978. General physiology and ecology of photosynthetic bacteria, in: Clayton, R.K., Sistrom, W.R. (Eds.), *The Photosynthetic Bacteria*. Plenum, New

York, pp. 3–18.

- Pollmann, T., Böttcher, M.E., Giani, L., 2021. Young soils of a temperate barrier island under the impact of formation and resetting by tides and wind. *Catena* 202, 105275. <https://doi.org/10.1016/j.catena.2021.105275>
- Price, F.T., Shieh, Y.N., 1979. Fractionation of sulfur isotopes during laboratory synthesis of pyrite at low temperatures. *Chem. Geol.* 27, 245–253.
- Reichow, M.K., Pringle, M.S., Al’Mukhamedov, A.I., Allen, M.B., Andreichev, V.L., Buslov, M.M., Davies, C.E., Fedoseev, G.S., Fitton, J.G., Inger, S., Medvedev, A.Y., Mitchell, C., Puchkov, V.N., Safonova, I.Y., Scott, R.A., Saunders, A.D., 2009. The timing and extent of the eruption of the Siberian Traps large igneous province: Implications for the end-Permian environmental crisis. *Earth Planet. Sci. Lett.* 277, 9–20.
<https://doi.org/10.1016/j.epsl.2008.09.030>
- Retallack, G.J., Veevers, J.J., Morante, R., 1996. Global coal gap between Permian-Triassic extinction and Middle Triassic recovery of peat-forming plants. *GSA Bull.* 108, 195–207.
- Sahney, S., Benton, M.J., 2008. Recovery from the most profound mass extinction of all time. *Proc. R. Soc. B Biol. Sci.* 275, 759–765.
<https://doi.org/10.1098/rspb.2007.1370>
- Sandwell, D., Garcia, E., Soofi, K., Wessel, P., Chandler, M., Smith, W.H.F., 2013. Toward 1-mGal accuracy in global marine gravity from CryoSat-2, Envisat, and Jason-1. *Lead. Edge* 32, 892–899.
- Sandwell, D.T., Müller, R.D., Smith, W.H.F., Garcia, E., Francis, R., 2014. New global marine gravity model from CryoSat-2 and Jason-1 reveals buried tectonic structure. *Science.* 346, 65–67. <https://doi.org/10.1126/science.1258213>
- Sandwell, D.T., Smith, W.H.F., 2009. Global marine gravity from retracked Geosat

- and ERS-1 altimetry: Ridge segmentation versus spreading rate. *J. Geophys. Res. Solid Earth* 114, B01411. <https://doi.org/10.1029/2008JB006008>
- Sass, A.M., Sass, H., Coolen, M.J.L., Cypionka, H., Overmann, J., 2001. Microbial Communities in the Chemocline of a Hypersaline Deep-Sea Basin (Urania Basin, Mediterranean Sea). *Appl. Environ. Microbiol.* 67, 5392–5402. <https://doi.org/10.1128/AEM.67.12.5392-5402.2001>
- Scaife, J.D., Ruhl, M., Dickson, A.J., Mather, T.A., Jenkyns, H.C., Percival, L.M.E., Hesselbo, S.P., Cartwright, J., Eldrett, J.S., Bergman, S.C., Minisini, D., 2017. Sedimentary Mercury Enrichments as a Marker for Submarine Large Igneous Province Volcanism? Evidence From the Mid-Cenomanian Event and Oceanic Anoxic Event 2 (Late Cretaceous). *Geochemistry, Geophys. Geosystems* 18, 4253–4275. <https://doi.org/10.1002/2017GC007153>
- Schaefer, B., Grice, K., Coolen, M.J.L., Summons, R.E., Cui, X., Bauersachs, T., Schwark, L., Böttcher, M.E., Bralower, T.J., Lyons, S.L., Freeman, K.H., Cockell, C.S., Gulick, S.S., Morgan, J. V., Whalen, M.T., Lowery, C.M., Vajda, V., 2020. Microbial mayhem in the nascent chicxulub crater. *Geology* 48, 328–332. <https://doi.org/10.1130/G46799.1>
- Sedlacek, A.R.C.C., Saltzman, M.R., Algeo, T.J., Horacek, M., Brandner, R., Foland, K., Denniston, R.F., 2014. $^{87}\text{Sr}/^{86}\text{Sr}$ stratigraphy from the Early Triassic of Zal, Iran: Linking temperature to weathering rates and the tempo of ecosystem recovery. *Geology* 42, 779–782. <https://doi.org/10.1130/G35545.1>
- Shen, J., Algeo, T.J., Chen, J., Planavsky, N.J., Feng, Q., Yu, J., Liu, J., 2019a. Mercury in marine Ordovician/Silurian boundary sections of South China is sulfide-hosted and non-volcanic in origin. *Earth Planet. Sci. Lett.* 511, 130–140. <https://doi.org/10.1016/j.epsl.2019.01.028>
- Shen, J., Chen, J., Algeo, T.J., Yuan, S., Feng, Q., Yu, J., Zhou, L., O’Connell, B., Planavsky, N.J., 2019b. Evidence for a prolonged Permian–Triassic extinction

interval from global marine mercury records. *Nat. Commun.* 10, 1563.

<https://doi.org/10.1038/s41467-019-09620-0>

Shen, J., Schoepfer, S.D., Feng, Q., Zhou, L., Yu, J., Song, H., Wei, H., Algeo, T.J., 2015. Marine productivity changes during the end-Permian crisis and Early Triassic recovery. *Earth-Science Rev.* 149, 136–162.

<https://doi.org/10.1016/j.earscirev.2014.11.002>

Shen, Y., Wang, Y., Miao, Y., Yang, M., Zhao, X., Shen, X., 2020. High-Energy Interlayer-Expanded Copper Sulfide Cathode Material in Non-Corrosive Electrolyte for Rechargeable Magnesium Batteries. *Adv. Mater.* 32, 1–9.

<https://doi.org/10.1002/adma.201905524>

Sial, A.N., Chen, J., Lacerda, L.D., Korte, C., Spangenberg, J.E., Silva-Tamayo, J.C., Gaucher, C., Ferreira, V.P., Barbosa, J.A., Pereira, N.S., Benigno, A.P., 2020. Globally enhanced Hg deposition and Hg isotopes in sections straddling the Permian–Triassic boundary: Link to volcanism. *Palaeogeogr. Palaeoclimatol. Palaeoecol.* 540, 109537. <https://doi.org/10.1016/j.palaeo.2019.109537>

Song, H.H., Wignall, P.B., Chu, D., Tong, J., Sun, Y., Song, H.H., He, W., Tian, L., 2014. Anoxia/high temperature double whammy during the Permian-Triassic marine crisis and its aftermath. *Sci. Rep.* 4, 1–7.

<https://doi.org/10.1038/srep04132>

Sousa Júnior, G.R., Santos, A.Ô.L.S.S., De Lima, S.G., Lopes, J.A.D.D., Reis, F.A.M.M., Santos Neto, E. V., Chang, H.K., 2013. Evidence for euphotic zone anoxia during the deposition of Aptian source rocks based on aryl isoprenoids in petroleum, Sergipe-Alagoas Basin, northeastern Brazil. *Org. Geochem.* 63, 94–104. <https://doi.org/10.1016/j.orggeochem.2013.07.009>

Spaak, G., 2017. *Molecular and Isotopic Perspectives on Australian Petroleum Systems: Hydrocarbon Fluid Correlations and Source Rock Depositional Environments in the Canning and Browse Basins.* Curtin University.

-
- Summons, R.E., Jahnke, L.L., Hope, J.M., Logan, G.A., 1999. 2-Methylhopanoids as biomarkers for cyanobacterial oxygenic photosynthesis. *Nature* 400, 554–557. <https://doi.org/10.1038/23005>
- Summons, R.E., Powell, T.G., 1987. Identification of aryl isoprenoids in source rocks and crude oils: biological markers for green sulphur bacteria. *Geochim. Cosmochim. Acta* 51, 557–566.
- Taniwaki, T., Elders, C., Grice, K., 2021. Early Triassic paleogeography of the northern Perth Basin, and controls on the distribution of source rock facies. *Mar. Pet. Geol.* 133, 105314. <https://doi.org/10.1016/j.marpetgeo.2021.105314>
- Them, T.R., Jagoe, C.H., Caruthers, A.H., Gill, B.C., Grasby, S.E., Gröcke, D.R., Yin, R., Owens, J.D., 2019. Terrestrial sources as the primary delivery mechanism of mercury to the oceans across the Toarcian Oceanic Anoxic Event (Early Jurassic). *Earth Planet. Sci. Lett.* 507, 62–72. <https://doi.org/10.1016/j.epsl.2018.11.029>
- Thomas, B.M., Barber, C.J., 2004. A re-evaluation of the hydrocarbon habitat of the northern Perth Basin. *APPEA J.* 44, 59–92.
- Thomas, B.M., Willink, R.J., Grice, K., Twitchett, R.J., Purcell, R.R., George, A.D., Tye, S., Alexander, R., Foster, C.B., Barber, C.J., George, A.D., Tye, S., Alexander, R., Foster, C.B., Unique, C.J.B., Barber, C.J., 2004. Unique marine Permian-Triassic boundary section from Western Australia. *Aust. J. Earth Sci.* 51, 423–430.
- Tulipani, S., Grice, K., Greenwood, P.F., Schwark, L., Böttcher, M.E., Summons, R.E., Foster, C.B., 2015. Molecular proxies as indicators of freshwater incursion-driven salinity stratification. *Chem. Geol.* 409, 61–68. <https://doi.org/10.1016/j.chemgeo.2015.05.009>
- Twitchett, R.J., Krystyn, L., Baud, A., Wheeley, J.R., Richoz, S., 2004. Rapid marine recovery after the end-Permian mass-extinction event in the absence of marine

- anoxia. *Geology* 32, 805–808. <https://doi.org/10.1130/G20585.1>
- Wang, X., Cawood, P.A., Zhao, H., Zhao, L., Grasby, S.E., Chen, Z.Q., Zhang, L., 2019. Global mercury cycle during the end-Permian mass extinction and subsequent Early Triassic recovery. *Earth Planet. Sci. Lett.* 513, 144–155. <https://doi.org/10.1016/j.epsl.2019.02.026>
- Wei, H., Shen, J., Schoepfer, S.D., Krystyn, L., Richoz, S., Algeo, T.J., 2015. Environmental controls on marine ecosystem recovery following mass extinctions, with an example from the Early Triassic. *Earth-Science Rev.* 149, 108–135. <https://doi.org/10.1016/j.earscirev.2014.10.007>
- Whiteside, J.H., Grice, K., 2016. Biomarker Records Associated with Mass Extinction Events. *Annu. Rev. Earth Planet. Sci.* 44, 581–612. <https://doi.org/10.1146/annurev-earth-060115-012501>
- Wignall, P.B., Twitchett, R.J., 1996. Oceanic anoxia and the end Permian mass extinction. *Science*. 272, 1155–1158. <https://doi.org/10.1126/science.272.5265.1155>
- Wijsman, J.W.M., Middelburg, J.J., Herman, P.M.J., Böttcher, M.E., Heip, C.H.R., 2001. Sulfur and iron speciation in surface sediments along the northwestern margin of the Black Sea. *Mar. Chem.* 74, 261–278. [https://doi.org/10.1016/S0304-4203\(01\)00019-6](https://doi.org/10.1016/S0304-4203(01)00019-6)
- Woods, A.D., Bottjer, D.J., Mutti, M., Morrison, J., 1999. Lower Triassic large sea-floor carbonate cements: Their origin and a mechanism for the prolonged biotic recovery from the end-Permian mass extinction. *Geology* 27, 645–648. [https://doi.org/10.1130/0091-7613\(1999\)027<0645:LTLSTFC>2.3.CO;2](https://doi.org/10.1130/0091-7613(1999)027<0645:LTLSTFC>2.3.CO;2)
- Zatoń, M., Niedźwiedzki, G., Blom, H., Kear, B.P., 2016. Boreal earliest Triassic biotas elucidate globally depauperate hard substrate communities after the end-Permian mass extinction. *Sci. Rep.* 6, 36345.

Zhang, L., Zhao, L., Chen, Z.-Q., Algeo, T.J., Chen, J., Wang, R., Chen, L., Hou, J., Li, Y., Qiu, H., Feng, X., Lu, Z., Wang, X., Huang, Y., 2014. Amelioration of marine environments at the Smithian–Spathian boundary, Early Triassic, Biogeosciences Discussions. <https://doi.org/10.5194/bgd-11-15361-2014>

Zhang, L.J., Buatois, L.A., Gabriela Mángano, M., Qi, Y.A., Zhang, X., Sun, S., Tai, C., 2017. Early Triassic estuarine depauperate *Cruziana* Ichnofacies from the Sichuan area of South China and its implications for the biotic recovery in brackish-water settings after the end-Permian mass extinction. *Palaeogeogr. Palaeoclimatol. Palaeoecol.* 485, 351–360.
<https://doi.org/10.1016/j.palaeo.2017.06.025>

Chapter 4

The potential extent of Kockatea Shale equivalent
source rocks in the Northern Carnarvon and Perth Basins

Takashi Taniwaki, Chris Elders, Alex I. Holman and Kliti Grice

Petroleum Geoscience, submitted

Submitted: 26 March 2022

Abstract

In the northern Perth Basin, the Early Triassic Kockatea Shale is considered to be the primary petroleum source rock. Possible source rocks in the Northern Carnarvon Basin are more varied and include the Upper Jurassic Dingo Claystone as well as the Early Triassic Locker Shale. Biomarker analyses were conducted on petroleum samples from both the Perth and Northern Carnarvon basins to understand the nature of petroleum systems in these basins. Many of the analysed petroleum samples contain carotenoids (okenane, chlorobactane and isorenieratane) derived from sulfur bacteria, suggesting that their source rocks were deposited under conditions of photic zone euxinia (PZE) and/or derived from microbialites. In the northern Perth Basin, the major lithofacies contributing to the source rock are dark coloured mudstones deposited under PZE conditions and microbialites. In the southern Perth Basin, there is a potential source rock of Permian age indicated by the low concentrations or absence of both carotenoids and the Triassic biomarker *n*-C₃₃ alkylcyclohexane (ACH). There is also a possibility that the Lower Triassic Locker Shale is the source rock of petroleum in the Tubridgi Field on the Peedamullah Shelf of the Northern Carnarvon Basin, based on the similarity of biomarkers to Perth Basin petroleum sourced from the Kockatea Shale. However, the possibility of charge from the Upper Jurassic Dingo Claystone cannot be fully excluded.

1 Introduction

The Perth and Northern Carnarvon basins are located on the western and north-western coasts of Australia, respectively. In the northern Perth Basin, the Early Triassic Kockatea Shale is considered to be the primary source rock for petroleum based on Rock-Eval, biomarker and stable carbon isotope analyses (Boreham et al., 2000; Dawson et al., 2005; Grice et al., 2007, 2005a, 2005c, 2005b; Grosjean et al., 2017; Langhi et al., 2014; McIldowie and Alexander, 2005; Scott, 1994; Thomas, 1979; Thomas et al., 2004). The basal section of the Kockatea Shale, which is

assigned to the Hovea Member, has high total organic carbon (TOC, up to 5 %) and hydrogen indices (HI, up to 800 mg/gTOC) indicating good potential for petroleum generation (Taniwaki et al., 2021; Thomas and Barber, 2004). In large parts of the southern Perth Basin, the source rock is assumed to be Permian in age because younger source rocks in Jurassic and Cretaceous sequences are too immature for hydrocarbon generation and expulsion, while the Lower Triassic is dominated by sandy lithofacies (Crostella and Backhouse, 2000). However, in the central part of the basin such as the Vlaming Sub-basin, the Upper Jurassic Yarragadee Formation is buried deep enough to reach maturity and is a source rock for oils containing relatively high abundances of conifer-derived organic materials (Crostella and Backhouse, 2000). In the Northern Carnarvon Basin there are several potential source rocks. The Upper Jurassic Dingo Claystone is recognised as a source rock in the Barrow and Exmouth sub-basins (Tindale et al., 1998; van Aarssen et al., 1996; Volkman et al., 1983), Lower to Middle Jurassic marine and deltaic sequences are untested potential source rocks (Edwards and Zumberge, 2005) and the Middle to Upper Triassic fluvial-deltaic to marine Mungaroo Formation is also considered a source rock (Edwards and Zumberge, 2005). The Lower Triassic Locker Shale, which is an equivalent of the Lower Triassic Kockatea Shale, also has source rock potential with high TOC and HI (Molyneux et al., 2016). Triassic or older strata have been cited as possible source rocks for the Tubridgi Field on the Peedamullah Shelf (Edwards and Zumberge, 2005; Yasin et al., 1998).

During the Late Permian/Early Triassic, massive volcanic activity from the Siberian Traps caused global warming and global anoxia (Erwin, 1994; Knoll et al., 1996; Nabbefeld et al., 2010; Song et al., 2014; Twitchett et al., 2004; Whiteside and Grice, 2016; Wignall and Twitchett, 1996). Development of PZE in the ancient water-column has been recognized in Permian/Triassic sections around the globe, including the northern Perth Basin (Grice et al., 2005a). Under PZE conditions, anoxygenic photosynthetic bacteria can thrive at the chemocline (the transition between oxic and anoxic conditions) (Pfenning, 1978). These bacteria include purple,

green-green and green-brown sulfur bacteria. These organisms make specific carotenoid pigments (purple sulfur bacteria: okenone, green-green sulfur bacteria: chlorobactene; green-brown sulfur bacteria: isorenieratene) which yield biomarkers following diagenesis in the water column and in sediments (okenane, chlorobactane and isorenieratane, respectively). Such biomarkers have been identified in both sediments and petroleum, suggesting the development of PZE (Clifford et al., 1998; Grice et al., 2005a, 1996; Maslen et al., 2009; Pedentchouk et al., 2004; Sousa Júnior et al., 2013; Tulipani, 2013). In addition, similar bacterial communities can develop in microbialites (Brocks and Schaeffer, 2008; Fox et al., 2020; Pagès et al., 2014; Schaefer et al., 2020). In this study, biomarker analyses were conducted on petroleum samples (crude oils and condensates) from both the Perth and Northern Carnarvon basins to evaluate the nature of their petroleum systems.

2 Geological setting

The Perth Basin developed during several rifting, subsidence and uplift events from the Devonian to Early Cretaceous (Figure 4-1 and 4-2) (Jablonski and Saitta, 2004; Norvick, 2004). The Late Permian to Early Triassic Kockatea Shale was deposited in a transgressive deeper water setting as post-rift sediments following Late Permian rifting. Facies distribution in the Kockatea Shale was controlled by remnant topography created by the rift event (Taniwaki et al., 2021). The Middle Triassic Woodada Formation and younger strata were deposited during subsequent phases of extension.

The tectono-stratigraphy in the Northern Carnarvon Basin is similar to the Perth Basin (Ferdinando et al., 2007; I'Anson et al., 2019). Late Permian rifting is also evident in the Northern Carnarvon Basin, and the Early Triassic Locker Shale, the equivalent of the Kockatea Shale, was deposited during a transgression that forms part of the post rift sequence. The Middle Triassic Mungaroo Formation and younger strata were deposited during subsequent phases of subsidence and rifting. The Upper

Jurassic Dingo Claystone was mainly deposited in an open marine anoxic deeper water setting (Hocking, 1992). Parts of the basin experienced significant uplift and erosion in the Early Cretaceous, as expressed by the Valanginian Unconformity.

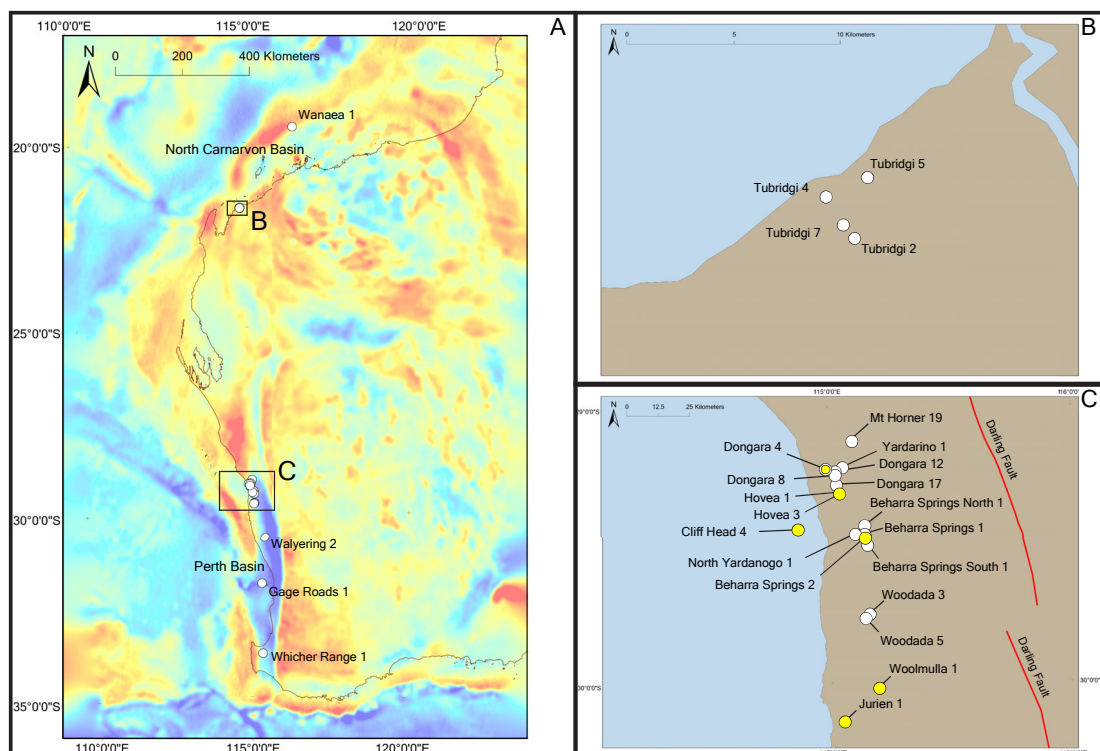


Figure 4-1. Location of both Perth and Northern Carnarvon basins and petroleum samples. A represents the location of both basins and samples with gravity anomaly map as background showing basin geometry. The public domain data used for the gravity map is published by the Scripps Institution of Oceanography (Sandwell et al., 2013, 2014; Sandwell and Smith, 2009). B shows the detailed sample location around the Tubridgi Field in the Northern Carnarvon Basin. C indicates the detailed sample location around the northern Perth Basin. Yellow points represent the location of wells where rock sample analysis was conducted (Taniwaki et al., 2021).

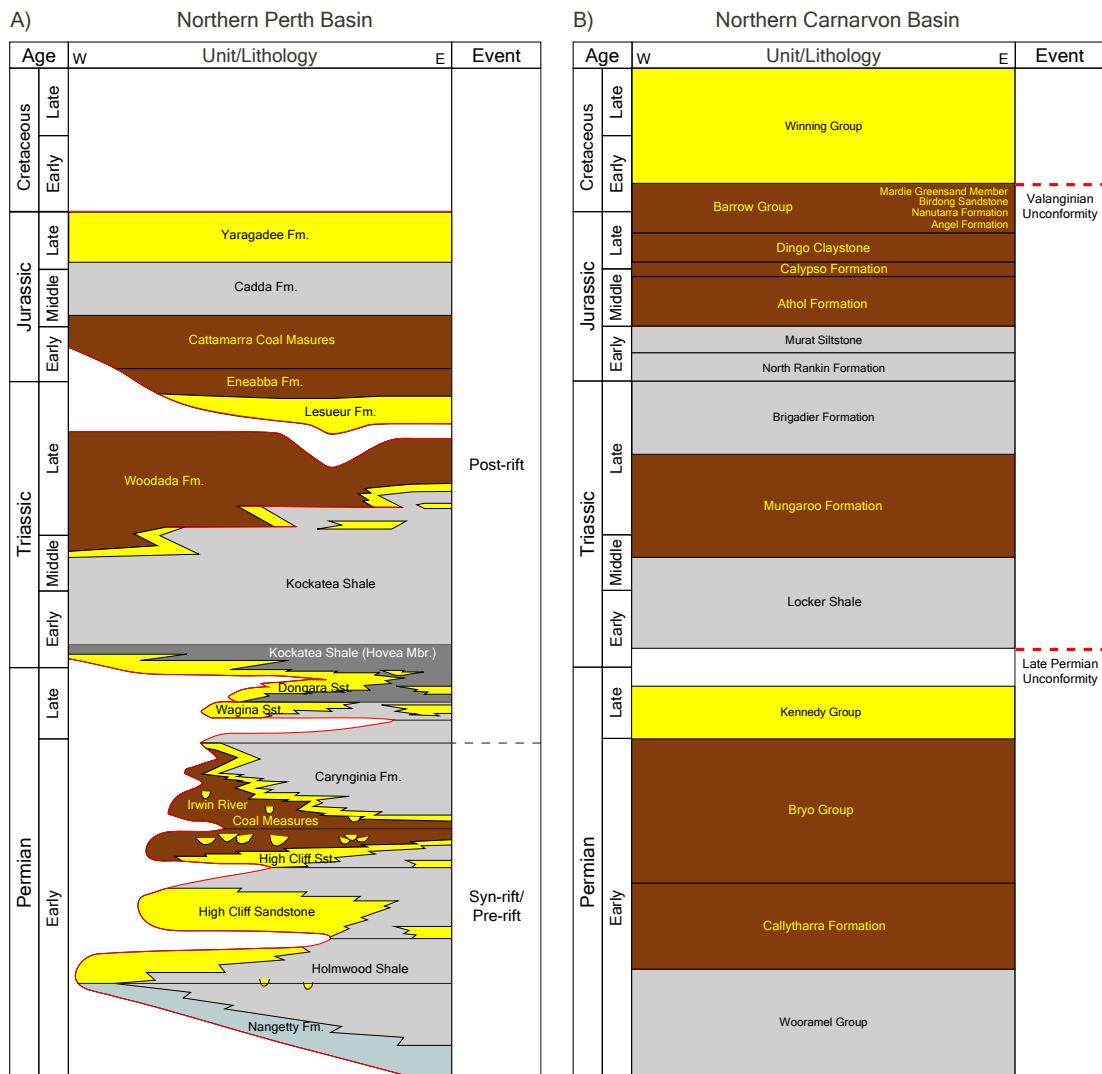


Figure 4-2. Stratigraphy in both (A) northern Perth and (B) Northern Carnarvon basins (Ferdinando et al., 2007; I'Anson et al., 2019). Light and dark grey: deeper water mudstone, yellow: shallow marine sandstone: brown: fluvial to deltaic/marine sediments, blue- green: open marine glacial sediments.

3 Data & Methodology

3.1 Samples

Twenty-one petroleum samples (crude oils and condensates) from both the Perth and Northern Carnarvon basins were used for this study (Figure 4-1, Table 4-1). In the Northern Carnarvon Basin, one sample (Wanaea 1) comes from the Dampier Sub Basin and four other samples are derived from the Tubridgi Field on the Peedamullah Shelf. The petroleum samples from the Northern Carnarvon Basin were recovered from the Cretaceous Birdrong Formation and Mardie Greensand Member (Tubridgi) and the Jurassic Angel Formation (Wanaea). In the Perth Basin, petroleum samples were derived from the Early Permian Carynginia Formation, Late Permian Dongara and Wagina Sandstones, Late Permian to Early Triassic Kockatea Shale and Jurassic Cattamarra Coal Measures and Cockleshell Gully Formation. In the southern Perth Basin, the Early Permian Irwin River Coal Measures and Jurassic Yaragadee Formation and Cattamarra Coal Measures are the reservoir formations for the samples.

3.2 Fractionation of samples

The petroleum samples were fractionated into saturated, aromatic, and polar fractions using small scale silica gel column chromatography. Samples (~10 mg) were weighed and put onto a 5.5 cm column packed with activated silica gel (160 °C overnight). The saturated hydrocarbons were eluted with 4 mL of *n*-hexane. The aromatic hydrocarbons were separated using a mixture of 1.2 mL dichloromethane and 2.8 mL of *n*-hexane. The polar fraction was eluted with a 1:1 mixture of methanol (2 mL) and dichloromethane (2 mL). Each fraction was evaporated to dryness with a nitrogen purge and then weighed.

Table 4-1. Type of fluids, basin location, reservoir age and Formation and for each petroleum sample.

Well	Type	Basin	Formation	Age
Beharra Springs 1	Condensate	North Perth Basin	Carynginia Fm.	Permian
Beharra Springs North 1	Oil	North Perth Basin	Wagina Sandstone	Permian
Beharra Springs South 1	Oil	North Perth Basin	Kockatea Shale	Permian/Triassic
Dongara 04	Oil	North Perth Basin	Irwin River Coal Measures	Permian
Dongara 08	Oil	North Perth Basin	Dongara Sandstone	Permian
Dongara 12	Oil	North Perth Basin	Wagina Sandstone	Permian
Dongara 17	Oil	North Perth Basin	Dongara Sandstone	Permian
Hovea 1	Oil	North Perth Basin	Dongara Sandstone	Permian
Mt Horner 09	Oil	North Perth Basin	Cattamarra Coal Measures	Jurassic
North Yardanogo 1	Oil	North Perth Basin	Cockleshell Gully Fm.	Jurassic
Woodada 03	Oil	North Perth Basin	Carynginia Fm.	Permian
Woodada 05	Oil	North Perth Basin	Carynginia Fm.	Permian

Yardarino 1	Oil	North Perth Basin	Wagina Sandstone	Permian
Gage Roads 1	Oil	South Perth Basin	Yaraggadee Fm.	Jurassic
Walyering 2	Oil	South Perth Basin	Cattamarra Coal Measures	Jurassic
Whicher Range 1	Oil	South Perth Basin	Irwin River Coal Measures	Permian
Tubridgi 02	Oil	North Carnarvon Basin	Birdong Sandstone	Cretaceous
Tubridgi 04	Oil	North Carnarvon Basin	Mardie Greensand Mbr. & Birdong Sandstone	Cretaceous
Tubridgi 05	Oil	North Carnarvon Basin	Mardie Greensand Mbr.	Cretaceous
Tubridgi 07	Oil	North Carnarvon Basin	Mardie Greendand Mbr., Birdong Sandstone & Nanutarra Fm.	Cretaceous
Wanaea 1	Oil	North Carnarvon Basin	Angel Fm.	Jurassic

3.3 Analysis

Gas chromatography-mass spectrometry (GC-MS) analyses were conducted on both saturated and aromatic hydrocarbon fractions. Gas chromatography-metastable reaction monitoring-mass spectrometry (GC-MRM-MS) was also conducted on all samples.

3.3.1 Gas Chromatography-Mass Spectrometry (GC-MS)

For the saturated fractions, an Agilent 5973B MSD interfaced to an Agilent 7890B gas chromatograph was used for GC-MS analysis. A J&W Scientific DB-1MS column of 60 m length, 250 μm inner diameter and 0.25 μm film thickness was installed. The GC oven was programmed from 40 $^{\circ}\text{C}$ to 325 $^{\circ}\text{C}$ at a heating rate of 3 $^{\circ}\text{C}/\text{min}$. The holding time at initial and final temperature was 1 and 30 minutes, respectively. The MS was set with an ionisation energy of 70 eV and measured a mass range from 50 to 550 Daltons.

For the aromatic fractions, an Agilent 5975B MSD interfaced to an Agilent 6890N gas chromatograph was used for GC-MS analysis. A J&W DB-5MS column of 60 m length, 250 μm inner diameter and 0.25 μm film thickness was used. The oven program and scanned range of the MS was the same as that used for the saturated fractions.

3.3.2 GC-MS, metastable reaction monitoring- (GC-MRM-MS)

Saturated and aromatic fractions were combined in equal amounts for GC-MRM-MS analysis. An Agilent 7890B GC interfaced to an Agilent 7010B Triple Quadrupole MS operated in metastable reaction monitoring (MRM) mode was used for the analysis. A DB-5MS UI capillary column of 60 m length, 250 μm inner diameter, and 0.25 μm film thickness was installed. The temperature of the GC oven was set from 40 $^{\circ}\text{C}$ to 325 $^{\circ}\text{C}$ with a heating rate of 4 $^{\circ}\text{C}/\text{min}$. The final holding time was 20.75 minutes. The MS was programmed at 50 eV ionisation energy. The QQQ temperature was set at 150 $^{\circ}\text{C}$. D4-C₂₇ $\alpha\alpha\alpha$ cholestane was added as an internal

standard. Compounds were identified by comparing with reference standards, matching retention times and elution order.

3.3.3 Rock samples

Rock samples from the earliest Triassic part of the Kockatea Shale from the northern Perth Basin were used for comparison with petroleum samples. The rock samples were analysed and described in detail by Taniwaki et al. (2021) and Chapter 3.

4 Results and discussions

4.1 Thermal maturity influence

The thermal maturity of each sample was determined based on C_{32} $22S/(22S+22R)$ $\alpha\beta$ -homohopane, $17\beta,21\alpha$ C_{30} hopane/ $17\alpha,21\beta$ C_{30} hopane (moretane/hopane), C_{29} $20S/(20S+20R)$ ($\alpha\alpha\alpha+\alpha\beta\beta$) sterane ratio, $\alpha\beta\beta/(\alpha\beta\beta+\alpha\alpha\alpha)$ C_{29} sterane, $18\alpha,22,29,30$ -*trishnor*hopane (Ts) to $17\alpha,22,29,30$ -*trishnor*hopane (Tm) ratio (Ts/(Ts+Tm)) and diasteranes/(diasteranes+regular steranes): ΣC_{27-29} diasteranes/ $(\Sigma C_{27-29}$ diasteranes+ ΣC_{27-29} steranes) (abbreviated as Dia/(Dia+Reg)) (Table 4-1). C_{32} $22S/(22S+22R)$ $\alpha\beta$ -homohopane, moretane/hopane and C_{29} $20S/(20S+20R)$ ($\alpha\alpha\alpha+\alpha\beta\beta$) sterane ratios reached their thermal equilibrium values, indicating that the thermal maturity is equivalent to at least 0.8 % vitrinite reflectance (Ro). $\alpha\beta\beta/(\alpha\beta\beta+\alpha\alpha\alpha)$ C_{29} sterane, Ts/(Ts+Tm) and Dia/(Dia+Reg) are still lower than their thermal equilibrium values indicating that the thermal maturity for all samples is less than 0.9 % Ro equivalent. Therefore, the thermal maturity level of samples ranges between 0.8 and 0.9 % Ro equivalent.

Table 4-2. C₃₂ 22*S*/(22*S*+22*R*) αβ-homohopane, Moretane/Hopane, C₂₉ 20*S*/(20*S*+20*R*) (ααα+αββ) sterane ratio, αββ/(αββ+ααα) C₂₉ Sterane, Ts/(Ts+Tm) and Dia/(Dia+Reg) of each sample for thermal maturity evaluation.

Well	Basin		C ₃₂ 22 <i>S</i> /(22 <i>S</i> +22 <i>R</i>) αβ-homohopane	Moretane/Hopane	C ₂₉ 20 <i>S</i> /(20 <i>S</i> +20 <i>R</i>) sterane ratio	αββ/(αββ+ααα) C ₂₉ Sterane	Ts/(Ts+Tm)	Dia/(Dia+Reg)
Beharra Springs 1	North Basin	Perth	0.61	0.06	0.42	0.63	0.61	0.49
Beharra Springs North 1	North Basin	Perth	0.61		0.29	0.72		0.35
Beharra Springs South 1	North Basin	Perth	0.58	0.07	0.43	0.64	0.69	0.55
Dongara 04	North Basin	Perth	0.61	0.06	0.47	0.59	0.49	0.35
Dongara 08	North Basin	Perth	0.58	0.06	0.44	0.61	0.65	0.49
Dongara 12	North Basin	Perth	0.58	0.07	0.44	0.54	0.56	0.54

Dongara 17	North Basin	Perth	0.60	0.07	0.46	0.50	0.70	0.32
Hovea 1	North Basin	Perth	0.60	0.07	0.46	0.46	0.54	0.27
Mt Horner 09	North Basin	Perth	0.55	0.05	0.47	0.58	0.76	0.42
North Yardanogo 1	North Basin	Perth	0.59	0.05	0.46	0.58	0.71	0.34
Woodada 03	North Basin	Perth	0.57	0.06	0.46	0.57	0.78	0.41
Woodada 05	North Basin	Perth	0.55	0.06	0.47	0.60	0.84	0.60
Yardarino 1	North Basin	Perth	0.58	0.04	0.45	0.64	0.77	0.57
Gage Roads 1	South Basin	Perth	0.60	0.09	0.45	0.50	0.31	0.64
Walyering 2	South Basin	Perth	0.56	0.04	0.41	0.59	0.74	0.54

Whicher Range 1	South Basin	Perth	0.60	0.04	0.47	0.66	0.65	0.56
Tubridgi 02	North Carnarvon Basin		0.63	0.05	0.48	0.59	0.56	0.23
Tubridgi 04	North Carnarvon Basin		0.61	0.05	0.45	0.57	0.56	0.40
Tubridgi 05	North Carnarvon Basin		0.59	0.05	0.48	0.58	0.61	0.42
Tubridgi 07	North Carnarvon Basin		0.58	0.09	0.34	0.45	0.64	0.38
Wanaea 1	North Carnarvon Basin		0.58	0.06	0.48	0.65	0.80	0.70

4.2 Characteristics of major biomarkers (Pr/Ph, C₃₅ homohopane index, gammacerane index, and C₂₇₋₂₉ regular sterane ratio)

Tubridgi petroleum appears to have experienced biodegradation based on the elevated unresolved complex mixture in total ion chromatograms, most significantly in Tubridgi 7. Samples from other fields do not show significant biodegradation.

Pr/Ph ratios show significant difference between the basins: 1.7-4.1 for most of the Northern Carnarvon Basin petroleum, 0.4-1.3 for the northern Perth Basin and 1.4-1.8 for the southern Perth Basin. However, Pr/Ph in the Tubridgi petroleum appears to be influenced by biodegradation (Table 4-3). C₃₅ homohopane and gammacerane indices (hopane index: C₃₅ (22*S*+22*R*) αβ-homohopane/C₃₄ (22*S*+22*R*) αβ-homohopane, gammacerane index: gammacerane/(gammacerane+C₃₀αβ-homohopane)) overlap between basins (C₃₅ homohopane indices: 0.4-1.0 in the Northern Carnarvon Basin, 0.4-0.7 in the northern Perth Basin and 0.1-0.7 in the southern Perth Basin, gammacerane indices: 0.01-0.06 in the Northern Carnarvon Basin, 0.02-0.08 in the northern Perth Basin and 0.01-0.05 in the southern Perth Basin) (Table 4-3). C₂₇ to C₂₉ regular sterane ratio also shows similar characteristics between basins, except petroleum from Gage Roads 1. C₂₇ and C₂₉ regular steranes generally range between 30-50%, and C₂₈ regular steranes generally range between 20-30%. However, the sterane ratio in Gage Roads 1 shows a higher abundance of C₂₉ regular sterane reaching 81% (Table 4-3).

4.3 Carotenoid biomarkers (okenane, chlorobactane and isorenieratane) in petroleum samples

4.3.1 Okenane, isorenieratane and chlorobactane

Most of the petroleum samples contain biomarkers derived from anoxygenic photosynthetic sulfur bacteria (okenane: purple sulfur bacteria, chlorobactane: green-green sulfur bacteria, isorenieratane: green-brown sulfur bacteria) (Figure 4-3)

(Brocks and Schaeffer, 2008; French et al., 2014; Grice et al., 2005a). Beharra Springs North 1 does not contain either chlorobactane or okenane but does contain isorenieratane. Beharra Springs South 1, Whicher Range 1 and Tubridgi 7 contain both chlorobactane and isorenieratane but no okenane. Wanaea 1 and Walyering 2 do not contain chlorobactane, isorenieratane nor okenane (Figure 4-4).

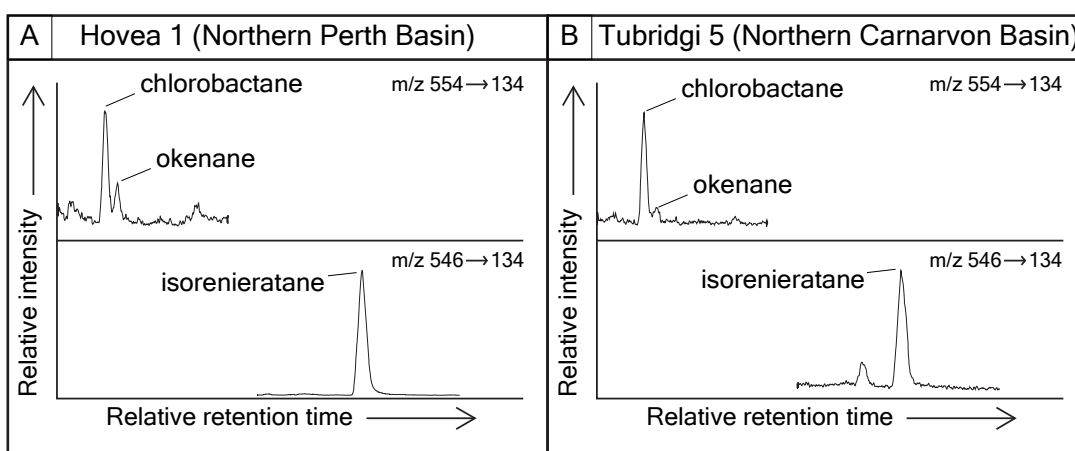


Figure 4-3. GC-MRM-MS peaks of okenane, isorenieratane and chlorobactane from petroleum samples (A: Hovea 1, B: Tubridgi 5). Hovea 1 is located on the northern Perth Basin and Tubridgi 5 is located on the Peedamullah Shelf in the Northern Carnarvon Basin.

Table 4-3. Characteristics of major biomarkers (Pr/Ph, C₃₅ homohopane index, gammacerane index, and C₂₇₋₂₉ regular sterane ratio)

		Pr/Ph	C₃₅ homohopane index	Gammacerane index	C₂₇₋₂₉ regular sterane ratio
Northern Basin	Carnarvon	1.7-4.1	0.4-1.0	0.01-0.06	C ₂₇ : 30-50%
					C ₂₈ : 30-50%
					C ₂₉ : 20-30%
Northern Perth Basin		0.4-1.3	0.4-0.7	0.02-0.08	C ₂₇ : 30-50%
					C ₂₈ : 30-50%
					C ₂₉ : 20-30%
Southern Perth Basin		1.4-1.8	0.1-0.7	0.01-0.05	C ₂₇ : 30-50%
					C ₂₈ : 30-50%
					C ₂₉ : 20-30%
					*Gage Roads 1
					C ₂₇ : 8%
					C ₂₈ : 11%
C ₂₉ : 81%					

4.3.2 Thermal maturity influence on okenane, chlorobactane and isorenieratane

The effect of thermal maturity on the concentrations of okenane, chlorobactane and isorenieratane is evaluated by comparing these biomarkers with $\alpha\beta\beta/(\alpha\beta\beta+\alpha\alpha\alpha)$ C₂₉ sterane (Figure 4-5). The concentrations of okenane, chlorobactane and isorenieratane generally decrease with increasing thermal maturity, suggesting that the compounds are likely affected by thermal maturity. The most significant change in concentrations occurs when $\alpha\beta\beta/(\alpha\beta\beta+\alpha\alpha\alpha)$ C₂₉ sterane ratio reaches 0.6. The rate of decrease of each carotenoid concentration is similar. The okenane ratio, which is the relative abundance of okenane to chlorobactane and isorenieratane, distinguishes PZE dominated conditions (lower okenane ratio) and microbialite facies (higher okenane ratio) in less mature rock samples (Brocks and Schaeffer, 2008; Pagès et al., 2014; Schaefer et al., 2020) but this ratio could be influenced by thermal maturity in the more mature petroleum samples and caution is therefore required if using it for comparison between samples from different wells.

The absence of some of these carotenoid biomarkers in Beharra Springs North 1, Beharra Springs South 1, Whicher Range 1 and Wanaea 1 could be the result of relatively higher thermal maturity, as $\alpha\beta\beta/(\alpha\beta\beta+\alpha\alpha\alpha)$ C₂₉ sterane of these samples is higher than 0.64, which is nearly the thermal equilibrium value. However, $\alpha\beta\beta/(\alpha\beta\beta+\alpha\alpha\alpha)$ C₂₉ sterane of Tubridgi 7 and Walyering 2 is lower (0.45 and 0.59, respectively), although Tubridgi 7 does not have okenane and Walyering 2 lacks all three carotenoid biomarkers. The absence of okenane in Tubridgi 7 appears to be the result of biodegradation. The absence of these biomarkers from Walyering 2 could indicate a difference in paleoenvironmental conditions during deposition of their source rocks. Gage Roads 1 and Whicher Range 1 in the southern Perth Basin contain carotenoids, but their concentrations are low compared to oils from the northern Perth and Northern Carnarvon basins.

4.3.3 Relative abundance of between okenane, chlorobactane and isorenieratane

Figure 4-6 shows peaks for okenane, chlorobactane and isorenieratane from Tubridgi 2, 4, 5 and 7. These samples show a similar distribution of carotenoid biomarkers to rock (PZE and microbialite facies) and petroleum samples from the northern Perth Basin (Figure 4-3). The similarity implies that the source of the Tubridgi petroleum samples shares similar paleoenvironmental conditions to the Kockatea Shale in the northern Perth Basin.

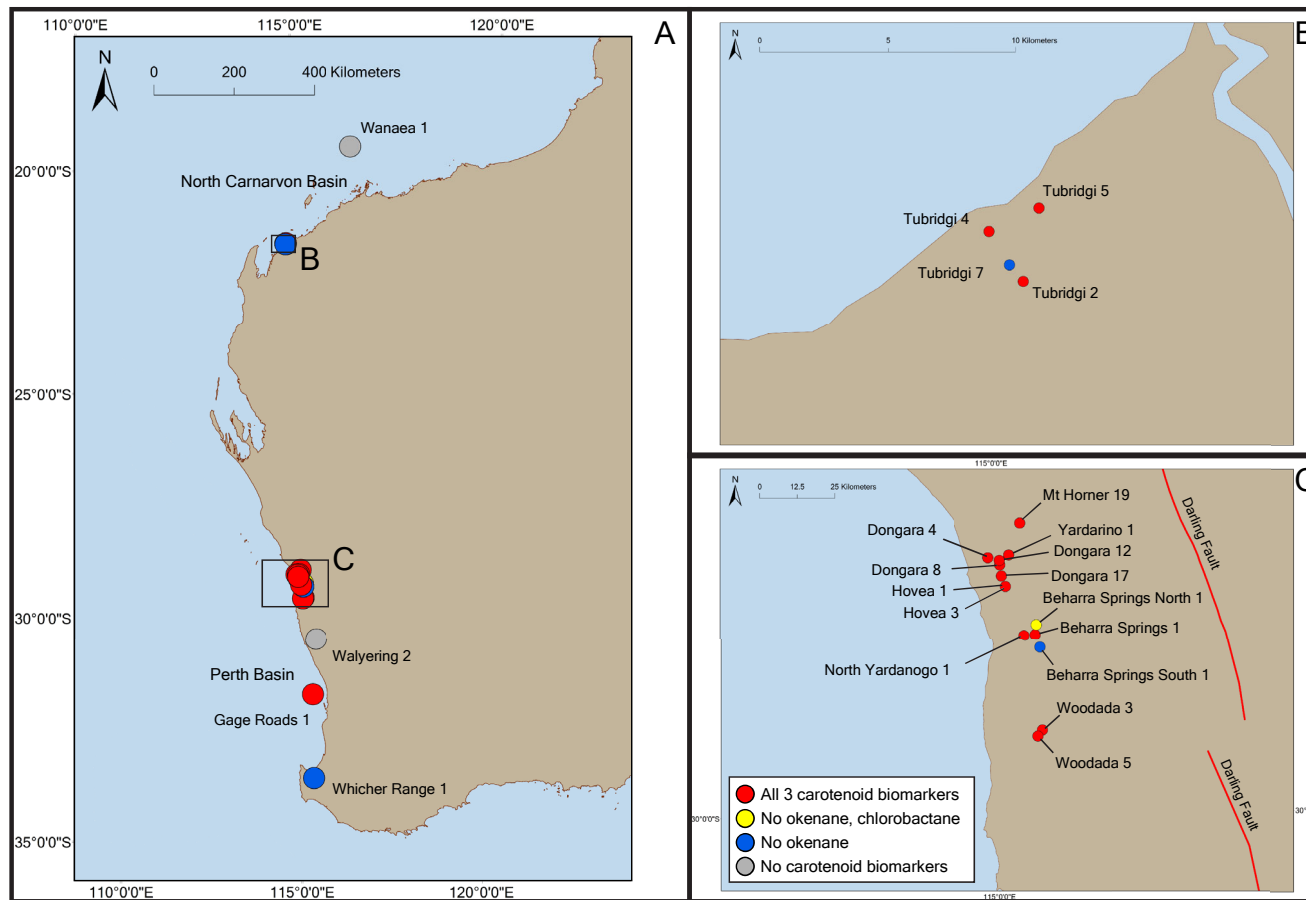


Figure 4-4. Distribution of carotenoid biomarkers (okenane, chlorobactane and isorenieratane). A shows the entire region covering samples from the Northern Carnarvon Basin to the southern Perth Basin. B represents the detailed distribution around the Tubridgi Field in the Northern Carnarvon Basin. C indicates the distribution around the northern Perth Basin.

4.4 Implications to source rocks

4.4.1 Perth Basin

In the northern Perth Basin, the Kockatea Shale is considered to be a primary source rock based on source-oil correlation, especially using the C₃₃ *n*-alkylcyclohexane ratio (*n*-C₃₃ ACH ratio, *n*-C₃₃ACH/*n*-C₃₄) (Dawson et al., 2005; Grice et al., 2005c; McIlldowie and Alexander, 2005; Owens et al., 2018). The samples analysed in this study also show variable abundances of *n*-C₃₃ ACH (Figure 4-7). In addition to *n*-C₃₃ ACH, the presence of carotenoid biomarkers (okenane, chlorobactane and isorenieratane) provides further evidence that the Lower Triassic Kockatea Shale is the primary source rock for oils in the basin. In the Kockatea Shale rock samples, these carotenoid biomarkers and *n*-C₃₃ ACH were only identified in the dark coloured shale deposited under PZE conditions, and in microbialite samples (Chapter 3). Rock-Eval analysis shows that these lithofacies have higher source rock potential than other lithofacies that comprise the Kockatea Shale (TOC: up to 3.4% and HI: up to 579 mg/gTOC), suggesting they are the main contributors to the petroleum systems (Taniwaki et al., 2021).

In the southern Perth Basin, oils from Gage Roads 1 and Whicher Range 1 contains some carotenoids, but their concentrations are low compared with the concentration in the northern Perth Basin. Walyering 2 does not contain these carotenoids. In addition, *n*-C₃₃ ACH is absent from these petroleum samples. The low concentration of carotenoids in Whicher Range 1 and their absence from Walyering 2 could be because these samples have a higher level of thermal maturity (Figure 4-5). In addition, the high relative abundance of C₂₉ steranes in Gage Roads 1 indicates significant input of terrigenous organic material. It is possible therefore that the low concentration of carotenoid biomarkers in this sample could be the result of dilution by terrestrial organic material. However, the low concentrations and/or absence of carotenoids and the lack of *n*-C₃₃ ACH also favours the assumption that the source rock is Permian or Jurassic, rather than the Lower Triassic Kockatea

Shale. This is consistent with the observation that the Lower Triassic is dominated by sandy lithofacies in this part of the basin 15 and the assumption that Permian age shaly coals and, where it is sufficiently deeply buried, the Upper Jurassic Yarragadee Formation are the main sources.

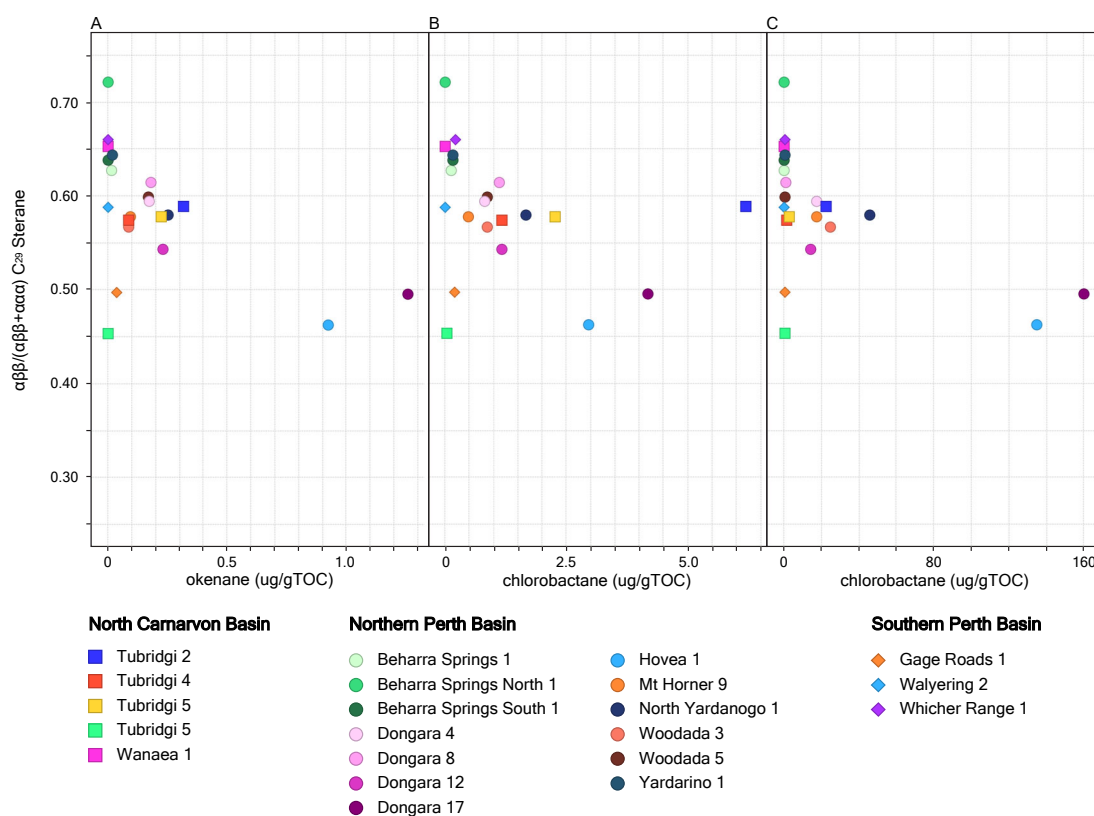


Figure 4-5. The influence of thermal maturity on carotenoid biomarkers (A: okenane, B: chlorobactane, C: isorenieratane).

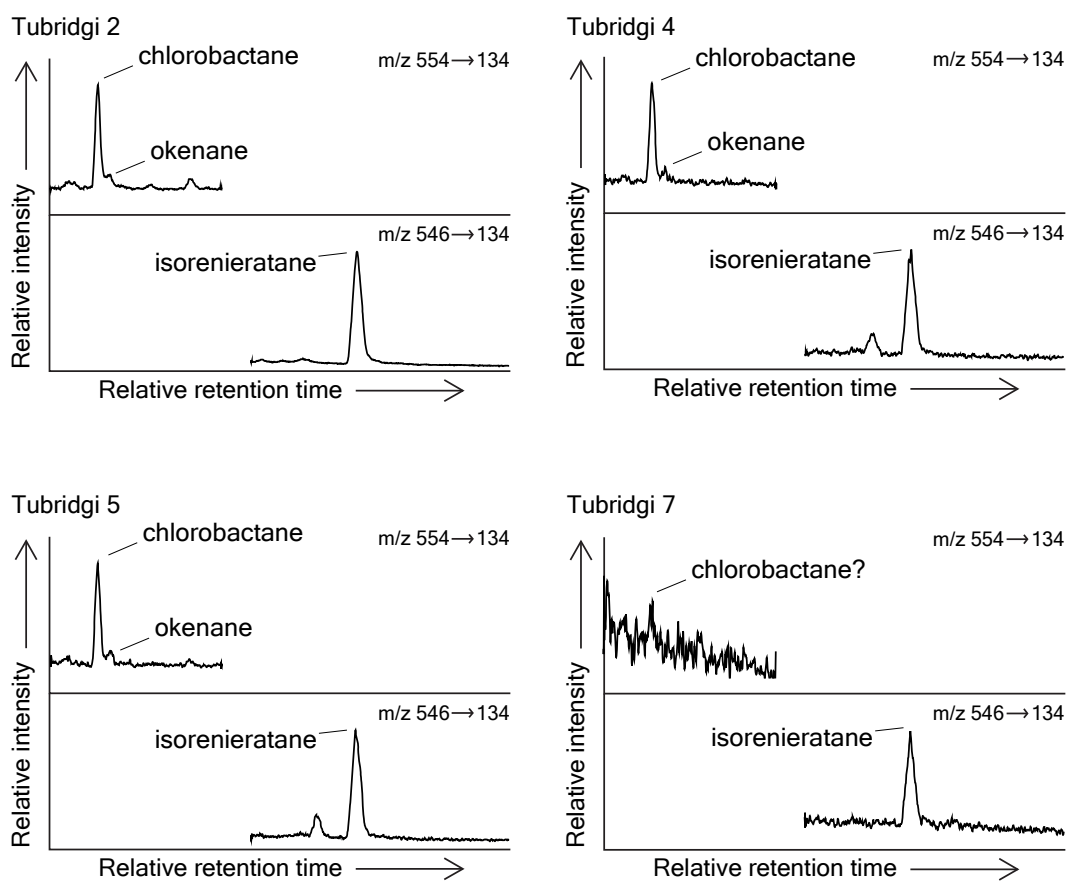
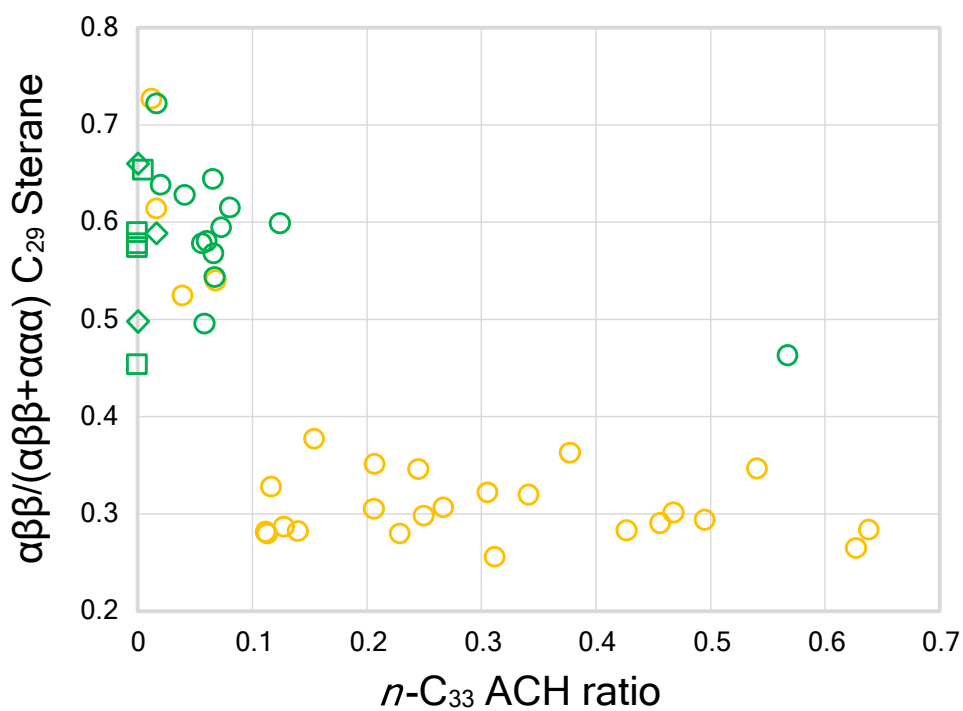


Figure 4-6. GC-MRM-MS peaks of okenane, isorenieratane and chlorobactane from petroleum samples of Tubridgi 2, 4, 5 and 7.



- Northern Carnarvon Basin petroleum samples
- Northern Perth Basin petroleum samples
- ◇ Southern Perth Basin petroleum samples
- Early Triassic Kockatea Shale rock samples (Northern Perth Basin)

Figure 4-7. The thermal maturity influence on $n\text{-C}_{33}$ ACH ratio. $n\text{-C}_{33}$ ACH ratio = $n\text{-C}_{33}$ ACH / C_{34} n -alkane.

4.4.2 Northern Carnarvon Basin

The Upper Jurassic Dingo Claystone is traditionally considered to be one of the main petroleum source rocks in the Northern Carnarvon Basin. This is based on source-oil correlation using steranes, hopanes and plant-derived aromatic biomarker evidence in the Barrow sub-basin (van Aarssen et al., 1996; Volkman et al., 1983). However, there are some questions as to the validity of these conclusions because some of the biomarker parameters are also influenced by thermal maturity (Peters et al., 2004). Basin modeling shows that the Dingo Claystone reached the oil window after the Late Cretaceous in the Exmouth sub-basin and generated large volumes of hydrocarbons (Tindale et al., 1998).

The presence of carotenoid biomarkers derived from sulfur bacteria in the Tubridgi petroleum samples suggests that their source rock was probably developed under PZE conditions and/or was formed by microbialites. The biomarker characteristics of the Tubridgi petroleum samples are similar to the petroleum from the northern Perth Basin, as well as the mudstones deposited under PZE conditions and the microbialites from the Lower Triassic Kockatea Shale. Triassic and older strata subcrop the Valanginian unconformity on the Peedamullah Shelf and are present beneath the Tubridgi Field (Iasky et al., 2002) and have been suggested as potential sources (Edwards and Zumberge, 2005; Yasin et al., 1998). The biomarker characteristics supports the possibility that Tubridgi petroleum comes from the Lower Triassic Locker Shale which is an equivalent of the Lower Triassic Kockatea Shale.

Further evidence that the Triassic acts as a source of oil in the Northern Carnarvon Basin comes from oil inclusions reported from the Upper Triassic Mungaroo Formation in the Pinhoe 1/ST1 well on the Exmouth Plateau, which indicate the presence of a paleo oil column (Bourdet, 2016). It is difficult to envisage migration of petroleum from the Upper Jurassic Dingo Claystone because there is no large fault displacing the stratigraphically younger Dingo Claystone into a downdip

position against the Middle Triassic Mungaroo Formation (Bernecker et al., 2018). Therefore, the stratigraphic relationship suggests that the Lower Triassic Locker Shale is the most likely source rock for the paleo oil column of the Upper Triassic Mungaroo Formation.

The relative abundance of *n*-C₃₃ ACH is a key biomarker used for source correlation to the Lower Triassic Kockatea Shale in the northern Perth Basin, but it is absent from the Northern Carnarvon Basin samples including the Tubridgi wells. However, this could be a result of thermal maturation because this compound reduces in concentration as thermal maturity increases (Thomas and Barber, 2004) (Figure 4-7). Although the Tubridgi Field petroleum comes from a source rock deposited under PZE conditions, there are no published analyses to indicate whether or not the Dingo Claystone was also deposited under these conditions. Furthermore, it cannot be determined if the petroleum in the Barrow and Exmouth sub-basins migrated from a source rock developed under PZE conditions and/or a microbialite source rock because published analyses are focused on steranes, hopanes and parameters related to terrestrial organic matter (van Aarssen et al., 1996; Volkman et al., 1983). This different analytical approach, and the limited nature of published analyses, precludes a direct comparison of the Tubridgi petroleum samples analysed in this study with both the Dingo Claystone and the oils from the Barrow sub-basin. Therefore, despite the evidence to support a Lower Triassic source rock, a contribution from an Upper Jurassic source rock to Tubridgi petroleum in the Peedamullah Shelf cannot be completely excluded. Further analysis of the Northern Carnarvon Basin petroleum and source rocks is clearly required. If the contribution from the Lower Triassic Locker Shale is substantiated, this opens up the potential for new plays on the southern margin of the Northern Carnarvon Basin and potentially more broadly in the basin.

5 Conclusion

Petroleum samples from the Perth Basin and the Tubridgi Field on the Peedamullah Shelf of the Northern Carnarvon Basin contain carotenoid biomarkers derived from sulfur bacteria, suggesting that the source rocks developed under PZE conditions and/or were formed by microbialites. In the northern Perth Basin, biomarkers proved that the microbialites and/or dark coloured mudstone deposited under PZE conditions in the Kockatea Shale are a major contributing lithofacies to the petroleum system. On the other hand, in the southern Perth Basin, it is possible that the source rock is Permian or Jurassic in age based on the low concentrations or absence of carotenoids, the lack of *n*-C₃₃ ACH and the overall geological setting. The presence of carotenoid biomarkers in the Tubridgi petroleum on the Peedamullah Shelf shows that petroleum also migrated from a source rock developed under PZE conditions and/or formed by microbialites. The similarity of biomarker characteristics to the Perth Basin petroleum suggests that the Tubridgi petroleum may have migrated from the Lower Triassic Locker Shale. However, the possibility of the Dingo Claystone contribution to the Tubridgi petroleum cannot be excluded due to the absence of *n*-C₃₃ ACH and the lack of previous analyses targeting the carotenoids in the Dingo Claystone and oils derived from it. Further analysis of Northern Carnarvon Basin petroleum and source rocks has the potential to resolve this issue and to open up new plays on the southern margin of the Northern Carnarvon Basin and possibly more broadly in the basin.

Acknowledgements

We acknowledge Peter Hopper for technical support, and Roger Summons for arranging the GC-MRM-MS analysis. This is a part of the PhD project for the first author funded by INPEX Corporation. Alex Maftai is thanked for drawing our attention to the oil inclusions in the Pinhoe 1/ST1 well.

References

- Bernecker, T., Bernardel, G., Orlov, C., Rollet, N., 2018. Petroleum geology of the 2018 offshore acreage release areas. *APPEA J.* 58, 437–461.
<https://doi.org/10.1071/aj17056>
- Boreham, C.J., Hope, J.M., Hartung-Kagi, B., van Aarssen, B.J.K., 2000. More sources for gas and oil in Perth Basin. *AGSO Res. Newsl.* 5–9.
- Bourdet, J., 2016. Fluid charge history in the Upper Triassic Mungaroo Fm at Pinhoe 1 / ST1 , Exmouth Plateau, Carnarvon Basin, Australia. *Confid. Rep.* EP159238, CSIRO Energy, Perth Aust.
- Brocks, J.J., Schaeffer, P., 2008. Okenane, a biomarker for purple sulfur bacteria (Chromatiaceae), and other new carotenoid derivatives from the 1640 Ma Barney Creek Formation. *Geochim. Cosmochim. Acta* 72, 1396–1414.
<https://doi.org/10.1016/j.gca.2007.12.006>
- Clifford, D.J., Clayton, J.L., Sinninghe Damsté, J.S., 1998. 2,3,6-/3,4,5-Trimethyl substituted diaryl carotenoid derivatives (Chlorobiaceae) in petroleums of the Belarussian Pripyat River Basin. *Org. Geochem.* 29, 1253–1267.
[https://doi.org/10.1016/S0146-6380\(98\)00086-2](https://doi.org/10.1016/S0146-6380(98)00086-2)
- Crostella, A., Backhouse, J., 2000. *Geology and Petroleum Exploration of the Central and Southern Perth Basin.* West. Aust. Geol. Surv. Report 57, 85p.
- Dawson, D., Grice, K., Alexander, R., 2005. Effect of maturation on the indigenous

- δ D signatures of individual hydrocarbons in sediments and crude oils from the Perth Basin (Western Australia). *Org. Geochem.* 36, 95–104.
<https://doi.org/10.1016/j.orggeochem.2004.06.020>
- Edwards, D.S., Zumberge, J.E., 2005. The oils of Western Australia II-regional petroleum geochemistry and correlation of crude oils and condensates from western Australia and Papua New Guinea. *Geosci. Aust. Rep.* 37512.
- Erwin, D.H., 1994. The Permo-Triassic extinction. *Nature* 367, 231–236.
- Ferdinando, D., Baker, J.C., Gongora, A., Pidgeon, B.A., 2007. Illite/smectite clays preserving porosity at depth in Lower Permian reservoirs, northern Perth Basin. *APPEA J.* 47, 69–88. <https://doi.org/10.1071/aj06004>
- Fox, C.P., Cui, X., Whiteside, J.H., Olsen, P.E., Summons, R.E., Grice, K., 2020. Molecular and isotopic evidence reveals the end-Triassic carbon isotope excursion is not from massive exogenous light carbon. *Proc. Natl. Acad. Sci.* 117, 30171–30178. <https://doi.org/10.1073/pnas.1917661117>
- French, K.L., Sepúlveda, J., Trabucho-Alexandre, J., Gröcke, D.R., Summons, R.E., 2014. Organic geochemistry of the early Toarcian oceanic anoxic event in Hawsker Bottoms, Yorkshire, England. *Earth Planet. Sci. Lett.* 390, 116–127. <https://doi.org/10.1016/j.epsl.2013.12.033>
- Grice, K., Cao, C., Love, G.D., Böttcher, M.E., Twitchett, R.J., Grosjean, E., Summons, R.E., Turgeon, S.C., Dunning, W., Jin, Y., 2005a. Photic zone euxinia during the Permian-Triassic superanoxic event. *Science.* 307, 706–709. <https://doi.org/10.1126/science.1104323>
- Grice, K., Nabbefeld, B., Maslen, E., 2007. Source and significance of selected polycyclic aromatic hydrocarbons in sediments (Hovea-3 well, Perth Basin, Western Australia) spanning the Permian-Triassic boundary. *Org. Geochem.* 38, 1795–1803. <https://doi.org/10.1016/j.orggeochem.2007.07.001>

-
- Grice, K., Schaeffer, P., Schwark, L., Maxwell, J., 1996. Molecular indicators of palaeoenvironmental conditions in an immature Permian shale (Kupferschiefer, *Org. Geochem.* 25, 131–147.
- Grice, K., Summons, R.E., Grosjean, E., Twitchett, R.J., Dunning, W., Wang, S.X., Böttcher, M.E., 2005b. Depositional conditions of the Northern Onshore Perth Basin (Basal Triassic). *APPEA J.* 45, 263–274.
- Grice, K., Twitchett, R.J., Alexander, R., Foster, C.B., Looy, C., 2005c. A potential biomarker for the Permian-Triassic ecological crisis. *Earth Planet. Sci. Lett.* 236, 315–321. <https://doi.org/10.1016/j.epsl.2005.05.008>
- Grosjean, E., Hall, L., Boreham, C., Buckler, T., 2017. Source rock geochemistry of the offshore northern Perth Basin: regional hydrocarbon prospectivity of the offshore northern Perth Basin. *Rec. 2017/18. Geosci. Aust. Canberra.* <https://doi.org/10.11636/Record.2017.018>
- Hocking, R.M., 1992. Jurassic deposition in the central and southern North West Shelf, Western Australia. *Geol. Surv. West. Aust. Rec.* 1992/7 101p.
- I'Anson, A., Elders, C., McHarg, S., 2019. Marginal fault systems of the Northern Carnarvon Basin: Evidence for multiple Palaeozoic extension events, North-West Shelf, Australia. *Mar. Pet. Geol.* 101, 211–229. <https://doi.org/10.1016/j.marpetgeo.2018.11.040>
- Iasky, R.P., Mory, A.J., Blundell, K.A., Ghori, K.A.R., 2002. Prospectivity of the Peedamullah Shelf and Onslow Terrace revisited, in: *The Sedimentary Basins of Western Australia 3: Proceedings of the Petroleum Exploration Society of Australia Symposium.* pp. 741–759.
- Jablonski, D., Saitta, A.J., 2004. Permian To Lower Cretaceous Plate Tectono-Stratigraphic Development of the Western Australian Margin. *APPEA J.* 44, 287–328. <https://doi.org/10.1071/AJ03011>

-
- Knoll, A.H., Bambach, R.K., Canfield, D.E., Grotzinger, J.P., 1996. Comparative earth history and late Permian mass extinction. *Science*. 273, 452–457.
<https://doi.org/10.1126/science.273.5274.452>
- Langhi, L., Ross, A., Croke, E., Jones, A., Nicholson, C., Stalvies, C., 2014. Integrated hydroacoustic flares and geomechanical characterization reveal potential hydrocarbon leakage pathways in the Perth Basin, Australia. *Mar. Pet. Geol.* 51, 63–69. <https://doi.org/10.1016/j.marpetgeo.2013.11.016>
- Maslen, E., Grice, K., Gale, J.D., Hallmann, C., Horsfield, B., 2009. Crocetane: A potential marker of photic zone euxinia in thermally mature sediments and crude oils of Devonian age. *Org. Geochem.* 40, 1–11.
<https://doi.org/10.1016/j.orggeochem.2008.10.005>
- McIldowie, M., Alexander, R., 2005. Identification of a novel C33 n-alkylcyclohexane biomarker in Permian-Triassic sediments. *Org. Geochem.* 36, 1454–1458. <https://doi.org/10.1016/j.orggeochem.2005.06.009>
- Molyneux, S., Goodall, J., McGee, R., Mills, G., Hartung-Kagi, B., 2016. Observations on the Lower Triassic petroleum prospectivity of the offshore Carnarvon and Roebuck basins Lead author. *APPEA J.* 56, 173–202.
- Nabbefeld, B., Grice, K., Summons, R.E., Hays, L.E., Cao, C., 2010. Significance of polycyclic aromatic hydrocarbons (PAHs) in Permian/Triassic boundary sections. *Appl. Geochemistry* 25, 1374–1382.
<https://doi.org/10.1016/j.apgeochem.2010.06.008>
- Norvick, M.S., 2004. Tectonic and Stratigraphic History of the Perth Basin. *Geosci. Aust.* 2004/16, 18p.
- Owens, R.J., Borissova, I., Hall, L.S., Bernardel, G., Southby, C., Grosjean, E., Mitchell, C., 2018. Geology and prospectivity of the northern Houtman Sub-basin. *Geosci. Aust.* 2018/25, 101 pp.

-
- Pagès, A., Grice, K., Vacher, M., Welsh, D.T., Teasdale, P.R., Bennett, W.W., Greenwood, P., 2014. Characterizing microbial communities and processes in a modern stromatolite (Shark Bay) using lipid biomarkers and two-dimensional distributions of porewater solutes. *Environ. Microbiol.* 16, 2458–2474. <https://doi.org/10.1111/1462-2920.12378>
- Pedentchouk, N., Freeman, K.H., Harris, N.B., Clifford, D.J., Grice, K., 2004. Sources of alkylbenzenes in Lower Cretaceous lacustrine source rocks, West African rift basins. *Org. Geochem.* 35, 33–45. <https://doi.org/10.1016/j.orggeochem.2003.04.001>
- Peters, K., Walters, C., Moldowan, J., 2004. *The Biomarker Guide*, 2nd ed. Cambridge University Press.
- Pfenning, N., 1978. General physiology and ecology of photosynthetic bacteria, in: Clayton, R.K., Sistrom, W.R. (Eds.), *The Photosynthetic Bacteria*. Plenum, New York, pp. 3–18.
- Sandwell, D., Garcia, E., Soofi, K., Wessel, P., Chandler, M., Smith, W.H.F., 2013. Toward 1-mGal accuracy in global marine gravity from CryoSat-2, Envisat, and Jason-1. *Lead. Edge* 32, 892–899.
- Sandwell, D.T., Müller, R.D., Smith, W.H.F., Garcia, E., Francis, R., 2014. New global marine gravity model from CryoSat-2 and Jason-1 reveals buried tectonic structure. *Science*. 346, 65–67. <https://doi.org/10.1126/science.1258213>
- Sandwell, D.T., Smith, W.H.F., 2009. Global marine gravity from retracked Geosat and ERS-1 altimetry: Ridge segmentation versus spreading rate. *J. Geophys. Res. Solid Earth* 114, B01411. <https://doi.org/10.1029/2008JB006008>
- Schaefer, B., Grice, K., Coolen, M.J.L., Summons, R.E., Cui, X., Bauersachs, T., Schwark, L., Böttcher, M.E., Bralower, T.J., Lyons, S.L., Freeman, K.H., Cockell, C.S., Gulick, S.S., Morgan, J. V., Whalen, M.T., Lowery, C.M., Vajda, V., 2020. Microbial mayhem in the nascent chicxulub crater. *Geology* 48, 328–

332. <https://doi.org/10.1130/G46799.1>

- Scott, J., 1994. Source rocks of Western Australia - distribution, character and models, in: *The Sedimentary Basins of Western Australia: Proceedings of the Petroleum Exploration Society of Australia Symposium*. pp. 141–155.
- Song, H.H.H.H., Wignall, P.B., Chu, D., Tong, J., Sun, Y., Song, H.H.H.H., He, W., Tian, L., 2014. Anoxia/high temperature double whammy during the Permian-Triassic marine crisis and its aftermath. *Sci. Rep.* 4, 4132. <https://doi.org/10.1038/srep04132>
- Sousa Júnior, G.R., Santos, A.Ô.L.S.S., De Lima, S.G., Lopes, J.A.D.D., Reis, F.A.M.M., Santos Neto, E. V., Chang, H.K., 2013. Evidence for euphotic zone anoxia during the deposition of Aptian source rocks based on aryl isoprenoids in petroleum, Sergipe-Alagoas Basin, northeastern Brazil. *Org. Geochem.* 63, 94–104. <https://doi.org/10.1016/j.orggeochem.2013.07.009>
- Taniwaki, T., Elders, C., Grice, K., 2021. Early Triassic paleogeography of the northern Perth Basin, and controls on the distribution of source rock facies. *Mar. Pet. Geol.* 133, 105314. <https://doi.org/10.1016/j.marpetgeo.2021.105314>
- Thomas, B.M., 1979. Geochemical analysis of hydrocarbon occurrences in northern Perth Basin, Australia. *Am. Assoc. Pet. Geol. Bull.* 63, 1092–1107. <https://doi.org/10.1306/2F9184BE-16CE-11D7-8645000102C1865D>
- Thomas, B.M., Barber, C.J., 2004. A re-evaluation of the hydrocarbon habitat of the northern perth basin. *APPEA J.* 44, 59–92.
- Thomas, B.M., Willink, R.J., Grice, K., Twitchett, R.J., Purcell, R.R., George, A.D., Tye, S., Alexander, R., Foster, C.B., Barber, C.J., George, A.D., Tye, S., Alexander, R., Foster, C.B., Unique, C.J.B., Barber, C.J., 2004. Unique marine Permian-Triassic boundary section from Western Australia. *Aust. J. Earth Sci.* 51, 423–430.

-
- Tindale, K., Newell, N., Keall, J., Smith, N., 1998. Structural Evolution and Charge History of the Exmouth Sub-basin, Northern Carnarvon Basin, Western Australia, in: *The Sedimentary Basins of Western Australia 2: Proceedings of the Petroleum Exploration Society of Australia Symposium*. pp. 447–472.
- Tulipani, S., 2013. Novel biomarker and stable isotopic approaches for palaeoenvironmental reconstruction of saline and stratified ecosystems: The modern Coorong Lagoon and Devonian reefs of the Canning Basin. Curtin University.
- Twitchett, R.J., Krystyn, L., Baud, A., Wheeley, J.R., Richoz, S., 2004. Rapid marine recovery after the end-Permian mass-extinction event in the absence of marine anoxia. *Geology* 32, 805–808. <https://doi.org/10.1130/G20585.1>
- van Aarsen, B.G.K., Alexander, R., Kagi, R.I., 1996. The origin of Barrow Sub-basin crude oils: A geochemical correlation using land-plant biomarkers. *APPEA J.* 36, 465–476.
- Volkman, K., Alexandert, R., Kagi, R.I., Noble, R.A., Woodhouse, G.W., 1983. A geochemical reconstruction of oil generation in the Barrow Sub-basin of Western Australia. *Geochim. Cosmochim. Acta* 47, 2091–2105.
- Whiteside, J.H., Grice, K., 2016. Biomarker Records Associated with Mass Extinction Events. *Annu. Rev. Earth Planet. Sci.* 44, 581–612. <https://doi.org/10.1146/annurev-earth-060115-012501>
- Wignall, P.B., Twitchett, R.J., 1996. Oceanic anoxia and the end Permian mass extinction. *Science*. 272, 1155–1158. <https://doi.org/10.1126/science.272.5265.1155>
- Yasin, A.R., Iasky, R.P., Sub-basin, B., 1998. Petroleum Geology of the Peedamullah Shelf, Northern Carnarvon Basin, in: *The Sedimentary Basins of Western Australia 2: Proceedings of the Petroleum Exploration Society of Australia Symposium*. pp. 473–491.

Chapter 5

Conclusions and significance

1 Summary of this PhD research

This PhD research demonstrates the practical integration of geology and organic geochemistry to investigate the basin-scale distribution and fluctuation of paleoenvironmental depositional conditions of the Lower Triassic Kockatea Shale in the northern Perth Basin, and the organic geochemical characteristics of microbialites and PZE (Figure 5-1). In addition, the source-oil and oil-oil correlations in the Perth and Northern Carnarvon basins confirm the importance of the Kockatea Shale as a source rock in the northern Perth Basin and suggest additional source rock potential in the Northern Carnarvon Basin.

Core observations reveal a large variation in lithofacies at the base of the Kockatea Shale: dark coloured mudstone, light coloured mudstone, microbialites, tidal sandstone, storm/gravity sandstones and bioturbated mudstones. The microbialites in cores correspond to an irregular log facies on wireline logs and this facies is recognized in several wells. In addition, seismic interpretation demonstrates that the paleogeography during the Late Permian and Early Triassic was influenced by remnant topography associated with Permian faults. The integrated analysis of core, well logs and seismic data shows the lateral distribution of paleogeography during the Early Triassic and the factors that control the development and distribution of microbialites in the northern Perth Basin. In addition, organic geochemical analyses (biomarker, stable carbon isotope and sulfur isotope analyses of organic matter and pyrite, respectively) are used to reconstruct the paleoenvironments of corresponding lithofacies.

The light coloured mudstones and interbedded sandstone were deposited in an oxygenated, tidally influenced shallow marine setting near the southern basin margin without any indication of sulfur bacteria development. PZE was established away from the margin due to a combination of the restricted nature of the basin and greater water depths with high abundance of sulfur bacteria, resulting in the deposition of dark coloured mudstone. Microbialites were confined to intra-basinal structural highs

(Beagle Ridge and Turtle Dove Ridge) away from basin margins, which were shallow enough for sufficient light to penetrate to allow the development of microbial mats, but in conditions that were unfavourable for other fauna. The presence of sulfur bacteria is identified in microbialite facies based on biomarker characteristics. High abundances of cyanobacterial biomarkers are identified from microbial mats developed under oxic conditions compared with the mats developed under PZE. Microbialite facies contain more abundant purple sulfur bacteria relative to green sulfur bacteria (higher okenane ratio) compared with PZE. The source of *n*-C₃₃ ACH is unknown, but it is observed to be abundant in microbialite layers as well as in intervening mudstones, suggesting that *n*-C₃₃ ACH is associated with the development of the microbialites themselves. The $\delta^{13}\text{C}$ of bulk organic matter and $\delta^{34}\text{S}$ of pyrite are isotopically lighter in the microbialite facies than in PZE. The isotopically light $\delta^{13}\text{C}_{\text{OM}}$ in microbialite facies is consistent with the abundance of purple sulfur bacteria utilizing the C₃ pathway for their carbon fixation which is depleted in ¹³C. The fractionation of $\delta^{34}\text{S}$ values between PZE and microbialites appears to indicate that differences in the microbial communities including the relative abundance of purple sulfur bacteria, is a cause of the fractionation and is likely related to the different metabolism of each microbe. The okenane ratio, *n*-C₃₃ ACH ratio, $\delta^{13}\text{C}_{\text{OM}}$ and $\delta^{34}\text{S}$ of pyrite are good proxies for distinguishing PZE and microbialite facies and are related to the relative abundance of purple and green sulfur bacteria. In addition, chemo-isotope stratigraphy suggests cyclic fluctuations of PZE and oxic conditions. This results in fluctuations in the depth of the chemocline (boundary of oxic and anoxic/euxinic conditions). This research reveals how chemo-isotope stratigraphy can be used for unravelling the history of extinction events.

During the period of ecological recovery that followed the end-Permian mass extinction, the development of microbialites was controlled by two local factors.

1) Paleogeographic control: anoxic conditions away from the basin margins inhibited grazing organisms, allowing microbial mats to flourish. On the other hand,

oxic, shallow marine, tidal settings with major clastic input closer to the basin margins promoted grazing organisms, which are unfavourable for microbial mat formation.

2) Topographic control: topographic highs in the anoxic part of the basin provided good habitats with sufficient light for microbial mat forming organisms.

The microbialites and dark coloured mudstone have good source rock potential with high TOC and HI. The distribution of these lithofacies matches the distribution of discovered hydrocarbon fields highlighting the more prospective parts of the basin. On the other hand, the light coloured mudstone deposited under oxic conditions have no to poor source rock potential with low TOC and HI. Petroleum samples from the Perth Basin contain carotenoid biomarkers derived from sulfur bacteria, suggesting that the source rocks developed under PZE and/or were formed by microbialites. In the northern Perth Basin, biomarkers demonstrated that the microbialites and/or dark coloured mudstone deposited under PZE in the Kockatea Shale are the major lithofacies contributing to the petroleum system.

In the southern Perth Basin, it is possible that the source rock is Permian in age based on the low concentrations or absence of carotenoids, the lack of *n*-C₃₃ ACH and the overall geological setting.

The presence of carotenoid biomarkers derived from sulfur bacteria in the Tubridgi petroleum on the Peedamullah Shelf suggested a contribution from a source rock developed under PZE and/or formed by microbialites. The similarity of biomarker characteristics to the Perth Basin petroleum and the Kockatea Shale indicate that the Tubridgi petroleum may have migrated from the Lower Triassic Locker Shale. However, the possibility of the Dingo Claystone source rock contributing to the Tubridgi petroleum cannot be excluded due to the lack of *n*-C₃₃ ACH, and the lack of previous analyses targeting the carotenoids in the Dingo Claystone. Further analysis of Northern Carnarvon Basin petroleum and source rocks in this regard may open up potential new plays on the southern margin of the Northern Carnarvon Basin and possibly more broadly in the basin.

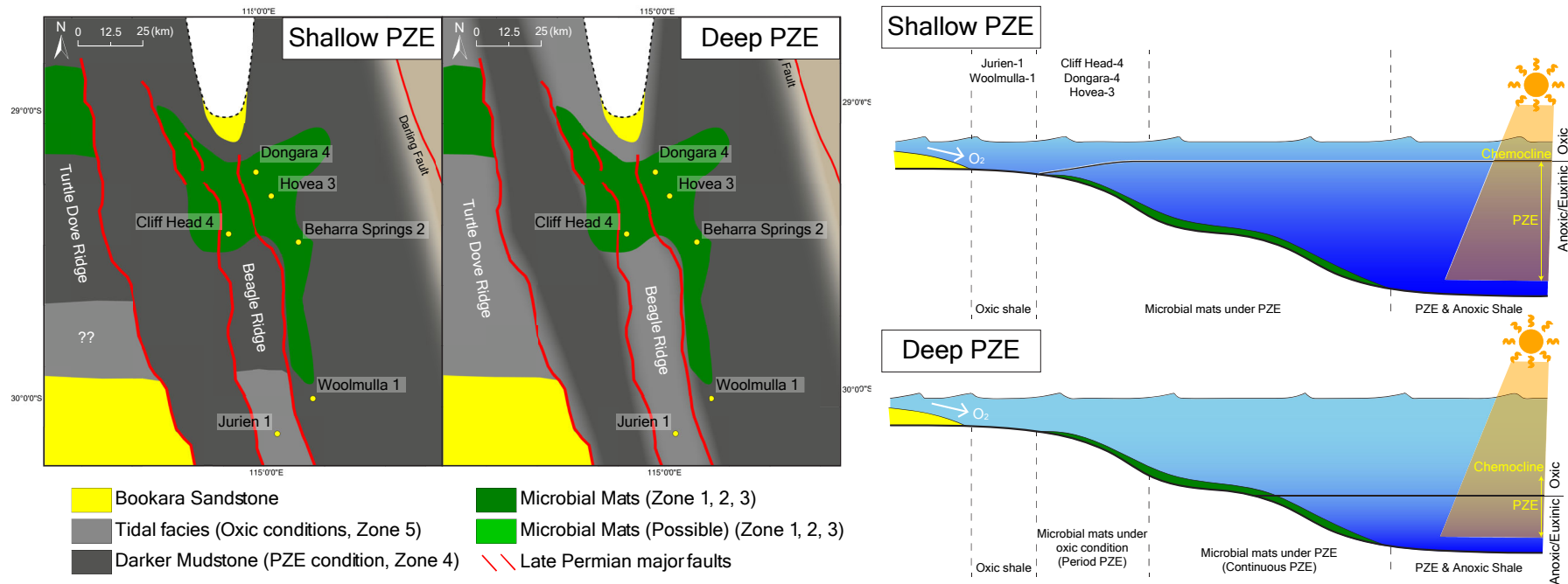


Figure 5-1. Summary figures of this research, showing the basin scale extent of paleoenvironments and their fluctuation during deposition of the Early Triassic Kockatea Shale.

2 Significance of this research

2.1 Organic geochemical difference between PZE and microbialites

This research demonstrates that the carotenoids derived from sulfur bacteria are indicative of both PZE and microbialites. However, purple sulfur bacteria is relatively more abundant than green sulfur bacteria in microbialites compared with PZE. The abundance of okenane relative to chlorobactane and isorenieratane (relative abundance of purple sulfur bacteria to green sulfur bacteria) and stable carbon isotopes can be used to distinguish microbialites from PZE. Many previous studies around the end-Permian mass extinction identified PZE mainly based on the presence of isorenieratane and aryl isoprenoids (Cao et al., 2009; Grice et al., 2005; Hays et al., 2012, 2007; Nabbefeld et al., 2010) which is insufficient to distinguish between PZE and/or microbialites. Around the end-Permian mass extinction, microbialites were also extensively developed globally. Therefore, careful evaluation of the organic geochemical characteristics is required to identify the contribution of PZE and/or microbialites. Some cases previously identified as indicative of PZE could have some contributions from microbialites, which do not necessarily require PZE to form.

Petroleum samples containing carotenoids derived from sulfur bacteria suggest the sources of these hydrocarbons were deposited under PZE and/or are from microbialites. High okenane ratios in petroleum may be indicative of significant contributions from microbialites, but the influence of thermal maturity needs to be considered. These carotenoids decrease in concentration during maturation, but because this rate of decrease is not the same for each carotenoid, the ratios will also be affected. This makes it difficult to use them as environmental indicators in thermally matured samples, while low maturity samples preserve the original biomarker information which more closely reflects their constituent ecological communities.

2.2 Application of chemo-isotope stratigraphy

In this research, paleoenvironmental zones are defined in each well to identify the paleoenvironmental depositional conditions and correlate them between wells. Each well has the same superposition of paleoenvironments, showing the fluctuation of PZE and oxic conditions through time, with development of microbialites during the early stage of evolution.

This research shows the effectiveness of applying the concept of chemo-isotope stratigraphy. The fluctuation of PZE and oxic conditions in the northern Perth Basin suggests the development of multiple episodes of harsh environmental conditions after the end-Permian mass extinction, consistent with the recurrent environmental perturbations observed during the Early Triassic in other regions (south China and northern India) (Wei et al., 2015), although it cannot be proven that the chronological scale of fluctuation identified in this research corresponds to the fluctuation in other basins. The similarity of the superposition in each well shows a similar environmental transition through time and across the basin, but better stratigraphic control is required for the precise correlation of zones between wells.

2.3 Global variation in source rock quality around the end-Permian mass extinction

Source rock quality around the end-Permian mass extinction shows variation globally. This research shows the northern Perth Basin has excellent source rock potential with high TOC (up to 3.4 %) at the PZE interval. The Peace River Basin (Canada) also shows high TOC (up to 3%) at the PZE interval (Hays et al., 2007). On the other hand, Meishan (China), Kap Stosch (Greenland) and Lusitaniadalen (Spitsbergen) have low TOC (generally less than 1%) at the PZE interval (Cao et al., 2009; Hays et al., 2012, 2007).

These basins are located in intra-continental restricted conditions, apart from Meishan which is located on a micro-continental fragment. Other factors such as climate and paleogeographic controls are required for the development of good quality source rock. In addition, imperfect correlation depending on the available data could cause the apparent difference in source rock quality.

Zhou et al. (2017) and Zhu et al. (2019) suggest one of the causes for the regional variation of PZE is an increase in riverine nutrition fluxes enhanced by the warming climate and terrestrial ecosystem collapse. Around the Permian-Triassic boundary, the northern Perth Basin, Meishan, Peace River Basin and Lusitaniadalen were located in the tropical to temperate climate zone, and Kap Stosch was located in the arid climate zone (Figure 5-2). However, source rock quality does not always correlate with climate zones. Source rock potential is high in both the northern Perth Basin and Peace River Basin in temperate climate zones and low in Kap Stosch in an arid climate zone. This appears to be consistent with the notion of riverine nutrient fluxes in different climate zones, but the source rock potential in Meishan and Lusitaniadalen are poor even although they are in temperate climate zones. Climate zones may influence source rock quality, but other factors such as paleogeography may also play a role.

In Meishan, the basin was located on the margin of a microcontinent. The riverine nutrient fluxes may not be sufficient to develop good quality source rock due to the smaller hinterland expected in microcontinents compared with major continents, and consequently lower primary productivity (Katz, 2011). The basins in both Lusitaniadalen and Kap Stosch were developed adjacent to the mountain range of the Appalachian orogenic belt, causing the dilution of organic materials by high sedimentary influx (Katz, 2011).

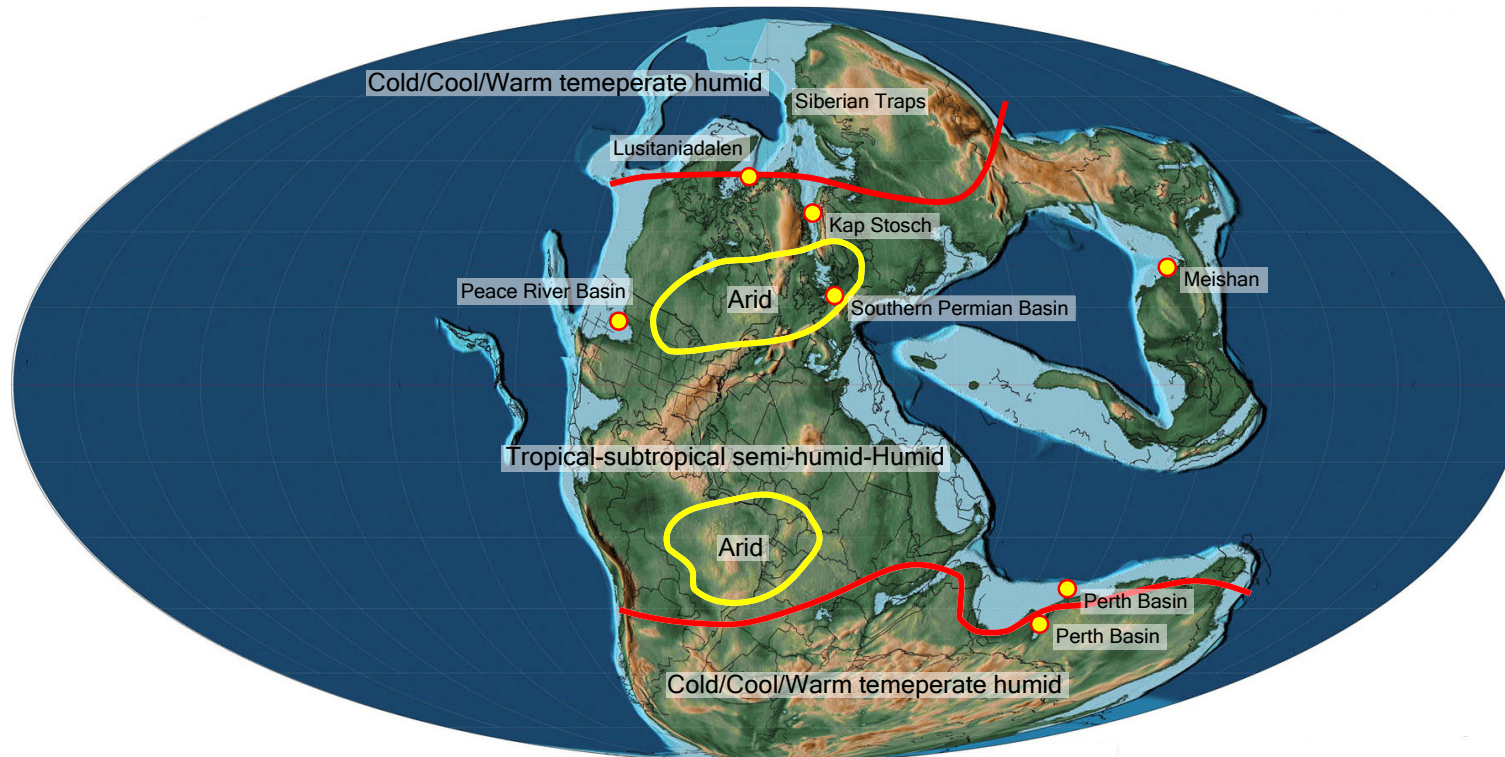


Figure 5-2. Plate reconstruction around 250Ma and locations of each basin (after Matthews et al., 2016; Scotese, 2003; Thomas et al., 2004; Zhu et al., 2019). The paleogeographic reconstruction in this figure shows the large continent around Meishan, but some other reconstructions show a micro-continental fragment (Matthews et al., 2016; Thomas et al., 2004).

The Upper Permian of the Southern Permian Basin in Poland is another example which shows the importance of the relationship between basin-scale paleogeographic variations and the potential for source rock development related to PZE. In the Southern Permian Basin, strata were deposited around the onset of the end-Permian mass extinction (García-Veigas et al., 2011), and record PZE in a slope setting, while PZE is absent on the basin margin (Słowakiewicz et al., 2015). The basin was located in the arid climate zone near Kap Stosch (Zhu et al., 2019). However, TOC values in the slope setting are high (up to 2 %) at the PZE interval, but values in the basin margin are low (less than 1 %) (Słowakiewicz et al., 2015). High source rock potential is confirmed under PZE at greater water depth away from the basin margin in the both the northern Perth Basin and the Upper Permian of the Southern Permian Basin.

The last factor is not geological, but is important for comparisons between basins. The basin scale paleoenvironmental distribution has been reconstructed based on several wells in the northern Perth Basin in Australia (this research) and in the Late Permian Southern Permian Basin in Europe. Therefore, the role of PZE and its effect on source rock quality are clearly illustrated in these basins. On the other hand, the paleoenvironments in other basins (Peace River Basin, Meishan, Lusitaniadalen and Kap Stosch) are based on a single data point or on limited data points from wells or outcrops without the reconstruction of regional paleoenvironmental conditions. Great caution is required when comparing paleoenvironments and source rock quality between basins because the material analysed in each basin could have been deposited under different paleoenvironmental conditions. Therefore, basin-scale distribution of paleogeography and paleoenvironmental conditions are essential factors for investigating source rock potential in a basin and to correlate paleoenvironmental conditions between basins.

3 Future work

3.1 Application of the northern Perth Basin analogues: Source rock potential and distribution in the Bedout Sub-basin

The Bedout Sub-basin is the southern sub-basin of the Roebuck Basin located between the Northern Carnarvon and Browse basins on the North West Shelf, and was part of the same depocentre as the south-eastern part of the Northern Carnarvon Basin during the Triassic (Minken et al., 2019). The Bedout Sub-basin and the south-eastern part of the Northern Carnarvon Basin have several recent oil discoveries from the Middle Triassic Lower Keraudren and Archer Formations in the Phoenix South, and Dorado Fields and in the Oxfordian Calypso Formation in the Nebo Field (Figure 5-3) (Grosjean et al., 2021, 2017; Lech, 2013; Rollet et al., 2019; Thompson, 2020; Woodward et al., 2018).

The Bedout Sub-basin and the northern Perth Basin are considered to have developed as part of the East Gondwana Interior Rift (EGIR) during this period (Figure 5-4) (Haig et al., 2017). The northern Perth Basin is located in the middle part of the EGIR and is restricted. On the other hand, the Bedout Sub-basin is located on the eastern edge of the EGIR and is bounded by the Sibmasu-Argo blocks adjacent to the Neo Tethys Ocean. The basin may have had more open marine connections to the Neo Tethys Ocean with more circulation of the water column, depending on the location and topography of these blocks. However the eastern end of the Triassic depocenter in the Bedout sub-basin may also represent a restricted environment.

In the Northern Carnarvon Basin, the Early Triassic Locker Shale was deposited as an equivalent of the lower part of the Kockatea Shale (northern Perth Basin) during the Early Triassic (Induan to Olenekian, Figure 5-3) and is suggested to be a possible source rock further west in the Northern Carnarvon Basin, on the Peedamullah Shelf (Chapter 4). The Archer and Lower Keraudren Formations overlie the Locker Shale in the eastern part of the Northern Carnarvon Basin and in the Beagle sub-basin, and were deposited as a series of deltaic sequences during the Early Triassic Olenekian to

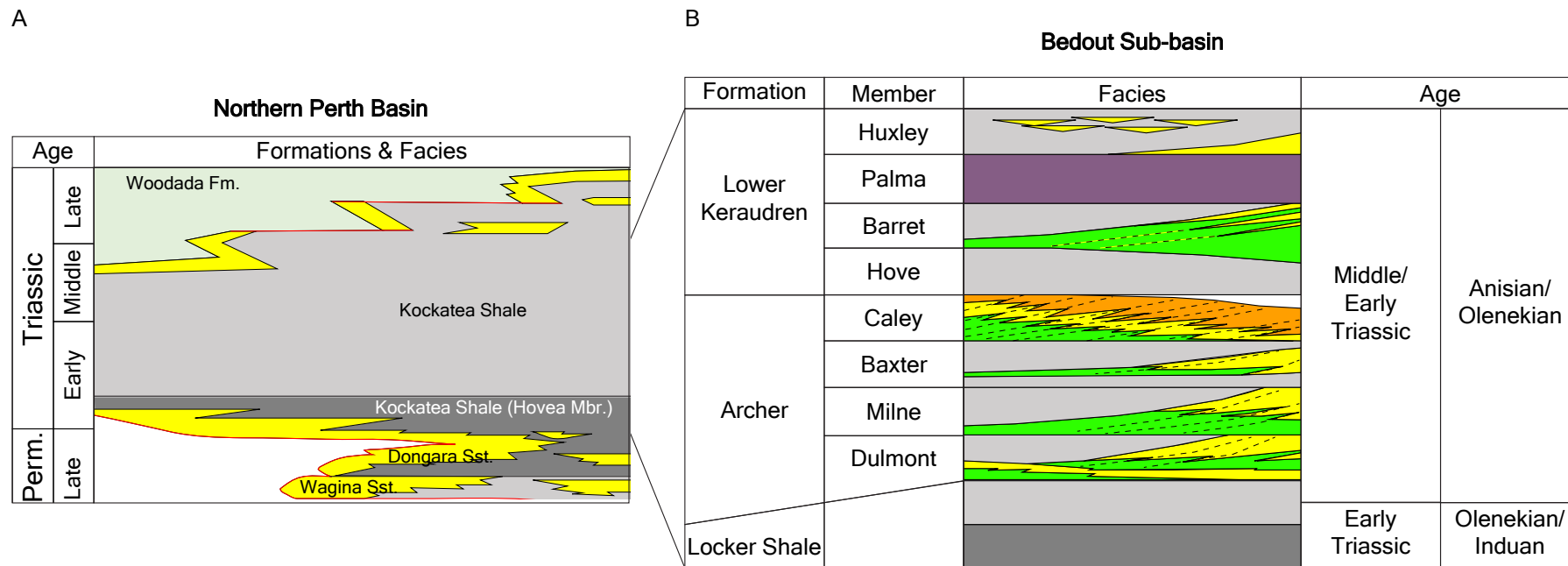
Middle Triassic Anisian (*T. playfordii* palynological zone) (Thompson, 2020; Woodward et al., 2018). The main source rock potential in the Bedout Sub-basin is considered to be the intraformational mudstones of the Archer and Lower Keraudren Formations, including the Caley Member in the uppermost part of the Archer Formation (Grosjean et al., 2021; Rollet et al., 2019; Woodward et al., 2018). The Lower Keraudren Formation is the main reservoir for the recent oil discoveries.

Although the Kockatea Shale extends into the *T. playfordii* palynological zone (Early Triassic Olenekian to Middle Triassic Anisian), the Caley Member is slightly younger than the interval that is the focus of this research (the Hovea Member in the Kockatea Shale in the northern Perth Basin, *K. saeptatus* and *P. samoilovichii* palynological zone corresponding to the Early Triassic Induan to Olenekian) (Jablonski and Saitta, 2004; Marshall and Lang, 2013; Rollet et al., 2019). However, the *T. playfordii* palynological zone lies partially within the recovery phase from the end-Permian mass extinction (Chen and Benton, 2012; Marshall and Lang, 2013), although the source rock potential for the Upper Kockatea Shale in the *T. playfordii* palynological zone equivalent in the Perth Basin is generally low (Thomas and Barber, 2004). There is no evidence to suggest that PZE developed in the Upper Kockatea Shale in the Perth Basin, although this cannot be confirmed due to the lack of previous research focusing on PZE biomarkers. In the Caley Member, source rocks deposited in deltaic environments are inferred to include organic materials derived from terrigenous and brackish algae (Allgöwer and Lignum, 2019; Grosjean et al., 2021; Woodward et al., 2018), but again the development of PZE cannot be confirmed due to the lack of biomarker analysis. It is thus unclear the extent to which the deposition of source rocks in the Bedout sub-basin is related to environmental conditions that persisted after the end-Permian mass extinction, as opposed to local depositional controls.

In the Bedout Sub-basin, the narrowing Triassic depocenter created a restricted environment, bounded by the Bedout High to the north and the Lambert Shelf to the south (Figure 5-5) (Rollet et al., 2019). The oil discoveries are located in the middle

of this area of local restricted topography. The Roc 1 and 2 wells have excellent source rock potential in the Early Triassic Olenekian to Middle Triassic Anisian (TOC: 2 to 15 % and HI: 150 to 400 mg/gTOC). Bruce 1 and Poissonnier 1 are located on the basin margin outside the area of local restricted topography and have fair source rock quality with low TOC and HI (TOC: less than 1 % and HI: less than 200 mg/gTOC). Keraudren 1 is located closer to the margin and has fair source rock potential (TOC: 0.5 to 2 % and HI: 150 to 200 mg/gTOC). This is analogous to the northern Perth Basin where the basin margins have poor source rock quality with Type III kerogen (TOC: 0.2-0.5%, HI: 59-127mg/gTOC) while the high potential source rocks were deposited away from the basin margin. In both instances, the controls on the development of high potential source rock are a combination of regional restricted basin geometry and local paleogeography including the water depth and distance from basin margins.

This research reveals the basin-scale extent of PZE and microbial mat activity during the Early Triassic in the Perth Basin, and the possible contribution of the Early Triassic source rock in on the Peedamullah Shelf on the Northern Carnarvon Basin. It is not clear to what extent these conditions extended in to the Bedout Sub-basin, or how much longer they persisted given that the main source rock interval is slightly different compared to both the Perth and Northern Carnarvon basins. Further research is required to show the way in which ecological recovery continued after the end Permian mass extinction and how it impacted on different parts of the northern and western Australian continental margin. Such research also has the potential unravel the contributions from different oil-prone source rocks and to open up new plays on the North West Shelf.



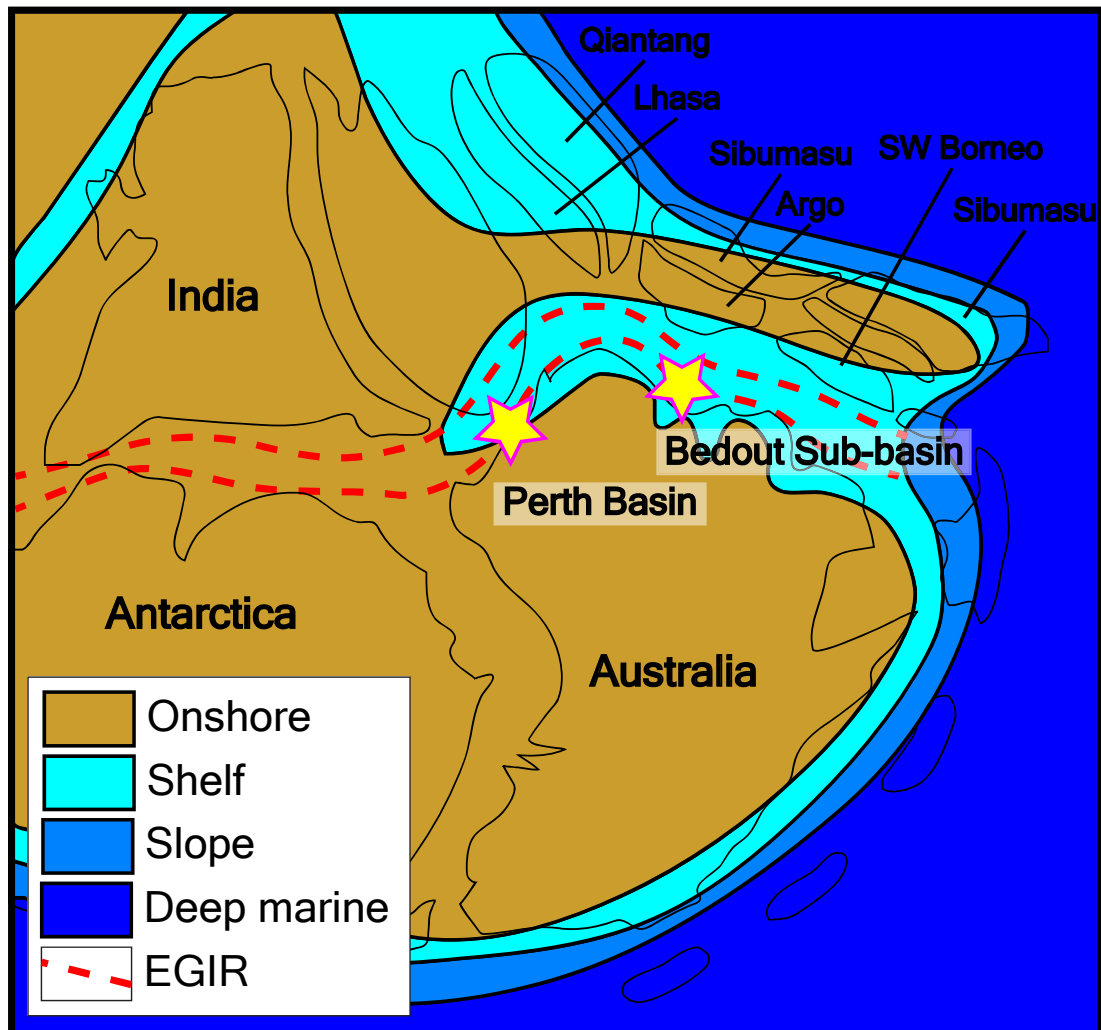


Figure 5-4. The distribution of the East Gondwana Interior Rift (EGIR) (after Minken et al., 2019).

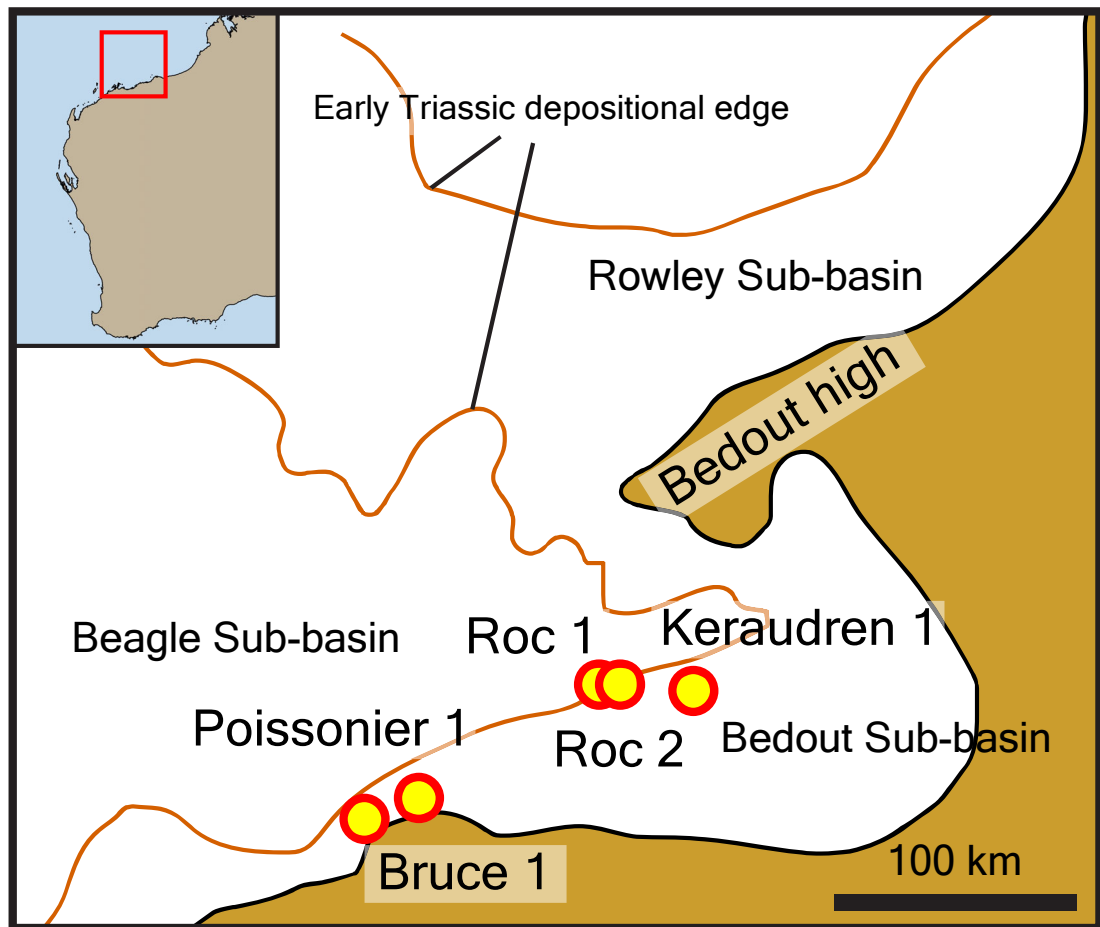


Figure 5-5. Reconstructed paleogeography during the Early Triassic Olenekian to Middle Triassic Anisian (after Rollet et al., 2019).

Bibliography

Every reasonable effort has been made to acknowledge the owners of copyright material. I would be pleased to hear from any copyright owner who has been omitted or incorrectly acknowledged.

A

Algeo, T.J., Chen, Z.Q., Fraiser, M.L., Twitchett, R.J., 2011. Terrestrial-marine teleconnections in the collapse and rebuilding of Early Triassic marine ecosystems. *Palaeogeogr. Palaeoclimatol. Palaeoecol.* 308, 1–11.

<https://doi.org/10.1016/j.palaeo.2011.01.011>

Allgöwer, A.M., Lignum, J.S., 2019. Fine-scale variations in distributary mouth-bar morphology in the Middle Triassic Caley Member of the Bedout Sub-basin , Western Australia. KeeP, M. MOSS, S.j. (eds), *Sediment. Basins West. Aust. V Proc. Pet. Explor. Soc. Aust. Symp. Perth, WA* 23.

Anderson, L.G., Dyrssen, D., Hall, P.O.J., 1988. On the sulphur chemistry of a super-anoxic fjord, Framvaren, South Norway. *Mar. Chem.* 23, 283–293.

Armitage, D.W., Gallagher, K.L., Youngblut, N.D., Buckley, D.H., Zinder, S.H., 2012. Millimeter-scale patterns of phylogenetic and trait diversity in a salt marsh microbial mat. *Front. Microbiol.* 3, 1–16.

B

Baillie, P.W., Powell, C.M.A., Li, Z.X., Ryall, A.M., 1994. The tectonic framework of Western Australia's Neoproterozoic to Recent sedimentary basins, in: *The Sedimentary Basins of Western Australia: Proceedings of the Petroleum Exploration Society of Australia Symposium.* pp. 45–62.

- Beatty, T.W., Zonneveld, J.P., Henderson, C.M., 2008. Anomalously diverse Early Triassic ichnofossil assemblages in northwest Pangea: A case for a shallow-marine habitable zone. *Geology* 36, 771–774. <https://doi.org/10.1130/G24952A.1>
- Becker, L., Poreda, R.J., Basu, A.R., Pope, K.O., Harrison, T.M., Nicholson, C., Iasky, R., 2004. Bedout : A Possible End-Permian Impact Crater Offshore of Northwestern Australia. *Science*. 304, 1469–1476.
- Benton, M.J., 2016. The Triassic. *Curr. Biol.* 26, R1214--R1218. <https://doi.org/10.1016/j.cub.2016.10.060>
- Bernasconi, S.M., Meier, I., Wohlwend, S., Brack, P., Hochuli, P.A., Bläsi, H., Wortmann, U.G., Ramseyer, K., 2017. An evaporite-based high-resolution sulfur isotope record of Late Permian and Triassic seawater sulfate. *Geochim. Cosmochim. Acta* 204, 331–349. <https://doi.org/10.1016/j.gca.2017.01.047>
- Boreham, C.J., Hope, J.M., Hartung-Kagi, B., van Aarssen, B.J.K., 2000. More sources for gas and oil in Perth Basin. *AGSO Res. Newsl.* 5–9.
- Borel, G.D., Stampfli, G.M., 2002. Geohistory of the North West Shelf: A tool to assess the Palaeozoic and Mesozoic motion of the Australian Plate, in: *The Sedimentary Basins of Western Australia 3: Proceedings of the Petroleum Exploration Society of Australia Symposium*. pp. 119–128.
- Böttcher, M.E., Voss, M., Schulz-Bull, D., Schneider, R., Leipe, T., Knöller, K., 2010. Environmental changes in the Pearl River Estuary (China) as reflected by light stable isotopes and organic contaminants. *J. Mar. Syst.* 82, S43–S53. <https://doi.org/10.1016/j.jmarsys.2010.02.004>
- Bralower, T.J., Cosmidis, J., Heaney, P.J., Kump, L.R., Morgan, V., Harper, D.T., Lyons, S.L., Freeman, K.H., Grice, K., Wendler, E., Zachos, J.C., Artemieva, N., Athena, S., Gulick, S.P.S., House, C.H., Jones, H.L., Lowery, C.M., Nims, C., Schaefer, B., Thomas, E., Vajda, V., 2020. Origin of a global carbonate layer deposited in the aftermath of the Cretaceous-Paleogene boundary impact. *Earth Planet. Sci. Lett.* 548, 116476. <https://doi.org/10.1016/j.epsl.2020.116476>
- Brocks, J.J., Schaeffer, P., 2008. Okenane, a biomarker for purple sulfur bacteria (Chromatiaceae), and other new carotenoid derivatives from the 1640 Ma Barney

Creek Formation. *Geochim. Cosmochim. Acta* 72, 1396–1414.

<https://doi.org/10.1016/j.gca.2007.12.006>

Bunt, R.J.W., Powell, W.D., Scholefield, T., 2001. The Tubridgi gas field rejuvenated. *APPEA J.* 41, 429–447.

Burgess, S.D., Bowring, S.A., 2015. High-precision geochronology confirms voluminous magmatism before, during, and after Earth's most severe extinction. *Sci. Adv.* 1, 1–14. <https://doi.org/10.1126/sciadv.1500470>

C

Cadman, S.J., Pain, L., Vuckovic, V., 1994. Perth Basin, Western Australia. *Aust. Pet. Accumulations Rep.* 10, 1–103.

Canfield, D.E., Farquhar, J., 2009. Animal evolution, bioturbation, and the sulfate concentration of the oceans. *Proc. Natl. Acad. Sci. U. S. A.* 106, 8123–8127. <https://doi.org/10.1073/pnas.0902037106>

Cao, C., Love, G.D., Hays, L.E., Wang, W., Shen, S., Summons, R.E., 2009. Biogeochemical evidence for euxinic oceans and ecological disturbance presaging the end-Permian mass extinction event. *Earth Planet. Sci. Lett.* 281, 188–201. <https://doi.org/10.1016/j.epsl.2009.02.012>

Chen, Z.-Q., Benton, M.J., 2012. The timing and pattern of biotic recovery following the end-Permian mass extinction. *Nat. Geosci.* 5, 375–383. <https://doi.org/10.1038/ngeo1475>

Chen, Z.-Q., Fraiser, M.L., Bolton, C., 2012. Early Triassic trace fossils from Gondwana Interior Sea: Implication for ecosystem recovery following the end-Permian mass extinction in south high-latitude region. *Gondwana Res.* 22, 238–255. <https://doi.org/10.1016/j.gr.2011.08.015>

Chen, Z.Q., Wang, Y., Kershaw, S., Luo, M., Yang, H., Zhao, L., Feng, Y., Chen, J., Yang, L., Zhang, L., 2014. Early Triassic stromatolites in a siliciclastic nearshore setting in northern Perth Basin, Western Australia: Geobiologic features and

- implications for post-extinction microbial proliferation. *Glob. Planet. Change* 121, 89–100. <https://doi.org/10.1016/j.gloplacha.2014.07.004>
- Clifford, D.J., Clayton, J.L., Sinninghe Damsté, J.S., 1998. 2,3,6-/3,4,5-Trimethyl substituted diaryl carotenoid derivatives (Chlorobiaceae) in petroleums of the Belarussian Pripyat River Basin. *Org. Geochem.* 29, 1253–1267. [https://doi.org/10.1016/S0146-6380\(98\)00086-2](https://doi.org/10.1016/S0146-6380(98)00086-2)
- Connock, G.T., Nguyen, T.X., Philp, R.P., 2018. The development and extent of photic-zone euxinia concomitant with Woodford Shale deposition. *Am. Assoc. Pet. Geol. Bull.* 102, 959–986. <https://doi.org/10.1306/0726171602017224>
- Crostella, A., 1995. An evaluation of the hydrocarbon potential of the onshore northern perth basin, western australia. *Geol. Surv. West. Aust. Report* 43, 67p.
- Crostella, A., Backhouse, J., 2000. *Geology and Petroleum Exploration of the Central and Southern Perth Basin*. West. Aust. Geol. Surv. Report 57, 85p.
- Cui, X., Liu, X.L., Shen, G., Ma, J., Husain, F., Rocher, D., Zumberge, J.E., Bryant, D.A., Summons, R.E., 2020. Niche expansion for phototrophic sulfur bacteria at the Proterozoic–Phanerozoic transition. *Proc. Natl. Acad. Sci. U. S. A.* 117, 17599–17606. <https://doi.org/10.1073/pnas.2006379117>

D

- Dargahi, H.J., Rezaee, R., 2014. The study of lateral variability of Kockatea Shale across the Perth Basin: an integration of electrofacies and lithofacies characteristics. *APPEA J.* 54, 241–248. <https://doi.org/10.1071/aj13024>
- Dawson, D., Grice, K., Alexander, R., 2005. Effect of maturation on the indigenous δD signatures of individual hydrocarbons in sediments and crude oils from the Perth Basin (Western Australia). *Org. Geochem.* 36, 95–104. <https://doi.org/10.1016/j.orggeochem.2004.06.020>
- Domeier, M., Torsvik, T.H., 2014. Plate tectonics in the late Paleozoic. *Geosci. Front.* 5, 303–350. <https://doi.org/10.1016/j.gsf.2014.01.002>

E

- Edwards, D.S., Zumberge, J.E., 2005. The oils of Western Australia II-regional petroleum geochemistry and correlation of crude oils and condensates from western Australia and Papua New Guinea. *Geosci. Aust. Rep.* 37512.
- Elders, C., Chen, P., Anson, A.I., Mahar, M., Neill, G.O., 2018. Triassic tectonics and sedimentation on the North West Shelf of Australia, in: *Australian Geoscience Council Convention*.
- Ellis, G., Bruce, R., 1998. Dongara Oil and Gas Field, Perth Basin, in: *The Sedimentary Basins of Western Australia 2: Proceedings of the Petroleum Exploration Society of Australia Symposium*. pp. 621–636.
- Erwin, D.H., 1994. The Permo-Triassic extinction. *Nature* 367, 231–236.

F

- Faure, G., Mensing, T.M., 2005. *Isotopes : principles and applications*, 3rd ed, Wiley. Wiley, Hoboken, N.J.
- Fenton, S., Grice, K., Twitchett, R.J., Böttcher, M.E., Looy, C. V., Nabbefeld, B., 2007. Changes in biomarker abundances and sulfur isotopes of pyrite across the Permian-Triassic (P/Tr) Schuchert Dal section (East Greenland). *Earth Planet. Sci. Lett.* 262, 230–239. <https://doi.org/10.1016/j.epsl.2007.07.033>
- Ferdinando, D., Baker, J.C., Gongora, A., Pidgeon, B.A., 2007. Illite/smectite clays preserving porosity at depth in Lower Permian reservoirs, northern Perth Basin. *APPEA J.* 47, 69–88. <https://doi.org/10.1071/aj06004>
- Forel, M.-B., 2013. The Permian–Triassic mass extinction: Ostracods (Crustacea) and microbialites. *Comptes Rendus Geosci.* 345, 203–211.
- Foster, W.J., Danise, S., Sedlacek, A., Price, G.D., Hips, K., Twitchett, R.J., 2015. Environmental controls on the post-Permian recovery of benthic, tropical marine ecosystems in western Palaeotethys (Aggtelek Karst, Hungary). *Palaeogeogr.*

Palaeoclimatol. Palaeoecol. 440, 374–394.
<https://doi.org/10.1016/j.palaeo.2015.09.004>

Foster, W.J., Heindel, K., Richoz, S., Gliwa, J., Lehrmann, D.J., Baud, A., Kolar-Jurkovšek, T., Aljinović, D., Jurkovšek, B., Korn, D., Martindale, R.C., Peckmann, J., 2020. Suppressed competitive exclusion enabled the proliferation of Permian/Triassic boundary microbialites. *Depos. Rec.* 6, 62–74.
<https://doi.org/10.1002/dep2.97>

Fox, C.P., Cui, X., Whiteside, J.H., Olsen, P.E., Summons, R.E., Grice, K., 2020. Molecular and isotopic evidence reveals the end-Triassic carbon isotope excursion is not from massive exogenous light carbon. *Proc. Natl. Acad. Sci.* 117, 30171–30178. <https://doi.org/10.1073/pnas.1917661117>

French, K.L., Rocher, D., Zumberge, J.E., Summons, R.E., 2015. Assessing the distribution of sedimentary C40 carotenoids through time. *Geobiology* 13, 139–151. <https://doi.org/10.1111/gbi.12126>

French, K.L., Sepúlveda, J., Trabucho-Alexandre, J., Gröcke, D.R., Summons, R.E., 2014. Organic geochemistry of the early Toarcian oceanic anoxic event in Hawsker Bottoms, Yorkshire, England. *Earth Planet. Sci. Lett.* 390, 116–127.
<https://doi.org/10.1016/j.epsl.2013.12.033>

G

García-Veigas, J., Cendón, D.I., Pueyo, J.J., Peryt, T.M., 2011. Zechstein saline brines in Poland, evidence of overturned anoxic ocean during the Late Permian mass extinction event. *Chem. Geol.* 290, 189–201.
<https://doi.org/10.1016/j.chemgeo.2011.09.016>

George, A.D., Chow, N., Trinajstić, K.M., 2014. Oxidic facies and the Late Devonian mass extinction, Canning Basin, Australia. *Geology* 42, 327–330.
<https://doi.org/10.1130/G35249.1>

Georgiev, S. V., Stain, H.J., Yang, G., Hannah, J.L., Böttcher, M.E., Grice, K., Holman, A.I., Turgeon, S., Simonsen, S., Cloquet, C., 2020. Late Permian–Early

- Triassic environmental changes recorded by multi-isotope (Re-Os-N-Hg) data and trace metal distribution from the Hovea-3 section, Western Australia. *Gondwana Res.* 88, 353–372. <https://doi.org/10.1016/j.bbamem.2019.183135>
- Ghori, K.A.R., 2017. Petroleum Systems Modelling of the Perth Basin, Western Australia. *Search Discov.* 10961, 25p.
- Ghori, K.A.R., 2015. Petroleum systems of the Perth Basin, Western Australia. *Search Discov.* 10805, 20p.
- Gorter, J., Nicoll, R.S., Metcalfe, I., Willink, R., Ferdinando, D., 2009. The Permian–Triassic boundary in Western Australia: evidence from the Bonaparte and Northern Perth basins—exploration implications. *APPEA J.* 49, 311–336. <https://doi.org/10.1071/AJ08020>
- Grahame, J., Cairns, E., Roy, S., Davidson, A., Waele, B. De, Ernst, R.A., Fitzsimons, I.C.W., Fuck, R.A., Gladkochub, D.P., Jacobs, J., Karlstrom, K.E., Lu, S., Natapov, L.M., Pease, V., Pisarevsky, S.A., Thrane, K., Vernikovskiy, V., 2017. Triassic paleogeography and petroleum systems of the North West Shelf, Australia: key insights from a new regional study. *APPEA J.* 57, 744–748. <https://doi.org/10.1071/AJ16156>
- Grasby, S.E., Shen, W., Yin, R., Gleason, J.D., Blum, J.D., Lepak, R.F., Hurley, J.P., Beauchamp, B., 2017. Isotopic signatures of mercury contamination in latest Permian oceans. *Geology* 45, 55–58. <https://doi.org/10.1130/G38487.1>
- Grice, K., Cao, C., Love, G.D., Böttcher, M.E., Twitchett, R.J., Grosjean, E., Summons, R.E., Turgeon, S.C., Dunning, W., Jin, Y., 2005a. Photic zone euxinia during the Permian-Triassic superanoxic event. *Science.* 307, 706–709. <https://doi.org/10.1126/science.1104323>
- Grice, K., Gibbison, R., Atkinson, J.E., Schwark, L., Eckardt, C.B., Maxwell, J.R., 1996. Maleimides (1H-pyrrole-2,5-diones) as molecular indicators of anoxygenic photosynthesis in ancient water columns. *Geochim. Cosmochim. Acta* 60, 3913–3924. [https://doi.org/10.1016/0016-7037\(96\)00199-8](https://doi.org/10.1016/0016-7037(96)00199-8)
- Grice, K., Nabbefeld, B., Maslen, E., 2007. Source and significance of selected polycyclic aromatic hydrocarbons in sediments (Hovea-3 well, Perth Basin,

- Western Australia) spanning the Permian-Triassic boundary. *Org. Geochem.* 38, 1795–1803. <https://doi.org/10.1016/j.orggeochem.2007.07.001>
- Grice, K., Schaeffer, P., Schwark, L., Maxwell, J.R., 1997. Changes in palaeoenvironmental conditions during deposition of the Permian Kupferschiefer (Lower Rhine Basin, northwest Germany) inferred from molecular and isotopic compositions of biomarker components. *Org. Geochem.* 26, 677–690.
- Grice, K., Schouten, S., Nissenbaum, A., Charrach, J., Sinninghe Damsté, J.S., 1998. A remarkable paradox: Sulfurised freshwater algal (*Botryococcus braunii*) lipids in an ancient hypersaline euxinic ecosystem. *Org. Geochem.* 28, 195–216. [https://doi.org/10.1016/S0146-6380\(97\)00127-7](https://doi.org/10.1016/S0146-6380(97)00127-7)
- Grice, K., Summons, R.E., Grosjean, E., Twitchett, R.J., Dunning, W., Wang, S.X., Böttcher, M.E., 2005b. Depositional conditions of the Northern Onshore Perth Basin (Basal Triassic). *APPEA J.* 45, 263–274.
- Grice, K., Twitchett, R.J., Alexander, R., Foster, C.B., Looy, C., 2005c. A potential biomarker for the Permian-Triassic ecological crisis. *Earth Planet. Sci. Lett.* 236, 315–321. <https://doi.org/10.1016/j.epsl.2005.05.008>
- Grosjean, E., Edwards, D.S., Rollet, N., Boreham, C.J., Nguyen, D., Buckler, T., 2021. Geochemical evidence for a new Triassic petroleum system on the western margin of Australia. *APPEA J.* 61, 616. <https://doi.org/10.1071/aj20027>
- Grosjean, E., Hall, L., Boreham, C., Buckler, T., 2017. Source rock geochemistry of the offshore northern Perth Basin: regional hydrocarbon prospectivity of the offshore northern Perth Basin. *Rec. 2017/18. Geosci. Aust. Canberra.* <https://doi.org/10.11636/Record.2017.018>
- Grotheer, H., Le Métayer, P., Piggott, M.J., Lindeboom, E.J., Holman, A.I., Twitchett, R.J., Grice, K., 2017. Occurrence and significance of phytanyl arenes across the Permian-Triassic boundary interval. *Org. Geochem.* 104, 42–52. <https://doi.org/10.1016/j.orggeochem.2016.12.002>

H

- Haig, D.W., Martin, S.K., Mory, A.J., McLoughlin, S., Backhouse, J., Berrell, R.W., Kear, B.P., Hall, R., Foster, C.B., Shi, G.R., Bevan, J.C., 2015. Early Triassic (early Olenekian) life in the interior of East Gondwana: Mixed marine-terrestrial biota from the Kockatea Shale, Western Australia. *Palaeogeogr. Palaeoclimatol. Palaeoecol.* 417, 511–533. <https://doi.org/10.1016/j.palaeo.2014.10.015>
- Haig, D.W., Mory, A.J., McCartain, E., Backhouse, J., Håkansson, E., Ernst, A., Nicoll, R.S., Shi, G.R., Bevan, J.C., Davydov, V.I., Hunter, A.W., Keep, M., Martin, S.K., Peyrot, D., Kossavaya, O., Santos, Z. Dos, 2017. Late Artinskian–Early Kungurian (Early Permian) warming and maximum marine flooding in the East Gondwana interior rift, Timor and Western Australia, and comparisons across East Gondwana. *Palaeogeogr. Palaeoclimatol. Palaeoecol.* 468, 88–121. <https://doi.org/10.1016/j.palaeo.2016.11.051>
- Hall, L.S., Sanchez, G., Borissova, I., Pryer, L., Southby, C., Shi, Z., Hackney, R., 2017. Crustal Structure and Tectonic Evolution of the Northern Perth Basin , Australia. AAPG/SEG Conf. Search Discov. Artic. #11027.
- Hall, P.B., Kneale, R.L., 1992. Perth Basin rejuvenated. *APPEA J.* 32, 33–43.
- Hallam, A., 1991. Why was there a delayed radiation after the end-palaeozoic extinctions? *Hist. Biol.* 5, 257–262. <https://doi.org/10.1080/10292389109380405>
- Hayes, J.M., Freeman, K.H., Popp, B.N., Hoham, C.H., 1990. Compound-specific isotopic analyses: A novel tool for reconstruction of ancient biogeochemical processes. *Org. Geochem.* 16, 1115–1128. [https://doi.org/10.1016/0146-6380\(90\)90147-R](https://doi.org/10.1016/0146-6380(90)90147-R)
- Hays, L.E., Beatty, T., Henderson, C.M., Love, G.D., Summons, R.E., 2007. Evidence for photic zone euxinia through the end-Permian mass extinction in the Panthalassic Ocean (Peace River Basin, Western Canada). *Palaeoworld* 16, 39–50. <https://doi.org/10.1016/j.palwor.2007.05.008>

- Hays, L.E., Grice, K., Foster, C.B., Summons, R.E., 2012. Biomarker and isotopic trends in a Permian-Triassic sedimentary section at Kap Stosch, Greenland. *Org. Geochem.* 43, 67–82. <https://doi.org/10.1016/j.orggeochem.2011.10.010>
- Herndon, J.M., 2017. New concept on the origin of petroleum and natural gas deposits. *J. Pet. Explor. Prod. Technol.* 7, 341–352. <https://doi.org/10.1007/s13202-016-0271-5>
- Hocking, R.M., 1992. Jurassic deposition in the central and southern North West Shelf, Western Australia. *Geol. Surv. West. Aust. Rec.* 1992/7 101p.
- Hofman, R., 2016. The End-Permian Mass Extinction, in: Mángano, M.G., Buatois, L.A. (Eds.), *The Trace-Fossil Record of Major Evolutionary Events*. Springer, pp. 325–349.
- Hofmann, R., Goudemand, N., Wasmer, M., Bucher, H., Hautmann, M., 2011. New trace fossil evidence for an early recovery signal in the aftermath of the end-Permian mass extinction. *Palaeogeogr. Palaeoclimatol. Palaeoecol.* 310, 216–226. <https://doi.org/10.1016/j.palaeo.2011.07.014>

I

- I'Anson, A., Elders, C., McHarg, S., 2019. Marginal fault systems of the Northern Carnarvon Basin: Evidence for multiple Palaeozoic extension events, North-West Shelf, Australia. *Mar. Pet. Geol.* 101, 211–229. <https://doi.org/10.1016/j.marpetgeo.2018.11.040>
- Iasky, R.P., Mory, A.J., Blundell, K.A., Ghori, K.A.R., 2002. Prospectivity of the Peedamullah Shelf and Onslow Terrace revisited, in: *The Sedimentary Basins of Western Australia 3: Proceedings of the Petroleum Exploration Society of Australia Symposium*. pp. 741–759.

J

- Jablonski, D., Saitta, A.J., 2004. Permian To Lower Cretaceous Plate Tectono-Stratigraphic Development of the Western Australian Margin. *APPEA J.* 44, 287–328. <https://doi.org/10.1071/AJ03011>
- Jahnert, R.J., Collins, L.B., 2013. Controls on microbial activity and tidal flat evolution in Shark Bay, Western Australia. *Sedimentology* 60, 1071–1099. <https://doi.org/10.1111/sed.12023>
- Jones, A., Kennard, J.M., Nicholson, C.J., Bernardel, G., Mantle, D., Grosjean, E., Boreham, C.J., Jorgensen, D.C., Robertson, D., 2011. New exploration opportunities in the offshore northern Perth Basin. *APPEA J.* 51, 45–78. <https://doi.org/10.1071/aj10003>
- Jones, N.T., Hall, a D., 2002. The Cliff Head Oil Discovery – Offshore Perth Basin, in: *The Sedimentary Basins of Western Australia 3: Proceedings of the Petroleum Exploration Society of Australia Symposium*. pp. 901–909.
- Jorgensen, B.B., Fossing, H., Wirsén, C.O., Jannasch, H.W., 1991. Sulfide oxidation in the anoxic Black Sea chemocline. *Deep. Res. Part A* 38, S1083–S1103. [https://doi.org/10.1016/s0198-0149\(10\)80025-1](https://doi.org/10.1016/s0198-0149(10)80025-1)

K

- Kaiho, K., Saito, R., Ito, K., Miyaji, T., Biswas, R., Tian, L., Sano, H., Shi, Z., Takahashi, S., Tong, J., Liang, L., Oba, M., Nara, F.W., Tsuchiya, N., Chen, Z.Q., 2016. Effects of soil erosion and anoxic–euxinic ocean in the Permian–Triassic marine crisis. *Heliyon* 2, e00137. <https://doi.org/10.1016/j.heliyon.2016.e00137>
- Kaplan, I.R., Rittenberg, S.C., 1964. Microbiological fractionation of sulphur isotopes. *J. Gen. Microbiol.* 34, 195–212. <https://doi.org/10.1099/00221287-34-2-195>

- Katz, B.J., 2011. Controlling Factors on Source Rock Development—A Review Of Productivity, Preservation, and Sedimentation Rate. *Depos. Org. Sediments Model. Mech. Consequences* 7–16. <https://doi.org/10.2110/pec.05.82.0007>
- Kershaw, S., Crasquin, S., Li, Y., Collin, P.Y., Forel, M.B., Mu, X., Baud, A., Wang, Y., Xie, S., Maurer, F., Guo, L., 2012. Microbialites and global environmental change across the Permian-Triassic boundary: A synthesis. *Geobiology* 10, 25–47. <https://doi.org/10.1111/j.1472-4669.2011.00302.x>
- Knaust, D., 2010. The end-Permian mass extinction and its aftermath on an equatorial carbonate platform: Insights from ichnology. *Terra Nov.* 22, 195–202. <https://doi.org/10.1111/j.1365-3121.2010.00934.x>
- Knoll, A.H., Bambach, R.K., Canfield, D.E., Grotzinger, J.P., 1996. Comparative earth history and late Permian mass extinction. *Science.* 273, 452–457. <https://doi.org/10.1126/science.273.5274.452>
- Kuhn, T.K., Krull, E.S., Bowater, A., Grice, K., Gleixner, G., 2010. The occurrence of short chain n-alkanes with an even over odd predominance in higher plants and soils q. *Org. Geochem.* 41, 88–95. <https://doi.org/10.1016/j.orggeochem.2009.08.003>
- Kump, L.R., Pavlov, A., Arthur, M.A., 2005. Massive release of hydrogen sulfide to the surface ocean and atmosphere during intervals of oceanic anoxia. *Geology* 33, 397–400. <https://doi.org/10.1130/G21295.1>

L

- Langhi, L., Ross, A., Crooke, E., Jones, A., Nicholson, C., Stalvies, C., 2014. Integrated hydroacoustic flares and geomechanical characterization reveal potential hydrocarbon leakage pathways in the Perth Basin, Australia. *Mar. Pet. Geol.* 51, 63–69. <https://doi.org/10.1016/j.marpetgeo.2013.11.016>
- le Poidevin, S.R., Lowden, R.D., 1994. Petroleum resources of the Western Australian Basins, in: *The Sedimentary Basins of Western Australia: Proceedings of the Petroleum Exploration Society of Australia Symposium.* pp. 119–125.

- Lech, M.E., 2013. New Observations of the Post-Triassic Succession in the Central Beagle Sub-basin, Northern Carnarvon Basin, North West Shelf, Australia, in: *The Sedimentary Basins of Western Australia 4: Proceedings of the Petroleum Exploration Society of Australia Symposium*. pp. 1–20.
- Logan, B.W., 1974. Inventory of Diagenesis in Holocene-Recent Carbonate Sediments, Shark Bay, Western Australia. *AAPG Mem. M22*, 195–245.
- Longley, I.M., Buessenschuett, C., Clydsdale, L., Cubitt, C.J., Davis, R.C., Johnson, M.K., Marshall, N.M., Murray, A.P., Somerville, R., Spry, T.B., 2002. The North West Shelf of Australia—a Woodside perspective. *Sediment. Basins West. Aust. 3 Proc. Pet. Explor. Soc. Aust. Symp. Perth, Aust. 10041*, 27–88.
<https://doi.org/10.1017/CBO9781107415324.004>
- Lowery, C.M., Bralower, J., Owens, J.D., Rodríguez-Tovar, F.J., Jones, H., Smit, J., Whalen, M.T., Claeys, P., Farley, K., Gulick, S.P.S., Morgan, J. V, Green, S., Chenot, E., Christeson, G.L., Cockell, C.S., Coolen, M.J.L., Poelchau, M.H., Rae, A.S.P., Rasmussen, C., Rebolledo-Vieyra, M., Riller, U., Sato, H., Tikoo, S.M., Tomioka, N., Urrutia-Fucugauchi, J., Vellekoop, J., Wittmann, A., Zylberman, W., 2018. Rapid recovery of life at ground zero of the end- Cretaceous mass extinction. *Nature* 558, 288–291.
- Luo, M., Chen, Z.Q., 2014. New arthropod traces from the Lower Triassic Kockatea Shale Formation, northern Perth Basin, Western Australia: Ichnology, taphonomy and palaeoecology. *Geol. J.* 49, 163–176. <https://doi.org/10.1002/gj.2506>
- Luo, M., Chen, Z.Q., Shi, G.R., Feng, X., Yang, H., Fang, Y., Li, Y., 2018. Microbially induced sedimentary structures (MISSs) from the Lower Triassic Kockatea Formation, northern Perth Basin, Western Australia: Palaeoenvironmental implications. *Palaeogeogr. Palaeoclimatol. Palaeoecol.* 519, 236–247. <https://doi.org/10.1016/j.palaeo.2018.06.040>

M

- Manske, A.K., Glaeser, J., Kuypers, M.M.M., Overmann, J., 2005. Physiology and phylogeny of green sulfur bacteria forming a monospecific phototrophic assemblage at a depth of 100 meters in the Black Sea. *Appl. Environ. Microbiol.* 71, 8049–8060. <https://doi.org/10.1128/AEM.71.12.8049-8060.2005>
- Marshall, N.G., Lang, S.C., 2013. A New Sequence Stratigraphic Framework for the North West Shelf, Australia. *Sediment. Basins West. Aust.* 4 Proc. Pet. Explor. Soc. Aust. Symp. 18–21. <https://doi.org/10.1016/B978-0-12-415894-8.00009-9>
- Maslen, E., Grice, K., Gale, J.D., Hallmann, C., Horsfield, B., 2009. Crocetane: A potential marker of photic zone euxinia in thermally mature sediments and crude oils of Devonian age. *Org. Geochem.* 40, 1–11. <https://doi.org/10.1016/j.orggeochem.2008.10.005>
- Matthews, K.J., Maloney, K.T., Zahirovic, S., Williams, S.E., Seton, M., Müller, R.D., 2016. Global plate boundary evolution and kinematics since the late Paleozoic. *Glob. Planet. Change* 146, 226–250. <https://doi.org/10.1016/j.gloplacha.2016.10.002>
- McGee, R., Goodall, J., Molyneux, S., 2017. A re-evaluation of the Lower to Middle Triassic on the Candace Terrace, Northern Carnarvon Basin. *APPEA J.* 57, 263–276. <https://doi.org/10.1071/AJ16003>
- McIlldowie, M., Alexander, R., 2005. Identification of a novel C33 n-alkylcyclohexane biomarker in Permian-Triassic sediments. *Org. Geochem.* 36, 1454–1458. <https://doi.org/10.1016/j.orggeochem.2005.06.009>
- Metcalf, I., Nicoll, R.S., Willink, R.J., 2008. Conodonts from the Permian-Triassic transition in Australia and position of the Permian-Triassic boundary. *Aust. J. Earth Sci.* 55, 365–377. <https://doi.org/10.1080/08120090701769480>
- Meyer, K.M., Macalady, J.L., Fulton, J.M., Kump, L.R., Schaperdoth, I., Freeman, K.H., 2011. Carotenoid biomarkers as an imperfect reflection of the anoxygenic phototrophic community in meromictic Fayetteville Green Lake. *Geobiology* 9, 321–329. <https://doi.org/10.1111/j.1472-4669.2011.00285.x>

- Minken, J., Thompson, M., Woodward, J., Ryan, R., Fabrici, R., Allen, M., Fernandes, F., 2019. Tectonics of the Bedout Sub-basin and deposition of the Archer and Lower Keraudren Formations ; influence of tectonics in a rapidly deposited succession, in: *The Sedimentary Basins of Western Australia V: Proceedings of the Petroleum Exploration Society of Australia Symposium, Perth*. pp. 1–26.
- Molyneux, S., Goodall, J., McGee, R., Mills, G., Hartung-Kagi, B., 2016. Observations on the Lower Triassic petroleum prospectivity of the offshore Carnarvon and Roebuck basins Lead author. *APPEA J.* 56, 173–202.
- Mory, A.J., 1994. Structural evolution of the onshore northern Perth basin, Western Australia. *Sediment. Basins West. Aust. Proc. Pet. Explor. Soc. Aust. Symp. Perth 1994* 781–790.
- Mory, A.J., Haig, D.W., McLoughlin, S., Hocking, R.M., 2005. Geology of the northern Perth Basin, Western Australia- A field guide. *Geol. Surv. West. Aust.* 2005/9, 71p.
- Mory, A.J., Iasky, R.P., 1996. Stratigraphy and structure of the onshore northern Perth Basin, Western Australia. *Geol. Surv. West. Aust. Report 46*, 101pp.
- Müller, R.D., Goncharov, A., Kritski, A., 2005. Geophysical evaluation of the enigmatic Bedout basement high, offshore northwestern Australia. *Earth Planet. Sci. Lett.* 237, 264–284. <https://doi.org/10.1016/j.epsl.2005.06.014>

N

- Nabbefeld, B., Grice, K., Twitchett, R.J., Summons, R.E., Hays, L., Böttcher, M.E., Asif, M., 2010. An integrated biomarker, isotopic and palaeoenvironmental study through the Late Permian event at Lusitaniadalen, Spitsbergen. *Earth Planet. Sci. Lett.* 291, 84–96. <https://doi.org/10.1016/j.epsl.2009.12.053>
- Naehrer, S., Grice, K., 2015. Novel 1H-Pyrrole-2,5-dione (maleimide) proxies for the assessment of photic zone euxinia. *Chem. Geol.* 404, 100–109. <https://doi.org/10.1016/j.chemgeo.2015.03.020>

Noffke, N., 2010. *Geobiology-Microbial Mats in Sandy Deposits from the Archean Era to Today*-. Springer.

Norvick, M.S., 2004. Tectonic and Stratigraphic History of the Perth Basin. *Geosci. Aust.* 2004/16, 18p.

O

Olierook, H.K.H.H., Barham, M., Fitzsimons, I.C.W.W., Timms, N.E., Jiang, Q., Evans, N.J., McDonald, B.J., 2019. Tectonic controls on sediment provenance evolution in rift basins: Detrital zircon U–Pb and Hf isotope analysis from the Perth Basin, Western Australia. *Gondwana Res.* 66, 126–142.
<https://doi.org/10.1016/j.gr.2018.11.002>

Orlov, C., Hall, L., Borissova, I., Southby, C., Owens, R., 2017. Reconstructing the Tectonic Evolution of the Houtman Sub-basin, Western Australia, in: *Specialist Group in Tectonics and Structural Geology 2017*. p. 115702.

Owens, R.J., Borissova, I., Hall, L.S., Bernardel, G., Southby, C., Grosjean, E., Mitchell, C., 2018. Geology and prospectivity of the northern Houtman Sub-basin. *Geosci. Aust.* 2018/25, 101 pp.

P

Pagès, A., Grice, K., Vacher, M., Welsh, D.T., Teasdale, P.R., Bennett, W.W., Greenwood, P., 2014. Characterizing microbial communities and processes in a modern stromatolite (Shark Bay) using lipid biomarkers and two-dimensional distributions of porewater solutes. *Environ. Microbiol.* 16, 2458–2474.
<https://doi.org/10.1111/1462-2920.12378>

Paschke, C., O’Halloran, G., Dempsey, C., O’Halloran, G., 2018. Interpretation of a Permian conjugate basin margin preserved on the outer Northwest Shelf of Australia, in: *AEGC 2018 Extended Abstracts*. pp. 1–8.
https://doi.org/10.1071/ASEG2018abM3_2B

- Payne, J.L., Lehrmann, D.J., Wei, J., Orchard, M.J., Schrag, D.P., Knoll, A.H., 2004. Large perturbations of the carbon cycle during recovery from the end-Permian extinction. *Science*. 305, 506–509. <https://doi.org/10.1126/science.1097023>
- Pedentchouk, N., Freeman, K.H., Harris, N.B., Clifford, D.J., Grice, K., 2004. Sources of alkylbenzenes in Lower Cretaceous lacustrine source rocks, West African rift basins. *Org. Geochem.* 35, 33–45. <https://doi.org/10.1016/j.orggeochem.2003.04.001>
- Peters, K., Walters, C., Moldowan, J., 2004. *The Biomarker Guide*, 2nd ed. Cambridge University Press.
- Peters, K.E., 1986. Guidelines for Evaluating Petroleum Source Rock Using Programmed Pyrolysis. *Am. Assoc. Pet. Geol. Bull.* 70, 318–329. <https://doi.org/10.1306/94885688-1704-11d7-8645000102c1865d>
- Pfenning, N., 1978. General physiology and ecology of photosynthetic bacteria, in: Clayton, R.K., Sistrom, W.R. (Eds.), *The Photosynthetic Bacteria*. Plenum, New York, pp. 3–18.
- Playford, P.E., Cockbain, A.E., Low, G.H., 1976. Geology of the Perth Basin, Western Australia. *Geol. Surv. West. Aust.* 124, 311. <https://doi.org/10.1360/zd-2013-43-6-1064>

Q

- Quaife, P., Rosser, J., Pagnozzi, S., 1994. The structural architecture and stratigraphy of the offshore northern Perth Basin, Western Australia, in: *The Sedimentary Basins of Western Australia: Proceedings of the Petroleum Exploration Society of Australia Symposium*. pp. 811–822.

R

Raup, D.M., Sepkoski, J.J., 1982. Mass Extinctions in the Marine Fossil Record. *Science*. 215, 1501–1504.

Reichow, M.K., Pringle, M.S., Al’Mukhamedov, A.I., Allen, M.B., Andreichev, V.L., Buslov, M.M., Davies, C.E., Fedoseev, G.S., Fitton, J.G., Inger, S., Medvedev, A.Y., Mitchell, C., Puchkov, V.N., Safonova, I.Y., Scott, R.A., Saunders, A.D., 2009. The timing and extent of the eruption of the Siberian Traps large igneous province: Implications for the end-Permian environmental crisis. *Earth Planet. Sci. Lett.* 277, 9–20. <https://doi.org/10.1016/j.epsl.2008.09.030>

Retallack, G.J., Veevers, J.J., Morante, R., 1996. Global coal gap between Permian-Triassic extinction and Middle Triassic recovery of peat-forming plants. *GSA Bull.* 108, 195–207.

Rollet, N., Grosjean, E., Edwards, D., Kempton, R., Nguyen, D., Abbott, S., Orlov, C., Bernardel, G., Nicholson, C., 2019. Triassic petroleum systems on the central North West Shelf – Learnings from the greater Phoenix area seismic mapping and geochemical studies, in: AEGC 2019 Extended Abstracts. pp. 1–7.

S

Sahney, S., Benton, M.J., 2008. Recovery from the most profound mass extinction of all time. *Proc. R. Soc. B Biol. Sci.* 275, 759–765. <https://doi.org/10.1098/rspb.2007.1370>

Sandwell, D., Garcia, E., Soofi, K., Wessel, P., Chandler, M., Smith, W.H.F., 2013. Toward 1-mGal accuracy in global marine gravity from CryoSat-2, Envisat, and Jason-1. *Lead. Edge* 32, 892–899.

Sandwell, D.T., Müller, R.D., Smith, W.H.F., Garcia, E., Francis, R., 2014. New global marine gravity model from CryoSat-2 and Jason-1 reveals buried tectonic structure. *Science*. 346, 65–67. <https://doi.org/10.1126/science.1258213>

- Sandwell, D.T., Smith, W.H.F., 2009. Global marine gravity from retracked Geosat and ERS-1 altimetry: Ridge segmentation versus spreading rate. *J. Geophys. Res. Solid Earth* 114, B01411. <https://doi.org/10.1029/2008JB006008>
- Sanei, H., Grasby, S.E., Beauchamp, B., 2012. Latest permian mercury anomalies. *Geology* 40, 63–66. <https://doi.org/10.1130/G32596.1>
- Sass, A.M., Sass, H., Coolen, M.J.L., Cypionka, H., Overmann, J., 2001. Microbial Communities in the Chemocline of a Hypersaline Deep-Sea Basin (Urania Basin, Mediterranean Sea). *Appl. Environ. Microbiol.* 67, 5392–5402. <https://doi.org/10.1128/AEM.67.12.5392-5402.2001>
- Scaife, J.D., Ruhl, M., Dickson, A.J., Mather, T.A., Jenkyns, H.C., Percival, L.M.E., Hesselbo, S.P., Cartwright, J., Eldrett, J.S., Bergman, S.C., Minisini, D., 2017. Sedimentary Mercury Enrichments as a Marker for Submarine Large Igneous Province Volcanism? Evidence From the Mid-Cenomanian Event and Oceanic Anoxic Event 2 (Late Cretaceous). *Geochemistry, Geophys. Geosystems* 18, 4253–4275. <https://doi.org/10.1002/2017GC007153>
- Schaefer, B., Grice, K., Coolen, M.J.L., Summons, R.E., Cui, X., Bauersachs, T., Schwark, L., Böttcher, M.E., Bralower, T.J., Lyons, S.L., Freeman, K.H., Cockell, C.S., Gulick, S.S., Morgan, J. V., Whalen, M.T., Lowery, C.M., Vajda, V., 2020. Microbial mayhem in the nascent chicxulub crater. *Geology* 48, 328–332. <https://doi.org/10.1130/G46799.1>
- Schidlowski, M., 1988. A 3,800-million-year isotopic record of life from carbon in sedimentary rocks. *Nature* 333, 313–318. <https://doi.org/10.1038/333313a0>
- Scholle, P.A., Peryt, T.M., Ulmer-Scholle, D.S., 1995. *The Permian of Northern Pangea: Volume 1: Paleogeography, Paleoclimates, Stratigraphy*. Springer-Verlag. <https://doi.org/10.1007/978-3-642-78593-1>
- Schouten, S., Klein Breteler, W.C.M., Blokker, P., Schogt, N., Rijpstra, W.I.C., Grice, K., Baas, M., Sinninghe Damsté, J.S., 1998. Biosynthetic effects on the stable carbon isotopic compositions of algal lipids: implications for deciphering the carbon isotopic biomarker record. *Geochim. Cosmochim. Acta* 62, 1397–1406. [https://doi.org/10.1016/S0016-7037\(98\)00076-3](https://doi.org/10.1016/S0016-7037(98)00076-3)

- Scotese, C.R., 2003. PALEOMAP Project [WWW Document]. URL <http://www.scotese.com/> (accessed 1.17.19).
- Scott, J., 1994. Source rocks of Western Australia - distribution, character and models, in: *The Sedimentary Basins of Western Australia: Proceedings of the Petroleum Exploration Society of Australia Symposium*. pp. 141–155.
- Sedlacek, A.R.C.C., Saltzman, M.R., Algeo, T.J., Horacek, M., Brandner, R., Foland, K., Denniston, R.F., 2014. $^{87}\text{Sr}/^{86}\text{Sr}$ stratigraphy from the Early Triassic of Zal, Iran: Linking temperature to weathering rates and the tempo of ecosystem recovery. *Geology* 42, 779–782. <https://doi.org/10.1130/G35545.1>
- Shen, J., Algeo, T.J., Chen, J., Planavsky, N.J., Feng, Q., Yu, J., Liu, J., 2019a. Mercury in marine Ordovician/Silurian boundary sections of South China is sulfide-hosted and non-volcanic in origin. *Earth Planet. Sci. Lett.* 511, 130–140. <https://doi.org/10.1016/j.epsl.2019.01.028>
- Shen, J., Chen, J., Algeo, T.J., Yuan, S., Feng, Q., Yu, J., Zhou, L., O’Connell, B., Planavsky, N.J., 2019b. Evidence for a prolonged Permian–Triassic extinction interval from global marine mercury records. *Nat. Commun.* 10, 1563. <https://doi.org/10.1038/s41467-019-09620-0>
- Shen, J., Schoepfer, S.D., Feng, Q., Zhou, L., Yu, J., Song, H., Wei, H., Algeo, T.J., 2015. Marine productivity changes during the end-Permian crisis and Early Triassic recovery. *Earth-Science Rev.* 149, 136–162. <https://doi.org/10.1016/j.earscirev.2014.11.002>
- Sial, A.N., Chen, J., Lacerda, L.D., Korte, C., Spangenberg, J.E., Silva-Tamayo, J.C., Gaucher, C., Ferreira, V.P., Barbosa, J.A., Pereira, N.S., Benigno, A.P., 2020. Globally enhanced Hg deposition and Hg isotopes in sections straddling the Permian–Triassic boundary: Link to volcanism. *Palaeogeogr. Palaeoclimatol. Palaeoecol.* 540, 109537. <https://doi.org/10.1016/j.palaeo.2019.109537>
- Słowakiewicz, M., Tucker, M.E., Perri, E., Pancost, R.D., 2015. Nearshore euxinia in the photic zone of an ancient sea. *Palaeogeogr. Palaeoclimatol. Palaeoecol.* 426, 242–259. <https://doi.org/10.1016/j.palaeo.2015.03.022>

- Smith, S.A., Tingate, P.R., Griffiths, C.M., Hull, J.N.F., 1999. The structural development and petroleum potential of the Roebuck Basin. *APPEA J.* 39, 364–385.
- Song, H.H., Wignall, P.B., Chu, D., Tong, J., Sun, Y., Song, H.H., He, W., Tian, L., 2014. Anoxia/high temperature double whammy during the Permian-Triassic marine crisis and its aftermath. *Sci. Rep.* 4, 1–7.
<https://doi.org/10.1038/srep04132>
- Song, T., Cawood, P.A., 2000. Structural styles in the Perth Basin associated with the Mesozoic break-up of Greater India and Australia. *Tectonophysics* 317, 55–72.
[https://doi.org/10.1016/S0040-1951\(99\)00273-5](https://doi.org/10.1016/S0040-1951(99)00273-5)
- Sousa Júnior, G.R., Santos, A.Ô.L.S.S., De Lima, S.G., Lopes, J.A.D.D., Reis, F.A.M.M., Santos Neto, E. V., Chang, H.K., 2013. Evidence for euphotic zone anoxia during the deposition of Aptian source rocks based on aryl isoprenoids in petroleum, Sergipe-Alagoas Basin, northeastern Brazil. *Org. Geochem.* 63, 94–104. <https://doi.org/10.1016/j.orggeochem.2013.07.009>
- Spaak, G., Edwards, D.S., Allen, H.J., Grotheer, H., Summons, R.E., Coolen, M.J.L., Grice, K., 2018. Extent and persistence of photic zone euxinia in Middle–Late Devonian seas – Insights from the Canning Basin and implications for petroleum source rock formation. *Mar. Pet. Geol.* 93, 33–56.
<https://doi.org/10.1016/j.marpetgeo.2018.02.033>
- Stal, L.J., van Gemerden, H., Krumbein, W.E., 1985. Structure and development of a benthic marine microbial mat. *FEMS Microbiol. Lett.* 31, 111–125.
[https://doi.org/10.1016/0378-1097\(85\)90007-2](https://doi.org/10.1016/0378-1097(85)90007-2)
- Stephenson, A.E., Blevin, J.E., West, B.G., 1998. The paleogeography of the beagle sub-basin, Northern Carnarvon Basin, Australia. *J. Sediment. Res.* 68, 1131–1145.
<https://doi.org/10.2110/jsr.68.1131>
- Summons, R.E., Powell, T.G., 1987. Identification of aryl isoprenoids in source rocks and crude oils: biological markers for green sulphur bacteria. *Geochim. Cosmochim. Acta* 51, 557–566.

Summons, R.E.E., Powell, T.G.G., 1987. Identification of aryl isoprenoids in source rocks and crude oils: biological markers for green sulphur bacteria. *Geochim. Cosmochim. Acta* 51, 557–566.

T

Tao, C., Bai, G., Liu, J., Deng, C., Lu, X., Liu, H., Wang Dapeng, 2013. Mesozoic lithofacies palaeogeography and petroleum prospectivity in North Carnarvon Basin, Australia. *J. Palaeogeogr.* 2, 81–92.
<https://doi.org/10.3724/SP.J.1261.2013.00019>

Them, T.R., Jagoe, C.H., Caruthers, A.H., Gill, B.C., Grasby, S.E., Gröcke, D.R., Yin, R., Owens, J.D., 2019. Terrestrial sources as the primary delivery mechanism of mercury to the oceans across the Toarcian Oceanic Anoxic Event (Early Jurassic). *Earth Planet. Sci. Lett.* 507, 62–72.
<https://doi.org/10.1016/j.epsl.2018.11.029>

Thibodeau, A.M., Ritterbush, K., Yager, J.A., West, A.J., Ibarra, Y., Bottjer, D.J., Berelson, W.M., Bergquist, B.A., Corsetti, F.A., 2016. Mercury anomalies and the timing of biotic recovery following the end-Triassic mass extinction. *Nat. Commun.* 7, 11147.

Thomas, B.M., 1979. Geochemical analysis of hydrocarbon occurrences in northern Perth Basin, Australia. *Am. Assoc. Pet. Geol. Bull.* 63, 1092–1107.
<https://doi.org/10.1306/2F9184BE-16CE-11D7-8645000102C1865D>

Thomas, B.M., Barber, C.J., 2004. A re-evaluation of the hydrocarbon habitat of the northern Perth Basin. *APPEA J.* 44, 59–92.

Thomas, B.M., Willink, R.J., Grice, K., Twitchett, R.J., Purcell, R.R., George, A.D., Tye, S., Alexander, R., Foster, C.B., Barber, C.J., George, A.D., Tye, S., Alexander, R., Foster, C.B., Unique, C.J.B., Barber, C.J., 2004. Unique marine Permian-Triassic boundary section from Western Australia. *Aust. J. Earth Sci.* 51, 423–430.

- Thompson, M., 2020. Dorado discovery – unlocking a major new oil and gas play in the Bedout Sub-basin. *APPEA J.* 60, 778–783. <https://doi.org/10.1071/aj19128>
- Thompson, M., Wehr, F., Woodward, J., Minken, J., D’Orazio, G., Fernandes, F., Kongowoin, M., Hansen, L., Kuek, D., Fabrici, R., D’Orazio, G., Fernandes, F., Kongowoin, M., Hansen, L., Kuek, D., 2018. Recent exploration results in the Lower Triassic , Bedout Sub-basin : Australia ’ s next petroleum province ? *APPEA J.* 58, 871–877.
- Tian, L., Tong, J., Algeo, T.J., Song, Haijun, Song, Huyue, Chu, D., Shi, L., Bottjer, D.J., 2014. Reconstruction of Early Triassic ocean redox conditions based on framboidal pyrite from the Nanpanjiang Basin, South China. *Palaeogeogr. Palaeoclimatol. Palaeoecol.* 412, 68–79. <https://doi.org/10.1016/j.palaeo.2014.07.018>
- Tindale, K., Newell, N., Keall, J., Smith, N., 1998. Structural Evolution and Charge History of the Exmouth Sub-basin, Northern Carnarvon Basin, Western Australia, in: *The Sedimentary Basins of Western Australia 2: Proceedings of the Petroleum Exploration Society of Australia Symposium.* pp. 447–472.
- Torghabeh, A.K., Rezaee, R., Harami, R.M., Pimentel, N., 2014. Unconventional resource evaluation: Kockatea Shale, Perth Basin, Western Australia. *Int. J. Oil, Gas Coal Technol.* 8, 16–30. <https://doi.org/10.1504/IJOGCT.2014.064420>
- Tulipani, S., 2013. Novel biomarker and stable isotopic approaches for palaeoenvironmental reconstruction of saline and stratified ecosystems: The modern Coorong Lagoon and Devonian reefs of the Canning Basin. Curtin University.
- Tulipani, S., Grice, K., Greenwood, P.F., Schwark, L., Böttcher, M.E., Summons, R.E., Foster, C.B., 2015. Molecular proxies as indicators of freshwater incursion-driven salinity stratification. *Chem. Geol.* 409, 61–68. <https://doi.org/10.1016/j.chemgeo.2015.05.009>
- Tupper, N., Matthews, E., Cooper, G., Furniss, A., Hicks, T., Hunt, S., 2016. The Waitsia Field , onshore North Perth Basin , Western Australia Lead author. *APPEA J.* 56, 29–44.

Twitchett, R.J., 2006. The palaeoclimatology, palaeoecology and palaeoenvironmental analysis of mass extinction events. *Palaeogeogr. Palaeoclimatol. Palaeoecol.* 232, 190–213.
<https://doi.org/10.1016/j.palaeo.2005.05.019>

Twitchett, R.J., Krystyn, L., Baud, A., Wheeley, J.R., Richoz, S., 2004. Rapid marine recovery after the end-Permian mass-extinction event in the absence of marine anoxia. *Geology* 32, 805–808. <https://doi.org/10.1130/G20585.1>

V

van Aarssen, B.G.K., Alexander, R., Kagi, R.I., 1996. The origin of Barrow Sub-basin crude oils: A geochemical correlation using land-plant biomarkers. *APPEA J.* 36, 465–476.

Volkman, K., Alexandert, R., Kagi, R.I., Noble, R.A., Woodhouse, G.W., 1983. A geochemical reconstruction of oil generation in the Barrow Sub-basin of Western Australia. *Geochim. Cosmochim. Acta* 47, 2091–2105.

W

Wang, X., Cawood, P.A., Zhao, H., Zhao, L., Grasby, S.E., Chen, Z.Q., Zhang, L., 2019. Global mercury cycle during the end-Permian mass extinction and subsequent Early Triassic recovery. *Earth Planet. Sci. Lett.* 513, 144–155.
<https://doi.org/10.1016/j.epsl.2019.02.026>

Wei, H., Shen, J., Schoepfer, S.D., Krystyn, L., Richoz, S., Algeo, T.J., 2015. Environmental controls on marine ecosystem recovery following mass extinctions, with an example from the Early Triassic. *Earth-Science Rev.* 149, 108–135. <https://doi.org/10.1016/j.earscirev.2014.10.007>

Westphal, H., Aigner, T., 1997. Seismic stratigraphy and subsidence analysis in the Barrow-Dampier Subbasin, Northwest Australia. *Am. Assoc. Pet. Geol. Bull.* 81, 1721–1749. <https://doi.org/10.1306/3b05c42e-172a-11d7-8645000102c1865d>

- Whiteside, J.H., Grice, K., 2016. Biomarker Records Associated with Mass Extinction Events. *Annu. Rev. Earth Planet. Sci.* 44, 581–612.
<https://doi.org/10.1146/annurev-earth-060115-012501>
- Wignall, P.B., Twitchett, R.J., 1996. Oceanic anoxia and the end Permian mass extinction. *Science*. 272, 1155–1158.
<https://doi.org/10.1126/science.272.5265.1155>
- Woods, A.D., 2014. Assessing Early Triassic paleoceanographic conditions via unusual sedimentary fabrics and features. *Earth-Science Rev.* 137, 6–18.
<https://doi.org/10.1016/j.earscirev.2013.08.015>
- Woods, A.D., Bottjer, D.J., Mutti, M., Morrison, J., 1999. Lower Triassic large sea-floor carbonate cements: Their origin and a mechanism for the prolonged biotic recovery from the end-Permian mass extinction. *Geology* 27, 645–648.
[https://doi.org/10.1130/0091-7613\(1999\)027<0645:LTLSFC>2.3.CO;2](https://doi.org/10.1130/0091-7613(1999)027<0645:LTLSFC>2.3.CO;2)
- Woodward, J., Minken, J., Thompson, M., Kongawoin, M., Hansen, L., Fabrici, R., 2018. The Lower Triassic Caley Member: depositional facies, reservoir quality and seismic expression. *APPEA J.* 58, 878–883. <https://doi.org/10.1071/aj17172>

Y

- Yasin, A.R., Iasky, R.P., Sub-basin, B., 1998. Petroleum Geology of the Peedamullah Shelf, Northern Carnarvon Basin, in: *The Sedimentary Basins of Western Australia 2: Proceedings of the Petroleum Exploration Society of Australia Symposium*. pp. 473–491.

Z

- Zatoń, M., Niedźwiedzki, G., Blom, H., Kear, B.P., 2016. Boreal earliest Triassic biotas elucidate globally depauperate hard substrate communities after the end-Permian mass extinction. *Sci. Rep.* 6, 36345.

- Zhang, L., Zhao, L., Chen, Z.-Q., Algeo, T.J., Chen, J., Wang, R., Chen, L., Hou, J., Li, Y., Qiu, H., Feng, X., Lu, Z., Wang, X., Huang, Y., 2014. Amelioration of marine environments at the Smithian–Spathian boundary, Early Triassic, Biogeosciences Discussions. <https://doi.org/10.5194/bgd-11-15361-2014>
- Zhang, L.J., Buatois, L.A., Gabriela Mángano, M., Qi, Y.A., Zhang, X., Sun, S., Tai, C., 2017. Early Triassic estuarine depauperate *Cruziana* Ichnofacies from the Sichuan area of South China and its implications for the biotic recovery in brackish-water settings after the end-Permian mass extinction. *Palaeogeogr. Palaeoclimatol. Palaeoecol.* 485, 351–360. <https://doi.org/10.1016/j.palaeo.2017.06.025>
- Zhou, W., Algeo, T.J., Ruan, X., Luo, G., Chen, Z.-Q., Xie, S., 2017. Expansion of photic-zone euxinia during the Permian–Triassic biotic crisis and its causes: Microbial biomarker records. *Palaeogeogr. Palaeoclimatol. Palaeoecol.* 474, 140–151. <https://doi.org/10.1016/j.palaeo.2016.06.027>
- Zhu, Z., Liu, Y., Kuang, H., Benton, M.J., Newell, A.J., Xu, H., An, W., Ji, S., Xu, S., Peng, N., Zhai, Q., 2019. Altered fluvial patterns in North China indicate rapid climate change linked to the Permian-Triassic mass extinction. *Sci. Rep.* 9, 16818. <https://doi.org/10.1038/s41598-019-53321-z>
- Zyakun, A.M., Lunina, O.N., Prusakova, T.S., Pimenov, N. V., Ivanov, M. V., 2009. Fractionation of stable carbon isotopes by photoautotrophically growing anoxygenic purple and green sulfur bacteria. *Microbiology* 78, 757–768. <https://doi.org/10.1134/S0026261709060137>

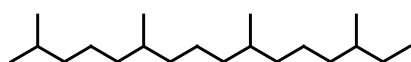
Appendices

Appendix 1

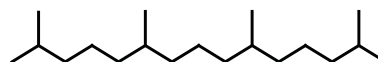
Biomarkers appearing in this thesis

Biomarkers appearing in this thesis are listed as follows.

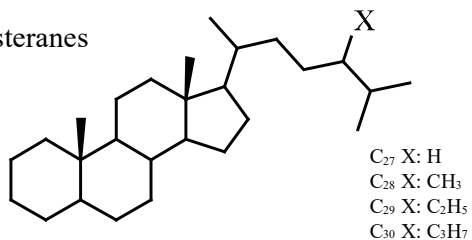
phytane



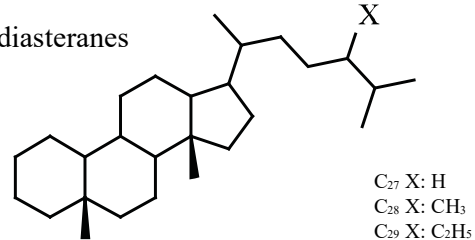
pristane



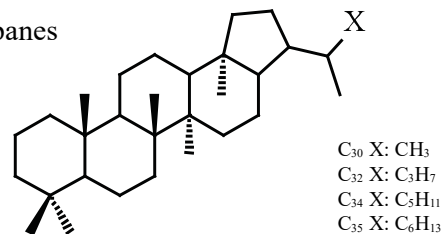
steranes



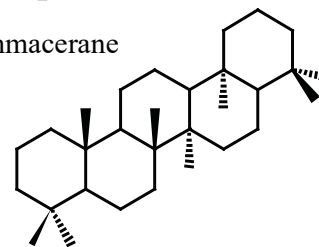
diasteranes



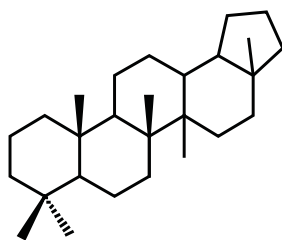
hopanes



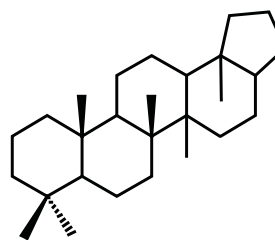
gammacerane



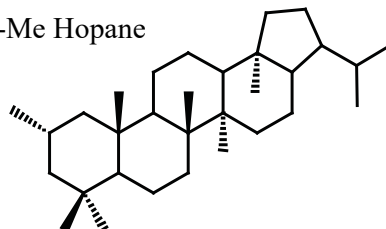
Ts



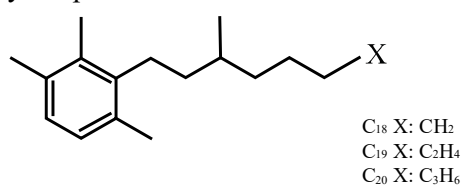
Tm



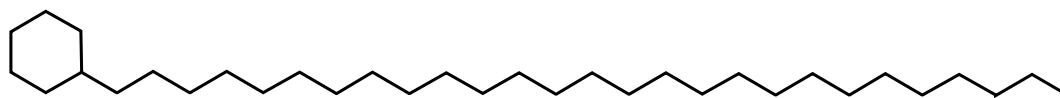
2-Me Hopane



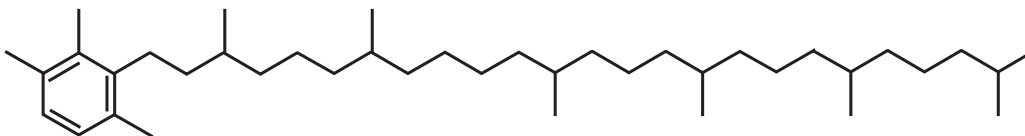
aryl isoprenoids



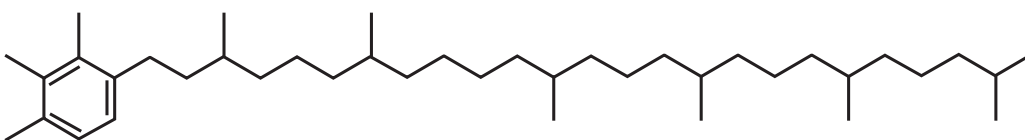
n-alkylcyclohexane



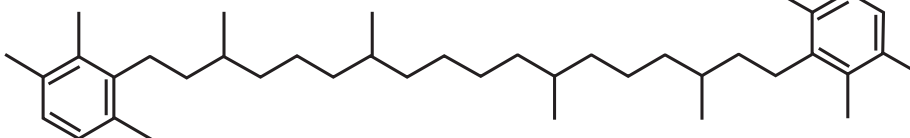
okenane



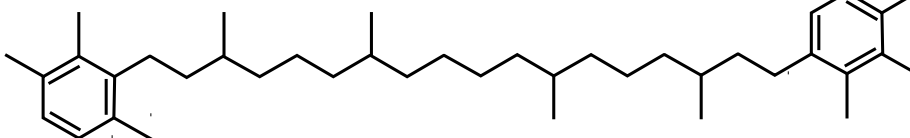
chlorobactane



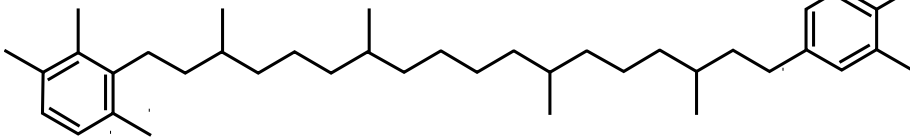
isorenieratane



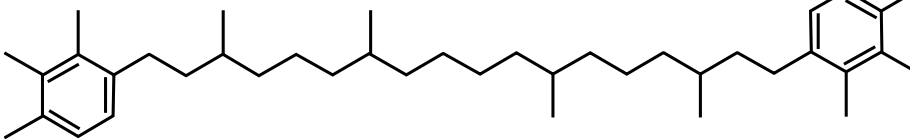
renieratane



paleorenieratane



renierapurpurane



Appendix 2

The rights to reproduce the contributions from printed volumes

The following pages contain a statement about the rights of the first author of the publication to reproduce the contribution in any printed volume (book or thesis), granted by Elsevier. This statement relates to Chapter 2 (*Marine and Petroleum Geology*),³ (*Geochimica et Cosmochimica Acta*) and 4 (*Organic Geochemistry*).

Copyright

[Overview](#) [Author rights](#) [Institution rights](#) [Government rights](#) [Find out more](#)

Overview

In order for Elsevier to publish and disseminate research articles, we need certain publishing rights from authors, which are determined by a publishing agreement between the author and Elsevier.

For articles published open access, the authors license exclusive rights in their article to Elsevier where a CC BY-NC-ND end user license is selected, and license non-exclusive rights where a CC BY end user license is selected.

For articles published under the subscription model, the authors transfer copyright to Elsevier.

Regardless of whether they choose to publish open access or subscription with Elsevier, authors have many of the same rights under our publishing agreement, which support their need to share, disseminate and maximize the impact of their research.

For open access articles, authors will also have additional rights, depending on the Creative Commons end user license that they select. This Creative Commons license sets out the rights that readers (as well as the authors) have to re-use and share the article: please see [here](#) for more information on how articles can be re-used and shared under these licenses.

This page aims to summarise authors' rights when publishing with Elsevier; these are explained in more detail in the [↓ publishing agreement](#) between the author and Elsevier.

Irrespective of how an article is published, Elsevier is committed to protect and defend authors' works and their reputation. We take allegations of infringement, plagiarism, ethical disputes, and fraud very seriously.

Author rights

The below table explains the rights that authors have when they publish with Elsevier, for authors who choose to publish either open access or subscription. These apply to the corresponding author and all co-authors.

Author rights in Elsevier's proprietary journals	Published open access	Published subscription
Retain patent and trademark rights	✓	✓
Retain the rights to use their research data freely without any restriction	✓	✓
Receive proper attribution and credit for their published work	✓	✓
Re-use their own material in new works without permission or payment (with full acknowledgement of the original article): 1. Extend an article to book length 2. Include an article in a subsequent compilation of their own work 3. Re-use portions, excerpts, and their own figures or tables in other works.	✓	✓
Use and share their works for scholarly purposes (with full acknowledgement of the original article): 1. In their own classroom teaching. Electronic and physical distribution of copies is permitted 2. If an author is speaking at a conference, they can present the article and distribute copies to the attendees 3. Distribute the article, including by email, to their students and to research colleagues who they know for their personal use 4. Share and publicize the article via Share Links, which offers 50 days' free access for anyone, without signup or registration 5. Include in a thesis or dissertation (provided this is not published commercially) 6. Share copies of their article privately as part of an invitation-only work group on commercial sites with which the publisher has a hosting agreement	✓	✓
Publicly share the preprint on any website or repository at any time.	✓	✓
Publicly share the accepted manuscript on non-commercial sites	✓	✓ using a CC BY-NC-ND license and usually only after an embargo period (see Sharing Policy for more information)
Publicly share the final published article	✓ in line with the author's choice of end user license	✗
Retain copyright	✓	✗

Institution rights

Regardless of how the author chooses to publish with Elsevier, their institution has the right to use articles for classroom teaching and internal training. Articles can be used for these purposes throughout the author's institution, not just by the author:

Institution rights in Elsevier's proprietary journals (providing full acknowledgement of the original article is given)	All articles
Copies can be distributed electronically as well as in physical form for classroom teaching and internal training purposes	✓
Material can be included in coursework and courseware programs for use within the institution (but not in Massive Open Online Courses)	✓
Articles can be included in applications for grant funding	✓
Theses and dissertations which contain embedded final published articles as part of the formal submission can be posted publicly by the awarding institution with DOI links back to the formal publication on ScienceDirect	✓

Government rights

For US government employees, works created within the scope of their employment are considered to be public domain and Elsevier's publishing agreements do not require a transfer or license of rights for such works.

In the UK and certain commonwealth countries, a work created by a government employee is copyrightable, but the government may own the copyright (Crown copyright). Click [here](#) for information about UK government employees publishing open access.

Appendix 3

Copies of published material and abstracts submitted at conferences

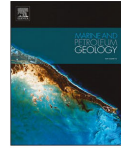
Taniwaki, T., Elders, C., Grice, K., 2021. Early Triassic paleogeography of the northern Perth Basin, and controls on the distribution of source rock facies. *Marine and Petroleum Geology*. 133, 105314, <https://doi.org/10.1016/j.marpetgeo.2021.105314>, impact factor 4.348.

The copy of manuscript published at *Marine and Petroleum Geology* is as follow.



Contents lists available at ScienceDirect

Marine and Petroleum Geology

journal homepage: www.elsevier.com/locate/marpetgeo

Early Triassic paleogeography of the northern Perth Basin, and controls on the distribution of source rock facies

Takashi Taniwaki^{a,b,*}, Chris Elders^c, Kliti Grice^a^a Western Australian Organic & Isotope Geochemistry Centre, The Institute for Geoscience Research, School of Earth and Planetary Sciences, Curtin University, Perth, WA, Australia^b INPEX Corporation, Minato-ku, Tokyo, Japan^c School of Earth and Planetary Sciences, Curtin University, Perth, Western Australia, Australia

ARTICLE INFO

Keywords:
Perth Basin
Kockatea Shale
Early Triassic
Microbial mats
Anoxia

ABSTRACT

The facies distribution of the Lower Triassic Kockatea Shale in the northern Perth Basin is an important factor for assessing the Lower Triassic source rock potential in the basin. Seismic interpretation and well analyses demonstrate that Permian-aged faults are responsible for the morphology of the basin in the Early Triassic and created remnant topography that controls the deposition of Lower Triassic sediments. Cores from petroleum wells and their correlated wireline logs show the lithological variation and lateral distribution of facies across the base of the Kockatea Shale. Darker coloured mudstones were deposited under anoxic conditions in the deeper part of the basin, while lighter coloured mudstones and tidally influenced sediments with bioturbation were deposited under oxic conditions in a shallow marine setting. Microbial mats developed in shallower water depths on structural highs (Beagle Ridge and Turtle Dove Ridge) in the anoxic parts of the basin.

The distribution of microbial mats is controlled by two factors during the period of ecological recovery from the end-Permian mass extinction: 1) the presence of topographic highs and, 2) distance from the edge of the basin. The source rock potential of both darker coloured mudstone and microbial mat facies is demonstrated by TOC values between 0.3 and 3.4% and HI values between 39 and 579 mg/gTOC. On the other hand, the lighter coloured mudstones, deposited under more aerobic tidal settings, have poor source rock quality and TOC values between 0.2 and 0.5% and HI values between 59 and 127 mg/gTOC.

1. Introduction

The Perth Basin is an oil-producing basin located on the western coast of Australia (Crostella, 1995; Ghori, 2015; Jones et al., 2011). One of the main sources of oil is the Lower Triassic Kockatea Shale (Boreham et al., 2000; Grosjean et al., 2017; Langhi et al., 2014; Scott, 1994; Thomas, 1979; Thomas et al., 2004), the source rock potential and organic geochemical characteristics of which are well documented based on biomarker and carbon and hydrogen stable isotopic studies (Dawson et al., 2005; Grice et al., 2005a, 2005b, 2005c, 2007; McIl Dowie and Alexander, 2005; Thomas and Barber, 2004). The basal section of the Kockatea Shale is distinctive and displays increased total organic carbon (TOC) and hydrogen index (HI) values both of which are good indicators of oil source rock quality. Key biomarker correlation confirms that this part of the Kockatea Shale is the primary source of hydrocarbons in many fields of the Perth Basin (e.g. Hovea, North Yardanogo,

Dongara, My Horner, Jिंगemia and Woodada) (Thomas and Barber, 2004).

The Kockatea Shale was deposited from the Late Permian to the Early Triassic, and therefore spans a part of the end-Permian mass extinction. The development of anoxic condition and photic zone euxinia (PZE) around this mass extinction is recognized globally, and is thought to be related to volcanic activity of the Siberian Trap eruptions (Erwin, 1994; Grice et al., 2005a; Knoll et al., 1996; Nabbefeld et al., 2010; Song et al., 2014; Twitchett et al., 2004; Whiteside and Grice, 2016; Wignall and Twitchett, 1996). The presence of these conditions in the Perth Basin has been established on the basis of biomarker analysis (Grice et al., 2005a), and they played an important role in the development of organic-rich source rocks in the Kockatea Shale (Grosjean et al., 2017; Thomas and Barber, 2004). In addition, the development of microbial mats following the mass extinction is recognized globally and is an indication of the severe conditions that existed during and after the mass extinction

* Corresponding author. School of Earth Planetary Sciences, Curtin University, Kent Street, Bentley, Western Australia, 6102, Australia.

E-mail addresses: takashi.taniwaki@postgrad.curtin.edu.au, takashi.taniwaki@inpx.co.jp (T. Taniwaki).

<https://doi.org/10.1016/j.marpetgeo.2021.105314>

Received 12 April 2021; Received in revised form 26 August 2021; Accepted 29 August 2021

Available online 1 September 2021

0264-8172/© 2021 Elsevier Ltd. All rights reserved.

which were not suitable for other organisms (Foster et al., 2020; Ker-shaw et al., 2012; Luo et al., 2019; Woods, 2014). Microbial mats are well documented from outcrops of the Kockatea Shale in the Perth Basin (Chen et al., 2014; Luo et al., 2019; Luo and Chen, 2014), although they are less well-studied in the subsurface (Thomas et al., 2004).

Although it is expected that the Kockatea Shale is widely distributed in the northern Perth Basin, the lateral extent of organic matter-rich source rock facies within the Kockatea Shale is poorly constrained (Crostella, 1995; Crostella and Backhouse, 2000; Haig et al., 2015; Mory, 1994). Recognising the factors that influence facies distribution, and microbial mat development in particular, will contribute to understanding the controls on source rock distribution and quality, as well as the impact of the end-Permian mass extinction on the Perth Basin. In this study, we identify several lithofacies, including microbial mats, from the base of the Kockatea Shale from a selection of petroleum exploration wells, and document lithological variation in the Kockatea Shale from cores. Seismic data is utilized to demonstrate the extent to which Permian rifting influenced basin geomorphology in the Early Triassic. Core data is correlated to well logs to investigate the lateral distribution of lithofacies and source rock quality. These results are integrated to evaluate the paleogeography, and identify controls on microbial mat development and distribution. Source rock analysis is also conducted to investigate the petroleum potential of these beds.

2. Geological setting

The northern Perth Basin (Fig. 1) has experienced several rift, subsidence and uplift events from the Devonian to the Early Cretaceous (Jablonski and Saitta, 2004; Norvick, 2004). Late Permian rifting is one of the most prominent events in the evolution of the basin (Jablonski and Saitta, 2004). The Lower Permian Nangetty Formation, Holmwood Shale, High Cliff Sandstone, Irwin River Coal Measures and Carynginia Formation were deposited in open marine, fluvial and deltaic settings, and are interpreted as pre-rift or syn-rift sequences (Mory et al., 2005; Mory and Jasky, 1996) (Fig. 2). The Late Permian Unconformity was developed regionally at the end of this rift event (Jablonski and Saitta, 2004; Jones et al., 2011). In parts of the basin, the Upper Permian Wagina Sandstone, Beekeeper Formation and Dongara Sandstone were

deposited in deltaic and shallow marine settings as the first post-rift sediments. Subsequently, in the Late Permian to Early Triassic, the thermal subsidence phase of the rift produced a local marine transgression with deposition of the Kockatea Shale facies in deeper water. At the same time, the Bookara Sandstone was developed in the shallow water parts of the basin. Deltaic sediments of the Middle Triassic Woodada Formation were deposited after the Kockatea Shale as a result of subsequent regression. The overlying Late Triassic to Late Jurassic Lesueur, Eneabba, Cattamarra Coal Measures, Cadda, and Yarragadee Formations were deposited during subsequent rift events. Extensive uplift and erosion caused by the breakup of Greater India in the Early Cretaceous is prominent (Jablonski and Saitta, 2004), especially in the offshore northern Perth Basin, resulting in a significant unconformity that separates these sequences from the Lower Cretaceous Winning Group.

3. Data & methodology

3.1. Seismic data

A large amount of public domain 2D and 3D seismic data is available from the northern Perth Basin. The 3D seismic surveys used in this study are listed in Table 1. In addition, the location of 2D and 3D seismic data is shown in Fig. 1.

The quality of both 2D and 3D seismic data is generally good offshore and poor to moderate onshore. Onshore 2D seismic lines were mainly acquired pre-2000. Seismic resolution of both 2D and 3D seismic data is generally good enough for interpretation as far down as the Late Permian Unconformity. However, the 2D seismic data in the southern portion of the onshore basin is relatively poor. Therefore it is difficult to identify horizons with a high degree of confidence in the regions covered solely by 2D seismic data.

3.2. Seismic interpretation

Interpretation was conducted on time domain data in Petrel (2017) Software (Schlumberger). Interpreted seismic horizons were picked based on well tops from 46 wells (Fig. 1 and Table 1), and synthetic

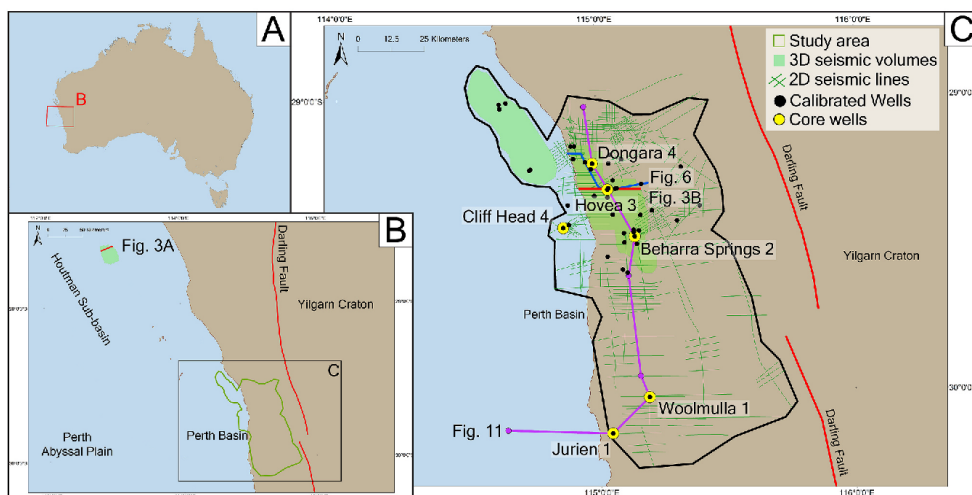


Fig. 1. Location of the study area within the northern Perth Basin, interpreted 3D seismic volumes, 2D seismic lines, calibrated wells, core interpreted wells, and the location of lines used in subsequent figures.

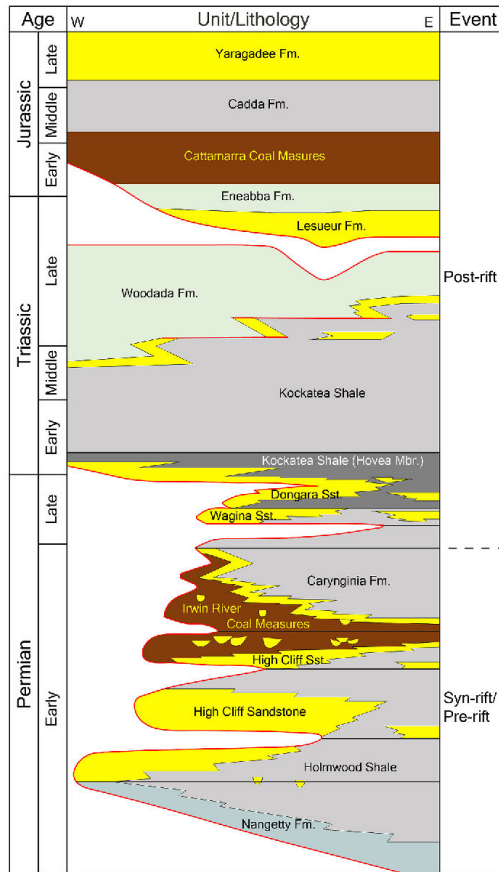


Fig. 2. Stratigraphy of the northern Perth Basin (after [Ferdinando et al., 2007](#); [Mory et al., 2005](#)). Light and dark grey: deeper water mudstone, yellow: shallow marine sandstone; brown: fluvial to deltaic sediments, bluish green (Nangetty Fm.): open marine glacial sediments, yellowish green (Eneabba and Woodada Fms.): fluvial to deltaic sediments. (For interpretation of the references to colour in this figure legend, the reader is referred to the Web version of this article.)

Table 1
Details of 3D seismic volumes used in this study.

Survey name	Setting	Year acquired	Area (sq. Km)	Record depth (s)	Inline spacing (m)	Crossline spacing (m)
Beharra Springs 3D	Onshore	2002	210	3.8	20	20
Denison 3D	Onshore	2004	580	4.2	20	20
Dongara North 3D	Onshore	1994	70	4	12.5	12.5
Diana 3D	Marine	2008	620	4	25	12.5
Macellan 3D	Marine	2003	550	5.6	25	25

seismograms were created for 3 wells (Beharra Springs 2, Hovea 3 and Apium 1) to confirm the tie between well tops and seismic data. Horizons were created for each 2D and 3D survey. All interpreted horizons were merged into a single horizon after eliminating overlap. The merged horizon data was used to create surfaces.

The Base and Top Kockatea Shale are the main seismic horizons interpreted for this study, and are used to identify basin geometry and paleogeography from the Late Permian to the Early Triassic. The Late Permian Unconformity was also interpreted where it is distinct from the Base Kockatea Shale, and where the Dongara and/or Wagina Sandstone are also present. The Late Permian Unconformity is a prominent unconformity in the northern Perth Basin. It forms an angular unconformity in the offshore, but it is represented by a disconformity or a subtle angular unconformity onshore. The Base Kockatea Shale is generally defined as a continuous reflection above the Late Permian Unconformity where the Dongara and/or Wagina Sandstone are present. The Top Kockatea Shale is defined as a continuous reflection at the top of the low amplitude seismic facies that represents the Kockatea Shale. However, the Woodada Formation, which generally lies above the Kockatea Shale, sometimes shares a similar lithology. Therefore, the seismic reflection corresponding to the Top Kockatea Shale is unclear in these places. In this case, the nearest reflection was picked. Based on correlation with wells, the vertical difference between the Top Kockatea Shale and the nearest picked reflection is small (~20 ms), and this approximation does not affect the interpretation of regional structural trends and thickness variations.

3.3. Well data for core description

Forty-one wells cored some part of the Kockatea Shale in the northern Perth Basin. Six wells were selected for core description and interpretation (Beharra Springs 2, Cliff Head 4, Dongara 2, Hovea 3, Jurien 1 and Woolmulla 1; [Fig. 1](#) and [Table S1](#)) because they contain cores near the base of the Kockatea Shale, covering both the Upper Permian and Lower Triassic sections, and have well-defined formation tops, well reports and mostly complete well logs. Furthermore, these wells are sufficiently well-spaced to evaluate the basin-scale lateral distribution of lithofacies and depositional setting. All core materials are stored in the Perth Core Library managed by the Department of Mines, Industry Regulation and Safety, Government of Western Australia.

3.4. TOC and Rock-Eval analyses

A set of 69 samples of the basal section of the Kockatea Shale from cores of 6 wells were selected and analysed for TOC and Rock-Eval analyses ([Fig. 9](#)).

Samples were subjected to sonication for three intervals of 15 min each in a 9:1 DCM:MeOH (Dichloromethane:Methanol) mixture to remove any surface contamination. Sonicated samples were then ground into fine powder using a Rocklabs BTRM 1A rock grinder. TOC and Rock-Eval analyses was applied to ~1g rock samples.

A LECO Carbon Sulphur analyser was used for the TOC measurement after treatment with 3M HCl to remove carbonate. For the pyrolysis analysis, Vinci Technologies Rock-Eval 6 equipment was used with powdered rock samples. Thermal maturity was evaluated by measuring S1 (Free hydrocarbon in mg/g rock measured at lower temperatures), S2 (Hydrocarbon in mg/g rock measured through thermal cracking of kerogens at higher temperatures), T_{max} (temperature of maximum hydrocarbon production in °C) and S3 (amount of CO₂ in mg/g rock) using IFP1600000 as standard. For the analysis, the initial temperature was set at 300 °C with 3 min holding time and programmed to heat to 650 °C at a rate of 25 °C/min. The derivative parameters such as HI (S2*100/TOC) and OI (S3*100/TOC) were also calculated.

The rock samples were ground at Curtin University and TOC and Rock-Eval analyses were conducted by Intertek (Intertek Group plc) in Welshpool, Western Australia.

4. Results

4.1. Seismic interpretation

4.1.1. Seismic stratigraphy

The seismic cross sections in Fig. 3 shows typical structural and stratigraphic features from the northern Perth Basin. Below the Late Permian Unconformity, reflections generally dip to the west-southwest and are segmented by normal faults. Parallel reflector packages are correlated to the pre-rift High Cliff Sandstone and older sediments. The overlying wedge-shaped packages are correlated to the syn-rift Irwin River Coal Measures and Caringinia Formation. The Dongara and Wagina sandstones are thin, and are represented by only a few reflections on seismic data, making them difficult to distinguish. Where

present, they are expressed as high-amplitude, flat-lying parallel reflectors overlying the angular Late Permian Unconformity.

The Kockatea Shale conformably overlies the Dongara Sandstone, and is expressed as a package of low-amplitude, parallel to semi-parallel reflections. Both time-thickness maps (Fig. 4A and B) and seismic sections suggest limited variations in the thickness of this formation, although several local depocentres are evident on the time-thickness map (Fig. 4C). A number of large normal faults cut the Kockatea Shale; however, there are no obvious thickness variations across these faults, which are interpreted as being post-depositional.

The Woodada Formation conformably overlies the Kockatea Shale and generally shows higher amplitude reflections than in the Kockatea Shale. The Lesueur Sandstone conformably overlies the Woodada Formation and the top of the Lesueur Sandstone is eroded by the

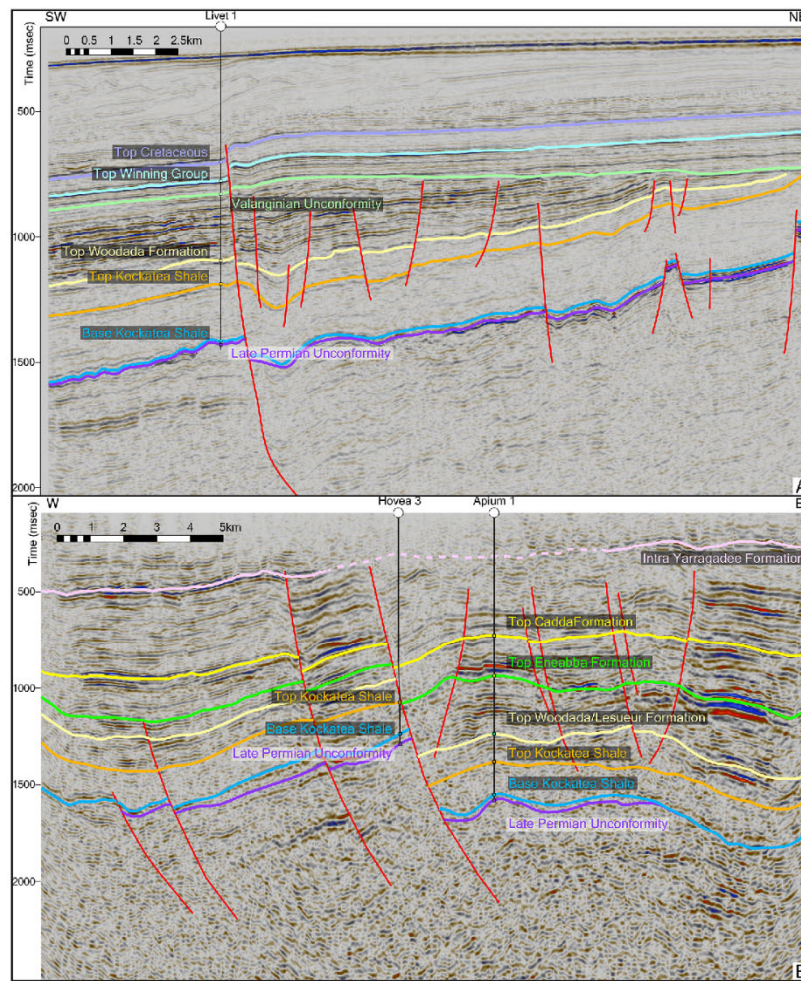


Fig. 3. Typical seismic section from the offshore (A) and onshore (B) northern Perth Basin. Dark purple (Oldest horizon): Late Permian Unconformity, Blue: Base Kockatea Shale, Orange: Top Kockatea Shale, Cream yellow: Top Woodada Formation/Lesueur Sandstone, Green: Top Eneabba Formation, Pink: Intra Yarragadee Formation, Cream green: Valanginian Unconformity, Light blue: Top Winning Group, Light purple: Top Cretaceous. The location of the lines is shown in Fig. 1. (For interpretation of the references to colour in this figure legend, the reader is referred to the Web version of this article.)

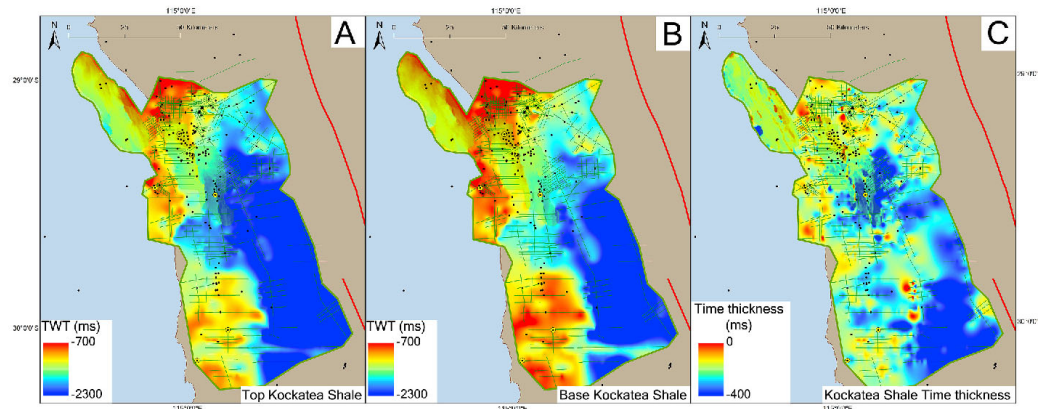


Fig. 4. Time structure maps of the (A) Top Kockatea Shale and (B) Base Kockatea Shale horizons and (C) time thickness map of the Kockatea Shale.

Valanginian Unconformity in the offshore. Where they are not eroded, the Eneabba and Cadda Formations conformably overlie the Lesueur Sandstone and show significant thickness variations across large normal faults. The Yarragadee Formation conformably overlies the Cadda Formation with poor definition of the top of the Yarragadee Formation due to poor seismic quality at shallower depth. The Cretaceous Winning Group overlies the Valanginian Unconformity. The reflections are sub-parallel to the sea bed and are low amplitude. Paleogene and Neogene packages with low amplitude reflections downlap onto the top Cretaceous horizon.

4.1.2. Structure

Both Top and Base Kockatea Shale structure maps and seismic sections show large normal faults (Figs. 3 and 4). The identified normal faults are consistent with faults that were previously identified by other authors (Cadman et al., 1994; Crostella and Backhouse, 2000; Hall and Kneale, 1992; Jablonski and Saitta, 2004; Jones et al., 2011; Mory et al., 2005; Quaife et al., 1994; Song and Cawood, 2000). The orientation of most onshore normal faults is NNW-SSE. The orientation rotates to NW-SE for the offshore normal faults. Faults dip to the east onshore and to the west offshore. In the northern onshore, NE-SW trending normal faults are also identified, such as the Allanooka Fault (Hall and Kneale, 1992). This fault dips to the south.

4.1.3. Structural evolution

4.1.3.1. Permian rifting. The large normal faults in the offshore are associated with inclined Permian packages that are truncated by the Late Permian Unconformity, indicating pre- and syn-rift sediments, suggesting that these faults were active during the Permian rifting phase. However, the seismic reflections beneath the Late Permian Unconformity in the onshore seismic data are not as clearly inclined, and indicate that the focus of Permian rifting occurs offshore.

4.1.3.2. Early post-rift. The Wagina Sandstone directly overlies the Late Permian Unconformity, but is limited to the middle part of the Dandaragan Trough (Fig. 6A). It is overlain by the Dongara Sandstone, which is more widespread and sits directly above the Late Permian Unconformity where the Wagina Sandstone is absent. Both units are absent from the south of the study area (Fig. 6B). The Permian Kockatea Shale developed in the middle part of study area around Hovea 3 and Beharra Springs 2 (Fig. 6C and D) and the Triassic Kockatea Shale sits directly above the Late Permian Unconformity in the south. The

combined thickness of these Upper Permian units is variable (Fig. 6D). They are thinner (~0–35 m) in the western part of the study area, which corresponds to the Beagle Ridge, and become thicker (>50 m) away from the ridge, toward the Dandaragan Trough. This is also evident from seismic data. For example, in the Denison 3D seismic survey both the Dongara and Wagina Sandstones are recognized in wells and can be identified as a single unit on seismic data. An arbitrary seismic section (Fig. 5) shows a major normal fault at the west end of the section, but the Dongara Sandstone can only be interpreted to the east of the fault, and is too thin (below seismic resolution) or absent to the west. The thickness variation, facies distribution and seismic stratigraphic relationships suggest a progressive infilling of remnant topography that remained after the Late Permian rift event. Alternatively, the thickness variation of the Upper Permian could be a result of erosion of more widespread Upper Permian units above structural highs. Either way, this indicates the persistence of remnant topography following Permian rifting.

The thickness of both Kockatea Shale and Woodada Formation is similar across most large faults (Fig. 3) which, combined with their position above the Late Permian Unconformity, allows these sequences to be interpreted as post-rift. However, there are some faults that propagate up from beneath the base of the Kockatea Shale, but do not cut the entire sequence (Fig. 3), indicating that minor movement continued from the Permian rift event in some places. The Kockatea Shale also show significant thickness variations across-faults in a few instances (i.e. ~280–470m in the foot wall and ~660–850m in the hanging wall, Fig. 4C), indicating continued fault activity, or alternatively, additional infilling of remnant topography created by the Late Permian rift event.

4.1.3.3. Late Triassic to Early Cretaceous reactivation. The Permian structure is partly disguised by fault reactivation in the Upper Triassic to Early Cretaceous. This is indicated by distinct thickness variations in the Upper Triassic to Middle Jurassic Eneabba and Cadda Formations across large normal faults (Fig. 3). On the other hand, the Upper Jurassic Yarragadee Formation is uniform in thickness, indicating a cessation of fault activity. In the offshore, the Upper Triassic Lesueur Sandstone package and younger units are rotated by fault movement after the deposition of this package because seismic reflections are parallel and uniform. The faults and the rotated sediments are truncated by the Valanginian Unconformity, and the thickness of the overlying post-Valanginian sediments, such as the Winning Group, are almost uniform. Therefore, the activity on these faults can be constrained to after the Middle Jurassic and before the development of the Valanginian

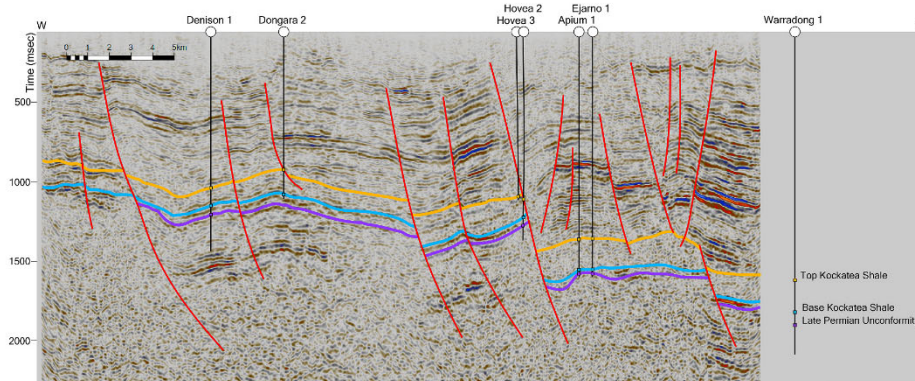


Fig. 5. The seismic expression of Permian faults. The major fault at the west end of the section represents one of the remnant Permian faults, based on thickness variations within the Upper Permian Sandstones. Location of the line is shown in Fig. 1. The colour of the seismic horizons is as in Fig. 3. (For interpretation of the references to colour in this figure legend, the reader is referred to the Web version of this article.)

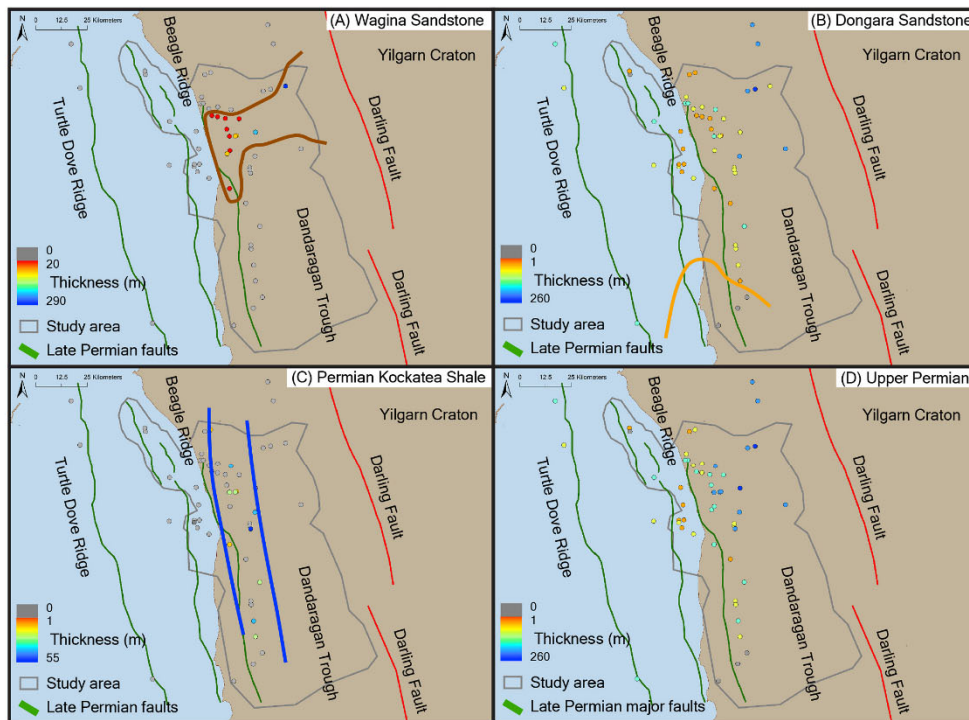


Fig. 6. Thickness variation in (A) the Wagina Sandstone, (B) the Dongara Sandstone, (C) the Permian Kockatea Shale, and (D) Upper Permian (Wagina and Dongara Sandstones and Permian Kockatea Shale) based on well log data. The brown polygon in (A) shows the extent of the Wagina Sandstone. The orange polygon in (B) shows the limit of the Dongara Sandstone. The blue polygon in (C) shows the extent of Permian Kockatea Shale. (For interpretation of the references to colour in this figure legend, the reader is referred to the Web version of this article.)

Unconformity. Reactivation of older Permian faults is indicated by the greater rotation of Permian packages beneath the Late Permian Unconformity. In addition, a number of new faults formed at this time, some of which detach in the Kockatea Shale.

4.2. Core description

Several different lithofacies are recognized in the Kockatea Shale, although "Shale" is used as a lithostratigraphic term in well reports. The Kockatea Shale contains dark and light coloured mudstones, microbial mat beds, storm/gravity sandstones, bioturbated siltstone and tidal sandstones (Fig. 8 and Fig. 9).

4.2.1. Mudstone facies (lighter coloured mudstone facies, darker coloured mudstone facies and fossiliferous facies)

Mudstone dominated intervals are identified in five of the six wells, but the mudstone type is variable and they are distinguished as: lighter coloured mudstone facies (medium grey mudstone), darker coloured mudstone facies (dark grey mudstone and black mudstone) and fossiliferous facies (Fig. 8). The latest Permian section is dominated by lighter coloured mudstones and fossiliferous grey mudstones beds which contain shells, small fossil fragments and erosional features. Bioturbation is less common in the latest Permian mudstone interval of Hovea 3. In the lowest Triassic section, black and dark-grey mudstone (darker coloured mudstone) are dominant in the northern wells (Hovea 3, Dongara 4). Black mudstone is common in Hovea 3 and dark grey mudstone is mainly observed in Dongara 4. Parallel laminations are commonly observed in all the mudstone facies, suggesting that the original sedimentary structures are preserved. Mudstone from the southern wells (Jurien 1, Woolmulla 1) are a medium grey colour (lighter coloured mudstone). This facies is lighter in colour than both the darker coloured mudstone and microbial mat facies in the northern wells.

4.2.2. Microbial mat facies

Cliff Head 4, Hovea 3 and Dongara 4 contain layered carbonates exhibiting a mounded or swelling geometry, with the colour of the carbonate layers varying from grey to cream (Fig. 7 and Fig. 8). Because

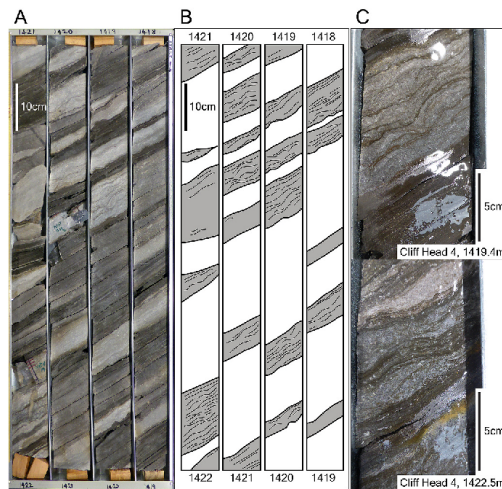


Fig. 7. Microbial mats in Cliff Head 4. Grey colour beds in (B) represent the microbial mats. (For interpretation of the references to colour in this figure legend, the reader is referred to the Web version of this article.)

of the mounded shape, the lateral thickness variation across individual beds is large, and is between 1 and 47 cm. The features of this lithofacies are similar to the cross-sections of stromatolites observed in outcrop (Chen et al., 2014; Luo and Chen, 2014), and this lithofacies was described as microbial beds in Hovea 3 by Thomas et al. (2004). Based on these features we interpret this lithofacies as containing microbial mats. In the Cliff Head 4 and Dongara 4 wells, the microbial mats are interbedded with dark grey mudstone. Both dark grey mudstone and black mudstone are interbedded with microbial mats in Hovea 3. The mudstone in this facies has no obvious bioturbation and parallel laminations are preserved, which are likely the original sedimentary structure. The contact between mudstone and microbial mat is sharp with no indication of a gradual lithologic change.

4.2.3. Tidal sandstone facies

Jurien 1 and Woolmulla 1 show alternations of sandstone and lighter coloured mudstone. Sandstone with wavy to flaser-like sedimentary structures and mud drapes are common in both wells (Fig. 8). This indicates that the sandstone was probably deposited in a shallow water setting with a tidal influence. The thickness of each bed ranges from 1 to 45 cm. The contacts between sandstone and mudstone are generally sharp and the base of some sandstone units shows erosion into the underlying mudstone. Bioturbation is not apparent in Jurien 1, indicating that the original sedimentary structures are preserved in this well. Conversely, tidal sandstones in Woolmulla 1 experienced significant bioturbation with vertical burrows such as *Planolites* and *Cylindrichnus*. However, the bioturbation cannot be easily identified in mudstone within this facies. In addition, the intensity of the bioturbation is not enough to completely destroy the original sedimentary structures, indicating a relatively sparse fauna. The preserved sedimentary structures of the sandstone units in Woolmulla 1 are similar to sandstones in Jurien 1 and indicate a probable tidal environment. The interbedded mudstone is medium-grey with parallel laminations.

4.2.4. Storm/gravity flow bed facies

Cliff Head 4 and Dongara 4 have an interval of interbedded mudstone and sandstone above and beneath the microbial mat facies. The thickness of the sandstone beds is generally 1–3 cm, and they are cream-yellow in colour. The sandstones are very fine to fine grained, and are massive, or contain weak parallel laminations (Fig. 8). There is a gradation from massive to finer grained parallel laminated units, which suggests deposition by a waning current. In places they also show boudin-like thickness variations, and are interbedded with laminated mudstone, suggesting deposition by a storm or gravity flow.

4.2.5. Bioturbated siltstone facies

Beharra Springs 2 contains chaotic, very poorly sorted siltstones in the Upper Permian. The facies is generally massive to weakly bedded. Bivalves and gastropods are frequently observed, although fossils are rare in other facies (Fig. 8). The original sedimentary structures are not obvious, and individual trace fossils are also rare in this facies, implying intense bioturbation, although in some cases vertical *Ophiomorpha*-like trace fossils are identified. The facies is medium-dark grey in colour and lighter than both the mudstone in the microbial mat facies and the darker coloured mudstone facies.

4.3. Core-well log correlation

There is a good correlation between core observations and well log response. Fig. 10 shows well logs (gamma ray (GR), sonic log, density log, neutron porosity log and resistivity log) and core logs of the six wells from which cores were described.

The typical response of the upper parts of the Kockatea Shale shows constant values of GR, sonic log, and neutron, with the high values of GR indicating the presence of mudstone. By contrast, some wells show an irregular log response in the lower part of the Kockatea Shale. In the

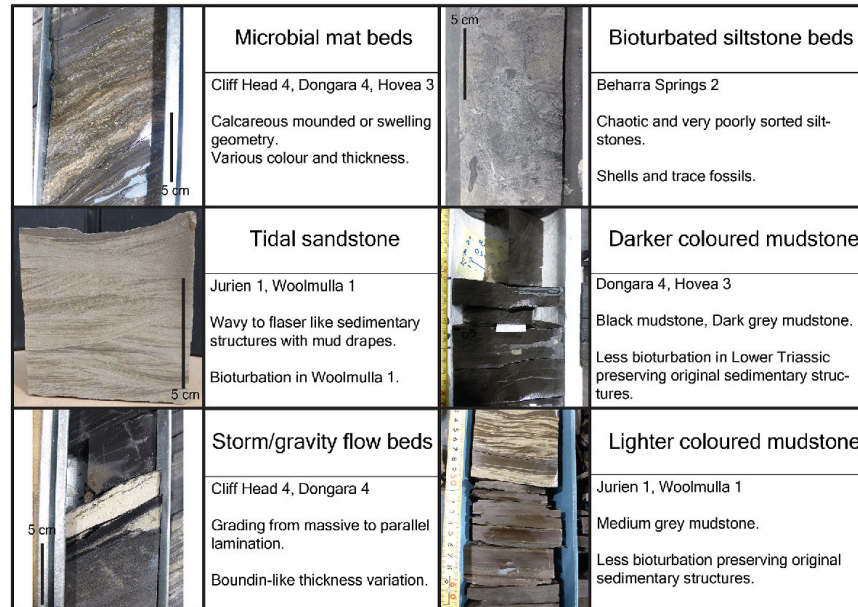


Fig. 8. Examples of typical lithologies observed in cores.

irregular log facies, the GR shows a serrated pattern and has lower values. The sonic log also shows a similar serrated pattern to GR, with slightly higher values that tend to decrease at the top of the irregular log facies. The neutron porosity log also shows a serrated pattern similar to the GR and sonic logs, and a decrease in values at the top of the irregular log facies. In the interval below the irregular log facies, the GR shows large variation in values. The sonic log decreases to typical Kockatea Shale values. The neutron porosity log tends to be higher in value compared the irregular log facies and typical Kockatea Shale.

The microbial mat facies is identified in three cores (Cliff Head 4, Dongara 4, Hovea 3), and in all cases the lithofacies corresponds to the irregular log facies (Fig. 10). In addition, cuttings description from these wells indicate the presence of limestone or calcareous lithofacies in the interval corresponding to the irregular log facies and microbial mats. Taken together, these observations indicate that the irregular log facies is a good proxy for identifying the development of microbial mats from wireline logs.

Beharra Springs 2, which does not contain the microbial mat facies in core, does not have this irregular log facies in the cored interval. However, an irregular log facies is identified on both the sonic and neutron porosity logs above the cored interval (Fig. 10), although GR cannot be used because of poor data quality. In addition, the cuttings description of Beharra Springs 2 also show the presence of limestone in the irregular log facies interval. Therefore, Beharra Springs 2 may have a microbial mat facies outside the cored interval. On the other hand, Jurien 1 and Woolmulla 1, which do not have microbial mat facies in the cored section, do not show the irregular log response in the cored interval or elsewhere in the well (Fig. 10).

4.4. Microbial mat distribution

Well logs from 63 wells were analysed to identify the irregular log facies (Fig. 11), starting from the cored wells (Dongara 4, Cliff Head 4 and Hovea 3) and extending to other wells. Wells with irregular log

facies are well developed around Dongara 4, Hovea 3 and Cliff Head 4 which are located around the northern Beagle Ridge. On the other hand, wells without irregular log facies tend to be located on the southern Beagle Ridge and in the Dandaragan Trough. Wells with irregular log facies are also identified on the Turtle Dove Ridge (Batavia 1 and Geelvink 1).

4.5. Source rock quality

The darker coloured mudstone have high TOC and HI and low OI (TOC: 0.6–2.7%, HI: 39–502mg/gTOC, OI: 7–65mg/gTOC), suggesting good source rock potential with type II-III kerogen (Fig. 12). The microbial mat facies also have high TOC and HI, as well as slightly high OI compared with the darker coloured mudstone (TOC: 0.3–3.4%, HI: 100–579mg/gTOC, OI: 16–410mg/gTOC), suggesting similar or slightly enhanced source rock potential compared to the darker coloured mudstones (Fig. 12). On the other hand, the lighter coloured mudstone has low TOC and HI and high OI indicating type III kerogen (TOC: 0.2–0.5%, HI: 59–127mg/gTOC, OI: 68–340mg/gTOC), suggesting poor source rock potential (Fig. 12).

5. Discussion

5.1. Lateral facies relationship

The distribution of different facies in the lower part of Kockatea Shale, based on core observations and well log analysis, is illustrated in Fig. 13.

The age of the formations in each well is based on post-drill palynological studies (Georgiev et al., 2020; Gorter et al., 2009; Metcalfe et al., 2008; Thomas et al., 2004). The Wagina Sandstone is Lower Wuchiapingian in age. The Permian Kockatea Shale is the same age as the Changhsinian and Upper Wuchiapingian Dongara Sandstone, and thus they are considered lateral equivalents.

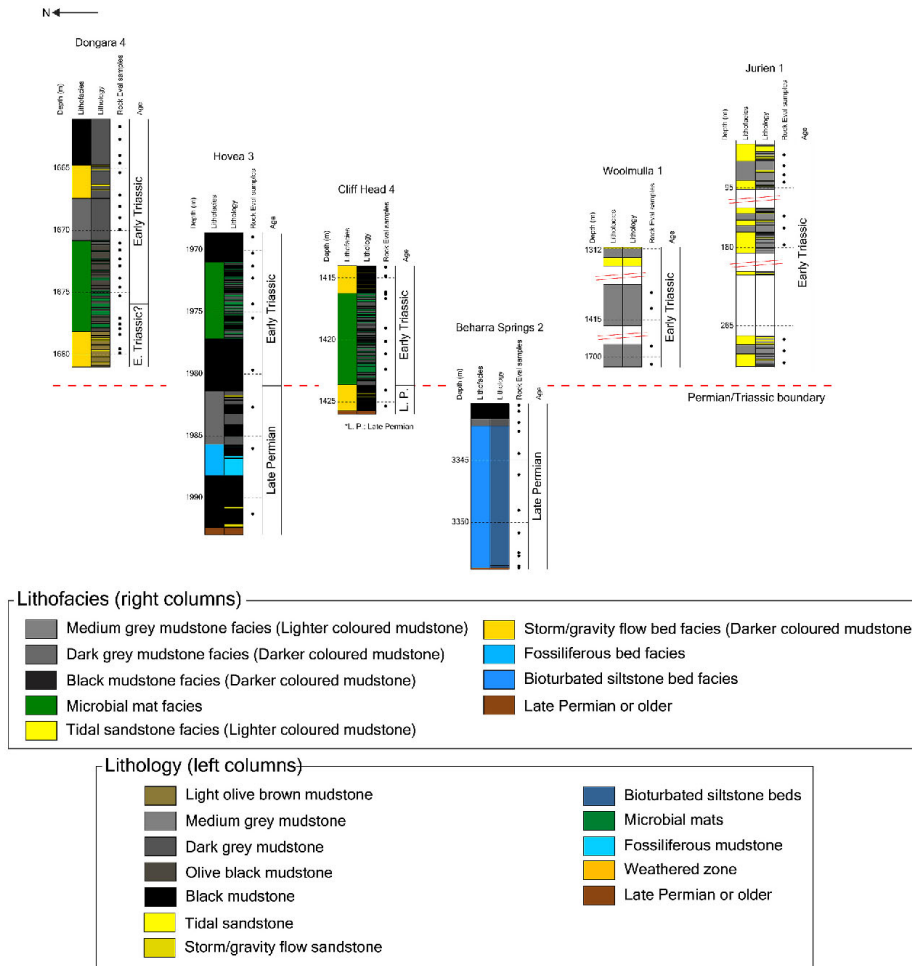


Fig. 9. Core observation logs and correlation of six wells. Points represent the location of samples for TOC and Rock-Eval analyses.

The cored Early Triassic sections of the Kockatea Shale are assigned to both the Griesbachian and Dienerian, which are parts of the Induan stage in the earliest Triassic. All of the microbial mats for which biostratigraphic samples are available indicate an Early Triassic age. Therefore it is highly likely that they are local representatives of typical Lower Triassic lithofacies, following a global pattern of microbial mat development (Foster et al., 2020; Kershaw et al., 2012; Luo et al., 2019; Woods, 2014). The Permo-Triassic boundary is located at the boundary of the sandstone (Dongara Sandstone) and mudstone (Kockatea Shale) in most wells, although this boundary is positioned within the Kockatea Shale in some wells where the Permian Kockatea Shale is present. The South Turtle Dove 1B well, located approximately 40 km west of Jurien 1, has a high proportion of sandstone in the lower part of the Lower Triassic which is assigned to the Bookara Sandstone, and is of equivalent age to the Kockatea Shale. The Permo-Triassic boundary in this well is positioned within sandstone facies, between the Dongara Sandstone and Bookara Sandstone.

5.2. Basin morphology

The morphology of the basin was created by Late Permian rifting. This persisted into the latest Permian and early Triassic post-rift phase either as remnant topography or as a consequence of minor continued fault movement, and influenced the distribution of both the Dongara and Wagina Sandstones and the Kockatea Shale (Fig. 14A). The Beagle Ridge formed a structural high at this time. A second ridge, comprising the Turtle Dove Ridge and Geelvink High (Jones et al., 2001) is located offshore and is parallel to the Beagle Ridge. The evolution of this ridge is less easy to define because of poor seismic resolution above it. However, several 2D seismic sections indicate thickening of Permian strata beneath the Late Permian Unconformity in the footwall of major faults that bound the ridge, indicating that the faults were active during Permian rifting and that the ridge also formed a structural high during the Upper Permian and Early Triassic. Structural lows such as the Dandaragan Trough are located both east and west of these highs. These

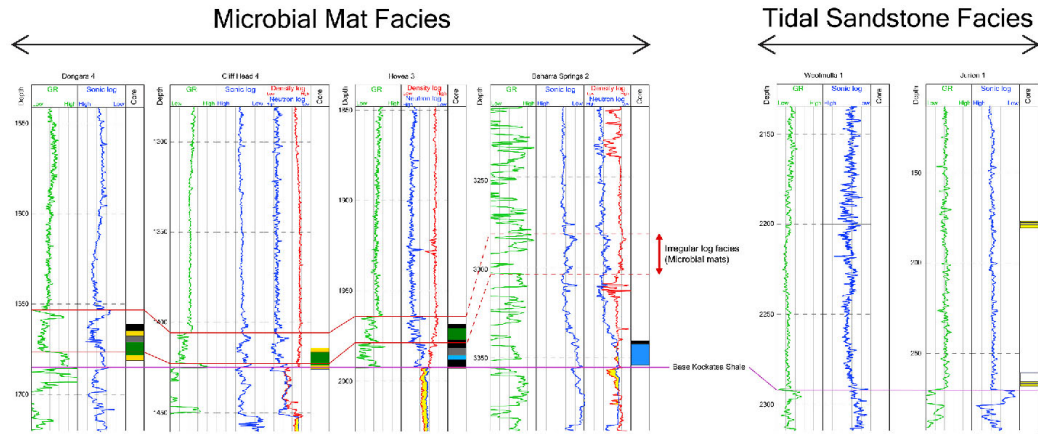


Fig. 10. Well log correlation to microbial mat facies. The base Kockatea Shale is indicated by purple lines. The intervals between red lines correspond to either the presence of microbial mat facies in cores or the irregular log facies which indicates the development of microbial mats. The microbial mat facies are absent from Jurien 1 and Woolmulla 1. Colours indicating the facies identified in core logs are the same as in Fig. 9. (For interpretation of the references to colour in this figure legend, the reader is referred to the Web version of this article.)

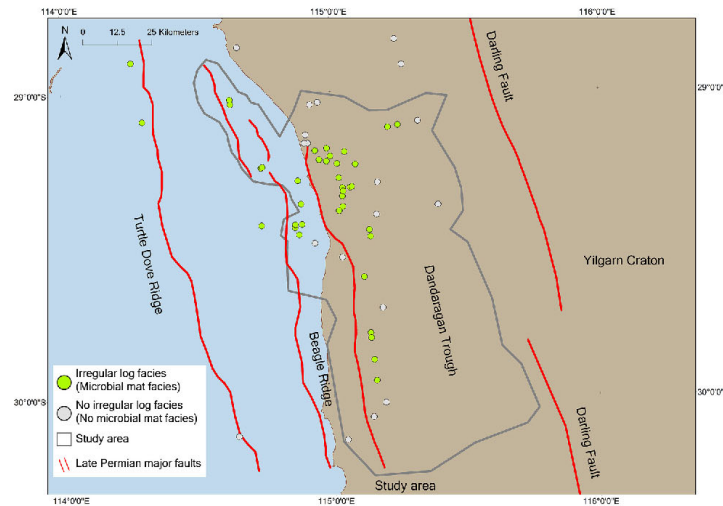


Fig. 11. Irregular log facies distribution indicating the distribution of microbial mat facies on well logs.

structural lows form the main depocentres and Upper Permian to Lower Triassic sedimentary sequences become thin, or are affected by hiatuses or erosion on the structural highs.

5.3. Lower Triassic paleogeography

Thomas and Barber (2004) identified the Permo-Triassic boundary in the Kockatea Shale although Georgiev et al. (2020) and Grice et al. (2005c) suggest that it may correspond to a short-lived hiatus. A major transgression commenced around the Permo-Triassic boundary. Consequently, mudstone deposition became dominant in the Early Triassic (Figs. 14B and 15). The main depocentres of the Kockatea Shale

correspond to structural lows (Fig. 4C). In addition, the onlap of reflections at the base of the Lower Triassic Kockatea Shale against a Permian fault (Fig. 3) shows that the morphology created by Permian faults continued to influence the deposition of the lower part of the Kockatea Shale.

The Bookara Sandstone is interpreted to have been deposited in a shallow marine setting with higher clastic input (Mory and Iasky, 1996) in the southern part of the Turtle Dove Ridge. Interbedding of the sandstone with mudstone containing coal fragments in South Turtle Dove 1B suggests that there is terrigenous input. The tidal sandstone facies recognized in Jurien 1 and Woolmulla 1 developed in the southern part of the Beagle Ridge. The high proportion of sandstone interbedded

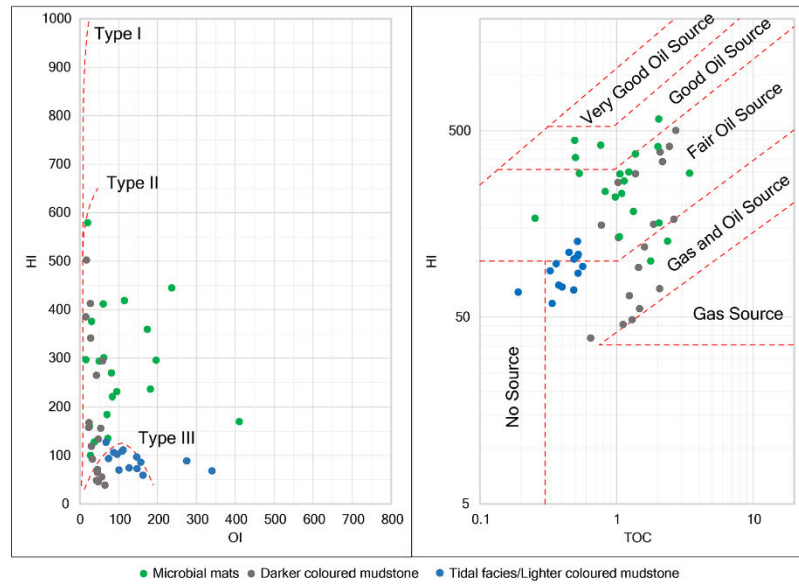


Fig. 12. III-OI and III-TOC plots of each lithofacies.

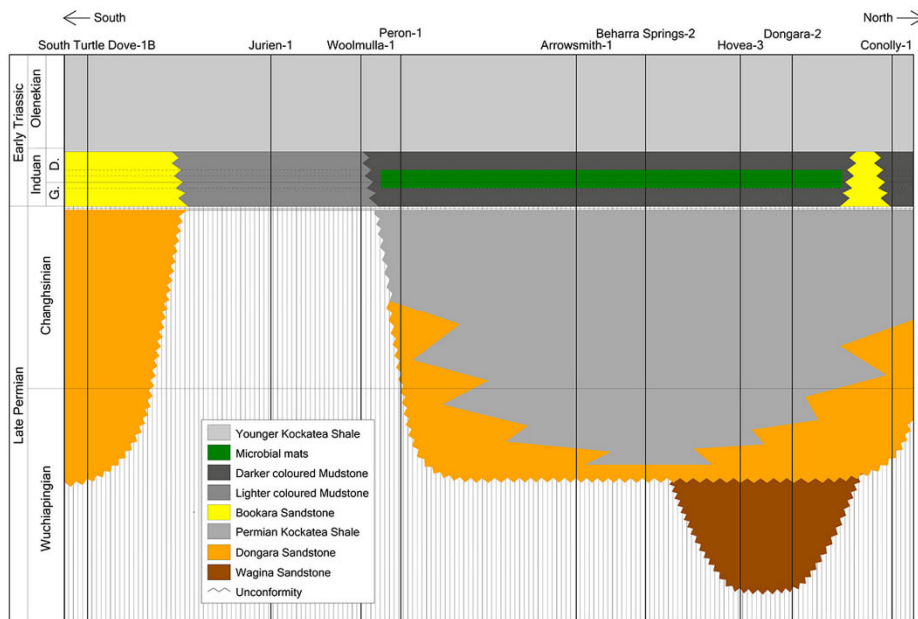


Fig. 13. N-S oriented lateral facies relationship from Upper Permian Dongara and Wagina Sandstone to Lower Kockatea Shale. G. = Griesbachian and D. = Dienerian. Location of wells is shown in Fig. 1.

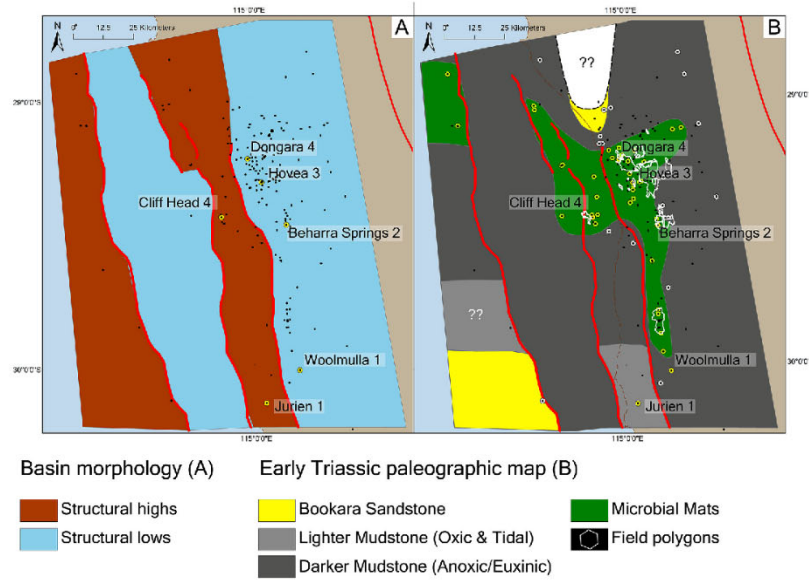


Fig. 14. Map of (A) reconstructed basin morphology during Late Permian and Early Triassic and (B) paleogeography in Early Triassic. The blank area in (B) represents a hiatus during the Early Triassic or erosion during younger rifting.

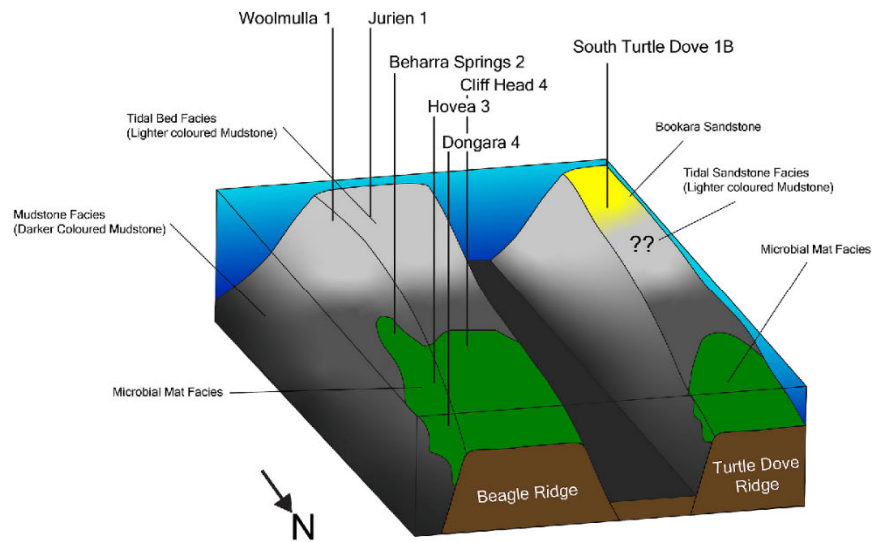


Fig. 15. Paleogeographic model of the Early Triassic viewed from north. Not to scale.

with mudstone in the tidal sandstone facies also suggests proximity to clastic input or the basin margin.

The association of the tidal sandstone facies with the lighter coloured mudstone in both Jurien-1 and Woolmulla-1 suggests oxic conditions, resulting in the deposition of a poor quality source rock. The sediments

of Cliff Head 4, Dongara 4 and Hovea 3 are dominated by darker coloured mudstone without significant bioturbation, suggesting that the mudstone was deposited under anoxic to euxinic conditions, resulting in higher source rock quality. Anoxic to euxinic condition have been reported by other authors (Grice et al., 2005a; Thomas and Barber, 2004)

and related to global anoxia or euxinia after the end-Permian mass extinction (Erwin, 1994; Grice et al., 2005a; Knoll et al., 1996; Nabbe-feld et al., 2010; Song et al., 2014; Twitchett et al., 2004; Whiteside and Grice, 2016; Wignall and Twitchett, 1996). In the north, some wells located on the Beagle Ridge (Bookara 1, Conder 1, Dibblers 1, Eleven Mile 1 and Wye 1) contain thin sandstone beds which are also assigned to the Bookara Sandstone, suggesting that clastic input and a shallower marine setting also developed in this area. The extent to which the Beagle Ridge persisted is unclear as other wells, such as Wakeford 1, are missing the Kockatea Shale as well as the Dongara and Wagina Sandstone and overlying units. This could either indicate a persistent high with a sedimentary hiatus during the latest Permian and Early Triassic or could be a result of erosion during Late Triassic to Early Cretaceous rifting.

Microbial mats are associated with the darker coloured mudstone found in the northern wells (Figs. 9 and 11). In addition, the distribution of wells containing the irregular log facies shows that microbial mats were mainly developed on the Beagle Ridge, on its eastern flank and on the Turtle Dove Ridge (i.e. in shallower water depths) in the anoxic part of the basin. They are absent from the Dandaragan Trough (i.e. greater water depths) and from the southern part of the basin where there was greater clastic input (Bookara Sandstone) and more oxygenated waters (tidal sandstone facies and lighter coloured mudstones).

5.4. Controls on microbial mat distribution

Fig. 15 shows a three dimensional representation of Early Triassic paleogeography showing the relationship between microbial mat development, clastic input, the presence of structural highs and relative paleo water depth.

Global anoxia or euxinia after the end-Permian mass extinction have been reported by several authors (Erwin, 1994; Grice et al., 2005a; Knoll et al., 1996; Nabbe-feld et al., 2010; Song et al., 2014; Twitchett et al., 2004; Whiteside and Grice, 2016; Wignall and Twitchett, 1996) and created the conditions globally for the development of microbial mats during the post-extinction recovery phase (Foster et al., 2020; Kershaw et al., 2012; Luo et al., 2019; Woods, 2014). However, these global conditions were not developed uniformly throughout the northern Perth Basin.

It is clear from the occurrence of bioturbated sediments that oxic conditions existed in shallow water conditions on the southern margin of the basin. These are associated with tidal sediments and clastic input (Bookara Sandstone) which may have provided nutrients that supported the establishment of grazing organisms that would in turn have inhibited the development of microbial mats.

Anoxic and euxinic conditions were established in the northern part of the basin, due to a combination of its restricted nature and greater water depth. While the absence of other fauna in this setting promoted the development of microbial mats, they are restricted to the intra-basinal structural highs (Beagle Ridge and Turtle Dove Ridge) where substrates were shallow enough for sufficient light to penetrate for the mats to develop. Anoxic mudstones were deposited in the adjacent deeper water troughs which are less favourable settings for mat development.

5.5. Source rock potential of microbial mats

Microbial mats and darker coloured mudstone have a good source rock quality with Type II-III kerogen. In addition, the discovered hydrocarbon fields are located in areas where anoxic darker coloured mudstones and microbial mats are present (Fig. 14B). The paleogeographic maps therefore highlight the more prospective parts of the basin.

6. Conclusions

Core observation reveals a large variation in lithofacies at the base of the Kockatea Shale: darker coloured mudstone, lighter coloured mudstone, microbial mats, tidal sandstone, storm/gravity sandstones and bioturbated mudstones. The microbial mats in cores correspond to an irregular log facies on wireline logs and this facies is recognized in several wells. In addition, seismic interpretation demonstrates that the paleogeography during the Late Permian and Early Triassic was influenced by remnant topography from Permian faults. The integrated analysis of core, well logs and seismic data shows the lateral facies distribution within the Kockatea Shale and the factors that control the development and distribution of microbial mats in the northern Perth Basin.

The lighter coloured mudstones and interbedded tidal sandstone were deposited in an oxygenated tidal setting along with the shallow marine Bookara Sandstone. Anoxic to euxinic conditions were established elsewhere in the basin due to a combination of its restricted nature and its greater water depths, resulting in the deposition of darker coloured mudstone with higher TOC values. Microbial mats developed in association with these darker coloured mudstone, but were confined to intra-basinal structural highs (Beagle Ridge and Turtle Dove Ridge) which were shallow enough for sufficient light to penetrate to allow the development of mats, but in harsh condition for other fauna.

During the period of ecological recovery that followed the end-Permian mass extinction, the development of microbial mats was controlled by two local factors.

- 1) Paleogeographic control: anoxic conditions away from the basin margin inhibited grazing organisms, allowing microbial mats to flourish while oxic, shallow marine, tidal settings with major clastic input closer to the basin margins promoted grazing organisms, which are unfavourable for microbial mat forming organisms.
- 2) Topographic control: topographic highs in the anoxic part of the basin provided good habitats with sufficient light for microbial mat forming organisms.

Therefore, the combination of global and local controls are important for the development of microbial mats.

The microbial mats and darker coloured mudstone have good source rock potential with higher TOC and HI. The distribution of these lithofacies matches the distribution of discovered hydrocarbon fields highlighting the more prospective parts of the basin. On the other hand, the lighter coloured shale deposited under oxic condition has poor source rock quality with lower TOC and HI.

Declaration of competing interest

The authors declare that they have no known competing financial interests or personal relationships that could have appeared to influence the work reported in this paper.

Acknowledgements

This study is a part of PhD research by the first author funded by INPEX Corporation and WA-OIGC. The authors thank Geoscience Australia and the Geological Survey of Western Australia for providing seismic and well log data. The Geological Survey of Western Australia is also thanked for permission to observe cores and collect rock samples (G004177), Intertek for TOC and Rock-Eval analyses, Schlumberger for providing Petrel interpretation software and ESRI for providing ArcGIS software. We also thank Darren Ferdinando and an anonymous referee for reviews of an earlier version of the manuscript which have improved it significantly.

Appendix A. Supplementary data

Supplementary data to this article can be found online at <https://doi.org/10.1016/j.marpetgeo.2021.105314>.

References

- Boreham, C.J., Hope, J.M., Hartung-Kagi, B., van Aarssen, B.J.K., 2000. More sources for gas and oil in Perth Basin. AGSO Res. Newsl. 5–9.
- Cadman, S.J., Pain, I., Vuckovic, V., 1994. Perth Basin, western Australia. *Aust. Pet. Accumul. Rep.* 10, 1–103.
- Chen, Z.Q., Wang, Y., Kershaw, S., Luo, M., Yang, H., Zhao, L., Feng, Y., Chen, J., Yang, L., Zhang, L., 2014. Early Triassic stromatolites in a siliciclastic nearshore setting in northern Perth Basin, Western Australia: geobiologic features and implications for post-extinction microbial proliferation. *Global Planet. Change* 121, 89–100. <https://doi.org/10.1016/j.gloplacha.2014.07.004>.
- Crostella, A., 1995. An evaluation of the hydrocarbon potential of the onshore northern Perth Basin, Western Australia. *Geol. Surv. West. Aust.* 43, 72.
- Crostella, A., Backhouse, J., 2000. *Geology and Petroleum Exploration of the Central and Southern Perth Basin*.
- Dawson, D., Grice, K., Alexander, R., 2005. Effect of maturation on the indigenous δD signatures of individual hydrocarbons in sediments and crude oils from the Perth Basin (Western Australia). *Org. Geochem.* 36, 95–104. <https://doi.org/10.1016/j.orggeochem.2004.06.020>.
- Erwin, D.H., 1994. The Permian-Triassic extinction. *Nature* 367, 231–236.
- Ferdinando, D., Baker, J.C., Gogora, A., Pidgeon, B.A., 2007. Illite/Smectite clays preserving porosity at depth in Lower Permian reservoirs, northern Perth Basin. *APPEA J* 47, 69–88. <https://doi.org/10.1071/apj06004>.
- Foster, W.J., Heindel, K., Richoz, S., Gliwa, J., Lehmann, D.J., Baud, A., Kolar-Jurkovič, T., Aljinović, D., Jurkovič, B., Korn, D., Martindale, R.C., Peckmann, J., 2020. Suppressed competitive exclusion enabled the proliferation of Permian/Triassic boundary microbialites. *Depos. Rec.* 6, 62–74. <https://doi.org/10.1002/dep2.97>.
- Georgiev, S.V., Stain, H.J., Yang, G., Hannah, J.L., Böttcher, M.E., Grice, K., Hofman, A.I., Turgeon, S., Simonsen, S., Cloquet, C., 2020. Late Permian–Early Triassic environmental changes recorded by multi-isotope (Re–Os–N–Hg) data and trace metal distribution from the Hovea-3 section, Western Australia. *Gondwana Res.* 88, 353–372. <https://doi.org/10.1016/j.gbs.2019.183135>.
- Ghori, K.A.R., 2015. *Petroleum Systems of the Perth Basin, Western Australia*, vol. 10895. Search Discov, p. 20.
- Gotter, J., Nicoll, R.S., Metcalfe, I., Willink, R., Ferdinando, D., 2009. The Permian–Triassic boundary in Western Australia: evidence from the Bonaparte and northern Perth basins—exploration implications. *APPEA J* 49, 311–336. <https://doi.org/10.1071/AP08020>.
- Grice, K., Cao, G., Love, G.D., Böttcher, M.E., Twitchett, R.J., Grosjean, E., Simonsen, R. E., Turgeon, S.C., Dunning, W., Jin, Y., 2005a. Photic zone euxinia during the Permian–Triassic superanoxic event. *Science* 307, 706–709. <https://doi.org/10.1126/science.1104323>.
- Grice, K., Nabbefeld, B., Maden, E., 2007. Source and significance of selected polycyclic aromatic hydrocarbons in sediments (Hovea-3 well, Perth Basin, Western Australia) spanning the Permian–Triassic boundary. *Org. Geochem.* 38, 1795–1803. <https://doi.org/10.1016/j.orggeochem.2007.07.001>.
- Grice, K., Simonsen, R.E., Grosjean, E., Twitchett, R.J., Dunning, W., Wang, S.X., Böttcher, M.E., 2005b. Depositional conditions of the northern onshore Perth Basin (basal Triassic). *APPEA J* 45, 262–274.
- Grice, K., Twitchett, R.J., Alexander, R., Foster, C.B., Looy, C., 2005c. A potential biomarker for the Permian–Triassic ecological crisis. *Earth Planet. Sci. Lett.* 236, 315–321. <https://doi.org/10.1016/j.epsl.2005.05.008>.
- Grosjean, E., Hall, L., Boreham, C., Buckler, T., 2017. Source Rock Geochemistry of the Offshore Northern Perth Basin. *Regional Hydrocarbon Prospectivity of the Offshore Northern Perth Basin*, Geoscience Australia. <https://doi.org/10.11636/Record.2017.018>.
- Haig, D.W., Martin, S.K., Mory, A.J., McLoughlin, S., Backhouse, J., Berrell, R.W., Keat, B.P., Hall, R., Foster, C.B., Shi, G.R., Bevan, J.C., 2015. Early Triassic (early Olenekian) life in the interior of east Gondwana: mixed marine-terrestrial biota from the Kockatea shale, western Australia. *Palaeogeogr. Palaeoclimatol. Palaeoecol.* 417, 511–533. <https://doi.org/10.1016/j.palaeo.2014.10.015>.
- Hall, P.B., Kneale, R.L., 1992. Perth Basin rejuvenated. *APPEA J* 32, 33–43.
- Jablonski, D., Saitta, A.J., 2004. Permian to lower cretaceous plate Tectono-stratigraphic development of the western Australian margin. *APPEA J* 44, 479–507. <https://doi.org/10.1071/AP03011>.
- Jones, A., Kennard, J.M., Nicholson, C.J., Bernard, G., Mantle, D., Grosjean, E., Boreham, C.J., Jørgensen, D.C., Robertson, D., 2011. New exploration opportunities in the offshore northern Perth Basin. *APPEA J* 51, 45–78. <https://doi.org/10.1071/apj0003>.
- Kershaw, S., Crasquin, S., Li, Y., Collin, P.Y., Forel, M.B., Mu, X., Baud, A., Wang, Y., Xie, S., Maurer, F., Guo, L., 2012. Microbialites and global environmental change across the Permian–Triassic boundary: a synthesis. *Geobiology* 10, 25–47. <https://doi.org/10.1111/j.1472-4669.2011.00302.x>.
- Knoll, A.H., Bambach, R.K., Canfield, D.E., Grotzinger, J.P., 1996. Comparative earth history and late Permian mass extinction. *Science* 273, 452–457. <https://doi.org/10.1126/science.273.5274.452>.
- Langhi, L., Ross, A., Crooke, E., Jones, A., Nicholson, C., Stalvies, C., 2014. Integrated hydroacoustic flares and geomechanical characterization reveal potential hydrocarbon leakage pathways in the Perth Basin, Australia. *Mar. Petrol. Geol.* 51, 63–69. <https://doi.org/10.1016/j.marpetgeo.2013.11.016>.
- Luo, M., Chen, Z.Q., 2014. New arthropod traces from the lower Triassic Kockatea shale formation, northern Perth Basin, western Australia: ichnology, taphonomy and palaeoecology. *Geol. J.* 49, 163–176. <https://doi.org/10.1002/gj.2506>.
- Luo, M., Chen, Z.Q., Shi, G.R., Feng, X., Yang, H., Fang, Y., Li, Y., 2019. Microbially induced sedimentary structures (MISSs) from the lower Triassic Kockatea formation, northern Perth Basin, western Australia: Palaeoenvironmental implications. *Palaeogeogr. Palaeoclimatol. Palaeoecol.* 519, 236–247. <https://doi.org/10.1016/j.palaeo.2018.06.040>.
- McIlldowie, M., Alexander, R., 2005. Identification of a novel C33 n-alkylcyclohexane biomarker in Permian–Triassic sediments. *Org. Geochem.* 36, 1454–1458. <https://doi.org/10.1016/j.orggeochem.2005.06.009>.
- Metcalfe, I., Nicoll, R.S., Willink, R.J., 2008. Conodonts from the Permian–Triassic transition in Australia and position of the northern Perth Basin. *Aust. J. Earth Sci.* 55, 365–377. <https://doi.org/10.1080/08120090701769480>.
- Mory, A.J., 1994. Structural evolution of the onshore northern Perth basin, Western Australia. In: *The Sedimentary Basins of Western Australia: Proceedings of the Petroleum Exploration Society of Australia Symposium*, pp. 781–789.
- Mory, A.J., Haig, D.W., McLoughlin, S., Hocking, R.M., 2005. *Geology of the northern Perth Basin, western Australia. A field guide*. *Geol. Surv. West. Aust.* 2005/9, 71pp.
- Mory, A.J., Iasky, R.P., 1996. Stratigraphy and structure of the onshore northern Perth Basin, western Australia. *Geol. Surv. West. Aust. Rep.* 46, 101pp.
- Nabbefeld, B., Grice, K., Simonsen, R.E., Hays, L.E., Cao, G., 2010. Significance of polycyclic aromatic hydrocarbons (PAHs) in Permian/Triassic boundary sections. *Appl. Geochem.* 25, 1374–1382. <https://doi.org/10.1016/j.apgeochem.2010.06.008>.
- Norvick, M.S., 2004. Tectonic and stratigraphic history of the Perth Basin. *Geo Australasia 2004/16*, 18pp.
- Quaife, P., Rosser, J., Pagnozzi, S., 1994. The structural architecture and stratigraphy of the offshore northern Perth Basin, Western Australia. In: *The Sedimentary Basins of Western Australia: Proceedings of the Petroleum Exploration Society of Australia Symposium*, pp. 811–822.
- Scott, J., 1994. Source rocks of Western Australia—distribution, character and models. In: *The Sedimentary Basins of Western Australia: Proceedings of the Petroleum Exploration Society of Australia Symposium*, pp. 141–155.
- Song, Haijun, Wignall, P.B., Chu, D., Tong, J., Sun, Y., Song, Haiyue, He, W., Tian, L., 2014. Anoxia/high temperature double whammy during the Permian–Triassic marine crisis and its aftermath. *Sci. Rep.* 4, 1–7. <https://doi.org/10.1038/srep04132>.
- Song, T., Cawood, P.A., 2000. Structural styles in the Perth Basin associated with the Mesozoic break-up of greater India and Australia. *Tectonophysics* 317, 55–72. [https://doi.org/10.1016/S0040-1951\(99\)00273-5](https://doi.org/10.1016/S0040-1951(99)00273-5).
- Thomas, B.M., 1979. Geochemical analysis of hydrocarbon occurrences in northern Perth Basin, Australia. *Am. Assoc. Petrol. Geol. Bull.* 63, 1092–1107. <https://doi.org/10.1306/2F9184BE-16CE-11D7-8645000102C1865D>.
- Thomas, B.M., Barber, C.J., 2004. A re-evaluation of the hydrocarbon habitat of the northern Perth Basin. *APPEA J* 44, 59–92.
- Thomas, B.M., Willink, R.J., Grice, K., Twitchett, R.J., Purcell, R.R., Archbold, H.W., George, A.D., Tye, S., Alexander, R., Foster, C.B., Barber, 2004. Unique marine Permian–Triassic boundary section from western Australia. *Aust. J. Earth Sci.* 51, 423–430.
- Twitchett, R.J., Krystyn, L., Baud, A., Whedey, J.R., Richoz, S., 2004. Rapid marine recovery after the end-Permian mass-extinction event in the absence of marine anoxia. *Geology* 32, 805–808. <https://doi.org/10.1130/G20585.1>.
- Whiteside, J.H., Grice, K., 2016. Biomarker records associated with mass extinction events. *Annu. Rev. Earth Planet. Sci.* 44, 581–612. <https://doi.org/10.1146/annurev-earth-060115-012501>.
- Wignall, P.B., Twitchett, R.J., 1996. Oceanic anoxia and the end Permian mass extinction. *Science* 272, 1155–1158. <https://doi.org/10.1126/science.272.5265.1155>.
- Woods, A.D., 2014. Assessing Early Triassic paleoceanographic conditions via unusual sedimentary fabrics and features. *Earth Sci. Res.* 137, 6–18. <https://doi.org/10.1016/j.earscirev.2013.08.015>.

Basin Workshop 2020

Taniwaki, T., Grice, K., Elders, C., Lateral facies distribution in the Upper Permian to Lower Triassic Kockatea Shale in the Northern Perth Basin. Basin Workshop 2020, Perth and online, December 2020, oral presentation.

No abstract was required for this conference.

AAPG Geosciences Technology Workshop (GTW)

Taniwaki, T., Elders, C., Grice, K., Biomarkers indicative of photic zone euxinia and microbial mats in the northern Perth and northern Carnarvon basins. AAPG Geosciences Technology Workshop (GTW), Perth and online, March 2021, oral presentation.

The end-Permian mass extinction is the greatest extinction event of the Phanerozoic. It is well established that a large igneous province (LIP) played a major role in the extinction due to massive volcanic activity associated with Siberian Trap eruptions that released large quantities of CO₂ and other gases leading to a rise in global temperature. It has also been shown that the paleo-seas (Panthalassa and Paleo Tethys) were generally stagnant and had anoxic bottom waters. Biomarkers indicative of photic zone euxinia (PZE) have been identified in many global deposits. Sulfate reducing bacteria anaerobically degrade organic matter in sediments and/or at the sediment water interface yielding H₂S which is then used by anoxygenic photosynthetic bacteria as an electron donor in photosynthesis to fix carbon dioxide near the chemocline (transition between oxic and anoxic conditions). Anoxygenic photosynthetic bacteria include obligate purple sulfur bacteria, strict green-green and green-brown sulfur bacteria. These organisms make specific carotenoids (purple sulfur bacteria: okenone, green-green sulfur bacteria: chlorobactene, green-brown sulfur bacteria: isorenieratene). Biomarkers of these compounds have been identified in oils and sediments and are regarded as indicators of open water column PZE. However, similar anaerobic photosynthetic sulfur bacteria can occur in microbial mats or microbialites which are often dominated by purple sulfur bacteria. In the northern Perth Basin, the development of open water PZE has been identified in the Early Triassic Kockatea Shale. The organic material in this interval is considered as an important source rock for oils in this basin. However, a potential source of these biomarkers from microbial mats needs to be carefully evaluated to better understand the paleoenvironmental conditions of deposition. In this study, nine lithofacies have been identified from core material of six wells penetrating the basal part of the

Kockatea Shale. These facies include bioturbated beds, black shale, dark grey shale, medium grey shale, light olive brown shale, olive black shale, microbial mat beds, storm/gravity flow sandstones and tidal sandstones. Most of the samples contain biomarkers indicative of anoxygenic photosynthetic sulfur bacteria. Darker coloured shales and microbial mats contain higher relative abundances of okenane (purple sulfur bacteria) in addition to chlorobactane (green-green sulfur bacteria) and isorenieratane (green-brown sulfur bacteria). Variations in these biomarkers in the Perth Basin sediments reflect two sources across much of the basin - open water column PZE and microbialites. However, they are not observed in tidal deposits from the southern region of this basin. The petroleum samples from the northern Perth Basin and the northern Carnarvon basins also contain okenane, chlorobactane and isorenieratane. The occurrence of these compounds indicate that the development of open water column PZE and microbial mat facies in the Early Triassic play an important role in the development of petroleum systems in these basins.

30th International meeting of Organic Geochemistry (IMOG 2021)

Taniwaki, T., Elders, C., Holman, A., I., Böttcher, M., E., Grice, K.,
Basin scale evaluation: Organic geochemical characteristics of
northern Perth Basin (Early Triassic). 30th International meeting of
Organic Geochemistry (IMOG 2021), Montpellier, France and online,
September 2021, poster.

The end Permian mass extinction event is the largest mass extinction of the Phanerozoic and led to 95% of marine and about 70% of terrestrial species being wiped out (Whiteside and Grice, 2016). Massive volcanic activity linked to the Siberian Trap eruptions is assumed to have played a critical role in the extinction. Large amounts of CO₂ and other gasses led to global warming and anoxia (Wignall and Twitchett, 1996). Photic zone euxinia (PZE) conditions have been identified in many global end-Permian locations (Grice et al., 2005), whereby H₂S is produced by sulfate reducing bacteria which anaerobically degrade organic matter in sediments and/or at the sediment water interface (Pfenning, 1978). Such organisms include purple sulfur bacteria, green-green and green-brown sulfur bacteria which make specific carotenoid pigments (purple sulfur bacteria: okenone; green-green sulfur bacteria: chlorobactene; green-brown sulfur bacteria: isorenieratene). These carotenoids are the source of biomarkers (okenane, chlorobactane and isorenieratane) respectively found in oils and source-rocks (Dawson et al., 2005; Grice et al., 2005; Maslen et al., 2009; Tulipani, 2013). Purple sulfur bacteria are also abundant in microbial mats (Brocks and Schaeffer, 2008; Pagès et al., 2014; Schaefer et al., 2020). In the northern Perth Basin, PZE has been established in the Lower Triassic Kockatea Shale. However, a basin wide study of the distribution of PZE conditions has never been undertaken.

Biomarker analysis has been conducted on rock samples from 6 wells of the basal Kockatea Shale including lithofacies containing microbial mats. The northern wells of the northern Perth Basin exhibit darker shale horizons and contain microbial mats.

These horizons contain abundant carotenoid biomarkers attributed to PZE and microbial mats. Such biomarkers are however, not identified in the southern wells of the northern Perth basin which are deposited under more oxic conditions in a tidal regime. In the northern wells, there are fluctuations of PZE conditions intruded by oxic conditions, caused by fluctuations of the chemocline. Elevated 2 α -methylhopanes index and higher renieratane and renierapurpurane/isorenieratane ratio (Fox et al., 2020; Schaefer et al., 2020) are identified in the microbial mats formed under oxic conditions. In addition, the higher proportion of both okenane against chlorobactane and isorenieratane and C₃₃ *n*-alkylcyclohexane ratio (n-C₃₃ ACH ratio) are identified in the microbial mat facies.

The combination of organic geochemistry (biomarker analysis) and geology (core observation, well analysis and seismic interpretation) show a strong relationship between basin morphology, paleogeography and paleoenvironmental conditions. The southern wells experienced higher influence of fluvial input (oxic conditions). The northern wells, which are far north of the fluvial input show evidence for PZE conditions.

GSA Earth Science Student Symposia Western Australia (GESSS WA)

Taniwaki, T., Elders, C., Holman, A., I., Grice, K., Basin scale paleoenvironmental conditions during deposition of the Early Triassic Kockatea Shale, northern Perth Basin. GSA Earth Science Student Symposia Western Australia (GESSS WA), Perth, November 2021, oral presentation.

The end Permian mass extinction is the largest mass extinction event in the Phanerozoic. Massive volcanic activity associated with Siberian Trap eruptions is considered to be a critical factor for the cause of this extinction event. These eruptions emitted large amount of CO₂ and other gasses, leading to global warming, anoxia and euxinia. Photic zone euxinia (PZE) conditions are formed when high H₂S concentration overlaps with the photic zone. PZE conditions have been reported globally around the Permian-Triassic boundary. Anaerobic sulfur bacteria are active when PZE conditions occur and show distinct zonation (top: purple sulfur bacteria (PSB), middle: green-green sulfur bacteria (GGSB), bottom: green-brown sulfur bacteria (GBSB)). These sulfur bacteria make characteristic carotenoid pigments giving rise to specific biomarkers (okenane: PSB, chlorobactane: GGSB, and isorenieratane: GBSB). Microbial mats are also known to contain anaerobic sulfur bacteria (especially PSB and GGSB).

In the northern Perth Basin, the Kockatea Shale was deposited during Late Permian to Early Triassic. The Lower Triassic Kockatea Shale shows lithological variations in core (*e.g.* darker coloured mudstone, lighter coloured mudstone and microbial mats). Darker coloured mudstones were deposited under deep water depth with PZE conditions. Microbial mats with sulfur bacteria developed under shallow water settings on intra-basinal structural highs away from basin margins. Lighter coloured mudstones were deposited under tidally influenced oxic settings without sulfur bacteria near basin margins. Microbial mats are characterised by higher abundance of okenane (PSB) and C₃₃ *n*-alkylcyclohexane and lighter values of $\delta^{13}\text{C}_{\text{OM}}$ and $\delta^{34}\text{S}$ of pyrite compared with

water column PZE conditions. These parameters are good proxies to distinguish between microbial mats and PZE based on the difference of relative abundance of purple sulfur bacteria.